UCRL-18735

ey. 2

INORGANIC MATERIALS RESEARCH DIVISION

Annual Report 1968

Lawrence Radiation Laboratory
University of California Berkeley

UCRL-18735

ey. 2

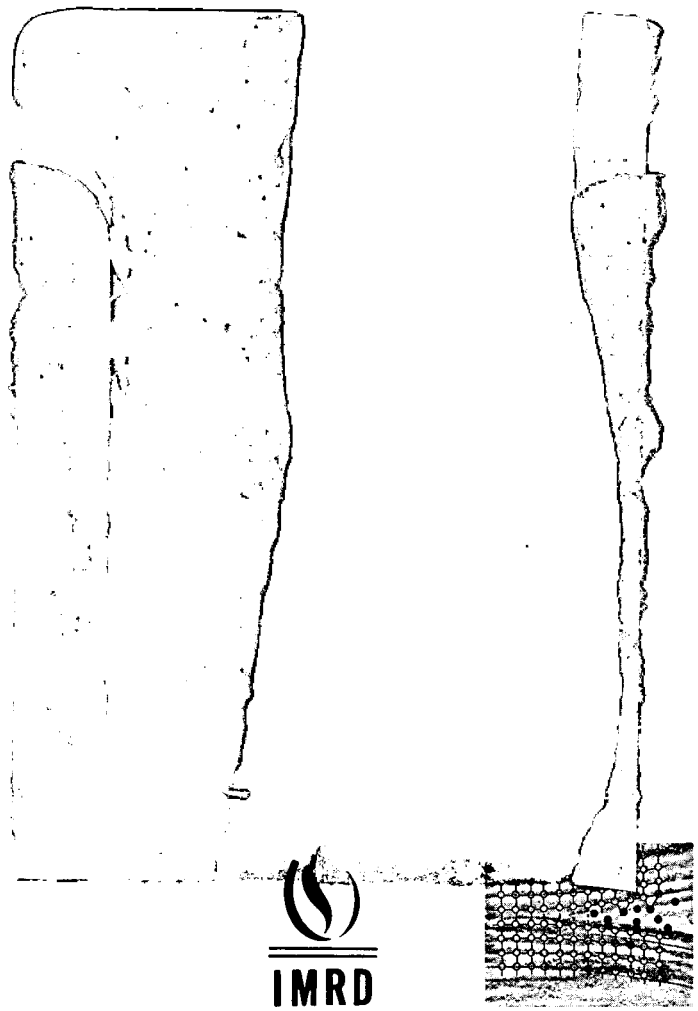

IMRD

Metallurgical Engineering

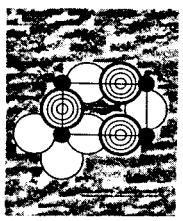

Chemistry

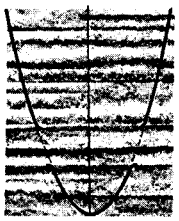

Solid-State Physics

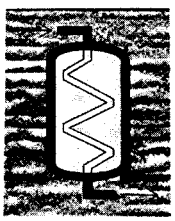

Chemical Engineering

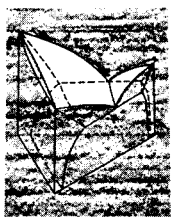

Ceramic Engineering

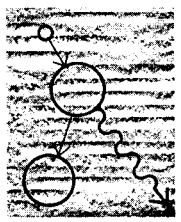

Nuclear Engineering

DISCLAIMER

UCRL-18735
UC-2 General, Miscellaneous,
and Progress Reports
TID-4500 (54th Ed.)

INORGANIC MATERIALS RESEARCH DIVISION
ANNUAL REPORT, 1968

April 1969

Lawrence Radiation Laboratory
University of California
Berkeley, California

Work done under
U.S. Atomic Energy Commission
Contract No. W-7405-eng-48

Printed in the United States of America
Available from
Clearinghouse for Federal Scientific and Technical Information
National Bureau of Standards, U.S. Department of Commerce
Springfield, Virginia 22151
Price: Printed Copy $3.00; Microfiche $0.65

INORGANIC MATERIALS RESEARCH DIVISION

ANNUAL REPORT,1968*

Contents

---

* Preceding Annual Reports: UCRL-18043, UCRL-17330.

GENERAL INTRODUCTION

Leo Brewer, Division Head
Victor F. Zackay, Associate Head

With the large influx of graduate students in the Fall, the total of IMRD graduate students would have topped 200 by December if a record number of students had not completed their degrees in the Fall. During the year 25 Ph. D. theses and 22 M. S. theses were filed.

The publications of the Division also expanded with 195 publications in technical journals or as chapters of books during 1968.

IMRD principal investigators continue their strong contribution to University administrative positions with Professors Bruce Mahan, Charles W. Tobias, and Jack Washburn as chairmen of the Departments of Chemistry, Chemical Engineering, and Materials Science and Engineering, respectively. Professor Harold S. Johnston is Dean of the College of Chemistry and Professor Gareth Thomas is Associate Dean of the Graduate Division. Dr. Norman Phillips is also an Associate Dean of the Graduate Division and Dr. Alan Portis is the Associate Director of the Lawrence Hall of Science.

Professor Bruce Mahan of the Chemistry Department was awarded the California Section of the ACS award. During the year Dr. Marshal Merriam, Dr. Joseph Pask, and Dr. Jack Washburn were granted sabbatical leaves from the Department of Materials Science and Engineering for advanced research in their respective fields.

The 650 kV high voltage microscopy program, under the directorship of Professor Gareth Thomas, should be operational in mid-1969. Its advantages are as follows: (1) Greater penetration, thus allowing use of thicker foils, heavier elements, and materials previously too difficult to make into foils for 100 kV examination (e.g., ceramics, composites, etc.); (2) higher resolution, mainly through a reduction in chromatic aberration due to reduced scattering in specimens; (3) lower radiation damage in non-metals due to reduced ionization cross sections at high voltage; thus, it becomes possible at ~300 kV to examine polymers (they decompose at 100 kV). Conversely, radiation damage in metals become appreciable above 500 kV The optimum range of high voltage work thus seems to be up to about 600 kV for most materials.

Weekly seminars based on current research of the Division and on the research of visiting scientists were continued. Among the speakers were Dr. M. E. Shank, Pratt and Whitney Aircraft Corporation, Middletown, Conn.; Mr. D. Mattox, Sandia Corporation, Albuquerque, New Mexico; Dr. R. Stern, Brooklyn Polytechnic Institute, Brooklyn, N. Y.; Dr. Peter Barrand, presently with Argonne National Laboratory, Argonne, Illinois; Dr. Osteryoung, North American Rockwell Science Center, Thousand Oaks, California; Dr. J. Kruger, National Bureau of Standards, Washington, D. C.; I. Blesh, Fairchild Semiconductor; Dr. A. J. Ardell, California Institute of Technology, Pasadena, California; Dr. J. E. Burke, General Electric Company, Pleasanton, California; Professor J. Cobble, Purdue University, Lafayette, Indiana; Dr. C. E. Birchenall, University of Delaware, Newark, Delaware; Dr. D. Rosner, Ritter Pfandler Corporation, Princeton, New Jersey; Dr. H. Goehr, University of Erlangen-Nuernberg, Germany; and Mr. W. Grimes, Reactor Chemistry Division, Oak Ridge National Laboratory, Oak Ridge, Tennessee.

The Fourth International Materials Symposium on the Structure and Chemistry of Solid Surfaces was held in June on the Berkeley campus. Three hundred and sixty-two registrants attended the four-day program which featured presentation of 84 papers in double sessions. Of the registrants, 27 attendees represented foreign countries. The next IMRD-sponsored symposium will be held in 1971 as a joint meeting on ceramics and metallurgy.

The 1965 policy of instituting salary reductions for graduate students who had not completed their degree work within five years was continued. During 1968 it was necessary to apply the salary reduction in five instances.

The third annual review symposium of the Inorganic Materials Research Division was held in January. All sessions of this interdisciplinary symposium are open to faculty,

students, and other scientific associates of the campus. Invited as reviewers were Professor Richard Spriggs, Lehigh University; Professor C. S. Barrett, James Frank Institute; Professor P. Duwez, California Institute of Technology; Professor John Chipman, Massachusetts Institute of Technology; Professor Robert Plane, Cornell University; and Professor T. H. Geballe, Stanford University. The Atomic Energy Commission representatives were Dr. Donald K. Stevens, Dr. A. R. Van Dyken, Dr. R. Epple, Dr. L. Ionniello, Dr. R. Kandel, and Dr. D. Richman. The meetings were held over a two day period with selected members of the IMRD staff presenting their current research in an open-discussion atmosphere.

REPRESENTATIVE HIGHLIGHTS OF THE 1968 RESEARCH PROGRAM

Spectroscopic studies of codeposited pairs Ag and Au, and Cu and Au in solid krypton have demonstrated that splittings and shifts of spectral lines of atoms isolated in rare-gas matrices are not due to long range solute-solute interactions. (Brewer)

A crossed molecular beam study of the reactions of thermal energy Li atoms with Cl_2, ICl, Br_2, $SnCl_4$, and PCl_3 indicates that the lithium halide product angular distributions are broader and more complex than had been observed in previous studies with Cs, Rb, K, and Na as reactants; this result strongly suggests an important mass effect in the overall reaction dynamics. (R. Herm)

A kinetic study of the sodium-urea reaction in liquid ammonia has yielded the rate constant of the reaction of the ammonium ion with the electron; the data suggest the formation of ammonium (NH_4) as an intermediate. (W. Jolly)

The resonance of ^{17}O bound to magnesium ion at ~ 0 °C has been made observable by broadening the bulk water resonance beyond detection through addition of manganous ion. The lifetime of a water molecule in the first coordination sphere of magnesium ion extrapolated to 25 °C is ca. 2×10^{-6} seconds. (R. Connick)

The critical role of ionic mass transport in anodic dissolution corresponding to electromachining conditions has been quantitatively demonstrated. Evidence was obtained to support the hypothesis that dissolution in the transpassive region occurs in part by entrainment of solid anodic reaction products. (C. W. Tobias)

The oxidation of a rotating disk of molybdenum has been measured over the temperature range from 840 to 1700 °C. The importance of diffusion limitations in obscuring the true activation energy of the gas-solid reaction was demonstrated. (D. Olander)

From ion-molecule beam studies of the reaction of N_2^+ with H_2, D_2, and HD, complete product velocity vector distributions, differential cross sections, and total cross section were determined. This is the most complete analysis of the dynamics of a chemical reaction ever accomplished. (B. Mahan)

Ellipsometry has been successfully used for determining adsorption isotherms on atomically clean metal single crystal faces. The results demonstrate that adsorption isotherms on single crystal surfaces can be obtained by ellipsometry, and heats of adsorption, cross sectional areas of adsorbed molecules, and coverage ratios of substrate and adsorbate atoms can be derived from the measurements. (R. Muller)

New molecular modulation spectrometers have been used to conclude what is by far the best study yet made of the infrared and ultraviolet spectra of the C100 and C10 radicals and the kinetics of these radicals. (H. Johnston)

Several adsorbed hydrocarbon gases form ordered surface structures on the platinum surface while remaining disordered on silver surfaces. (G. Somorjai)

Two theoretical analyses on solute atom interactions with dislocations were completed. One concerned the thermally activated unlocking of dislocations from a solute atmosphere, and the second concerned the effect of concentration of solute atoms on the yield stress; in the latter it was shown that the yield stress increased at first linearly with the square root of the concentration, reached a maximum value, and thereafter decreased as the concentration was further increased. (J. Dorn)

The effect of fine precipitates on the critical current densities of superconducting niobium 1% zirconium were studied. The model developed to explain the results predict that the critical current density is a function of the ratio of precipitate size to interprecipitate spacing. (L. Brewer et al.)

Intergranular fracture modes in Al-Zn binary alloys have been established. Fracture may involve either microvoid coalescence or a combined fracture mode of microvoid coalescence and "intergranular cleavage" (not true cleavage, due to the lack of crystallographic character). (E. Parker)

It has been shown that embrittlement in high strength martensites is correlated with transformation twinning (and composition). In order to avoid this control of alloying or changing, heat treatment to form lower bainite is necessary. (G. Thomas)

Phase boundaries in semi-infinite diffusion couples have been shown to move with the crystal having the higher diffusivities growing at the expense of the other. This was shown to occur with NiO-MgO (complete solid solution) and NiO-CaO (limited solid solution) couples in the temperature range 1200 to 1550°C in air. (J. Pask)

Theoretical study of evaporation kinetics shows that from comparison of apparent enthalpies and entropies of activation to enthalpies and entropies of the equilibrium evaporation processes it is frequently possible to show either a surface or the desorption step is probably rate determining. (A. Searcy)

A study of vacancy clustering in quenched aluminum has shown that both dislocation loops and voids are nucleated for a wide range of quenching and aging temperatures. The results provide direct evidence that the stress field of a dislocation loop significantly increases its efficiency as a vacancy sink. (J. Washburn)

A unique method of sintering lead zirconate titanate ferroelectric ceramics was developed. Impurities normally encountered in ceramic processing were identified to lead to liquid phase sintering kinetics. (R. Fulrath)

Evaluation of thermodynamic data for 95 elements and binary alloys was completed. (R. Hultgren)

The principles involved in obtaining excellent combinations of strength and ductility and combinations of strength and resistance to fracture have been established in TRIP steel. The first involves the prevention of local necking by enhancing the work-hardening rate from the transformation. The second involves the energy dissipation arising out of the crystallographic shear process. (V. Zackay)

The low temperature region of the lead-indium phase diagram was investigated using the superconducting transition temperature and x-ray diffraction. The results show that a narrowing of the stability ranges of the α_1 and fcc phases occurs below room temperature. (R. Hammond)

The ^{19}F resonance has been carefully studied in $KMnF_3$, yielding both an accurate indication of deviations in the structure from the ideal cubic perovskite and also indicating the extent to which the sublattice magnetization is modified by an external static field. (A. Portis)

The study of the interaction of far infrared radiation with superconducting Josephson junctions has led to the invention of a sensitive tunable narrow band regenerative far infrared receiver. (P. Richards)

A powerful tunable far infrared source can be obtained from the difference-frequency generation in a nonlinear crystal by mixing of two laser beams. (Y. R. Shen and P. Richards)

The flux jumping experiments on Pb-In alloys have shown that flux bundles enter or leave a superconductor with an exponential size distribution, and that jumping persists in the region $H_{c2} < H < H_{c3}$ above the bulk upper critical field. (G. Rochlin)

I. Chemistry

A. INORGANIC CHEMISTRY

1. THE DEPROTONATION OF WEAK ACIDS WITH POTASSIUM HYDROXIDE*

William L. Jolly, Douglas S. Rustad, Thomas Birchall, and David J. Chazan

Potassium hydroxide may be used to deprotonate extremely weak acids if hydroxylic solvents such as water and alcohols are avoided.[1] Several syntheses have been devised to illustrate the general applicability of this procedure to organometallic syntheses.

The synthesis of methyl cyclopentadienylmolybdenum tricarbonyl illustrates how a potassium cyclopentadienyl solution may be prepared and then used to prepare a typical transition metal cyclopentadienyl complex. By analogous procedures, one may prepare a wide variety of metal complexes of the anions of cyclopentadiene, indene, etc. The syntheses of ferrocene and nickelocene illustrate how the procedure may be adapted to the simultaneous deprotonation of cyclopentadiene and the dehydration of a transition metal salt. Methylphosphine and dimethylphosphine syntheses show how alkyl derivatives of a volatile hydride may be prepared in amounts as great as 0.05 mole. A methylgermane synthesis shows a somewhat simpler procedure applicable to amounts less than 0.005 mole.

The compounds synthesized, together with the chemical reactions involved, are listed below.

a. σ-Methyl-π-Cyclopentadienylmolybdenum Tricarbonyl

$$2KOH + C_5H_6 \rightarrow K^+ + C_5H_5^- + KOH \cdot H_2O$$

$$Mo(CO)_6 + C_5H_5^- \rightarrow Mo(CO)_3C_5H_5^- + 3CO$$

$$CH_3I + Mo(CO)_3C_5H_5^- \rightarrow CH_3Mo(CO)_3C_5H_5 + I^-$$

b. Biscyclopentadienyliron (Ferrocene)

$$8KOH + 2C_5H_6 + FeCl_2 \cdot 4H_2O \rightarrow Fe(C_5H_5) + 2KCl + 6KOH \cdot H_2O$$

c. Biscyclopentadienylnickel (Nickelocene)

$$10KOH + 2C_5H_6 + NiCl_2 \cdot 6H_2O \rightarrow Ni(C_5H_5)_2 + 2KCl + 8KOH \cdot H_2O$$

d. Methylphosphine

$$2KOH + PH_3 \rightarrow K^+ + PH_2^- + KOH \cdot H_2O$$

$$CH_3I + PH_2^- \rightarrow CH_3PH_2 + I^-$$

e. Dimethylphosphine

$$2KOH + PH_3 \rightarrow K^+ + PH_2^- + KOH \cdot H_2O$$

$$CH_3I + PH_2^- \rightarrow CH_3PH_2 + I^-$$

$$2KOH + CH_3PH_2 \rightarrow K^+ + CH_3PH^- + KOH \cdot H_2O$$

$$CH_3I + CH_3PH^- \rightarrow (CH_3)_2PH + I^-$$

f. Methylgermane

$$2KOH + GeH_4 \rightarrow K^+ + GeH_3^- + KOH \cdot H_2O$$

$$CH_3I + GeH_3^- \rightarrow CH_3GeH_3 + I^-.$$

*Abstracted from Inorg. Syn. 11, 113 (1968).
1. See 1967 IMRD Annual Report (UCRL-18043), pp. 10-11.

2. STUDIES OF THE HYDRIDES OF GROUPS IV AND V

a. Syntheses of the Hydrides

Arlan D. Norman, John Webster, and William L. Jolly

We have written an extensive review[1] of methods for preparing the hydrides of the elements of Groups IV and V, exclusive of carbon and nitrogen. The review is concerned principally with the hydrides of silicon, germanium, tin, phosphorus, arsenic, and antimony. Usually a given hydride can be prepared by several different methods, and there are many methods each of which is applicable to several different hydrides. Our aim was to describe the important methods that have been used, emphasizing, when possible, the generality of their application. Specific synthetic methods are recommended for particular hydrides, and suggestions are made for future synthetic research, particularly for higher hydrides and ternary hydrides. Finally, we list those physical properties of the hydrides that are pertinent to their manipulation and identification in the laboratory.

Silane, germane, and stannane can be synthesized by the reduction of a variety of silicon, germanium, or tin compounds with active metal hydrides. We have found that the general method,[2] involving the lithium hydroaluminate ($LiAlH_4$) reduction of silicon tetrachloride and stannic chloride, is convenient for the efficient preparation of 1 to 50 millimoles of silane and stannane. The method is easily adapted to the synthesis of deuterio compounds, i.e., silane-d_4, germane-d_4, and stannane-d_4 by substituting lithium deuterioaluminate for lithium hydroaluminate in the appropriate reactions. Silane-d_4 and germane-d_4 are useful in structural and mechanistic studies, and undoubtedly stannane-d_4 will have similar applications.

We list below the hydrides synthesized, together with the chemical reactions involved.

a. Silane and Silane-d_4

$$SiCl_4 + LiAlH_4 \rightarrow LiCl + AlCl_3 + SiH_4$$

$$SiCl_4 + LiAlD_4 \rightarrow LiCl + AlCl_3 + SiD_4$$

b. Germane-d_4

$$GeCl_4 + LiAlD_4 \rightarrow LiCl + AlCl_3 + GeD_4$$

c. Stannane and Stannane-d_4

$$SnCl_4 + LiAlH_4 \rightarrow LiCl + AlCl_3 + SnH_4$$

$$SnCl_4 + LiAlD_4 \rightarrow LiCl + AlCl_3 + SnD_4.$$

1. Abstracted from Prep. Inorg. Reactions 4, 1 (1968).
2. Abstracted from Inorg. Syn. 11, 170 (1968).

b. Potassium Germyltrihydroborate*

Douglas S. Rustad and William L. Jolly

Potassium germyltrihydroborate, KH_3GeBH_3, is formed by the reaction of diborane with potassium germyl. The salt melts with little decomposition at 98-99° and decomposes at 200° to germanium, germanium hydrides, hydrogen, and potassium hydroborate. Alkaline aqueous solutions are fairly stable, but addition of acid causes complete hydrolysis to germane, hydrogen, and boric acid. The infrared and nmr spectra are given.

*Abstracted from Inorg. Chem. 7, 213 (1968).

c. The Chemistry of Potassium Germyl

Paul M. Kuznesof, Robert Dreyfuss, and William L. Jolly

Last year we reported the synthesis and characterization of potassium 2-germaacetate, $K^+GeH_3CO_2^-$, from potassium germyl and carbon dioxide.[1] This year we have examined reactions of $KGeH_3$ with CS_2, BH_3CO, BF_3, and CH_3COCl, with the aim of preparing

$GeH_3CS_2^-$, $GeH_3C(=O)BH_3^-$, $GeH_3BF_3^-$,

and $GeH_3C(=O)CH_3$.

The first two would be isostructural and isoelectronic, respectively, with $GeH_3CO_2^-$; the third would be isostructural with $GeH_3BH_3^-$; the last would be an analog of acetone.

The reactions of $KGeH_3$ with CS_2 and BH_3CO in 1,2-dimethoxyethane appear extremely complicated. Both reactions produce some GeH_4. The CS_2 reaction proceeds through dramatic color changes from yellow to deep red on warming from -196° to room temperature, finally yielding a moisture-sensitive purple-brown residue. The BH_3CO reaction also yields H_2, CO, and a non-volatile, colorless, apparently polymeric solid which reacts with water to give H_2. No B_2H_6 was produced in the reaction nor was any BH_3CO recovered. Reaction of $KGeH_3$ with BF_3 in 1,2-dimethoxyethane yields a white solid which decomposes at room temperature to give H_2 and GeH_4. Further studies of these systems are planned.

From the reaction of $KGeH_3$ with CH_3COCl, in the absence of a solvent, we have obtained a mixture of volatile liquids which we are presently trying to separate. Infrared and mass spectral data suggest GeH_3COCH_3 may be one of the products. However, other species containing more than one acetyl group and Ge atom also are indicated. We would like to compare the electronic and chemical properties of GeH_3COCH_3 with those of triorgano-α-germyl methyl ketones.

An attempt has been made to prepare phenylgermane by the reaction of potassium germyl, $KGeH_3$, with phenyl iodide, using monoglyme, diglyme, and dimethyl sulfoxide as solvents. The desired nucleophilic substi-

tution (which takes place readily with aliphatic halides) did not occur. Instead benzene and a germanium-hydrogen polymer were formed:[2]

$$NaGeH_3 + C_6H_5Br \rightarrow C_6H_6 + GeH_2 + NaBr.$$

This is a reaction in which the germyl acts as a hydride donor instead of as a simple Lewis base.

We intend to study the reaction of potassium germyl with several substituted aromatic halides in order to determine the conditions under which the two kinds of reaction occur. We hope to see if the reactions are quantitative and to isolate any new arylgermanes that might be formed. A preliminary experiment, for example, indicates that potassium germyl and benzyl bromide yield benzylgermane.

In order to facilitate future work, a system has been devised whereby a stock solution of potassium germyl in diglyme may be prepared, standardized, and stored indefinitely at 0° in the presence of dry nitrogen. Aliquots of the solution may be withdrawn with a pipet; this is an improvement over the usual techniques where a researcher has to make and standardize the reagent each time he wishes to use it.

---

1. Described in detail in Inorg. Chem. 7, 2574 (1968).
2. Last year we described the preparation of GeH_2 by the liquid ammonia-catalyzed disproportionation of Ge_2H_6. This work has been published in Inorg. Chem. 7, 2643 (1968).

3. BORON HYDRIDE CHEMISTRY

a. The Synthesis of Diborane*

Arlan D. Norman and William L. Jolly

Diborane can be prepared by a variety of methods, the most common being the reduction of boron trihalides with active metal hydrides and the reaction of hydroborate salts with stannous chloride, sulfuric acid, methanesulfonic acid, orthophosphoric acid, or polyphosphoric acid. Although diborane is commercially available in bulk quantities, we have found the reaction of potassium hydroborate (KBH_4) with 85% orthophosphoric acid to be convenient for the rapid preparation in a vacuum line of small quantities of this material.

$$KBH_4 + H_3PO_4 \rightarrow 1/2\ B_2H_6 + H_2 + K^+ + H_2PO_4^-.$$

Using this method, diborane is obtained in only 50% of the theoretical yield; however, the absence of volatile solvents, the high purity of the product, and the simplicity of the reaction apparatus make this method superior.

By using approximately 100% orthophosphoric acid, we have increased the yield of diborane to 60-65%. However, under these conditions extensive foaming occurs, necessitating the use of an overhead stirrer in the reaction apparatus. We believe the advantage of this increased yield is offset by the relative unavailability of the more concentrated acid and the increased difficulty of stirring.

---

*Abstracted from Inorg. Syn. 11, 15 (1968).

b. Intermediates in the Hydrolysis of Boron Hydrides

Patricia Finn, Francis Wang, and William L. Jolly

Our study of the isolation and identification of intermediates in the hydrolysis of boron hydrides continues. Preliminary kinetic data show that BH_4^- and $B_3H_8^-$ undergo hydrolysis in cold 8 M HCl by a series of consecutive hydrogen-evolution steps. We tentatively suggest the following steps:

$$\begin{matrix} & \text{f} & & \text{s} & & \text{s} \\ & \text{a} & & \text{l} & & \text{l} \\ BH_4^- & \text{s} & & \text{o} & & \text{o} \\ \text{or} & \text{t} & & & & \\ B_3H_8^- & \rightarrow & BH_2(OH_2)_2^+ & \overset{\text{w}}{\rightarrow} & BH(OH)_2 & \overset{\text{w}}{\rightarrow} B(OH)_3. \end{matrix}$$

We have found that when an intimate mixture of diborane and excess water (formed by co-condensation at -196°) is warmed to -130°, no hydrogen is evolved and no vapor pressure of diborane can be detected (even though diborane itself has an easily measurable vapor pressure at this temperature). We conclude that a hydrate of diborane is formed. When a known excess of diborane is employed in the reaction, the unreacted diborane can be pumped off at -130° and measured. The stoichiometry corresponds to $B_2H_6 \cdot 2H_2O$. It will be interesting to compare this compound with the well-known ammonia analog, which has the structure $BH_2(NH_3)_2^+BH_4^-$.

4. SULFUR-NITROGEN CHEMISTRY*

a. The Reactions of $Mo(CO)_6$ with $S_3N_3Cl_3$ and with S_4N_4†

Kenneth J. Wynne and William L. Jolly

We have observed that molybdenum hexacarbonyl reacts with $S_3N_3Cl_3$ in dichloromethane solution to form a dark brown microcrys-

talline solid of composition $MoS_3N_3Cl_3$:

$$Mo(CO)_6 + S_3N_3Cl_3 \rightarrow MoS_3N_3Cl_3 + 6\ CO.$$

The compound is soluble in donor solvents such as pyridine, dimethyl sulfoxide, and nitromethane, but we have been unable to isolate any stable products from these solutions. When $MoS_3N_3Cl_3$ is exposed to air, sulfur dioxide is evolved (as in the case of $S_3N_3Cl_3$); it therefore seems likely that S-Cl bonds are present in the solid. The compound is insoluble in non-polar solvents; this observation and the observed low ratio of $S_3N_3Cl_3$ to Mo suggest a polymeric structure involving metal-metal bonding. When heated in vacuo, $MoS_3N_3Cl_3$ decomposes with formation of a dark brown amorphous sublimate of composition $MoS_9N_3Cl_6$.

Molybdenum hexacarbonyl reacts with S_4N_4 in refluxing benzene to form a black amorphous explosive solid of composition MoS_5N_5CO. The compound is insoluble in all common organic solvents.

---

*For a review of our recent work in this area, see the chapter by W. L. Jolly in The Chemistry of the Sulfides, A. V. Tobolsky, ed. (Interscience, New York, 1968), pp. 3-7.

†Abstracted from J. Inorg. Nucl. Chem. 30, 2851 (1968).

b. The Structure of the Antimony Pentachloride Diadduct of Disulfur Dinitride

Robert L. Patton and K. Raymond

Suitable crystals of $S_2N_2(SbCl_5)_2$ were grown and mounted for a single crystal x-ray diffraction study, and three-dimensional x-ray data were collected by counter methods. The material crystallizes in space group $I\bar{4}2d$ of the tetragonal system with 8 molecules in a unit cell of dimensions a=b=14.933(3)Å and c=15.547(3)Å. The calculated density of 2.67 g/cm^3 agrees well with the value 2.70 g/cm^3 measured by flotation. Refinement of the structure on F^2 by least-squares methods resulted in a final conventional R factor of 3.8% for 768 independent reflections above background.

The structure consists of $SbCl_5$ groups bonded via the antimony atoms to opposite nitrogen atoms of a planar S_2N_2 ring, with equal S-N bond distances of 1.62 Å, S-N-S angles of 95°, and N-S-N angles of 85°. The nitrogens, antimonys, and axial chlorines of the two nearly octahedral $NSbCl_5$ groups lie on the same twofold rotation axis through the molecule in which both Sb-N distances equal 2.28 Å.

The molecule $S_2N_2(SbCl_5)_2$ is the first compound prepared containing the S_2N_2 group that is sufficiently stable to form crystals suitable for room temperature x-ray structure analysis. This structure is in agreement with that predicted from the infrared spectra of $S_2N_2(SbCl_5)_2$ and, by extrapolation, supports also the planar, 4-membered ring structure proposed by Warn and Chapman[1] for S_2N_2 on the basis of its infrared spectrum.

---

1. J. R. W. Warn and D. Chapman, Spectrochim. Acta 22, 1371 (1966).

c. S_4N_4-H_2SO_4 Solutions

Steven Lipp and William L. Jolly

Our study of the species formed by the reaction of S_4N_4 with 100% sulfuric acid continues. We are using nuclear magnetic resonance to determine the ammonium ion concentration. The complex $[Co(NH_3)_6]_2(SO_4)_2$ is a useful internal standard because it has a large number of protons per mole and has an nmr signal sufficiently upfield so as not to overlap the NH_4^+ triplet. From comparisons of integrated intensities we find that about 1.3 NH_4^+ ions are formed per mole of dissolved S_4N_4.

Cryoscopic studies have shown that the species $HS_2O_7^-$ is present in these solutions. The addition of water to the solutions causes the freezing point to increase, corresponding to a decrease in the total number of species in solution. This result is caused by the $H_2S_2O_7$ which is in equilibrium with the $HS_2O_7^-$:

$$H_2S_2O_7 + H_2O \rightleftharpoons 2H_2SO_4.$$

We are now attempting to calibrate the cryoscopic method so as to permit the quantitative determination of $HS_2O_7^-$ concentrations.

d. The Behavior of S_7NH in Non-Aqueous Solutions

Marshall Mendelsohn and William L. Jolly

It has been known for several years that S_7NH turns purple when added to a methanolic solution of KOH;[1] however, these colored solutions have not been studied extensively. Not only will S_7NH turn blue in various solvents in the presence of KOH but also in some pure solvents such as DMSO, DMF, isopropylamine, and other strongly basic solvents. The blue color is due to an absorption at 5900 Å. There is also an intermediate absorption at ~4200 Å which disappears with time.

At this time it is not clear exactly what part water plays in these systems. However, when water is added to fresh solutions of S_7NH in DMSO and in pyridine, an increase in the intensity of the peak at 5900 Å is observed.

1. H. Garcia-Fernandez, Bull. Soc. Chim. France 265 (1958).

5. STUDIES IN LIQUID AMMONIA

a. The Reaction of Sodium with Urea in Liquid Ammonia: The Rate Constant of the Reaction of the Ammonium Ion with the Ammoniated Electron*

William L. Jolly and Leonardo Prizant

Kinetic studies of the reactions of alcohols[1, 2] and water[2] with sodium in liquid ammonia have been interpreted[2, 3] in terms of the following mechanism:

$$HA + NH_3 \underset{k_2}{\overset{k_1}{\rightleftharpoons}} NH_4^+ + A^-$$

$$NH_4^+ + e^- \xrightarrow{k_3} NH_3 + \tfrac{1}{2}H_2,$$

where HA represents an alcohol or water molecule. The kinetic data are consistent with a low steady-state concentration of ammonium ion and the corresponding rate law

$$-d[e^-]/dt = k_1[HA][e^-]/\{(k_2/k_3)[A^-] + [e^-]\}.$$

Evaluation of the rate constants from the data is difficult because of the strong complexing of the alkoxide ion by dissolved alcohol[3] and of the hydroxide ion by dissolved water.[4] However, we have found that the same type of rate law (and presumably the same mechanism) applies to the reaction of sodium with urea, in which complex-formation of this type is absent. In this case the rate constants may be evaluated relatively unambiguously. It seems possible that the above mechanism, characterized by the lack of a direct reaction between the electron and the species HA, is fairly general for the reaction of metal-ammonia solutions with protic acids.

We followed the course of the urea-sodium reaction by measuring the electrical conductivity of the solution as a function of time at -45°. Several runs, with initial urea-sodium ratios ranging from 1.3:1 to 10:1, yielded the values $k_1 = 3.6 \times 10^{-4}$ sec^{-1} and $k_2/k_3 = 0.30$.

Urea is one of the few acids whose ionization constants in ammonia are known. Herlem[5] has determined that $K_a = 1.25 \times 10^{-13}$ for urea at -60°. By combining this value with our value for k_1, we obtain $k_2 \approx 3 \times 10^9$ M^{-1} sec^{-1}. Apparently the transfer of a proton from an ammonium ion to the anion of urea is essentially a diffusion-controlled reaction.

From the values for k_2 and k_2/k_3 we calculate $k_3 \approx 10^{10}$ M^{-1} sec^{-1}.[2] This value again corresponds to a diffusion-controlled reaction having a low activation energy. There is reason to question whether the rate-determining step for the liquid ammonia reaction can be formulated as it has been for the aqueous reaction:

$$NH_4^+ + e^- \rightarrow NH_3 + H.$$

The heats of formation in liquid ammonia for the first three species in this equation are known,[3] and that for atomic hydrogen may be estimated (probably with an accuracy of ± 3 kcal/mole) by assuming zero heat of solution. Thus we calculate $\Delta H° = 15 \pm 3$ kcal/mole for the liquid ammonia reaction. Now if this process is the rate-determining step, then $\Delta H^‡$ must be at least 15 ± 3 kcal/mole, corresponding to a slow reaction. Thus the formation of atomic hydrogen is inconsistent with the rate constant in liquid ammonia. Perhaps the rate-determining process is better represented by the equation

$$NH_4^+ + e^- \rightarrow NH_4.$$

The ammonium radical might be expected to react further, as in either of the following sequences:

$$NH_4 + e^- \rightarrow NH_2^- + H_2$$
$$NH_4^+ + NH_2^- \rightarrow 2NH_3$$

$$NH_4 \rightarrow NH_2 + H_2$$
$$NH_2 + e^- \rightarrow NH_2^-$$
$$NH_4^+ + NH_2^- \rightarrow 2NH_3.$$

*Abstracted from Chem. Commun. 1345 (1968).

1. E. J. Kelly, H. V. Secor, C. W. Keenan, and J. F. Eastham, J. Amer. Chem. Soc. 84, 3611 (1962).
2. R. R. Dewald and R. V. Tsina, Chem. Commun. 647 (1967); R. R. Dewald and R. V. Tsina, paper presented before the Division of Physical Chemistry at the National A. C. S. Meeting in Chicago, September 1967.
3. W. L. Jolly, Advances in Chemistry Series, American Chemical Society, Washington, 1965, No. 50, p. 27; W. L. Jolly and C. J. Hallada, Non-Aqueous Solvent Systems, T. C. Waddington, ed. (Academic Press, London, 1965), p. 1.

4. W. L. Jolly, J. Chem. Educ. 44, 304 (1967); J. Phys. Chem. 58, 250 (1954).
5. M. Herlem, Bull. Soc. Chim. France 1687 (1967).

b. Ammonium Ion Determination and Acid-Base Titrations in Liquid Ammonia Using a Glass Electrode*

Robert A. Shiurba and William L. Jolly

The glass membranes of ordinary pH-sensitive glass electrodes show essentially infinite resistance and consequently no detectable sensitivity toward ammonium ion concentration when used in cells having liquid ammonia solutions.[1] However, we have observed that a commercial cationic glass electrode,[2] sensitive in varying degrees to Na^+, H_3O^+, K^+, NH_4^+, Ag^+, and Li^+, can be used to follow ammonium ion concentration in liquid ammonia solutions.

In one series of measurements, the potential of a cell without liquid junction was determined as a function of the ammonium ion concentration. The cell may be represented as Ag, AgCl, 8 M HCl(aq), glass membrane, ammonia solution (varying molarity of NH_4Br; 0.001 M $AgNO_3$), Ag. The data are plotted in Fig. 1. The slope of the line drawn through the points in Fig. 1 corresponds to 50 mV per decade change in concentration, as compared with the value 48 mV per decade calculated from the Nernst equation.

In another series of measurements, the potential of a cell with liquid junction was followed as weighed amounts of ammonium bromide were added to solutions of potassium amide or suspensions of potassium hydroxide. The cell may be represented as Ag, AgCl, 8 M HCl (aq), glass membrane, ammonia solution (varying NH_4^+ concentration during "titration"), asbestos-plugged capillary junction, ammonia solution (0.001 M $AgNO_3$, ca. 0.2 M KNO_3), Ag. A plot of emf vs. weight of added ammonium bromide for a "titration" of a KOH suspension gave a sharp inflection point corresponding to the weight of potassium converted to KOH. A curve of essentially the same shape was obtained for the titration of a solution of potassium amide with ammonium bromide.

In view of the simplicity of the apparatus, the rapidity with which measurements can be made (electrode equilibrium was usually established within 20 sec), and the results described above, the use of cationic glass electrodes appears to be a promising method for measuring pH values in liquid ammonia. Clearly the method will facilitate end-point determination for acid-base titrations in ammonia. It is hoped that it will permit the determination of absolute pK values for acids in ammonia. It will be interesting to apply cationic glass electrodes to the determination of alkali metal ion concentrations (for example, in metal-ammonia solutions).

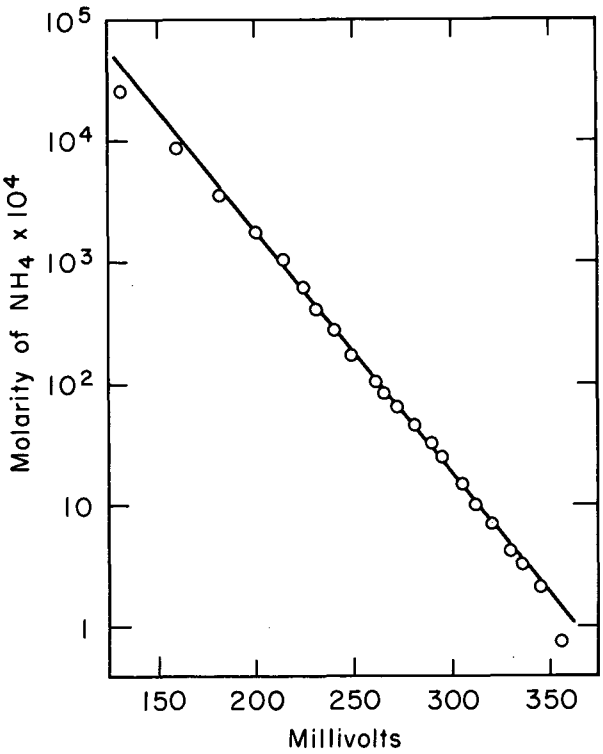

Fig. 1. Plot of logarithm of ammonium bromide concentration vs. millivolts.

*Abstracted from J. Am. Chem. Soc. 90, 5289 (1968).

1. A. H. A. Heyn and M. J. Bergin, J. Am. Chem. Soc. 75, 5120 (1953).
2. Beckman Instruments, Inc., Fullerton, Calif., Cationic Electrode No. 39137; see Beckman Bulletin 7017-a and Instructions 1154B.

c. Reactions of Atomic and Molecular Hydrogen with Liquid Ammonia Solutions

Kenneth Strom and William L. Jolly

Attempts to carry out the reaction

$$H + NH_2^- \rightarrow NH_3 + e^-_{am}$$

by bubbling atomic hydrogen through a solution of KNH_2 in liquid ammonia were unsuccessful, probably because, at the high pres-

sures required, no appreciable concentration of atomic hydrogen reached the ammonia solution from the electric discharge zone. However, by passing atomic hydrogen over frozen KNH_2-NH_3 solutions and over solid KNH_2, blue solids were obtained.

It is known[1] that molecular hydrogen reacts with amide-ammonia solutions to give the ammoniated electron:

$$1/2\ H_2 + NH_2^- \rightleftharpoons NH_3 + e^-_{am}.$$

Various solid catalysts for this reaction are known. We hope to reduce various oxidizing agents (ordinarily inert toward H_2) with molecular hydrogen by using this pre-equilibrium. Currently we are attempting the reduction of Cu(I) and Ag(I).

1. E. J. Kirschke and W. L. Jolly, Inorg. Chem. 6, 855 (1967).

6. PHOTOELECTRON SPECTROSCOPY

a. Nitrogen 1s Electron Binding Energies. Correlation with CNDO Charges*

Jack M. Hollander, David N. Hendrickson, and William L. Jolly

Recent developments in photoelectron spectroscopy have made possible the measurement of chemical shifts in inner-electron binding energies.[1] Binding energies for 1s electrons have been correlated with formal oxidation state in sulfur[1,2] and chlorine[1,3] compounds and with fractional atomic charge (calculated by a modification of Pauling's method[4]) in sulfur[1] and nitrogen compounds.[1,5] We have extended the group of nitrogen compounds for which nitrogen 1s binding energies have been measured and have shown that these binding energies are linearly related to nitrogen atomic charges calculated from CNDO molecular orbital eigenfunctions.[6]

The experimental binding energies and the CNDO-calculated nitrogen atom charges are plotted in Fig. 1. It will be noted that the points seem to fall on two lines—one characteristic of anions, and the other characteristic of neutral molecules and possibly cations (although insufficient data are available to show definitely that the cation points fall on the same line as the neutral molecules points). The observance of separate lines for anions and neutral species can be rationalized by the fact that anions in an ionic crystal lattice experience a greater positive lattice potential than neutral molecules in a molecular lattice. It may be that the separate lines are an artifact of the CNDO method for calculating atomic charges.

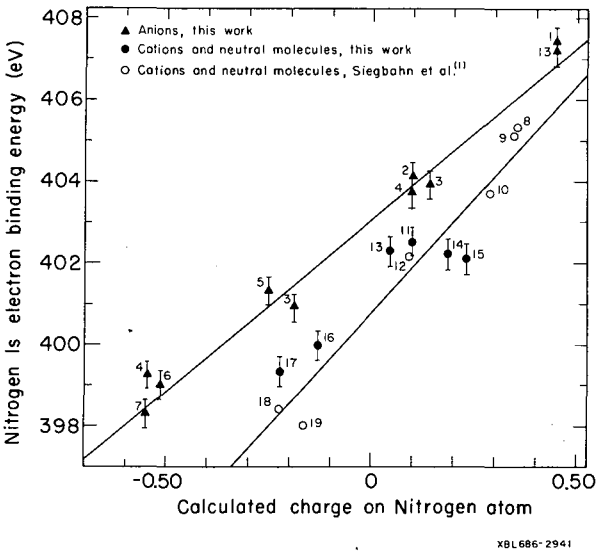

Fig. 1. Plot of nitrogen 1s binding energies vs. CNDO-calculated charges on nitrogen atoms.

A second feature of the plot is that all the data are reasonably well correlated; that is, there are no large discrepancies as were found in a previous attempt to correlate binding energies with charges calculated by Pauling's method.[1-5] Because of this better fit of the data, we conclude that the atomic charges calculated by the CNDO method are better approximations to the true charges than those calculated by Pauling's method. By combining a plot such as Fig. 1 with 1s binding energy data for compounds of uncertain structure it should be possible to estimate atomic charges and thus obtain useful structural information. Work along these lines is underway.

*Abstracted from J. Chem. Phys. 49, 3315 (1968).

1. K. Siegbahn, C. Nordling, A. Fahlman, R. Nordberg, K. Hamrin, J. Hedman, G. Johnasson, T. Bergmark, S.-E. Karlsson, I. Lindgren, and B. Lindberg, ESCA Atomic Molecular and Solid State Structure Studied by Means of Electron Spectroscopy (Almqvist and Wiksells AB, Stockholm, 1967).
2. A. Fahlman et al., Nature 210, 4 (1966).
3. A. Fahlman et al., Arkiv Kemi 25, 301 (1966).
4. L. Pauling, The Nature of the Chemical Bond, 34d. ed. (Cornell University Press, Ithaca, New York, 1960), p. 97.
5. R. Nordberg et al., Nature 214, 481 (1967).
6. J. A. Pople, D. P. Santry, and G. A.

Segal, J. Chem. Phys. 43, 5130 (1965). A modified CNDO/1 version involving empirically evaluated repulsion integrals was used, as per P. M. Kuznesof and D. F. Shriver, J. Am. Chem. Soc. 90, 1683 (1968).

b. Boron 1s and Phosphorus 2s and 2p Electron Binding Energies. Correlation with CNDO, EHMO, and Pauling Charges

David N. Hendrickson and William L. Jolly

Boron 1s binding energies have been measured for about 20 boron compounds. Good correlations of these binding energies with calculated atomic charges have been found for 7 compounds by using the CNDO method and for 11 compounds by using the EHMO (extended Hückel molecular orbital) method.

Phosphorus 2p (and some 2s) binding energies have been measured for about 50 phosphorus compounds. EMHO-calculated phosphorus charges have been found to correlate poorly with the phosphorus 2p binding energies for 25 compounds. Phosphorus atomic charges calculated by Pauling's method[1] with charge-independent atom electronegativities gave a similar poor correlation. A marked improvement in this later correlation was obtained by using the self-consistent Pauling method wherein the atom electronegativities are charge dependent. A similar improvement would be expected in the EHMO case if the calculation was made self-consistent with charge-dependent valence orbital ionization potentials.

1. L. Pauling, The Nature of the Chemical Bond, 3rd ed. (Cornell University Press, Ithaca, New York, 1960), p. 97.

7. NMR STUDIES

a. Proton Magnetic Resonance Spectrum of the Ruthenium (II) Pentammino Nitrogen Complex in Various Solvents

David N. Hendrickson and William L. Jolly

Proton magnetic resonance spectra have been obtained for solutions of $[Ru(NH_3)_5N_2](BF_4)_2$ dissolved in concentrated H_2SO_4, 66 wt % H_2SO_4, and formamide. The initial spectrum in each of the solvents consisted of two non-solvent peaks (-3.29 δ and -2.62 δ in conc. H_2SO_4) in the ratio of one to four, assignable to the trans and cis ammine protons, respectively. The appearance of new peaks in the sulfuric acid solution spectra indicated solvolytic reactions. The formamide solution spectrum remained unchanged for a period of two weeks.

The presence of the four-to-one p. m. r. pattern for this Ru(II) complex is to be compared with previous measurements in sulfuric acid showing similar spectra for Co(III) pentammines and only single resonances for the analogous Rh(III) and Ir(III) complexes.

b. Nitrogen NMR Chemical Shifts

David N. Hendrickson and Paul M. Kuznesof

Nitrogen-14 chemical shifts for NO_2^-, NO_3^-, NO_2^+, CN^-, N_3^-, and NH_4^+ ions have been calculated by an application of Pople's theory of chemical shifts[1] employing CNDO/1 molecular orbitals. Excited state eigenvectors and eigenvalues were obtained through a limited consideration of configuration interaction. The observed and calculated electronic spectra are given in Table I. For each ion the choice of ΔE, the average excitation energy for the magnetically allowed transitions, [1] was taken as a properly weighted average of the calculated eigenvalues for the lowest electronic states of proper symmetry.

The calculated and observed nitrogen chemical shifts also are listed in Table I. Only qualitative trends in the ^{14}N chemical shifts are obtained. The disparities may be attributed, at least in part, to differences in the effectiveness of the amount of configuration interaction considered for each ion. Also, it is clear that the selection of the ΔE values is very critical for a nitrogen chemical shift calculation for such a diversified series of ions.

1. M. Karplus and J. A. Pople, J. Chem. Phys. 38, 2803 (1963).

Table I. Electronic spectra and ^{14}N chemical shifts for some nitrogen ions.

Ion	Calculated electronic spectra		Observed[a] electronic spectra		^{14}N shielding constants and chemical shifts (ppm)		
	Energy (eV)	Oscillator strength	Energy (eV)	Oscillator strength	$-\sigma \times 10^6$	$\delta_{calc.}$	$\delta_{obs.}$[b]
NO_2^-	2.16($^1B_1$)	0.0024	3.50	0.0005			
	3.59($^1A_2$)	0	4.20	0.0004	1484	≡0	≡0
	4.91($^1B_2$)	0.038	5.95	0.20			
NO_3^-	4.39($^1E'$)	0.0054	4.10	0.0001			
	6.34($^1E'$)	0.25	6.26	0.15	1386	+98	+237
NO_2^+	7.92($^1\pi_u$)				1417	+67	+283
CN^-	5.69($^1\pi$)	0.013	3.92		534	+950	+380
N_3^- (inner)	8.61($^1\pi_u$)				1375	+109	+365
N_3^- (outer)	8.61($^1\pi_u$)				1038	+446	+514
NH_4^+	9.40($^1T_2$)				156	+1328	+592

a. References in K. McEwen, J. Chem. Phys. 34, 547 (1961).
b. References in M. Witanowski, J. Am. Chem. Soc. 90, 5683 (1968).

8. RESEARCH PLANS FOR CALENDAR YEAR 1969

William L. Jolly

Studies of the Hydrides of Groups IV and V

The preparation of compounds containing the GeH_3 group will continue. Such compounds are of interest because, by comparing them with the corresponding CH_3 compounds, we may obtain information about the ability of germanium to form double bonds and to use its empty d orbitals in bonding. Eventually we hope to prepare transition metal complexes of the GeH_3^- ion and of the isoelectronic hydrides, AsH_3 and PH_3. We hope to learn why it is that under certain conditions the GeH_3^- ion acts as a source of the hydride ion and under other conditions as a simple Lewis base. The stannyl halides (SnH_3X) will be characterized by physical methods such as infrared and mass spectrometry.

Boron Hydride Chemistry

We shall apply various physical chemical methods (e.g., kinetic studies, NMR, and possibly infrared and Raman spectroscopy) to the characterization of the intermediate species formed in the hydrolysis of boron hydride compounds in cold 8 M HCl. The reaction between diborane and water will be investigated by using a low-temperature infrared cell in order to determine the structure of the intermediates formed.

Studies in Liquid Ammonia

We plan to extend the kinetic study of the reaction of metal-ammonia solutions with urea to other protonic acids (for example, various substituted ureas) in order to correlate reactivity with acidity. The feasibility of using the electron electrode in ammonia as an analytical probe in such kinetic studies will be investigated. We shall use a cation-sensitive glass electrode to determine the activity of sodium ion in sodium-ammonia solutions; the data should be of particular interest in the concentrated region where unsolvated electrons become important. It is hoped that a cation-sensitive electrode system can be devised for measuring pH in liquid ammonia solutions; this would be useful for determining the pK values of weak acids.

Sulfur-Nitrogen Chemistry

A determination of the vapor pressure of $S_3N_3Cl_3(g)$ over $S_3N_3Cl_3(s)$ by a gas-flow saturation method will be completed. By com-

bining the results with data previously obtained from measurements of the equilibrium vapor pressure of NSCl(g) over $S_3N_3Cl_3$(s), we will be able to calculate thermodynamic data for the gaseous trimerization reaction.

We plan to determine the concentration of the radical formed by the dissolution of S_4N_4 in H_2SO_4 and to establish the composition of the radical by esr studies of ^{33}S-enriched S_4N_4.

9. 1968 PUBLICATIONS

William L. Jolly and Associates

Technical Journals

1. R. Dreyfuss and W. L. Jolly, The Disproportionation of Digermane in Liquid Ammonia, Inorg. Chem. 7, 2645 (1968).
2. J. Hollander, D. N. Hendrickson, and W. L. Jolly, Nitrogen 1s Electron Binding Energies. Correlation with CNDO Charges, J. Chem. Phys. 49, 3315 (1968).
3. W. L. Jolly, Recent Studies of Sulfur-Nitrogen Compounds, in The Chemistry of Sulfides, A. V. Tobolsky, ed. (Interscience Publishers, New York, 1968), pp. 3-7.
4. W. L. Jolly, editor, Preparative Inorganic Reactions, Vol. 4 (Interscience Publishers, New York, 1968).
5. W. L. Jolly, editor, Inorganic Syntheses, Vol. 11 (McGraw-Hill Book Company, New York, 1968).
6. W. L. Jolly and A. D. Norman, Hydrides of Groups IV and V, Prep. Inorg. Reactions 4, 1 (1968).
7. W. L. Jolly, σ-Methyl-π-Cyclopentadienylmolybdenum Tricarbonyl, Inorg. Syn. 11, 116 (1968).
8. W. L. Jolly, Bis(cyclopentadienyl) iron, Inorg. Syn. 11, 120 (1968).
9. W. L. Jolly and D. Chazan, Bis(cyclopentadienyl)nickel, Inorg. Syn. 11, 122 (1968).
10. W. L. Jolly, Methylphosphine, Inorg. Syn. 11, 124 (1968).
11. W. L. Jolly, Dimethylphosphine, Inorg. Syn. 11, 126 (1968).
12. W. L. Jolly and L. Prizant, The Reaction of Sodium with Urea in Liquid Ammonia: the Rate Constant of the Reaction of the Ammonium Ion with the Ammoniated Electron, Chem. Commun. 1345 (1968).
13. P. M. Kuznesof and W. L. Jolly, Potassium 2-Germaacetate, an Analog of Potassium Acetate, Inorg. Chem. 7, 2574 (1968).
14. A. D. Norman and W. L. Jolly, Diborane, Inorg. Syn. 11, 15 (1968).
15. A. D. Norman, J. Webster, and W. L. Jolly, Silane, Stannane, Silane-d_4, Germane-d_4, and Stannane-d_4, Inorg. Syn. 11, 170 (1968).
16. D. Rustad and W. L. Jolly, Potassium Germyltrihydroborate, Inorg. Chem. 7, 213 (1968).
17. R. A. Shiurba and W. L. Jolly, Ammonium Ion Determination and Acid-Base Titrations in Liquid Ammonia Using a Glass Electrode, J. Am. Chem. Soc. 90, 5289 (1968).
18. K. Wynne and W. L. Jolly, The Reactions of $Mo(CO)_6$ with $S_3N_3Cl_3$ and with S_4N_4, J. Inorg. Nucl. Chem. 30, 2851 (1968).

10. NUCLEAR MAGNETIC STUDY OF THE RATE OF WATER EXCHANGE FROM PARTIALLY COMPLEXED NICKEL ION

Kenneth Kustin* and Jack Vriesenga

The line width of the oxygen-17 nmr resonance of bulk water for solutions of various complexes of nickel was measured as a function of temperature. This type of data should yield information concerning the mechanism of oxygen-17 relaxation, the scalar coupling constant (A/h) between oxygen-17 nuclei and the unpaired electrons on the nickel, as well as the rate constant (k), enthalpy of activation ($\Delta H^{\ddagger}$) and the entropy of activation ($\Delta S^{\ddagger}$) for the water-exchange between the first coordination sphere of the complex and the bulk water.

Line width measurements from 0 to 100° were made on a solution 0.020 M in nickel perchlorate and 0.080 M in iminodiacetic acid (IDA) with the pH adjusted to 4.1. The water was enriched to approximately 10 at. % oxygen-17. The data could not be explained adequately in terms of a theory presupposing all the water molecules on the complex were exchanging at the same rate. The interpretation of the results was further clouded because three possible nickel species exist in equilibrium. These are the mono and bis IDA complexes, as well as free nickel. Since these equilibria are temperature dependent, the concentration of the mono IDA complex (the species of interest) is also temperature dependent. Attempts to estimate the concentration change as a function of temperature by using spectrophotometry indicate the change was less than 20% over the range investigated.

Attention was shifted to a simpler system, namely, the nitrilotriacetate (NTA) complex of nickel. This complex has the advantage that only one species is formed, and the equilibrium can be shifted almost completely in favor of this species, thereby establishing its concentration. Line widths of a solution 0.040 M in Ni^{2+} and 0.060 M in NTA at pH 4.1 were measured. The data clearly indicated that the two sites occupied by water on the complex were exchanging at different rates. Assuming

that the $\Delta\omega$ mechanism is the only relaxation mechanism, a non linear least-squares fit of the data yielded the following scalar coupling constants and reaction rate parameters at 25° for the rapid and slow exchanging sites respectively: $A/h = 2.9\times10^7$ Hz, $k = 1.0\times10^6$ sec^{-1}, $\Delta H^{\ddagger} = 12.2$ kcal/$mole^{-1}$, $\Delta S^{\ddagger} = 9.7$ eu, and $A/h = 3.1\times10^7$ Hz, $k = 3.0\times10^6$ sec^{-1}, $\Delta H^{\ddagger} = 10.6$ kcal/$mole^{-1}$, $\Delta S^{\ddagger} = -1.6$ eu.

An independent check of these parameters is being made by measuring the chemical shift of the oxygen-17 resonance of the bulk water as a function of temperature. These measurements should yield essentially the same information as the line width data and therefore will permit a more precise determination of the parameters.

*On a sabbatical leave from Brandeis University during academic year 1967-68.

11. STUDIES OF PROTON EXCHANGE FROM THE FIRST COORDINATION SPHERE OF CHROMIUM (III) SPECIES BY NUCLEAR MAGNETIC RESONANCE

Ronald T. Lee

The present study concerns the line-broadening of the proton resonance in aqueous solutions of hydrolyzed polymerized species of Cr(III), thought to be a dimer $[Cr_2(OH)_2(H_2O)_8^{4+}]$ and a trimer $[Cr_3(OH)_4(H_2O)_{10}^{5+}]$.

A temperature study of the trimer as a function of hydrogen-ion concentration was made from ~5 to ~60°. The line width is proportional to $[H^+]$ and increases with increasing temperature, indicating the exchange control region. At the lower temperatures the data also indicate appreciable effects in the second coordination sphere. Unfortunately the trimer decomposes at higher temperatures, which makes it impossible to enter the relaxation control region. The scalar contribution to the relaxation mechanism can be calculated if one has the scalar-coupling constant A/h and the correlation time--thought to be the longitudinal electronic relaxation time T_{1e}. Chemical shift measurements were carried out but have not yet been completed. Indications are that A/h will be close to the value for Cr^{3+} of 2.0×10^6 Hz. ESR experiments were attempted to obtain T_{2e}, and which give a lower limit to T_{1e} since $T_{1e} \geq T_{2e}$. Asymmetric non-Lorentzian lines were obtained which are attributed to decomposition to hexaquochromic ion and to the broad nature of the trimer lines. Further experiments will be done to verify these conclusions. Longitudinal relaxation times of the protons in this solution will also be measured in order to obtain the dipolar contribution to T_1, which will allow one to make an estimate of its contribution to T_2.

12. OXYGEN-17 NMR STUDIES OF WATERS IN THE FIRST COORDINATION SPHERE OF Mg^{2+} AND Ni^{2+}

James W. Neely

In the past the properties of metallic ions in aqueous solution have been studied extensively by the $H_2{}^{17}O$ NMR spectrum of the bulk waters,[1] the waters not directly bound to the metal ion. If the bound waters could be observed, much information could be obtained more easily. Also, additional information would be available. The difficulty in observing the bound waters is that only a fraction of the total water can ever be in the first coordination sphere, and in cases of interest the signals are exceedingly broad. Bound waters have been observed previously;[2] however, the application of this method was limited to ions with very slow exchange rates. Improved experimental techniques now allow a more general use of this method.

Thus far two systems have been studied in this manner. The first system was Mg^{2+}. Estimates of the water exchange rate constant at 25° have varied from 4×10^6 sec^{-1} to 1×10^5 sec^{-1}.[3] By observing the width of the ^{17}O NMR spectrum of the bound waters, a rate of ca. 6×10^5 sec^{-1} has been obtained with an enthalpy of activation of ca. 10 kcal/mole and an entropy of activation of ca. zero entropy units.

The second system thus far studied was Ni^{2+}. The bound waters on Ni^{2+} have been seen previously.[4] Improved experimental techniques now make it possible to get a much more accurate determination of the line width; a significantly narrower line has been obtained than was reported previously. From this line width it is possible to calculate the longitudinal relaxation time of the paramagnetic electrons on the Ni^{2+}. This value is too small to be measured directly by EPR. The T_{1e} has been calculated to be about 10^{-12} sec at 29° and 1.4×10^4 gauss assuming $T_{1e} = T_{2e}$. It is hoped that a future study of the line width as a function of temperature will give some idea as to the temperature dependence of T_{1e}.

1. Swift and Connick, J. Chem. Phys. 37, 307 (1962).

2. Connick and Fiat, J. Chem. Phys. 39, 1349 (1963).
3. Atkinson, J. Chem. Phys. 70, 3122 (1966), and Wawro and Swift, J. Am. Chem. Soc. 90, 2792 (1968).
4. Connick and Fiat, J. Chem. Phys. 44, 4103 (1966).

13. SECOND COORDINATION SPHERE PROPERTIES OF HYDRATED Cr^{3+} MEASURED BY NMR RELAXATION TIMES

William L. Earl

In recent studies of proton and oxygen-17 NMR transverse relaxation times in solutions of paramagnetic metal ions in methanol, dimethyl formanide, and water low temperature contributions to the line width have been ascribed to relaxation of solvent molecules outside the first coordination sphere.[1-4] Connick and Stover[5] measured the oxygen-17 NMR line width of the bulk waters in a solution of $Cr(ClO_4)_3$ and found that it is significantly broader than that of pure water. Through isotopic dilution studies, Hunt and Taube[6] earlier showed that the half-life for water exchange from the first coordination sphere of chromic ion is on the order of 40 hours at room temperature. Therefore, the relaxation measured by Connick and Stover must be due to second coordination sphere waters. Further, Alei has measured the chemical shift of the bulk water in a series of Cr^{3+} solutions in water.[7]

In order to study systematically the second coordination sphere effects on oxygen-17 relaxation in water solutions of paramagnetic metal ions, $[Cr(H_2O)_6]^{3+}$ was chosen. A temperature study of the ^{17}O relaxation in a 1.06 mm $Cr(ClO_4)_3$ solution in 1.73 mm $HClO_4$ has been made. The data, when plotted as log T_{2p} vs. $10^3/T$ give the expected straight line within experimental error. Using these data, two separate calculations have been done. First it was assumed that the relaxation was due entirely to scalar coupling and using Alei's data to calculate a scalar coupling constant and McCain's value for T_{1e},[8] a mean lifetime for water in the second coordination sphere of 3.0×10^{-10} sec was found necessary. In the second calculation it was assumed that the relaxation was due entirely to dipole-dipole coupling with a Cr^{3+} distance of 3.43 Å (calculated by assuming that second coordination sphere waters were on the faces of the octahedron). This calculation gave the correlation time for the dipole coupling as 5.6×10^{-10} sec. Since it is difficult to estimate the rotational correlation time, this result cannot be checked easily. The analogous calculation for quadrupole relaxation is complicated by rotation of the waters and cannot be reported at this time.

A measurement of T_1 as a function of temperature by sideband saturation techniques has been started. From the difference between T_1 and T_2 we expect to calculate the scalar coupling contribution to T_2. If the scalar coupling contribution is important, it should be possible to calculate the lifetime of water in the second coordination sphere of Cr^{3+}.

1. Z. Juz and S. Melboom, J. Chem. Phys. 40, 2686 (1964).
2. J. C. Sheppard and J. L. Burdett, Inorg. Chem. 5, 921 (1966).
3. J. S. Babiec, Jr., C. H. Langford, and T. R. Stengle, Inorg. Chem. 5, 1362 (1966).
4. K. Wuthrich and R. E. Connick, Inorg. Chem. 6, 583 (1967).
5. D. Stover and R. E. Connick, J. Phys. Chem. 65, 2075 (1961).
6. J. P. Hunt and J. Taube, J. Chem. Phys. 18, 757 (1950).
7. M. Alei, Jr., Inorg. Chem. 3, 44 (1964).
8. D. C. McCain, Thesis, UCRL-17064 (1966).

14. ^{17}O NMR STUDIES OF Ti^{3+} SOLUTIONS

Hubert Charles

The transverse relaxation of ^{17}O of the bulk waters has now been studied as a function of temperature and frequency. The results indicate that the relaxation controlled region is dominated by $\Delta\omega$ relaxation but that there is an appreciable contribution from the transverse relaxation of the oxygens when they are in the first coordination sphere of the titanium.

An attempt will be made to observe directly the resonance of the oxygens of the first coordination sphere waters.

15. RESEARCH PLANS FOR CALENDAR YEAR 1969

Robert E. Connick

The very promising studies started on partially complexed nickel ion will be extended to other ligands. Nuclear magnetic resonance work is providing more detail than is readily available by other methods. Results of these studies should contribute generally to our understanding of substitution reactions on metal ions. The work will have to be stopped in August when the funds now being used for Dr. Vriesinga run out.

Improvements in the detection of very broad resonances, as with Mg^{2+}, make it possible to study exchange rates of diamagnetic species up to 10^6 sec^{-1} in favorable cases. Other systems will be investigated.

The work on properties of water in the second coordination sphere of highly charged cations has just begun with the preliminary results on chromic ion. It is hoped that other promising systems can be studied.

The work on titanium (III) will be completed.

The studies of proton exchange on chromium (III) species has turned out to be more complex than anticipated. The work will be pursued as far as feasible.

It is hoped that the NMR measurements on the vanadyl system can be undertaken to yield the longitudinal relaxation time of the electronic system.

Dr. George Johannson of the Royal Institute of Technology in Stockholm is spending five months in our laboratory to familiarize himself with NMR techniques in the study of hydrolytic polymers of cations in aqueous solutions. He will undertake studies of the aluminum system.

16. 1968 PUBLICATIONS

Robert E. Connick and Associates

Technical Journals

1. D. Fiat and R. E. Connick, Oxygen-17 Magnetic Resonance Studies of Ion Solvation. The Hydration of Aluminum (III) and Gallium (III) Ions, J. Am. Chem. Soc. 90, 608 (1968).
2. K. Wüthrich and R. E. Connick, Nuclear Magnetic Resonance Studies of the Coordination of Vanadyl Complexes in Solution and the Rate of Elimination of Coordinated Water Molecules, Inorg. Chem. 7, 1377 (1968).

B. CHEMICAL THERMODYNAMICS

1. SPECTROSCOPIC INVESTIGATIONS OF HIGH-TEMPERATURE SPECIES TRAPPED AT LOW TEMPERATURES IN INERT MATRICES

Baldwin A. King*

Copper atoms have been trapped in Kr and Xe; Ag atoms in Ar, Kr, and Xe; and Au atoms in Kr, Xe, and SF_6 at 20°K. The transitions np $^2P \leftarrow$ ns ^2S were studied in absorption; the shifts from the positions of the gaseous spectral lines can be described in terms of a blue shift due to compression of the upper state by the matrix and a red shift increasing with polarizability of the matrix from Ar to Xe. The net shift was to the blue except for Au in Xe. Three strong bands are observed in all cases except for Au in SF_6, which gives two bands. The observation of three bands compared with two gaseous lines is ascribed to matrix splitting of the $^2P_{3/2}$ state.

To test the hypothesis that the splittings and shifts could be due to long range solute-solute interaction rather than interaction with matrix, the two pairs Ag and Au and Cu and Au were codeposited with Kr. The resulting Ag, Cu, and Au spectra were unchanged from their spectra when deposited individually with Kr, thus excluding solute-solute interactions as the cause of the splittings or shifts.

*Present address: E. I. du Pont de Nemours, Parlin, New Jersey.

2. INORGANIC SYNTHESES IN LOW TEMPERATURE MATRICES, NONAQUEOUS SOLVENTS, AND COCONDENSATION SYSTEMS

John Ling-Fai Wang, David Solan, Chin-An Chang, and Baldwin A. King*

Attempts have been made to synthesize diatomic MgO in rare gas matrices by simultaneous trapping of magnesium and oxygen atoms. Upon warming the matrix to allow diffusion of the oxygen atoms, the magnesium line spectrum has disappeared and a banded spectrum has appeared. However, the banded spectrum appears to be due to O_3 formed by the reaction of oxygen atoms with O_2 which is also present. It is hoped that the O_2 content can be minimized so that the ozone spectrum will not obscure the MgO spectrum.

It is also hoped that fluorinated hydrocarbons and other fluorinated compounds can be used as matrices for isolation of high temperature molecules. Such matrices offer the possibility of condensation at liquid nitrogen temperatures instead of liquid hydrogen temperatures and also offer the possibility of determining if the observed splittings of atomic lines are due to Stark splitting by varying the polarity of the matrix molecules. SF_6 was found to be a suitable matrix for Au, but Cu and Ag gave complex spectra which may be due to reactions to form CuF and AgF. SF_6 was passed through alkali metal solutions in liquid NH_3 to determine the behavior of SF_6 under reducing conditions. Reduction appears to take place to form alkali fluorides and sulfides. The spectrum of Au cocondensed with n-perfluor-heptane was surprisingly complex. It has not been determined whether the complexity is due to reaction or to strong coupling of the electronic transition of Au with vibrations of the matrix.

Further investigations of the phosphorus-fluorine high temperature system have been carried out. The cracking of P_2F_4 had been previously shown to yield PF_2 radicals, using mass spectroscopy. These radicals will react on a cold surface to form the unstable liquid $P(PF_2)_3$, whose formula has been confirmed via fluorine and phosphorus NMR spectroscopy. Matrix isolation infrared spectroscopy of PF_2 has given the frequencies of its three fundamentals, which, when extrapolated to gas phase values, are: ν_1 = 850K, ν_2 = 323K, ν_3 = 830K. From these values and other data the force constants and thermodynamic data for PF_2 have been determined. It is found not to be an important equilibrium species at the temperature of its formation from P_2F_4 (800°). The photolysis of P_2F_4 isolated in a rare gas matrix produces PF_3 and another species whose infrared spectrum has been obtained. This spectrum does not agree with the molecular constants of gas phase PF as determined by Douglas and Frackowiak.[1] Ultraviolet absorption and fluorescence studies in the matrix are contemplated to elucidate the nature of this new species.

Various cocondensation reactions were attempted with the PF_2 radical, which reacts readily with hydrogen-containing species (probably through hydrogen abstraction to form PHF_2). GeH_4 yielded many new non-polymeric

compounds, none of which have been analyzed as yet.

*Present address: E. I. du Pont de Nemours, Parlin, New Jersey.

1. A. E. Douglas and M. Frackowiak, Can. J. Phys. 40, 832 (1962).

3. THERMODYNAMIC COMPILATIONS

Gerd Rosenblatt* and Norman Lofgren†

The thermodynamic properties of the gaseous diatomic oxides of the elements have been reviewed and tabulated in a comprehensive paper that will be published in 1969. Enthalpies of sublimation of the elements and enthalpies of formation of the solid oxides have been combined with high temperature spectroscopic and equilibria data to obtain dissociation enthalpies and enthalpies of formation of the diatomic oxides, and free energy functions have been tabulated from 298 to 3000°K.

Work is continuing slowly on the compilation of thermodynamic properties of compounds of molybdenum.

*Present address: Department of Chemistry, University of Pennsylvania, College Park, Pa.
†Present address: Department of Chemistry Chico State College, Chico, Calif.

4. TRANSITION-METAL ALLOY SYSTEMS

Paul Wengert and James Roberts

Activity coefficients of Zr in noble metals have been determined by measuring the concentration of Zr in equilibrium with ZrC and graphite. The results show that the activity coefficient of Zr drops to a very low value in Pd, Pt, Rh, and Ir and rises again in Ru and Os in confirmation of the expectations of the Engel theory of metals. Only an upper limit could be set for metals of the ninth and tenth group metals, but it appears that the activity coefficient of dilute Zr solutions in ninth and tenth group metals may be as low as 10^{-17} at 1000°K.

The extreme stability of intermetallic compounds of third and fourth group transition metals with ninth and tenth group metals of the second and third transition series offers interesting possibilities for high temperature separation processes. Preliminary studies indicate high oxidation resistance for some of these intermetallic compounds.

5. RADIATIVE LIFETIME AND PREDISSOCIATION MEASUREMENTS FOR I_2 AND RECOMBINATION STUDIES

Joel Tellinghuisen, Shih-Ger Chang, Paul T. Cunningham,* and Karl Wieland†

The previously reported variation of lifetime with vibrational state of upper electronic state has been repeated with different equipment and with different frequencies in the phase shift apparatus. Somewhat different results have been obtained for some vibrational levels, but there is still considerable variation in lifetime as a function of vibrational level. In addition, a variation of lifetime with frequency of modulation has been found for some levels. It appears that the frequency dispersion is due to excitation of adjoining vibrational levels with different lifetimes. The I_2 fluorescence, which had previously been considered to be rather simple, seems to be quite complex.

Clear evidence of predissociation competing with fluorescence has been found through observation of ultraviolet iodine atomic fluorescence as a function of I_2 excitation in the red. Studies of the predissociation and of the atomic recombination are continuing.

The ultraviolet spectra of I_2 have been examined for two isotopes of iodine and previous analyses have been shown to be in error. A new analysis is in progress.

*Present address: Argonne National Laboratory, Argonne, Illinois.
†Visiting scientist, Fall 1968. Permanent address: Physikalisches Institut der Universitat Basel, Switzerland.

6. SPECTRA OF HIGH TEMPERATURE MOLECULES

Helen Johansen, Shih-Ger Chang, and Willis Callins

The analysis of rotational perturbations by using isotopic shifts in an effort to fix the energies of the low lying electronic states of diatomic molecules is in progress using the CaO spectrum.

The spectrum of TiO is being examined from the point of view of fixing low lying electronic states and with respect to the possibility of fixing the dissociation energy through observation of a predissociation or a dissociation limit in the ultraviolet. An alternative route to the determination of the dissociation energy, which is in dispute, is the determina-

11. MAGNETIC BEHAVIOR OF PLUTONIUM AT LOW TEMPERATURES

Warren Henry*

Magnetic measurements were made on plutonium metal encapsulated in aluminum from 300°K to below the lambda point of liquid helium in magnetic fields up to 93,000 G. Typical magnetization values in 90,000 G fields were 0.005 Bohr magnetons per atom of Pu at room temperature, 0.04 Bohr magnetons at temperatures between liquid nitrogen and liquid hydrogen temperatures, and down to 0.01 Bohr magnetons per atom of Pu at the lambda point of liquid helium. Time effects were evident as if a phase transformation were taking place. The anomalous magnetic behavior of plutonium is somewhat suggestive of the metamagnetism exhibited by $Mn_{2-x}SbCr_x$.

*Visiting scientist, Howard University and Lockheed Missiles and Space Company.

12. RESEARCH PLANS FOR CALENDAR YEAR 1969

Leo Brewer

Spectroscopic Studies of High Temperature Species in Low Temperature Matrices and Inorganic Syntheses in Low Temperature Matrices

Work will continue on the attempt to observe the spectra of MgO, CaO, and SrO diatomic molecules synthesized in low temperature matrices through reaction of metal atoms with atomic oxygen. The matrix materials will be extended to high boiling materials and more polar materials to characterize the nature of the interaction of the solutes with the matrix. A wider range of concentrations of metal atoms in inert matrices will be studied to characterize the behavior of metal atoms at high concentrations.

The work on the reactions of PF and PF_2 and the characterization of cocondensation products should be completed this year.

Radiative Lifetime and Predissociation Measurements for I_2

The characterization of the energy transfer processes upon excitation of I_2 in the red and in the ultraviolet should be completed this year.

Pseudopotential Calculations for Atomic and Diatomic Molecules

This program should be completed during this year.

Alkaline Earth and TiO Spectra

This program will be carried on actively with respect to use of rotational perturbations, analysis of new band systems, and determination of thermodynamic properties.

Transition-Metal Alloy Systems

Due to budgetary restrictions, this program will be combined with the superconductivity program. The types of studies that were carried out here during the last year will probably be taken over at Oak Ridge.

Compilations

It is hoped that progress will be made on the compilation of thermodynamic properties of compounds of molybdenum.

13. 1968 PUBLICATIONS

Leo Brewer and Associates

Technical Journals

1. L. Brewer, Bibliography of the High Temperature Chemistry and Physics of Gases and Gas-Condensed Phase Reactions (International Union of Pure and Applied Chemistry, Commission of High Temperature and Refractories), Nos. 26-29 (1968).
2. L. Bajema, M. Gouterman, B. Meyer, Spectra of Porphyrins, Part XI, J. Mol. Spec. 27, 225 (1968).
3. L. Brewer and R. Hauge, Near Infrared Bands of Diatomic CaO and SrO, J. Mol. Spec. 27, 330-9 (1968).
4. L. Brewer, Bonding and Structures of Transition Metals, Science 161, 115 (1968).
5. B. Meyer, L. F. Phillips, and J. J. Smith, Temperature Dependence of Intersystem Crossing: Lifetime and Intensity of SO_2 Phosphorescence in Low-Temperature Solids, Proc. Natl. Acad. Sciences 61, 7 (1968).
6. J. J. Smith and B. Meyer, The Absorption and Fluorescence Spectrum of SnS and SnO: Matrix-Induced Intersystem Crossing, J. Mol. Spec. 27, 304 (1968).
7. P. Cunningham, Lifetime Measurements of the $4s^2S_{1/2}$ and $3d^2D$ State of Aluminum by the Phase-Shift Method, J. Opt. Soc. Am. 58, 1507 (1968).
8. L. Brewer, B. King, J. L. Wang, B. Meyer, and G. F. Moore, Absorption Spectrum of Silver Atoms in Solid Argon, Krypton and Xenon, J. Chem. Phys. 49, 5209 (1968).

tion of the radiative lifetime along with the determination of the TiO absorption in a high temperature equilibrium system. Experiments are in progress to determine the most promising route.

7. THE PHOTOLYSIS OF MATRIX ISOLATED DISULFUR DICHLORIDE

Jerry J. Smith* and Beat Meyer*

S_2Cl_2 was photolyzed in various inert matrices at 20°K for the purpose of identifying the primary photolysis products and studying the nature of the disulfide bond. UV and IR spectroscopy were used to determine the products in Ar, Kr, Xe, CH_4, CO, and N_2. In each case, S_2 was found to be formed. The S_2 yield depends on the rigidity of the matrix. CO and N_2 are shown to yield third products. Solute-solute and solute-solvent interactions are excluded from being responsible for the observed results. A plausible mechanism based on the diffusion of photolysis fragments is discussed.

*Visiting scientists during summer 1968; permanent address: University of Washington, Seattle, Washington.

8. THE ABSORPTION AND FLUORESCENT SPECTRUM OF SnS AND SnO: MATRIX-INDUCED INTERSYSTEM CROSSING

Jerry J. Smith* and Beat Meyer*

The spectrum of SnS and SnO was studied in the 14000 to 50000 cm^{-1} region in argon, krypton, and xenon matrices at 20°K. The $D^1\Pi$-$X^1\Sigma$ absorption system is reported. All SnO spectra show a vibrational band to the red of the earlier reported (0, 0) band. This suggests that the numbering should be corrected to yield a new T_0 = 28,923 cm^{-1}. Excitation of the D state of both molecules leads to strong red fluorescence but not to the resonance fluorescence observed in the gas phase. The red fluorescence is attributed to the transition α-X where α is believed to be $^3\Pi$. The fluorescence results from matrix induced intersystem crossing, a process which is unusual in diatomic molecules. Absorption and fluorescence matrix shifts of T_0 and ω_0 are consistent with the heavy atom effect.

*Visiting scientists during summer 1968; permanent address: University of Washington, Seattle, Washington.

9. TEMPERATURE DEPENDENCE OF INTERSYSTEM CROSSING: LIFETIME AND INTENSITY OF SO_2 PHOSPHORESCENCE IN LOW TEMPERATURE SOLIDS

Beat Meyer,* Leon F. Phillips,† and Jerry J. Smith*

We observed large temperature-dependent changes in intensity of SO_2 phosphorescence in weakly interacting, low temperature, solid solutions, accompanied by small changes in the radiative lifetime. We concluded that the rate of $S_1 \rightarrow T_1$ intersystem crossing, relative to the rates of fluorescence and internal conversion, is a strong function of temperature. The rate of quenching from T_1 to S_0 shows only a small temperature dependence.

*Visiting scientists during summer 1968; permanent address: University of Washington, Seattle, Washington.
†Visiting scientist, 1968; permanent address: University of Canterbury, Christchurch, New Zealand.

10. SPECTRA OF PORPHYRINS: ABSORPTION AND FLUORESCENT SPECTRA OF MATRIX ISOLATED PHTHALOCYANINES

Larry Bajema,* Martin Gouterman,* and Beat Meyer*

Absorption and fluorescence spectra of free base and zinc phthalocyanines (H_2Pc and ZnPc) were studied in matrices of Ar, Kr, Xe, CH_4, N_2, and SF_6 at liquid hydrogen temperature. ZnPc was also studied in CO. The spectra show considerable fine structure whose resolution decreases along the series $Ar > CH_4 \gtrsim Kr > Xe > N_2 \gtrsim SF_6 > CO$. Only part of the fine structure seen in absorption appears in emission. Provisionally we view the spectrum as made up of a broad band arising from phonon exchange with the lattice and non-phonon lines arising from distinct sets of molecules. However, the lack of apparent correspondence between the line structure of the two Q bands of H_2Pc remains unexplained.

*Visiting scientists during summer 1968; permanent address: University of Washington, Seattle, Washington.

UCRL Reports

1. L. Brewer and D. Green, The Low Lying Electronic States of Scandium Monofluoride, UCRL-18474, September 1968.
2. J. G. Conway, B. Meyer, J. J. Smith, and L. J. Williamson, Zeeman Effect on Phosphorescent Lifetime of Matrix Isolated SO_2, UCRL-18657, December 1968.
3. P. Cunningham, Measurement of Lifetimes by the Phase-Shift Method. I. Radiative Lifetimes of Some Excited Atomic States. II. Lifetimes of Some v' Regions of the $B^3\Pi_{0^+}v$ State of I_2 (Ph. D. Thesis), UCRL-18419, University of California, Berkeley, November 1968.
4. D. Green, Molecular Beam Studies of Scandium Monofluoride (Ph. D. Thesis, I), UCRL-17961, University of California, Berkeley, January 1968.
5. D. Green, Arc Spectrum of Magnesium Oxide (Ph. D. Thesis, II), UCRL-17878 Rev., University of California, Berkeley, March 1968.
6. B. King, Optical Absorption Spectra of Matrix-Isolated Copper, Silver and Gold (Ph. D. Thesis), UCRL-18618, University of California, Berkeley, November 1968.
7. L. Phillips, Dissociation Energies from Inverse Predissociation, UCRL-18180, April 1968.
8. J. J. Smith and B. Meyer, Temperature Dependence of Quantum Yield and Lifetime of Phosphorescence of Matrix Isolated SO_2, UCRL-18247, May 1968.
9. J. J. Smith and B. Meyer, The Photolysis of Matrix Isolated Disulfur Dichloride, UCRL-10860, July 1968.
10. J. J. Smith and B. Meyer, Temperature Dependence of Quantum Yield and Lifetime of Phosphorescence of Matrix Isolated SO_2, UCRL-18247 Rev., July 1968.
11. T. S. Wauchop and L. F. Phillips, Luminescent Reactions of $H(^2P)$, UCRL-18302, July 1968.

C. SOLID STATE CHEMISTRY AND PHYSICS

1. LOW TEMPERATURE HEAT CAPACITIES OF DILUTE SOLUTIONS OF Fe

John C. F. Brock,* James C. Ho,† Gary P. Schwartz, and Norman E. Phillips

Most measurements of the heat capacities of dilute magnetic alloys have been interpreted in terms of the indirect (via the conduction electrons) exchange interaction between the magnetic ions. Overhauser[1] and Marshall[2] have derived, from somewhat different models, similar expressions for the low temperature heat capacity that predict a concentration-independent term proportional to temperature. Measurements on dilute Fe in Cu by Franck, Manchester, and Martin[3] above 0.4°K did not show this behavior but it was possible to extrapolate the data to 0°K in a way consistent with the predictions. More recently, experimental and theoretical evidence for the existence of a low-temperature spin-compensated state for isolated localized moments has been obtained,[4] and expressions predicting concentration-proportional heat capacities varying (at temperatures well below the Kondo temperature, T_K) as T,[5,6] T ln T,[7] and $T^{1/2}$,[8] have been derived. Separation of the two heat capacity contributions (arising from interactions between magnetic ions and from the thermal break-up of the spin-compensated state) therefore require measurements over a wide range of concentrations. We have recently made some new measurements on dilute solutions of Fe in Cu that cover concentration regions in which each contribution is expected to dominate the heat capacity. Heat capacity measurements have made on 0.070, 0.13, 0.18, and 0.27 at. % samples between ~ 0.60 and 1°K, and on a 0.01 at. % sample between 0.3 and 20°K. The results are shown in Fig. 1. At the lowest temperatures a small T^{-2} term, approximately proportional to concentration, is observed. For the 0.07 to 0.27 at. % samples, subtraction of the T^{-2} term leaves a well-defined linear term extending to about 0.11°K for the 0.07 at. % sample, and to higher temperatures for the others, in qualitative agreement with the extrapolations made by Franck et al.[3] The linear term however is not concentration independent, but increases by about 40% as the concentration increases from 0.07 to 0.27 at. % . This trend is similar to, but larger in magnitude than, that observed by Hill and Pickett[9] at higher temperatures and concentrations. The decrease in the linear term with decreasing concentration may itself be a consequence of the occurrence of the spin compensated state, since the formation of this state, in the more dilute solutions, can be expected to reduce the interactions between the localized moments. At the higher temperatures and lower concentrations the heat capacity in excess of that of pure copper becomes more nearly proportional to concentration (see Fig. 2, as suggested by the earlier work.[3] The 0.010 at. % sample does not appear to show the low-temperature rise in C/T associated with the "concentration-independent" interaction term, and the results for this sample may correspond to the concentration-proportional limit expected for the spin-compensated state. Further experiments are necessary to establish this definitely, but it is already clear that in this limit C varies more rapidly than $T^{1/2}$, and may in fact be proportional to T or to T ln T.

Daybell et al.,[10] have recently reported measurements between 0.04 and 1°K on 0.011 and 0.038 at. % samples, and interpret the results as showing a $T^{1/2}$ heat capacity for the spin-compensated state throughout this range. The 0.010 at. % results reported here are more precise by a factor of 5 than their 0.011 at. % results at comparable temperatures and, although they agree in magnitude, show that between 0.3 and 1°K, C is varying much more nearly as T. Furthermore, the marked deviations from proportionality to concentration found in this work strongly suggest that the low temperature upturn in C/T reported by Daybell et al., is associated with interactions between the Fe ions.

---

*Present address: University of the Witwatersrand, Johannesburg, South Africa.

†Present address: Battelle Memorial Institute, Columbus, Ohio.

1. A. W. Overhauser, Phys. Rev. Letters 3, 414 (1959); J. Phys. Chem. Solids 13, 71 (1960).
2. W. Marshall, Phys. Rev. 118, 1519 (1960)
3. J. P. Franck, F. D. Manchester, and D. L. Martin, Proc. Roy. Soc. A 263, 494 (1961).
4. M. S. Daybell and W. A. Steyert, Rev. Mod. Phys. 40, 380 (1968), have recently reviewed the work on the spin-compensated state and give references to the original publications.
5. Y. Nagaoka, Phys. Rev. 138, A 1112 (1965).

6. A. P. Klein, Phys. Letters 26A, 57 (1967).
7. J. A. Appelbaum and J. Kondo, Phys. Rev. Letters 19, 906 (1967).
8. P. E. Bloomfield and D. R. Hamann, Phys. Rev. 164, 856 (1967).
9. R. W. Hill and G. R. Pickett, Proceedings of the 10th International Conference on Low Temperature Physics, Moscow, 1966.
10. M. D. Daybell, W. F. Pratt, Jr., and W. A. Steyert, Phys. Rev. Letters 21, 353 (1968).

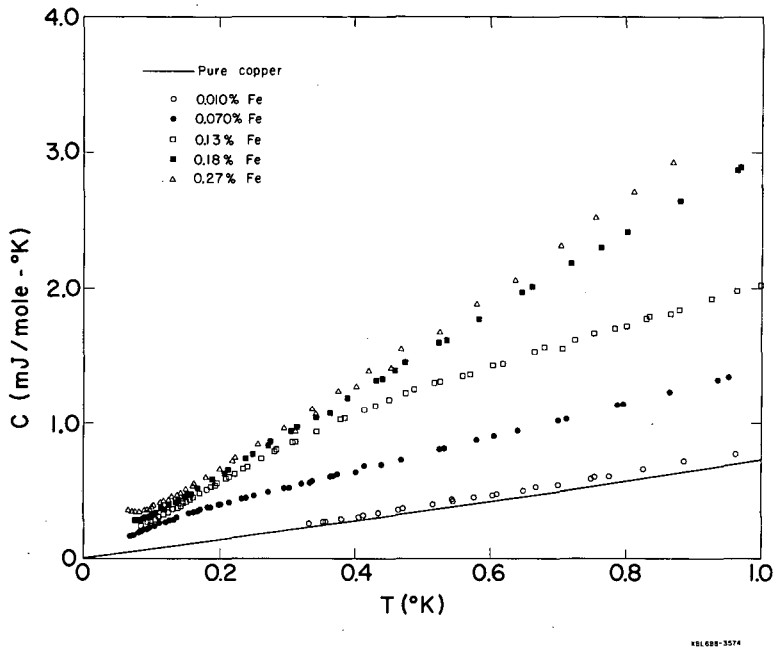

Fig. 1. The low-temperature heat capacities of dilute solutions of Fe in Cu.

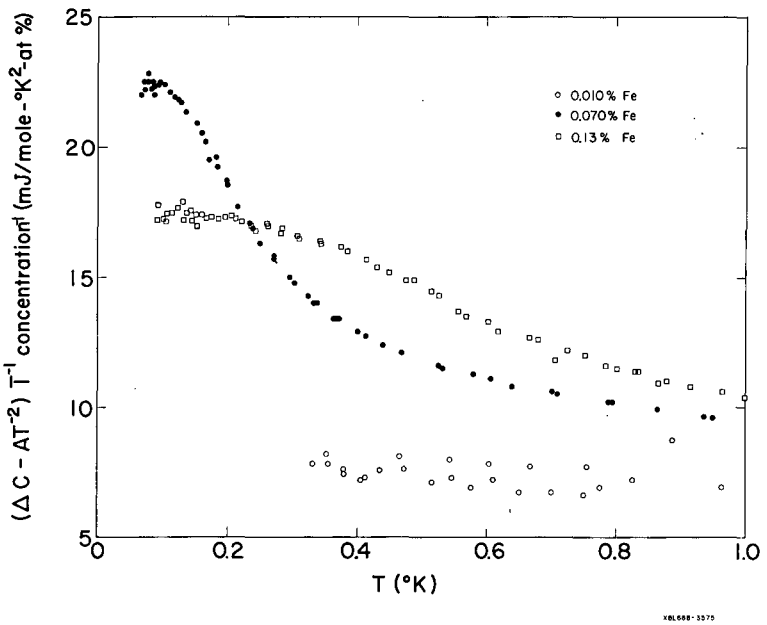

Fig. 2. The excess heat capacities of the dilute solutions (over that of pure copper) divided by T and by concentration.

2. LOW TEMPERATURE HEAT CAPACITY OF Ni-Rh ALLOYS

Baylor B. Triplett and Norman E. Phillips

The heat capacities of two Ni-Rh alloys with compositions near the critical concentration for the occurrence of ferromagnetism have been measured between 0.05 and 4°K. The temperature dependence is consistent with the theory for spin-fluctuation mass enhancement, but it is also possible that magnetic clusters are contributing to the observed heat capacity anomaly.

3. TEMPERATURE SCALE BETWEEN 0.25 AND 25°K

Mary M. Conway, Charles G. Waterfield, and Norman E. Phillips

An improved apparatus for calibrating thermometers, incorporating a gas thermometer, He^4 vapor pressure thermometer, and a magnetic thermometer has been constructed and initial experiments carried out.

4. RESEARCH PLANS FOR CALENDAR YEAR 1969

Norman E. Phillips

Dilute Alloys and Weakly Magnetic Materials

Further heat capacity measurements in these areas are planned. The Cu-Fe measurements will be extended to higher temperatures and other systems exhibiting the Kondo effect may be investigated. Recent developments suggest that the Ni-Rh system is not a simple example of a system showing spin fluctuation effects and our attention will probably be transferred to a different system.

Pressure Dependence of Electronic Heat Capacity of Lanthanide and Actinide Metals

Experiments in this area have been delayed by the failure of the calibrated germanium thermometer on the high pressure cell. This has necessitated the calibration of new thermometers (now completed) and the remeasurement of the heat capacity of the empty cell.

5. 1968 PUBLICATIONS

Technical Journals

1. B. J. Alder, W. R. Gardner, J. K. Hoffer, W. E. Phillips, and D. A. Young, Instability Modes Prior to Melting, Phys. Rev. Letters 21, 11 (1968).
2. L. Finegold, Determination of Mass of Large Gas Volumes by Direct Weighing, Rev. Sci. Instr. 44, 789 (1967).
3. J. K. Hoffer, C. G. Waterfield, W. R. Gardner, and N. E. Phillips, Phase Diagram of ^{4}He Below 1.2°K, Phys. Letters 27A, 1 (1968).
4. N. E. Phillips, J. C. Ho, and T. F. Smith, Heat Capacity of α-Cerium at a Pressure of 11 Kbar, Between 0.3 and 6°K, Phys. Letters 27A, 1 (1968).
5. N. E. Phillips, He^3-He^4 Solutions, Ann. Rev. of Phys. Chem. 19, 1968.
6. N. E. Phillips, J. C. Ho, and T. F. Smith, Calorimetric Investigation of Superconductivity in Alpha-Uranium, Proceedings of the 10th International Conference on Low Temperature Physics, Moscow, USSR, 1967, Vol. 2b, p. 189.

UCRL Reports

1. J. Brock, J. Ho, G. P. Schwartz, and N. Phillips, Low Temperature Heat Capacities of Dilute Solutions of Fe in Cu, UCRL-18385, October 1968.
2. L. Finegold and N. E. Phillips, The Low Temperature Heat Capacities of Solid Argon and Kyrpton, UCRL-18409, September 1968.
3. J. K. Hoffer, The Thermodynamic Properties of He^4 Near the Melting Line (Ph. D. Thesis), UCRL-18409, August 1968.
4. J. Hoffer, N. Gardner, C. Waterfield, and N. Phillips, Thermodynamic Properties of bcc He^4, UCRL-18384, October 1968.

6. HEAT CAPACITY

Albert Yee and George Jura

The earlier work with Dr. Walter Stark on the effect of pressure and temperature was reasonably good in that specific heat could be obtained for metals to several percent from liquid nitrogen to room temperature to pressures of about 125 kbars. In the circuit that was developed, the largest error in the determination of C_p was the measurement of the current. In general the best that could be done was 2%, and since this parameter appears to the third power, it is seen that a minimum error of 6% is introduced in this part of the measurement. The other errors were such that 8% on any single determination was the best that could be hoped for.

The circuit is being modified now so that the current is known to 0.1%. At the present time, the measurements are held up by a single factor, the length of the overlap of a square pulse in two arms of the circuit. The circuit is being modified, and the equipment should be productive by February 1969 at the latest.

This change and rebuilding of the apparatus should enable us to determine C_p to 0.5% with the same amount of effort as used in the past. This will enable us to undertake a much larger class of problems than before. For example, with the earlier results, it was not possible to really determine the Debye temperature with any degree of precision from the available data.

7. INFRARED REFLECTION MEASUREMENTS

Che-Kuang Wu and George Jura

Infrared measurements under pressure have been primarily exploratory in nature and, because of difficulties in making intensity measurements, limited in scope. It could be stated that a band that appeared at x cm^{-1} moved to y cm^{-1} at z kbars.

Reflectivity measurements under pressure should not have as many difficulties with respect to some of the problems that are inherent in the transmission measurements. Also, if they are feasible, they will yield considerably more information than the transmission measurements. For not only can the position of absorption peaks be determined, but in principle the real and imaginary parts of the refractive index as well as the molar extinction coefficient. Furthermore, there is an extensive theory associated with the reflectance. Dr. Cohen of the IMRD group is interested in these theories.

This year the necessary pressure cell was built and tested in transmission under low resolution. At the present time we are engaged in rebuilding a Perkin Elmer Model 21 spectrometer that belongs to Professor Pimentel of the Chemistry department, but which had in the course of time been pirated of various parts; also, many of the remaining parts had been modified for particular purposes.

Needless to say the transmission spectra

will also be determined.

8. POSITRON ANNIHILATION

John Przyblinski and George Jura

Earlier work with Dr. James Burton showed that positron annihilation measurements were feasible under pressure. In his work the movable counter was mounted horizontally and, because of the geometry of the pressure cell, the resolution was low, approximately 3 mrad. This was good enough to determine a Fermi momentum, and consequently a Fermi energy, but the data were not good enough for any other measurement. It was decided to redesign the equipment so that the movable counter moved vertically. The first construction was mechanically poor, and the equipment had to be rebuilt a second time. The apparatus is now in satisfactory condition. Its ultimate resolution is about 0.15 rad. Measurements have been made on aluminum to a pressure of 100 kbars with a resolution of 0.5 rad. This resolution is good enough to permit us to determine the density of states at each pressure at which the experiment has been performed. There are obvious changes as a function of pressure, but the calculations are not sufficiently complete to make the comparison and obtain the information that is desired.

9. RESEARCH PLANS FOR CALENDAR YEAR 1969

George Jura

Positron Annihilation

It is expected that the calculations on aluminum will be completed and similar measurements will be made on bismuth and ytterbium—the former because it exhibits several polymorphic transitions and the latter an electronic transition. These measurements should be completed by June and the choice of future studies will depend upon what is learned from the present and immediately projected experiments. It may even become essential to determine the effect of temperature as well as pressure.

Heat Capacity

As soon as the equipment is ready the heat capacity of bismuth will be determined. This material should be the most critical test of our ability to determine heat capacities because of the polymorphic transitions and the existence of a semiconducting state at low temperatures and pressures.

Reflectance Measurements

The first material whose spectrum will be determined is that of $KClO_3$. The reason for the choice is that Raman measurements are available, there is the presence of a forbidden band in the infrared, and it is an excellent choice for the detection of possible Davidoff splitting.

Mössbauer Measurements

Some preliminary measurements made several years ago show that it might be possible to determine the kinetics of the alpha-eta transition in iron at room temperatures as well as other temperatures. This should enable us to determine the rate constants for the transition, the activation energy, and all of the other quantities that might be of interest that can be obtained from such measurements.

10. 1968 PUBLICATIONS

George Jura and Associates

Technical Journals

1. J. Burton and G. Jura, The Fermi Momentum of Aluminum from 0 to 100 kbars, Phys. Rev. 171, 699 (1968).

UCRL Reports

1. J. Burton and G. Jura, Surface Phase Transformations: An Interpretation of LEED Results, UCRL-18202, July 1968.
2. J. Burton and G. Jura, Surface Phase Transformation on a Molecular Crystal, UCRL-18210, July 1968.
3. J. Burton and G. Jura, Adsorption and Diffusion on Three Structures of the (100) Surface of a Face Centered Cubic Crystal, UCRL-18209, July 1968.
4. J. Burton and G. Jura, Surface Phase Transformations on a Molecular Crystal, UCRL-18210 Rev., August 1968.
5. G. Jura and W. Stark, A Technique for Measurement of the Heat Capacity of Metals Under Pressure, UCRL-18497, September 1968.

11. VAPORIZATION KINETICS OF SOLIDS

a. Vaporization Kinetics of Gallium Arsenide Single Crystals

Catherine Lou and Gabor A. Somorjai

The vacuum evaporation rates of the

(111) gallium face and the ($\bar{1}\bar{1}\bar{1}$) arsenic face of gallium arsenide single crystals have been measured in the temperature range 650 - 900° by microbalance and mass-spectrometric techniques. The compound vaporizes according to the dominant net reaction

$$GaAs(solid) \rightarrow Ga(liquid) + \frac{x}{2}As_2(vapor) + \frac{(1-x)}{4}As_4(vapor).$$

The tetramer concentration is about 25-65 mole % of the total arsenic flux and it is increasing with increasing temperature. Both faces show an initial period of transient vaporization after which, reproducible steady state rates can be established. The total evaporation rates are identical for both faces. Microbalance studies yield an average activation energy of vaporization $\bar{E}^* = 90 \pm 4$ kcal/mole of solid, which is equal to the equilibrium heat of sublimation. The vacuum evaporation rates, however, are less than one-third of the maximum rates (Fig. 1). Thus, the average evaporation coefficient $\bar{\alpha}(T)$ is about $\alpha(T) \approx 0.27$.

Mass-spectrometric studies indicate that the ratio of dimer to tetramer arsenic molecules, As_2^+/As_4^+, is different for the two crystal faces (Table I). The activation energies of the tetramer arsenic molecules are also markedly different for the two, (111) and ($\bar{1}\bar{1}\bar{1}$), crystal faces; E^*(dimer) = 94.5 kcal/mole of vapor and E^*(tetramer) = 95.9 kcal/mole of vapor for the gallium or (111) face, E^*(dimer) = 99.6 kcal/mole of vapor and E^*(tetramer) = 142 kcal/mole of vapor for the arsenic or ($\bar{1}\bar{1}\bar{1}$) crystal face.

When the gallium face was covered with excess liquid gallium the total evaporation rate increased more than threefold and reached the maximum equilibrium value. The intensities of the As_2^+ and As_4^+ peaks increased markedly in the presence of liquid gallium but their ratio, As_2^+/As_4^+, remained the same as that for the pure sample. Thus, liquid gallium increases the vaporization rate but does not change the vapor composition or the activation energies of vaporization of the subliming products.

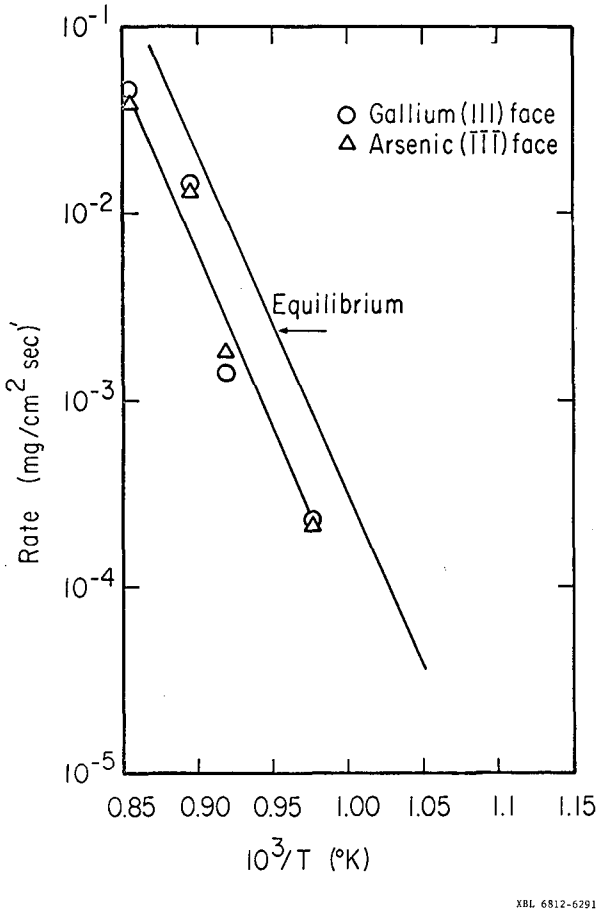

Fig. 1. Evaporation rate of GaAs single crystals as a function of temperature.

Table I. The intensity ratio, As_2^+/As_4^+, for the gallium (111) and arsenic ($\bar{1}\bar{1}\bar{1}$) faces at different temperatures.

Ga(111) face		As($\bar{1}\bar{1}\bar{1}$) face	
T(°C)	As_2^+/As_4^+	T(°C)	As_2^+/As_4^+
728	0.47	705	3.57[a]
730	0.48	746	0.81
758	0.44	798	0.78
780	0.49	809	0.73
782	0.51	842	0.71
832	0.44		
838	0.48		

[a]May not have reached steady state.

b. Kinetics of Sublimation of Ice Single Crystals

The vacuum sublimation rates of the c and a faces of ice single crystals have been measured in the temperature range -85 to -40° by using a microbalance. At low temperatures (< - 65°) the evaporation rate equals the maximum equilibrium rate; above -65° the sublimation rate decreases with respect to the maximum rate (Fig. 1). The two crystal faces (a and c faces) appear to have identical sublimation rates within the accuracy of the experiments. In the presence of ammonia gas, NH_3 (gas), the sublimation rate of ice decreases markedly.

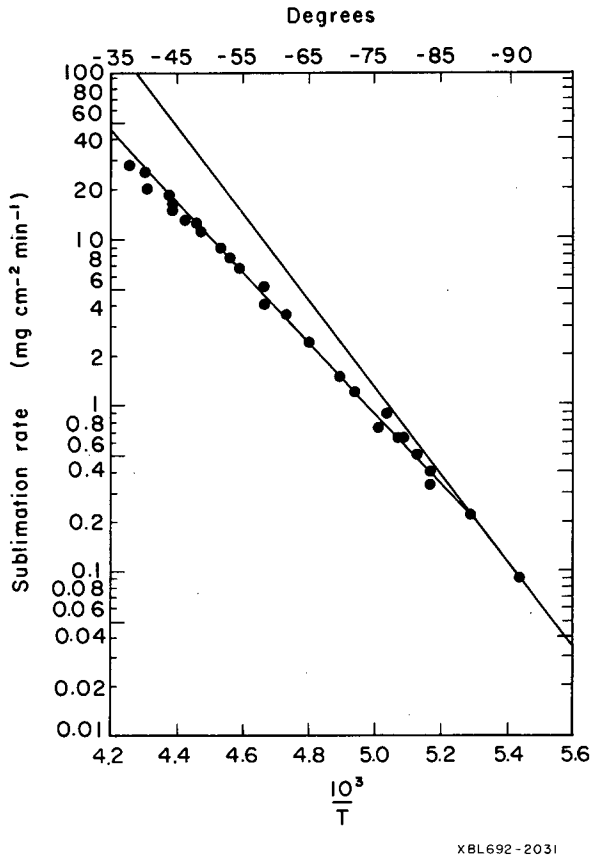

Fig. 1. Evaporation rate of ice single crystals as a function of temperature.

12. SURFACE STUDIES BY LOW ENERGY ELECTRON DIFFRACTION

a. The Properties of the Specular Low Energy Electron Beam Scattered by Face-Centered Cubic Metal Single Crystal Surfaces

Helen H. Farrell, Richard M. Goodman, and Gabor A. Somorjai

The intensity, $I_{00\ell}$, of the specularly reflected low energy (10-500 eV) electron beam was monitored for the different low index crystal faces of palladium, platinum, and lead as a function of electron energy (eV). The properties of the $I_{00\ell}$ (eV) curves were investigated as a function of temperature, crystal orientation, scattering angle, and the appearance of different ordered surface structures. For clean surfaces, the positions of the intensity peaks were insensitive to variation of temperature. They were found to change markedly, however, with variation of the scattering angle and the formation of new surface structures on the Pd (100) face. A "reduced" electron energy scale was used to compare the intensity curves obtained for the different face-centered cubic metal surfaces. The same crystal face of the different metals yields similar intensity curves. Correlations between intensity curves from different surfaces of the same metal have also been pointed out. The occurrences of maxima and minima in the intensity of the specularly scattered low energy electron beam are primarily determined by the periodicity of the crystal lattice rather than the nature of the crystal potential. However, the relative intensities of the diffraction features are sensitive to variations in the crystal potential.

b. Low Energy Electron Diffraction and Ellipsometry Studies of Physical Adsorption on the (110) Silver Surface at Low Temperatures

Joseph M. Morabito, Jr.,* Rolf F. Steiger,† Rolf Muller, and Gabor A. Somorjai

The physical adsorption of several gases (Kr, Xe, O_2, CH_4, C_2H_2, n-C_4H_{10}, and C_2H_4) on the (110) crystal face of silver has been studied in the temperature range -72 to -10° and pressure range 10^{-10} to 10^{-6} torr. The techniques of structure-sensitive low energy electron diffraction (LEED), coverage-sensitive ellipsometry, and mass spectroscopy have been combined in these investigations. While the diffraction technique allows one to distinguish between adsorption in random or ordered configurations on the single crystal substrate, the optically determined film thickness gives more quantitative information

on the amount of gas adsorbed. Mass spectroscopy has been used for the analysis of the residual gases in the vacuum chamber and to determine the composition of the gases used in the experiments.

The relative phase difference, Δ, between the parallel and perpendicular components of the polarized light beam has been measured during the adsorption of gas at a given temperature and pressure. From these data adsorption isotherms were derived. The surface area occupied by the adsorbed molecules on the single crystal surface and hence the number of surface atoms covered by each adsorbed molecule could be calculated from the isotherms. Isosteric heats of adsorption have also been calculated. These heats of adsorption increased with increasing film thickness, which indicates significant lateral interactions between the adsorbed molecules (clustering).

No ordered surface structures have been found under the conditions of the experiments. Adsorption at pressures below 10^{-8} torr has resulted in film coverages measurable by ellipsometry, while the LEED pattern was still representative of a clean surface. The gas molecules seem to adsorb in clusters on the silver single crystal surface.

---

*Present address: Philips Research Laboratories, Eindhoven, The Netherlands.

†Present address: CIBA Photochemical Ltd., Fribourg, Switzerland.

c. Low Energy Electron Diffraction Study of Surface Reactions on Platinum

Alan E. Morgan and Gabor A. Somorjai

Surface studies on platinum are being continued since the metal is an excellent catalyst for many chemical reactions involving gaseous reactants. Also the low index faces of platinum exhibit stable fractional order diffraction features that could result from the rearrangement of the platinum surface atoms into new ordered surface structures. The nature and geometry of these rearrangements are still in question.

The chemisorption of various gases (H_2, N_2O, N_2, O_2, CO, CO_2, CH_4, C_2H_6, C_2H_2, and C_2H_4) on the Pt(100) single crystal surface has been studied by using LEED, mass spectrometry, flash desorption, and work function measurements at gas pressures $\leq 1\times10^{-7}$ torr and at temperatures between 25 - 1200°. The Pt(100) substrate was characterized by a (5X1) surface structure. Those gases that chemisorbed on the platinum surface (CO, H_2, C_2H_2, and C_2H_4) formed ordered surface structures. Also, a further surface structure was formed by the co-adsorption of H_2 and CO. A strong affinity was found between carbon, or carbon-containing molecules, and the platinum surface. Carbon monoxide adsorbed in three bonding states on the (100) surface. The adsorption results differed somewhat from those observed in adsorption experiments performed at higher gas pressures.

These studies have been extended to the Pt(111) surface in order to investigate the role of the substrate in the adsorption process and in forming ordered surface structures. The chemisorption of propylene, 1,3-butadiene and the butenes, on both the (100) and (111) surfaces, is being examined in order to study how the size of the adsorbate influences the formation of surface structures.

A crystal manipulator has been designed and built to extend surface studies to liquid nitrogen temperature. Thus physical adsorption of gases can be examined in addition to chemisorption. It is still uncertain if physical adsorption is an ordered process and whether the adsorption can be detected by LEED. Ellipsometry will be used to obtain quantitative adsorption data. Eventually a specific reaction will be studied in order to carefully define the role of the surface in the catalytic process.

d. Surface Melting Studies by Low Energy Electron Diffraction

Richard M. Goodman and Gabor A. Somorjai

The structure of the low index crystal surfaces of lead (111), bismuth ($11\bar{2}0$), and tin (0001) has been studied by LEED below the melting points, during melting, and above the melting points. These surfaces retained their structure as the bulk melting point was approached. The surface structure seemed to collapse at the bulk melting points within the accuracy of the measurements. Above the melting points, the intensity distribution, which is characteristic of the short range order in liquids, could only be detected for the lead surfaces. Previous experiments[1] have shown that the mean displacement of surface atoms in these solids is much larger (about a factor of 2) than the mean displacement of bulk atoms. Thus the absence of surface pre-melting, as shown by these experiments, seems to refute the melting theory which predicts correlation between melting points of solids and their atomic root square displacements. Our results favor melting models that involve nucleation of

melting by defects that are generated at the surface.

1. R. H. Goodman, H. H. Farrell, and G. A. Somorjai, J. Chem. Phys. 48, 1046 (1968).

e. LEED Studies of the (0001) Face of Al_2O_3

Theodore French and Gabor A. Somorjai

This investigation was initiated to scrutinize the low energy electron scattering properties of insulator surfaces and the structural properties of α alumina. The incident electron beam in the energy range 5 - 70 eV induces a space charge at the alumina surface that deflects the impinging beam so that diffraction cannot occur. Above 70 eV the secondary electron emission overcomes the space charge and diffraction can take place from the discharged alumina surface. We have been able to obtain diffraction patterns at as low as 30 eV by the simultaneous use of two electron guns: one employed at high electon energy (> 70 eV) to discharge the surface and the other at low energy (< 70 eV) to obtain the diffraction pattern.

The (0001) crystal face of Al_2O_3 exhibits a structure below 1200° that is expected from the properties of the bulk unit cell [$Al_2O_3(0001)$ - (1×1)]. When the surface is heated above 1200° a new surface structure forms which can be designated as $Al_2O_3(0001)$ - $(\sqrt{31}\times\sqrt{31})$. When this surface structure is exposed to 2×10^{-4} torr oxygen at 1200° it converts into a new structure [$Al_2O_3(0001)$ - (2×2) O_2]. When this (2×2) structure is heated in vacuum above 1200° it reverts back to the $(\sqrt{31}\times\sqrt{31})$ surface structure, which seems to be the oxygen-deficient high temperature surface phase of the c face of Al_2O_3.

f. Studies of the Mean Displacement of Surface Atoms in the (100) and (110) Faces of Silver Single Crystals at Low Temperatures

Joseph M. Morabito, Jr.,* Rolf F. Steiger,† and Gabor A. Somorjai

The intensities of back-diffracted low energy (10-500 eV) electrons have been measured as a function of temperature for the (110) and (100) faces of single crystal silver in the temperature range -195 to 85°. From these data the mean displacements, $\langle u_\perp \rangle$, of surface atoms perpendicular to the surface planes have been calculated and the magnitude of the parallel components, $\langle u_\parallel \rangle$, estimated.

The perpendicular components of the surface mean displacements on silver (110) and (100) surfaces are 60% and 100% larger than those of bulk atoms. There is little difference in magnitude between the parallel and perpendicular components for these faces, as has also been reported for the (111) face. In addition, the parallel components of the mean displacements did not exhibit anisotropy within the accuracy of the measurements, and the physical adsorption of several noble gases had no effect on any of these measurements. The surface mean displacement for silver and those other face centered cubic metals studied are larger than predicted by theory which assumes bulk force constants for the surface atoms. This suggests that force constants for surface atoms are smaller than those of bulk atoms.

*Present address: Philips Research Laboratories, Eindhoven, The Netherlands.

†Present address: CIBA Photochemical Ltd., Fribourg, Switzerland.

g. Molecular Beam Scattering from Single Crystal Surfaces

Lloyd A. West and Gabor Somorjai

An apparatus was constructed to study the properties of molecular beams scattered from single crystal surfaces. The apparatus consists of three parts: 1) an "oven" which produces the gas flux, 2) a rotating disk velocity selector which selects the desired beam velocity and 3) an ultrahigh vacuum reaction chamber where the interaction between the beam and the single crystal surface takes place. The detector is a quadrupole mass spectrometer which can be rotated about the crystal both in and out of the incident plane to monitor the angular distribution of the scattered beam. The velocity of the scattered beam can be measured by suitable phase detection techniques. Studies will include the diffraction of molecular beams from metal surfaces and reactive scattering of beams from platinum surfaces.

h. Inelastic Scatterings of Low Energy Electron

Frederick Szalkowski and Gabor A. Somorjai

The purpose of these studies is to analyze the energy losses of the inelastically scattered electron from solid surfaces. The characteristic energy losses reveal the presence of surface impurities and provide information about the electronic binding energies of surface atoms. An apparatus was constructed which enables us to measure the

energy losses directly in the low energy electron diffraction chamber by suitable modifications of the electron optics.

13. RESEARCH PLANS FOR CALENDAR YEAR 1969

Gabor A. Somorjai

Our studies on the sublimation mechanism of ice will be completed. New vaporization studies will be initiated of non-congruently vaporizing solids and of several liquids.

Low energy electron diffraction studies will be extended to include molecular crystal surfaces. Our studies of melting will be completed. Structure analysis of low index face centered cubic metal surfaces will be completed.

14. 1968 PUBLICATIONS

Gabor A. Somorjai and Associates

Technical Journals

1. R. H. Goodman, H. H. Farrell, and G. A. Somorjai, The Mean Displacement of Surface Atoms in Palladium and Lead Single Crystals, J. Chem. Phys. 48, 1046 (1968).
2. R. H. Goodman, H. H. Farrell, and G. A. Somorjai, The Properties of the Specular Low Energy Electron Beam Scattered by Face Centered Cubic Metal Single Crystal Surfaces, J. Chem. Phys. 49, 692 (1968).
3. J. Lester and G. Somorjai, The Effect of Dislocations on the Vaporization Rate of NaCl Single Crystals, Phys. Rev. Letters 12, 216 (1968).
4. J. Lester and G. Somorjai, Studies of the Evaporation Mechanism of Sodium Chloride Single Crystals, J. Chem. Phys. 49, 2940 (1968).
5. A. E. Morgan and G. A. Somorjai, Adsorption Studies on Platinum Single Crystal Surfaces, Trans. Am. Cryst. Assoc. 4, 59 (1968).
6. J. M. Morabito, Jr., and G. A. Somorjai, Low Energy Electron Diffraction: The Technique and Its Application to Metallurgical Science, J. Metals 20, 17 (1968).
7. G. A. Somorjai, Small Angle X-Ray Scattering and Low Energy Electron Diffraction Studies of Catalyst Surfaces, in X-ray Electron Methods of Analysis (Plenum Press, New York, 1968).
8. G. A. Somorjai, Surface Chemistry, Ann. Rev. Phys. Chem. 19, 251 (1968).
9. G. A. Somorjai, The Mechanism of Sublimation, Science 162, 755 (1968).
10. G. A. Somorjai and D. H. Templeton, editors Proceedings of the Symposium on Low Energy Electron Diffraction (Am. Cryst. Association Publication, 1968).

UCRL Reports

1. H. Farrell and G. A. Somorjai, A Simple Relationship to Predict the Positions of Intensity Maxima for Diffracted Low Energy Electron Beams, UCRL-18373, August 1968.
2. E. Kozak and J. Morabito, A Low Temperature Crystal Manipulator for the Study of Metals Surfaces by LEED, UCRL-18038, February 1968.
3. J. M. Morabito, Jr., and P. F. Duby, The Relative Distribution of Energy on the $BaSO_4$ Surface: Part III, UCRL-17819, February 1968.
4. J. M. Morabito, Jr., and P. F. Duby, Theoretical Description of the Relative Distribution of Energy on a Solid Surface and Its Application to TiO_2, UCRL-17834, April 1968.
5. J. M. Morabito, Jr., R. F. Steiger, R. Muller, and G. A. Somorjai, LEED and Ellipsometry Studies of Physical Adsorption on a (110) Silver Surface at Low Temperatures, UCRL-18334, July 1968.
6. J. M. Morabito, Jr., R. J. Steiger, and G. A. Somorjai, Studies of the Mean Displacement of Surface Atoms in the (100) and (110) Faces of Silver Single Crystals at Low Temperatures, UCRL-18533, October 1968.
7. A. E. Morgan and G. A. Somorjai, Low Energy Electron Diffraction Studies of Gas Adsorption on the Platinum (100) Single Crystal Surface, UCRL-18333, July 1968.
8. R. H. Muller, R. F. Steiger, G. A. Somorjai, and J. M. Morabito, Jr., Gas Adsorption Studies by Ellipsometry in Combination with Low Energy Electron Diffraction and Mass Spectrometry, UCRL-18132, October 1968.
9. R. F. Steiger, J. M. Morabito, Jr., G. A. Somorjai, and R. H. Muller, A Study of the Optical Properties and of the Physical Adsorption of Gases on Silver Single Crystal Surfaces by Low Energy Electron Diffraction and Ellipsometry, UCRL-18480, November 1968.

D. ELECTROCHEMISTRY

1. FUNDAMENTAL STUDIES OF IONIC MASS TRANSFER

a. Laser Interferometer and Flow Cell for Mass Transfer Studies

Kirk W. Beach, Rolf H. Muller, and Charles W. Tobias

An electrolysis flow cell has been constructed for observation of concentration profiles in the mass transfer boundary layer during copper deposition. The flow channel, shown in Fig. 1, is 11 feet long and has an adjustable cross section of up to 10 × 10 cm. Presently, the channel is 2.5 cm high (electrode spacing) and 1.0 cm wide (optical path), the electrodes are 100 cm long, the entrance length measures 200 cm (140 hydraulic diameters). Glass sidewalls allow optical observations along the entire channel length.

A theoretical analysis of light propagation in the boundary layer has shown that under most conditions, because of the curved light path, concentration profiles are not simply related to the interferograms observed. Computational procedures have been devised to correct for the resulting distortions, which affect both the dimension and the concentration profile of the boundary layer. These errors depend on the optical parameters of the system.[1]

Two- and three-dimensional concentration fields require additional measurements for their determination. For this purpose, two optical systems, a focusing refractometer and a holographic interferometer, are being added to the laser interferometer.

A laser Doppler velocimeter is being developed to measure local fluid velocities in the cell. This will provide information on local velocity changes resulting from viscosity and density variations in the mass transfer

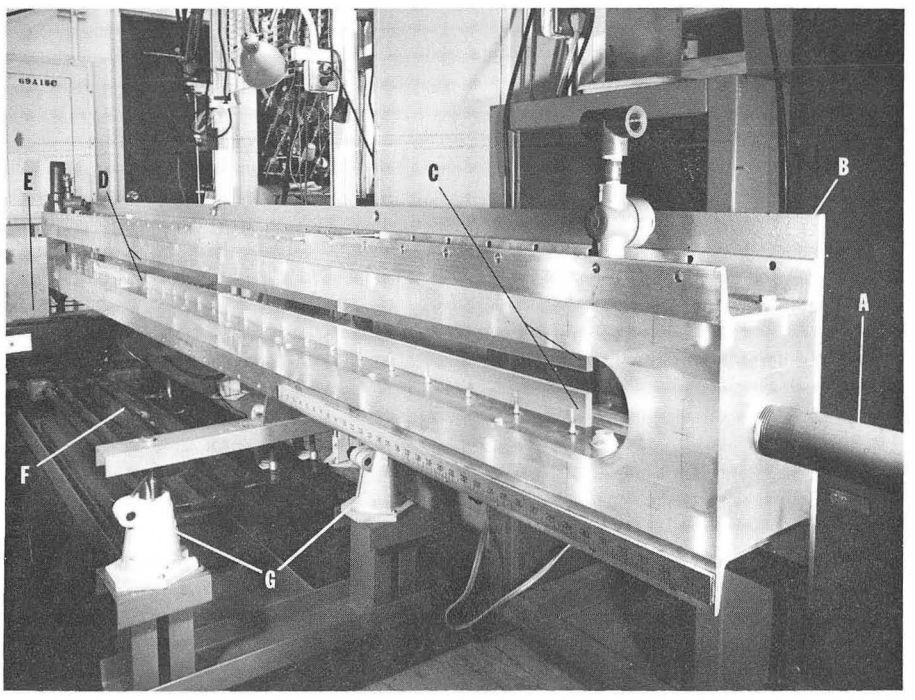

Fig. 1. Rectangular flow channel for the study of mass transfer boundary layers by laser interferometry. (A) electrolyte feed line, (B) mounting flange for glass wall (removed on side facing camera), (C) replaceable lucite spacers which form the top and bottom of the channel, (D) electrodes, (E) laser interferometer, (F) lathe bed for moving the interferometer, (G) cell mounting jacks. (XBB6811-6683A)

boundary regions.

1. Kirk W. Beach: A Laser Interferometer for Mass Transfer Studies (M.S. Thesis), UCRL-18037, February 1968.

b. Current and Potential Distribution in Convective Mass Transfer at Planar Electrodes

J. Robert Selman and Charles W. Tobias

Unsteady State Effects

The relationship between "apparent" and "real" limiting currents was studied in dilute potassium ferricyanide and ferrocyanide, with excess KOH, at a rotating-disk electrode. Either the current or the potential was controlled by means of a ramp-function generator. While at low rates of increase in current (small di/dt) well defined plateaus in the current-vs.-potential curves are obtained, at higher rates the plateau tends to disappear and becomes an inflection point that may exceed the steady state value of the limiting current, i_∞. As shown in Fig. 1, a correlation of the ratio of apparent to real limiting current, i/i_∞, with the current increase rate indicates that one obtains steady state limiting currents only when i_∞ is reached in not less than 20 $Sc^{1/3}/\Omega$ seconds. If the limiting condition is reached in shorter times, i/i_∞ can greatly exceed unity due to unsteady state diffusion. Under potential control, steady state limiting currents are observed when a 59 mV increase takes place in not less than 3 $Sc^{1/3}/\Omega$ seconds. When the potential is increased at a higher rate the current passes through a maximum before dropping to the apparent limiting current plateau. Both the experimental evidence and theoretical considerations indicate that potential control has distinct advantages over current control when precise values of limiting current are desired.

Construction of a Flow Circuit for Electrolysis at High Flow Rates

To minimize time-consuming changes in laying out the circuit,[1] e.g., to convert from gravity flow to pumping, a circuit was designed that combines several possibilities: gravity flow, pumping at moderate flow rates, pumping at high flow rates, and pressurization. The construction of this circuit is now in the final stages. Piping is of industrial glass, valves of PVC, pumps and main tank of 316

1. J. Robert Selman and Charles W. Tobias, Current and Potential Distribution in Convective Mass Transfer at Plane-Plate Electrodes, IMRD Annual Report, 1967, UCRL-18043 (March 1968), pp. 50-51.

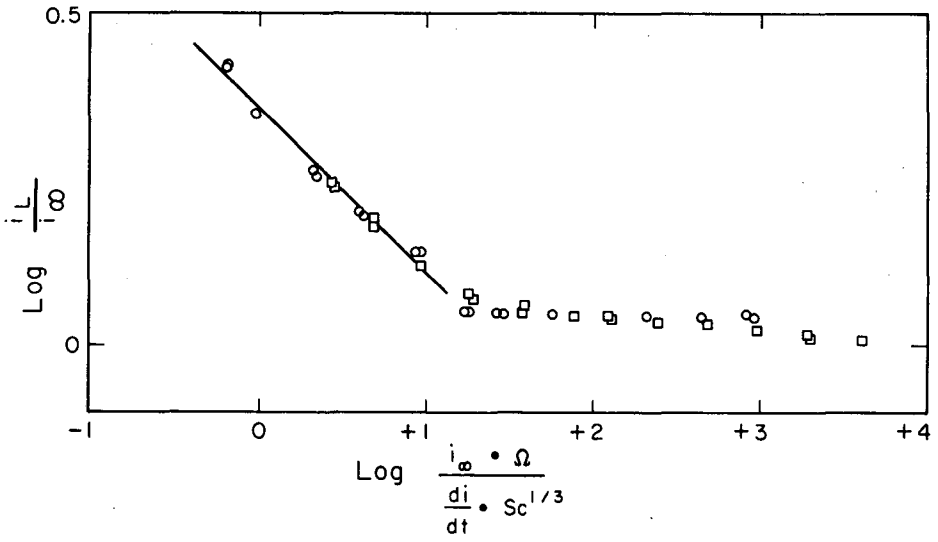

Fig. 1. Dependence of the apparent limiting current on linear current increase rate at a rotating disk. O: 115 RPM; □: 419 RPM; Ω: angular velocity in radians per second; $i_\infty/(di/dt)$, sec: time in which steady state limiting current would be reached; Sc: Schmidt number.

stainless steel. The circuit contains two pumps (70 GPM, 250 GPM), two reservoirs (50 gal, 85 gal) and two magnetic flowmeters (60 GPM, 200 GPM).

Physical Properties of the System $CuSO_4$-H_2SO_4-H_2O

Continuing the characterization of this electrolyte system for mass transfer studies, density, viscosity, and refractive index data were taken at 35° for solutions containing 0.05 M, 0.1 M, 0.2 M, 0.3 M, or 0.4 M $CuSO_4$ and H_2SO_4 concentrations between 0.5 M and 2.5 M. The results will be correlated with data for saturated solutions presently being gathered.

c. The Role of Ionic Mass Transport in Electropolishing

Kaoru Kojima and Charles W. Tobias

Phosphoric acid has been extensively used as an electrolyte for the electropolishing of metals such as copper, iron, and nickel. Polished surfaces are obtained when the dissolution occurs under limiting current conditions. However, the ionic species involved in the mass transfer rate-limiting step has not been satisfactorily clarified.

A review of available experimental evidence indicates that the transport of phosphoric acid to the anode surface is not a rate-limiting step. Rather, the limiting rate of diffusion of copper phosphate from the surface to the bulk electrolyte should be responsible for the onset of passivity, and result in polishing action. By using available data for transport properties and for the solubility of copper phosphate, transition times necessary for the onset of passivation have been calculated for pure diffusion in a semi-infinite column.[1-3]

In Fig. 1 theoretical transition times, calculated from

$$i\sqrt{\tau} = \frac{F\sqrt{\pi D_{Cu}}}{1 - t_{Cu}} (C_{Cu_s} - C_{Cu_b}) \cdots \quad (1)$$

are compared with those obtained experimentally for the galvanostatic dissolution of copper in various concentrations of phosphoric acid.

The discrepancies between theory and experimental results are most likely due to the lack of accurate transport property and solubility data in this complex electrolyte. Nevertheless the agreement is sufficient to give firm support to the view that in electropolishing of copper involving phosphoric acid, the controlling step is the transport of copper phosphate away from the anode.

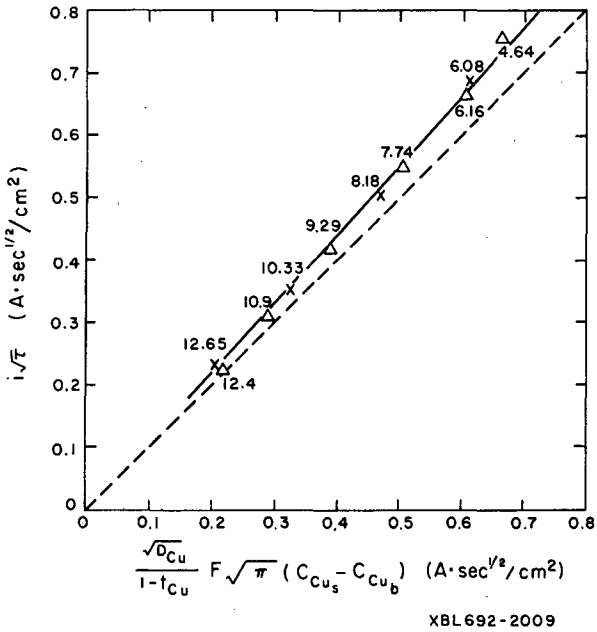

XBL692-2009

Fig. 1. The time required for onset of passivation in the galvonostatic dissolution of copper in phosphoric acid. The dashed line represents behavior derived from Eq. 1. Numbers at experimental points indicate bulk concentration of phosphoric acid. Data: Δ by Edwards[3], × by Elmore.[2]

τ = transition time, sec
i = applied current density, A/cm^2
D_{Cu} = diffusivity of copper phosphate, cm^2/sec
t_{Cu} = transference number of copper phosphate
C_{Cu_s} = saturation concentration of copper phosphate at the anode
C_{Cu_b} = concentration of copper phosphate in bulk electrolyte electrolyte, moles/cm^3.

1. S. I. Krichmar and V. P. Galushko, Russ. J. Inorg. Chem. I, 10, 2422-2424 (1956).
2. W. C. Elmore, J. Appl. Phys. 10, 724 (1939).
3. J. Edwards, J. Electrochem. Soc. 100, 189c (1953).

2. ELECTROLYSIS AT HIGH CURRENT DENSITIES

Electrochemical machining (ECM) has found widespread use in recent years for the shaping of metals. In this process the workpiece is dissolved anodically at current densities on the order of 100 A/cm^2, characteristically with electrolyte flow rates of 0.5 to 70 m/sec and electrode spacings of 0.1 to 0.5 mm. As an electrochemical process ECM is of particular interest because the current densities employed are about three orders of magnitude higher than those applied in conventional electrolysis. Most of the published literature of ECM deals with the correlation of practical process variables such as cathode feed rate, applied voltage, and electrolyte pressure, but little is known about the electrochemical factors involved. A more detailed understanding of ECM is not only expected to lead to further development and wider practical adoption of this highly interesting process, but it may also yield information relevant to the operation of other electrochemical processes at much higher rates than employed in current industrial practice. With this purpose in mind, the anodic dissolution of a metal with reasonably well understood electrochemical and metallurgical properties was subjected to study under conditions similar to those employed in ECM.

a. Stoichiometry of Anodic Copper Dissolution

Kimio Kinoshita, Rolf H. Muller, and Charles W. Tobias

Determination of the apparent valence of the anodic dissolution process of copper at high current densities has been extended to solutions of 1 N K_2SO_4 and 1 N H_2SO_4 in forced-convection systems. As found previously with 2 N KNO_3, the apparent valence, determined from the weight loss of the anode and the amount of charge passed, depends markedly on current density and flow rate. Again, a stepwise change in cell voltage has been found to coincide with an abrupt change in valence as a function of current density (Fig. 1).

The formation of passivating layers associated with these phenomena has now been confirmed in a motion picture study of anodic copper dissolution under natural convection conditions. The face of a copper anode has been observed through the transparent wall of a rectangular cell. Figure 2 shows the oscillogram of the cell voltage as a function of time during dissolution of Cu at 3.14 A/cm^2 in 2 N KNO_3. The inserted photographs show the appearance of the circular copper surface. After the electrolysis is begun the anode surface is gradually covered by a surface layer that grows from the periphery toward the center. After about two-thirds of the surface is covered the cell voltage increases rapidly until coverage is complete. Afterwards, removal of solid material and slight gas evolution is observed on the dissolving anode.

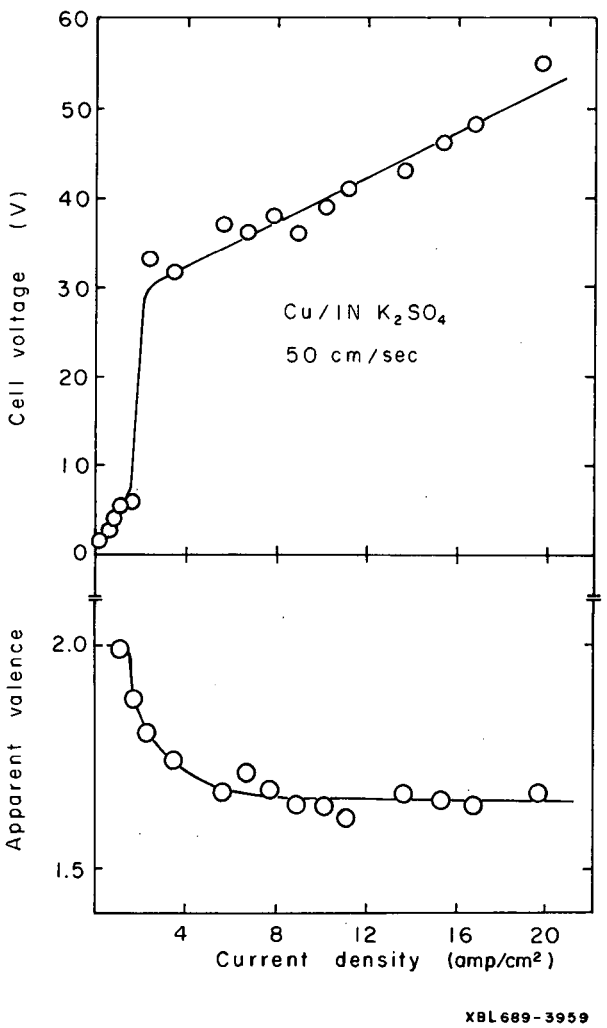

Fig. 1. Cell voltage and apparent valence behavior as a function of current density for anodic copper dissolution in 1 N K_2SO_4.

Qualitative analyses have been obtained of the anode precipitate formed during electrolysis under forced convection conditions.

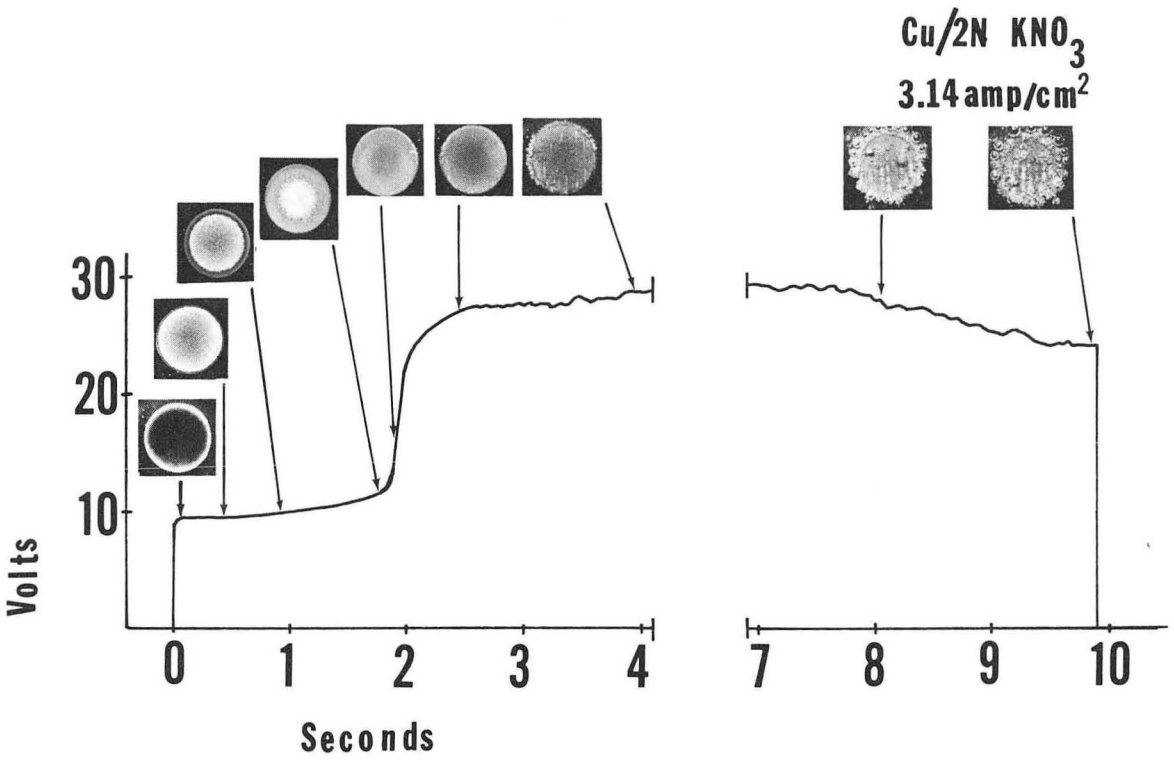

Fig. 2. Appearance of copper anode surface during transition from "active" to "passive" dissolution.

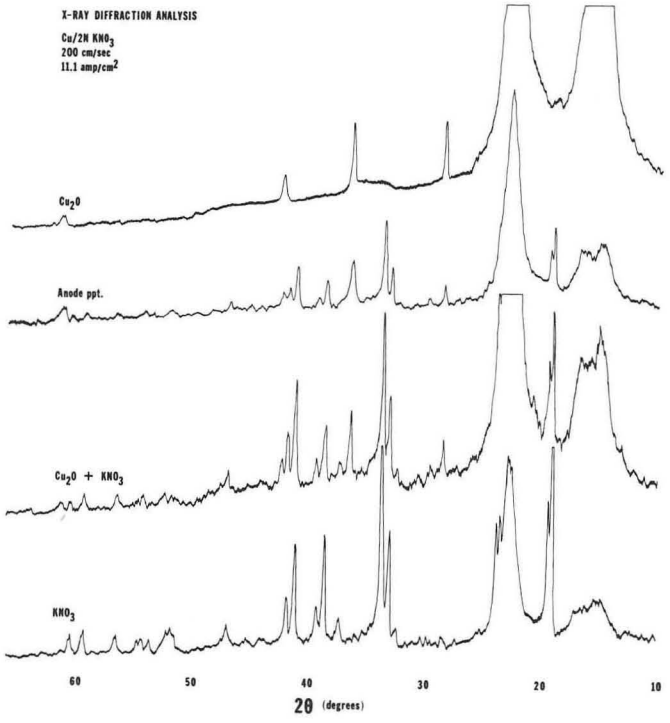

Fig. 3. X-ray diffraction analysis of anode precipitate resulting from the dissolution of copper in 2 N KNO_3, compared with known samples. (XBL6810-6087)

The specimens have been withdrawn with a portion of the electrolyte through an opening immediately downstream from the anode, collected on a filter paper, and analyzed by x-ray diffraction. The results have confirmed the presence of monovalent copper compounds, which have previously been postulated to account for the apparent valence of the dissolution process, and support the view that the voltage increase is primarily due to the ohmic resistance of an anodic surface layer. Figure 3 shows the x-ray diffraction pattern of anode precipitate from the Cu/2 N KNO_3 system in comparison with known specimens of Cu_2O, KNO_3, and a mixture of the two components. The diffraction peaks at 2θ less than 30° are due to specimen holder, adhesive, and filter paper.

b. Mass Transfer Considerations of High Rate Anodic Copper Dissolution

Dieter Landolt,* Rolf Muller, and Charles W. Tobias

Design criteria have been analyzed for the construction of an experimental flow system which allows us to perform electrochemical measurements of the anodic metal dissolution process under hydrodynamic conditions that are well defined and similar to those employed in the technical ECM process. The apparatus that has been built and extensively used contains a rectangular flow channel of 0.5×8 mm cross section and 120 mm length. Two rectangular electrodes 0.53×3.17 mm face each other, positioned flush with the channel walls, near the downstream end of the channel. This arrangement provides fully developed velocity profiles at the electrodes by use of a hydrodynamic entrance length of 77 hydraulic diameters. Linear flow rates up to 25 m/sec can be obtained with a maximum pressure at the channel inlet of approximately 150 psi. Capillaries drilled into the cell body near the two electrodes allow potential measurements against reference electrodes.

Copper dissolution experiments have been carried out in solutions of 2 M KNO_3 0.4 M KNO_3 and 0.2 M K_2SO_4. In all cases, anode potential and cell voltage have shown an abrupt change of 10-30 volts, depending on whether the dissolution proceeded in the

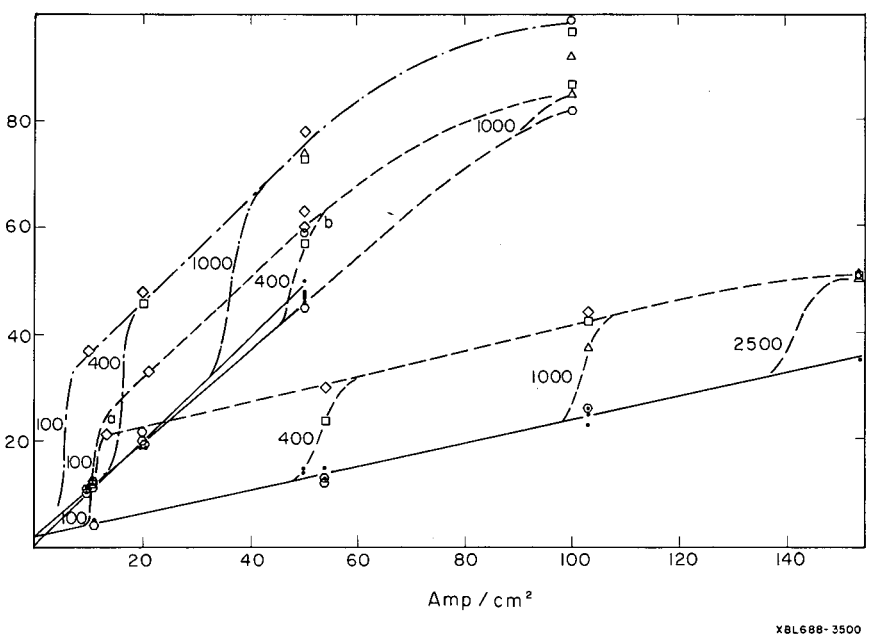

Fig. 1. Current cell voltage relationships during copper dissolution in nitrate and sulfate solutions.
——— least-square fit of values for active dissolution and initial step values for transpassive dissolution for all flow rates
— — — 2 M KNO_3 passive
---- 0.4 M KNO_3 passive
—.—. 0.2 M K_2SO_4 passive
Passivation: electrolyte flow rate ◇ = 100 cm/sec; □ = 400 cm/sec; △ = 1000 cm/sec; O = 2500 cm/sec.

"active" or "passive" mode. This transition could be accomplished by changing current density or flow rate as illustrated in Fig. 1 and coincides with a change in surface finish from a dull appearance with steps and etch pits within each grain to a bright appearance with round pits preferentially located along grain boundaries.

The results illustrated in Fig. 1 strongly indicate that the onset of passivation is controlled by mass transfer. The fact that, at both nitrate concentrations studied, passivation occurred in the same range of current density suggests that the transport of anions is not a controlling factor. The onset of passivity in sulfate solutions at lower current densities is qualitatively consistent with a salt precipitation mechanism. Current densities applied during "passive" dissolution were up to ten times higher than the minimum current density leading to passivation. Since the latter is believed to correspond to the highest rate at which cupric ions may be removed from the anode by convective diffusion, it appears that a large part of the oxidized copper is transported away from the anode in the form of solid dissolution products formed at or near the anode. It is probable that a similar transport mechanism may be involved in other ECM operations.

*Present address: University of California at Los Angeles.

c. Cathodic Gas Evolution in High-Current Electrolysis

Raul Acosta, Rolf Muller, and Charles W. Tobias

In order to evaluate the effect of cathodically generated hydrogen on the electrolysis at high current densities, size and distribution of gas bubbles evolved at the cathode have been observed by high speed stop-motion photography for current densities of 5 to 150 A/cm^2 and electrolyte flow rates of 40 to 2500 cm/sec.

For both electrolytes employed (2 N KCl and 2 N KNO_3) the bubble diameter and the thickness of the two-phase region have been found to decrease with decreasing current density and increasing flow rate (Fig. 2). For any given current density and flow rate the amount of gas evolved appears smaller in KNO_3 than in KCl electrolyte. Whether this difference is due to the partial reduction of the NO_3^- ion is presently being investigated.

The three dimensional extent of the gas bubble clouds to be observed has required the use of a telecentric optical system in order to avoid geometric distortions and extend the depth of field. The associated decrease in objective aperture, unfortunately, reduces the geometric resolution, which was 20μ for the system employed. Since the gas bubbles observed were unexpectedly small under most

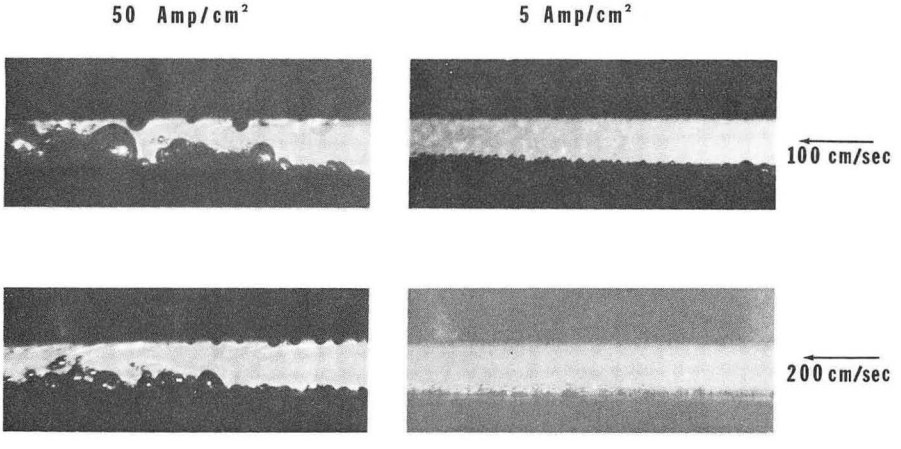

Fig. 2. Hydrogen evolution in a 0.05 cm gap. Cathode facing upward. Electrolyte: 2 N KCl.

XBB 6811-7025

conditions of electrolysis their diameter could only be determined at low flow rates and current densities. Gas volume fractions are being derived from these experiments in order to estimate the resulting change in electrolyte conductance.

3. DISTRIBUTION OF REACTION WITHIN FLOODED POROUS ELECTRODES

Richard C. Alkire, Edward A. Grens, and Charles W. Tobias

A technique has been developed for measuring the reaction distribution within flooded porous diffusion electrodes without sectioning or otherwise altering the electrodes before and during operation.[1-4] A porous metal anode is dissolved electrolytically, forming soluble reaction products, so that the porosity of the matrix changes from its original value. The resulting change in porosity distribution is equivalent to the time-average current distribution during dissolution.

The $Cu/CuSO_4/H_2SO_4$ system was used in this study. Electrodes of uniform porosity were fabricated by winding fine copper wire onto a large spool in hexagonal array, sintering it, and cutting electrodes from the fused mass along radial planes. The spaces between the wires constituted the pores. The porosity of the electrodes was 3.5%, the equivalent pore diameter was 25 μ, and the specific surface area was 1100 cm^2/cm^3 void volume. Gold was vapor-deposited onto the visible surface of some of these electrodes in order to prevent the reaction from occurring external to the pores.

Well defined mass transfer conditions external to the test electrode were maintained by mounting the electrode in the wall of a closed channel through which the electrolyte flowed under conditions assuring well developed turbulence. A secondary anode surrounded the test piece both to form a mass transport boundary layer that changed but little over the test section and also to maintain a uniform primary distribution over the test section. The polarization of the porous electrode was measured, during dissolution, with a reference electrode capillary inserted through the wall of the flow channel.[5]

Post-electrolysis examination was conducted by impregnating the reacted electrode with epoxy resin, sectioning, taking photomicrographs, and measuring electrode porosity as a function of distance from the external surface.

Electrolysis experiments have been performed with both gold-coated and "bare" copper electrodes. Porosity data were measured every 4 μ in depth. Most of the reaction was found to occur within 250 μ microns of the external surface. As could be expected the overpotential of the gold-coated electrode was higher than that of the bare copper electrode. After an initial transient the overpotentials decreased approximately along a straight line when plotted against the logarithm of time.

The existing theoretical framework[6, 7] has been extended to take into account the change in local specific surface area due to dissolution of the solid phase. Based on transport equations written for a macroscopic (one dimensional) model, calculations were made in the pseudo steady state that prevails during dissolution. These equations include terms describing diffusion, migration, and the convection which arises from displacement of fluid during dissolution. The initial transient response is not considered; the reaction rate is characterized by a Volmer-type double exponential expression. Solution of the coupled nonlinear equations was carried out on digital computing machinery.

As shown in Figs. 1 and 2 the model predicts the variations of the concentration, potential, current, and porosity distributions within the electrode as dissolution proceeds. The experimental data (porosity distributions and total polarizations) are in reasonable agreement with these predictions.

---

1. V. S. Daniel-Bekh, Zh. Fiz. Khim. 22, 697 (1948).
2. O. S. Ksenzhek and V. V. Stender, Zh. Fiz. Khim. 31, 117 (1957).
3. J. Euler and W. Nonnemacher, Electrochim. Acta 2, 268 (1960).
4. A. Winsel, Z. Elektrochem. 66, 287 (1962).
5. R. C. Alkire, Reaction Distribution in a Dissolving Porous Anode (Ph. D. Thesis), UCRL-18425, September 1968.
6. J. S. Newman and C. W. Tobias, J. Electrochem. Soc. 109, 1183 (1962).
7. E. A. Grens and C. W. Tobias, Ber. der Bunsen. fur physik. Chemie 68, 236 (1964).

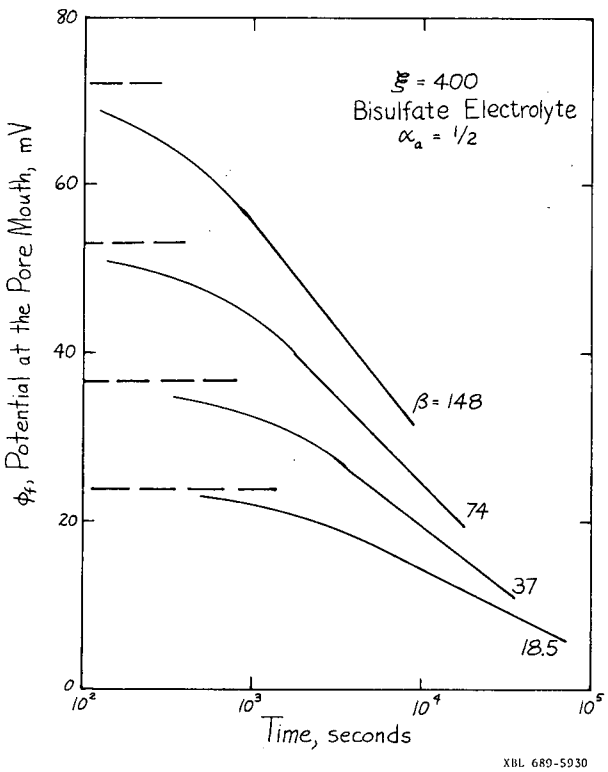

Fig. 1. Predicted potential variation for various applied currents. $\beta = i^* a_f d/nFc_{ref}D_{ref}$, dimensionless current density parameter, proportional to the applied current density, i^*.

4. ELECTROCHEMISTRY IN NONAQUEOUS SOLVENTS

Reduction of Active Metals in Propylene Carbonate

Jacob Jorne and Charles W. Tobias

Earlier work in this laboratory[1] first established the unique solvent properties of P.C., which make it potentially suitable for reactions requiring very high reduction potentials. A reactivation of this project involved the development of a reference electrode, thallium-thallous chloride for use in this solvent medium,[2] and the design and construction of a rotating disk electrode system operating in inert atmosphere.[3] Recent efforts have been concentrated on the acquisition of moisture-free halides of Mg, Al, Be, and of the group IV-VIb metals, and the preparation of coordinated complex solutions demonstrating sufficiently high conductivity to afford electrolysis. Complementing our vacuum-dry box, a second, inert atmosphere glove box has been assembled to allow all experimentation to be carried out under moisture- and air-free conditions.

1. W. S. Harris, Electrochemical Studies in Cyclic Esters (Ph. D. Thesis), UCRL-8381, July 1958.
2. F. G. K. Baucke and C. W. Tobias, Thallium Halide Reference Electrodes in Propylene Carbonate, UCRL-17892, November 1967.
3. F. G. K. Baucke, D. Landolt, and C. W. Tobias, J. Sci. Instr. 39, 1753 (1968).

5. RESEARCH PLANS FOR CALENDAR YEAR 1969

Charles W. Tobias and Associates

Fundamental Studies of Ionic Mass Transfer

Concentration profiles in combined free and forced convection at electrodes surfaces will be derived from interferograms. The development of a focusing refractometer will be undertaken to allow the evaluation of variation of electrolyte concentration in the direction of the incident laser beam. Attempts will be made for the measurement of velocity distribution by laser-Doppler effect.

Using the newly designed and constructed channel type cell, and associated high capacity flow circuit, the longitudinal distribution of limiting currents along planar electrodes will be measured in laminar and turbulent flow.

The study of the role of ionic mass transport in the mechanism of electropolishing will be continued. Emphasis will be given to the development of exact methods by which conditions appropriate for smoothing or brightening dissolution of anodes may be predicted.

Electrolysis at High Current Densities

The present investigation of the stoichiometry of the anodic copper dissolution at high current densities will be concluded by the analysis of gaseous anodic reaction products. The importance of solid reaction products for the mass transfer in the transpassive dissolution will be verified by motion picture photography. The influence of cathodically generated hydrogen on the electrolysis process and the occurrence of other cathodic reactions will be further investigated. Acquisition of a commercial ECM machine for the systematic investigation of rational cathode design, selection of electrolyte composition, flowrate, and current density is tentatively planned, subject to the availability of funding for the equipment and salaries for supporting personnel.

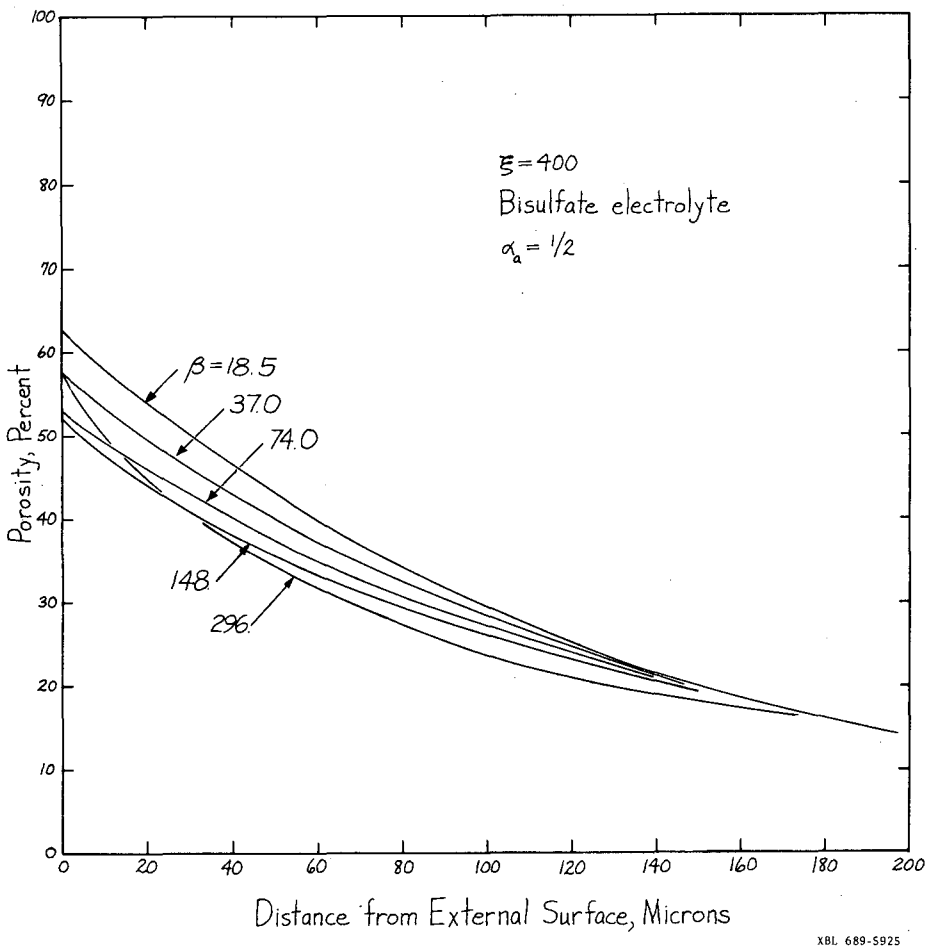

Fig. 2. Predicted porosity distributions for various applied currents.

Electrochemistry in Nonaqueous Solvents

Electrolyte compositions suitable for the reduction of active metals will be further explored. Attempts will be concentrated on the reduction of metals that at present cannot be obtained in pure form except by electrolysis in the melt.

6. 1968 PUBLICATIONS

Charles W. Tobias and Associates

Technical Journals

1. F. G. K. Baucke, D. Landolt, and C. W. Tobias, Rotating Disc System for the Study of Metal Deposition from Nonaqueous Solvents, J. Sci. Instr. 39, 1753 (1968).
2. H. Y. Cheh and C. W. Tobias, On the Dynamics of Hemispherical Phase Growth in Non-uniform Concentration Fields, Intern. J. Heat Mass Transfer 11, 709 (1968).
3. H. Y. Cheh and C. W. Tobias, Mass Transfer to Spherical Drops or Bubbles at High Reynolds Number, I and EC Fundamentals 7, 48 (1968).
4. D. Landolt and N. Ibl, On the Mechanism of Anodic Chlorate Formation in Dilute NaCl Solutions, J. Electrochem. Soc. 115, 713 (1968).
5. W. H. Smyrl and C. W. Tobias, Thermodynamic Properties of LiCl in Dimethyl Sulfoxide, J. Electrochem. Soc. 115, 33 (1968).
6. W. H. Smyrl and C. W. Tobias, The Effect of Diffusion of a Sparingly Soluble Salt on the EMF on a Cell Without Transference, Electrochim. Acta 13, 1581 (1968).

UCRL Reports

1. R. Alkire, Reaction Distribution in a Dissolving Porous Anode (Ph. D. Thesis), UCRL-18425, September 1968.
2. F. G. K. Baucke and C. W. Tobias,

Thallium-Thallous Reference Electrodes in Propylene Carbonate, UCRL-17892 Rev., August 1968.
3. K. N. Beach, A Laser Interferometer for Mass Transfer Studies (M.S. Thesis), UCRL-18037, February 1968.
4. D. Landolt, R. H. Muller, and C. W. Tobias, High Rate Anodic Dissolution of Copper, UCRL-18381, December 1968.

7. TRANSIENT BEHAVIOR IN A STAGNANT ELECTROLYTIC SOLUTION*

Limin Hsueh and John Newman

The analysis of mass transfer rates in a stagnant electrolytic solution by means of a similarity transformation shows that the current should be inversely proportional to the square root of time if a step change in the concentration at the electrode surface could be effected. In reality, the current density is limited by the ohmic resistance and surface overpotential at the very beginning; the surface concentration of reacting ions does not drop to zero instantaneously but is a function of time. The equation of unsteady state diffusion in a stagnant capillary is solved numerically with the consideration of these facts. The analysis[1] is similar to the one used by Parrish and Newman.[2]

The theoretically predicted curves of log current vs. log time generally agree well with the experimental observations except that for the nearly flat part the experimental curves are consistently lower than the predicted ones. However, the theory has successfully predicted an overshooting phenomenon, which was observed in many experimental curves at the transition region between the nearly flat part and the part of constant slope of -1/2.

The transient behavior of surface concentration was measured optically in a copper sulfate solution of 0.0385 M. Two separate runs of total applied voltages of 0.60 and 0.80 volt were measured and plotted in Fig. 1. There are no exchange current density i_0 data available in the literature for unsupported copper sulfate solutions. A reasonable estimation is that i_0 lies between 0.1 and 1.0 mA/cm^2. The theoretical predictions are also plotted in Fig. 1; the solid lines are the theoretical calculations at i_0 = 0.1 mA/cm^2, whereas the dashed lines are calculated at i_0 = 1.0 mA/cm^2. The plot shows that the solid lines fit the experimental results satisfactorily.

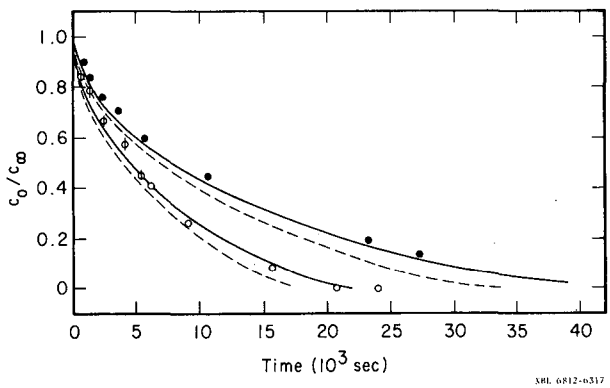

Fig. 1. Transient behavior of surface concentration of copper sulfate (0.0385 M) in a stagnant diffusion cell. (• = 0.60 V; o = 0.80 V; dashed lines i_0 = 1.0 mA/cm^2; solid lines i_0 = 0.1 mA/cm^2)

*This work is supported by the Petroleum Research Fund, administered by the American Chemical Society.

1. Limin Hsueh, Diffusion and Migration in Electrochemical Systems (Ph. D. Thesis), UCRL-18597, December 1968.
2. W. R. Parrish and John Newman, Current Distribution on a Plane Electrode below the Limiting Current, J. Electrochem. Soc. 116, 169-172 (1969). (Also UCRL-18160.)

8. ROLE OF THE BISULFATE ION IN A COPPER SULFATE-SULFURIC ACID SOLUTION ON THE EFFECT OF MIGRATION*

Limin Hsueh and John Newman

Many previous workers have ignored the incomplete dissociation of the bisulfate ion in solutions of copper sulfate and sulfuric acid. A theoretical analysis[1] has indicated that incomplete dissociation has a drastic effect on the migration and the surface concentration of supporting electrolyte. The existence of bisulfate ions would increase the effect of migration and decrease the concentration difference of supporting electrolyte between the bulk solution and the electrode surface.

Limiting current densities were measured with a stagnant diffusion cell in solutions of 0.1 M copper sulfate and 0.05 to 1.5 M sulfuric acid. In order to compare the results with the theoretical predictions,[1, 2] one may notice that the diffusion current i_D, i.e., the limiting current measured with an infinite amount of supporting electrolyte, cannot be measured without introducing a large viscous effect. Therefore, the measured values of $i_L\sqrt{t}$ are adjusted to $i_D\sqrt{t}$ by the theoretically predicted migration factor (see the curves labelled with

DROP in references 1, 2) and if the factor is correct, $i_D\sqrt{t}$ should be constant.

For the case of complete dissociation of bisulfate ion, the average of 13 values of $i_D\sqrt{t}$ is $26.2\sqrt{\text{sec}}$ -mA/cm^2 with a standard deviation of 2.2. For the case of incomplete dissociation and a dissociation constant of 0.0104, the average value is 23.4 with a standard deviation of 1.3. These results seem favorable to the assumption of incomplete dissociation of bisulfate ion in a solution of copper sulfate with sulfuric acid as the supporting electrolyte.

The surface concentrations of sulfuric acid were measured optically. The ratio $\Delta c_{H_2SO_4}/c_{CuSO_4}$, obtained experimentally, did not fall between the values calculated for complete dissociation and no dissociation of bisulfate ions. The cause of this discrepancy is unknown and should be subjected to further investigations.

---

*This work is supported by the Petroleum Research Fund, administered by the American Chemical Society.

1. J. R. Selman and John Newman, Laminar Free Convection at a Vertical Electrode in the Presence of Supporting Electrolyte, in Inorganic Materials Research Division Annual Report, 1967, UCRL-18043, March 1968, Figs. ID. 17-1 and 17-2.
2. John Newman, Effect of Ionic Migration on Limiting Currents, Ind. Eng. Chem. Fundamentals 5, 525-529 (1966).

9. CURRENT DISTRIBUTION ON A ROTATING DISK ELECTRODE

Vinay Marathe and John Newman

One of the advantages offered by the rotating disk electrode system is a uniform current density. This, however, is valid only at the limiting current. The aim of this work was to measure the current distribution on a rotating disk electrode, below the limiting current, for comparison with the theoretical results reported earlier. [1]

The copper deposition reaction, from copper sulfate-sulfuric acid, at copper rotating disk electrodes was chosen for experimental work. The deposit distribution should be proportional to the current density distribution if the deposit has uniform density. Thus, measurement of the deposit profile along a diameter of the disk electrode would yield the current density distribution.

The deposit distribution was obtained by observing the deposit optically along a diameter of the disk. The disk electrode was embedded in a hard epoxy resin, to prevent burring of the deposit, and one half was machined off on a milling machine, leaving about 0.005 in. for polishing and etching. The machined surface was then polished and etched for observation under a metallographic microscope. Deposit distribution was obtained from microphotographs of the deposit at various points along the disk diameter.

Measurements were made at several fractions of the limiting current density and have been reported elsewhere. [2] The experimental results were found to be in good agreement with Newman's numerical results.

---

1. John Newman, Current Distribution on a Rotating Disk below the Limiting Current, J. Electrochem. Soc. 113, 1235-1241 (1966).
2. Vinay Marathe, Current Distribution on a Rotating Disk Electrode (M.S. Thesis), pp. 30-33, UCRL-18264, June 1968.

10. CURRENT DISTRIBUTION ON PLANE PARALLEL ELECTRODES BELOW THE LIMITING CURRENT

William R. Parrish and John Newman

Primary and limiting current distributions are well known [1] for laminar channel flow between two plane, parallel electrodes. However, little is known about current distributions below the limiting current for this industrially important flow geometry. A numerical technique has been developed for treating such cases. The method uses the concept of having concentration variations confined to thin diffusion layers near the electrodes. [2] This concept allows separate treatment of the diffusion layers and the potential distribution outside the diffusion layers. The same approach has been applied to the rotating disk electrode. [3, 4] The numerical method used involved solving integral equations, which is thought to be more satisfactory for this type of problem than using power series solutions, or numerically solving partial differential equations.

The simpler case where the height to length ratio (h/L) is much greater than unity was treated first. [5] In this case each electrode had to be considered separately. Numerical results showed that, for the cathode at average current densities near the limiting current density, it was possible for the local current density to exceed the local limiting current density. It was also found that at the higher current densities the concentration would drop rapidly at the front of the electrode, but then increase slightly before dropping to near zero

at the rear of the electrode. In all cases the effect of mass transfer was to make the current distribution more nearly uniform near the back of the electrode.

The current distribution becomes more uniform as the ratio h/L is decreased. Although calculations are not completed, it appears that when h/L is 10 or greater, the two electrodes can be treated separately. This allows a great simplification, since the numerical problem is much more complicated when both electrodes must be considered.

1. John Newman, Engineering Design of Electrochemical Systems, Ind. Eng. Chem. 60 (no. 4), 12-27 (April 1968).
2. John Newman, The Effect of Migration in Laminar Diffusion Layers, Intern. J. Heat Mass Transfer 10, 983-997 (1967).
3. John Newman, Current Distribution on a Rotating Disk below the Limiting Current, J. Electrochem. Soc. 113, 1235-1241 (1966).
4. John Newman, The Diffusion Layer on a Rotating Disk Electrode, J. Electrochem. Soc. 114, 239 (1967).
5. W. R. Parrish and John Newman, Current Distribution on a Plane Electrode below the Limiting Current, J. Electrochem. Soc. 116, 169-172 (1969). (Also UCRL-18160, April 1968.)

11. PROPERTIES OF ELECTROLYTIC SOLUTIONS

Thomas W. Chapman* and John Newman

Data from the literature on properties of binary electrolytes in aqueous solutions are tabulated.[1] The properties include the density, viscosity, conductivity, transference number, diffusion coefficient, and activity coefficient.

*Present address: Department of Chemical Engineering, University of Wisconsin, Madison, Wisconsin.

1. Thomas W. Chapman and John Newman, A Compilation of Selected Thermodynamic and Transport Properties of Binary Electrolytes in Aqueous Solution, UCRL-17767, May 1968.

12. LAMINAR FREE CONVECTION AT A VERTICAL ELECTRODE IN THE PRESENCE OF A SUPPORTING ELECTROLYTE

J. Robert Selman and John Newman

Free Convection Under Uniform Flux Condition

The work reported earlier[1] concerned free convection under conditions of uniform concentration at the electrode. To supplement this, the equations of convective diffusion were also solved for the case of a uniform current density at the electrode. The results of interest are the concentration at the electrode and the shear stress, expressed in the appropriate variables:

$$c_s^0 - c_s^b = -\theta_s(0)\,\frac{Lj(1-t_R)}{D_s}\left(\frac{5x}{L\,Gr_s^*}\right)^{1/5},$$

$$\tau_{avg} = -\phi_s(0)\,\frac{\mu D_s}{L^2}\,(Gr_s^*)^{3/5},$$

where j is the prescribed flux at the electrode and

$$Gr_s^* = \frac{g\alpha_s j L^4}{\nu D_s^2}$$

is a modified Grashof number characteristic for free convection at uniform flux. All other variables are in the notation used earlier.[1]

The values found for $\theta_s(0)$ and $\phi_s(0)$ are in good agreement with the trend indicated by values for lower Sc numbers, given in Table I.

Unfortunately, a similarity transformation of the same type cannot be used for a ternary system, e.g., $CuSO_4$-H_2SO_4-H_2O, unless vanishingly small current densities are assumed.

Free Convection Under Conditions of Uniform Concentration at the Electrode

Earlier work[1] concerned the systems $CuSO_4$-H_2O and $CuSO_4$-H_2SO_4-H_2O. Next, the system $K_3Fe(CN)_6$-$K_4Fe(CN)_6$-H_2O was studied, preliminary to more complicated

Table I. Dimensionless concentration and shear stress as a function of Sc number.

	Sc →	0.1	1	10	100	∞[a]
$\theta_s(0)$	This work					1.14747
	Sparrow and Gregg[2]	1.7356	1.3574	1.2163	1.1697	
$\phi_s(0)$	This work					0.83789
	Sparrow and Gregg[2]	0.65425	0.72196	0.76962	0.79628	

[a]In the asymptotic limit of large Sc numbers the inertial terms are dropped from the equation of motion.

systems involving KOH or NaOH as supporting electrolyte. In these widely used redox systems the traditional method of calculating electrolyte composition at the electrode[3] reportedly leads to unsatisfactory results.

The values of current and shear stress, in the notation used earlier, [1] are given in Figs. 1 and 2 as functions of composition (solid line). In the same figures, values are indicated for three situations where physical properties have been simplified arbitrarily:

1. no specific densification, i.e., α_s is equal for ferricyanide and ferrocyanide (squares);
2. equal diffusivity of ferricyanide and ferrocyanide ion (diamonds);
3. no specific diffusivity, i.e., equal diffusivity for all three ions (triangles).

It appears that the results in case 3 are practically the same whether or not specific densification is assumed. Figure 3 shows the concentration of the supporting ion (i.e., the product ion) at the electrode; it is almost or entirely independent of composition. Likewise, the concentration profiles (Fig. 4) do not show appreciable variation with composition.

Both for the case of different diffusivities and for that of equal diffusivity of all three ions, the concentrations at the electrode do not depend on the value of the densification coefficient. In fact, the convective velocity along the electrode changes sign when densification coefficients are set equal, but the concentrations at the electrode are the same. They correspond closely to the values predicted by the stagnant diffusion model (Table II). For equal diffusivities there is an exact correspondence. As also shown in Table II, the migration contribution to the current is not correctly predicted by this model; convection does have an effect on the concentration gradients near the electrode.

The current and shear stress found for equal diffusivity of ferricyanide and ferrocyanide ion present an anomalous situation. The concentration of the product ion at the electrode is intermediate between that for

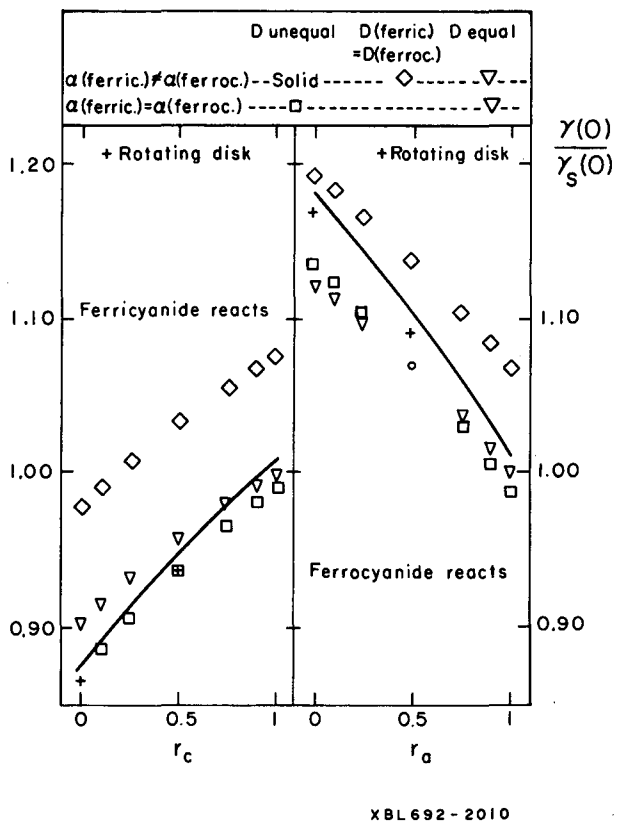

Fig. 1. Influence of migration on the current for cathodic reaction (left) and anodic reaction (right) of the system $K_3Fe(CN)_6$-$K_4Fe(CN)_6$-H_2O.

$$\left[r_c = \frac{K_4Fe(CN)_6}{K_3Fe(CN)_6 + K_4Fe(CN)_6}; \quad r_a = 1 - r_c \right].$$

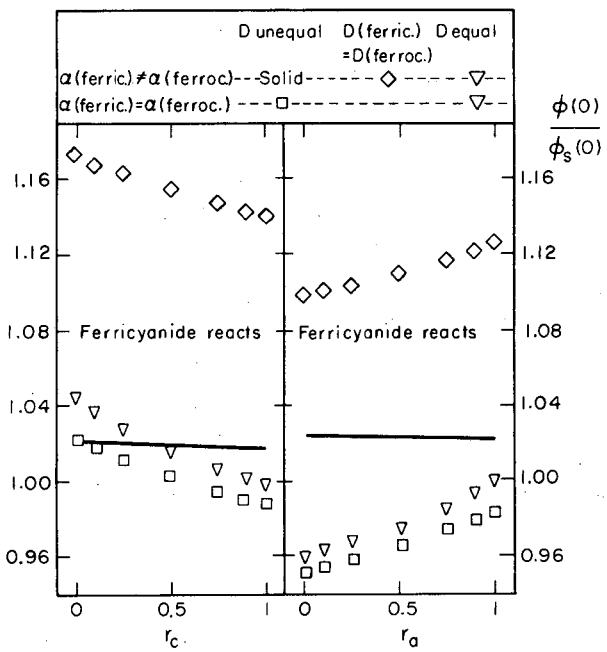

XBL692-2011

Fig. 2. Influence of migration on the shear stress for cathodic reaction (left) and anodic reaction (right) of the system $K_3Fe(CN)_6$-$K_4Fe(CN)_6$-H_2O.

$$\left[r_c = \frac{K_4Fe(CN)_6}{K_3Fe(CN)_6 + K_4Fe(CN)_6} ; \quad r_a = 1 - r_c \right].$$

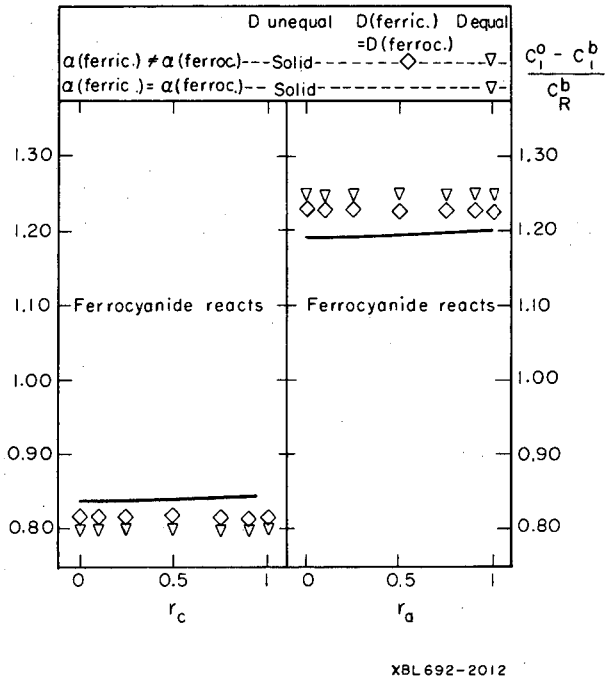

XBL692-2012

Fig. 3. Concentration of the product ion at the electrode, in the cathodic reaction (left) and anodic reaction (right) of the system $K_3Fe(CN)_6$-$K_4Fe(CN)_6$-H_2O.

$$\left[r_c = \frac{K_4Fe(CN)_6}{K_3Fe(CN)_6 + K_4Fe(CN)_6} ; \quad r_a = 1 - r_c \right].$$

Table II. Concentration at the electrode and migration current ratio.

	$(c_1^0 - c_1^b)/c_R^b$ cathodic		$(c_1^0 - c_1^b)/c_R^b$ anodic		$\gamma(0)_{r=0}/\gamma(0)_{r=1}$	
	r=0	r=1	r=0	r=1	cath.	anodic
Specific diffusivities:						
This work	0.838	0.845	1.192	1.202	0.876	1.183
Stagnant diff. model	0.829	0.843	1.186	1.206	0.660	1.483
Equal diffusivities:						
This work	0.800	0.800	1.250	1.250	0.903	1.124
Stagnant diff. model	0.800	0.800	1.250	1.250	0.800	1.250

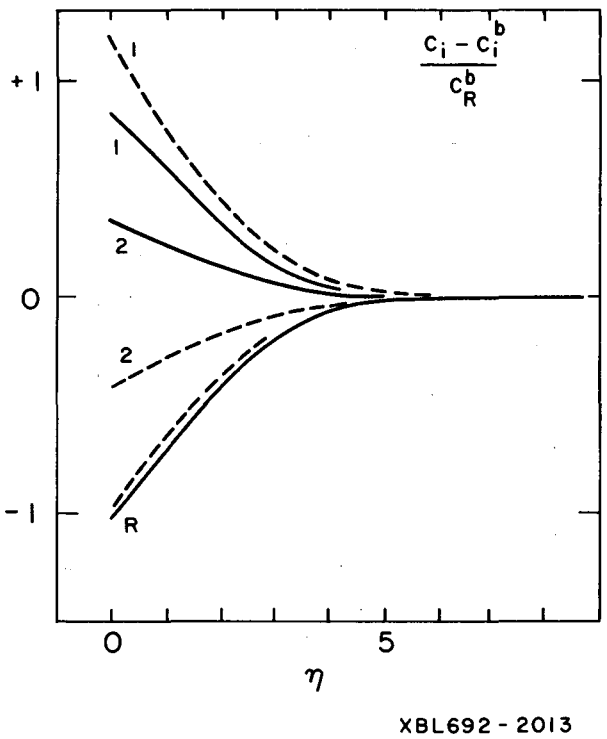

Fig. 4. Concentration profiles of the reacting ion (R), product ion (1) and K^+ (2) for the cathodic reaction (solid line) and anodic reaction (broken line) of ferricyanide-ferrocyanide in water, as a function of dimensionless distance from the electrode.

$$\left[\eta = \frac{y}{\left(\frac{4 x \nu D_R}{3 g \alpha_R c_R^b}\right)^{1/4}}\right].$$

unequal diffusivities and that for three equal diffusivities. Both the current and the shear stress, however, are considerably higher than in these cases. The reason for this behavior is not clear.

Work is continued with the system $K_3Fe(CN)_6$-$K_4Fe(CN)_6$-KOH-H_2O.

1. J. R. Selman and J. Newman, Laminar Free Convection at a Vertical Electrode in the Presence of Supporting Electrolyte, Inorganic Materials Division Annual Report, 1967, UCRL-18043, March 1968, pp. 66-68.
2. E. M. Sparrow and J. L. Gregg, Laminar Free Convection from a Vertical Plate with Uniform Surface Heat Flux, Trans. A. S. M. E. 78, 435-440 (1956).
3. C. R. Wilke, M. Eisenberg, C. W. Tobias, Correlation of Limiting Currents under Free Convection Conditions, J. Electrochem. Soc. 100, 513-523 (1953).

13. MOVING WALL TUNNEL

Ping Sih and John Newman

It was mentioned in the 1967 IMRD annual report that the fluid velocity profile in the flow tunnel was to be measured by means of a hot-wire anemometer. However, the hot-wire probes tested were not satisfactory. Better probes have just been obtained from the manufacturer.

Meanwhile, attempts were made to measure the velocities by a tracer, $KMnO_4$ solution, injected into the stream. It worked well at fast laminar flows but was rather poor for slow flows. This was because of the fact that the tracer tended to diffuse and sink by gravity. The proposed mass transfer experiment (see next article) involves velocities on the order of 0.002 ft/sec, which cannot be measured by either the hot-wire probes or the tracer method. Therefore, for the low flow rate range, we suggest as an alternative to measure the total volumetric flow rate by a rotameter, and define the characteristic Reynolds number by

$$Re = (G/A) \cdot 2R \cdot \rho/\mu,$$

where

G = volumetric flow rate,
A = cross-sectional area of flow tunnel,
R = radius of the circular cylinder,
ρ = density of the fluid,
μ = viscosity of the fluid.

At this low flow rate range the moving walls will not be in motion. In fact, in the mass transfer problem only the velocity gradient at the surface of the cylinder is needed. Therefore, the overall characteristic Reynolds number serves as a parameter particular to this flow tunnel. The method for measuring the surface velocity gradient is indicated in the next article.

14. MASS TRANSFER TO A CIRCULAR CYLINDER

Ping Sih and John Newman

The objective of this experimental study is to prove the theories proposed in two papers by Sih and Newman, [1] and Newman [2] concerning mass transfer to the rear of objects at slow fluid flows. An electrochemical system con-

sists of a solution of $K_4Fe(CN)_6$, $K_3Fe(CN)_6$, large excess of KNO_3, and nickel electrodes. A similar system, utilizing NaOH instead of KNO_3 as the supporting electrolyte, has been widely employed by many other investigators for mass transfer studies. The reason for choosing KNO_3 in this experiment is because KNO_3 is neutral while NaOH is caustic and extremely corrosive. The behavior of the system was tested by the rotating disk method. The current-voltage relationship appears to give a good limiting current plateau. Incidentally, the diffusivity of the ferricyanide ions will be measured by the rotating disk method.

For the experiment of mass transfer to a circular cylinder, a nickel circular cylinder is placed in the flow tunnel as the cathode, and the stainless steel walls of the tunnel act as the anode. In order to measure the local mass flux, for example, at the rear of a cylinder, a small section of the cylinder is isolated as a separate electrode. The limiting current of this small electrode gives the local mass flux. Three such cylinders have been constructed.

As mentioned in the previous article, mass transfer rate is related to the surface velocity gradient. To measure this gradient, the local flux $\underline{N}$ in the diffusion layer can be used:

$$N = \frac{-D(c_\infty - c_0)\cdot\sqrt{\beta}}{\Gamma(4/3)\left[9D\int_0^x \sqrt{\beta}\,dx\right]^{1/3}},$$

where

D = diffusivity,
c = concentration,
$\Gamma(4/3)$ = gamma function of 4/3,
β = local velocity gradient, $\partial v_x/\partial y|_{y=0}$,
x = distance along the cylinder surface starting from the leading edge of the mass transfer area,
y = distance normal to the cylinder surface.

For the small and isolated electrode, β may be considered as constant. Thus we have

$$\overline{\beta} = [9DR\theta]\left[\frac{N\Gamma(4/3)}{D(c_\infty - c_0)}\right]^3,$$

where θ is the angle covered by the small electrode.

The above diffusion layer approximation is invalid in the rear region. However, as the rear region is very small, its β values can be obtained by extrapolating from the diffusion layer to the rear stagnation point $\theta = 0$, where $\beta = 0$.

Experiments with higher flow rates will also be made in order to compare with literature values.

---

1. P. H. Sih and J. Newman, Mass Transfer to the Rear of a Sphere in Stokes Flow, Intern. J. Heat Mass Transfer 10, 1749-1756 (1967).
2. J. Newman, Mass Transfer to the Rear of a Cylinder at High Schmidt Numbers, UCRL-17599, June 1967.

15. MOVING-BOUNDARY TRANSFERENCE NUMBERS

Kong-Heong Tan and John Newman

In a previous endeavor,[1] a rigorous expression for the moving-boundary transference number was developed, viz.,

$$t_1 = -a_B z_3 \left(\frac{c_3}{c_0}\right)_A \left(\frac{FV}{tI} + \frac{M_e}{z_2\rho_e} + \frac{b_B}{z_2\nu_2 a_B}\right), \quad (1)$$

applicable for a boundary rising from a dissolving metallic anode, and for dilute as well as concentrated electrolytic solutions.

In conjunction with this effort, an experimental technique was established[1] in an attempt to determine the transference numbers of ammonium nitrate solutions at concentrations covering both the dilute and concentrated regimes, with silver nitrate as the following solution in all instances.

This particular technique yielded, for the system 0.213 $\underline{M}$ NH_4NO_3: 0.195 $\underline{M}$ $AgNO_3$ at 25°, a t_1 which equals 0.5140 ± 0.0024.[1]

Efforts are presently under way to extend the experimental endeavor and thereby obtain t_1 data for the ammonium nitrate system for as wide a concentration range as experimentally possible to render complete its set of transport properties. Accurate diffusion coefficient and electrical conductivity data are already available in the literature[2] for concentrations as great as 8 $\underline{M}$.

Of course, in this regard, the more pronounced IR heating effect introduced when concentrated electrolytic solutions are present will have to be dealt with satisfactorily.

Quite possibly, then, with these t_1 data at hand for a sufficiently wide concentration range, generalized correlations in the fashion proposed by Chapman[3] will be accessible, and subsequently be amenable for further theoret-

ical interpretations.

1. P. Milios, A Theoretical Analysis of the Moving-Boundary Measurement of Transference Numbers (M.S. Thesis), UCRL-17807, September 1967.
2. T. W. Chapman and J. Newman, A Compilation of Selected Thermodynamic and Transport Properties of Binary Electrolytes in Aqueous Solution, UCRL-17767, May 1968.
3. T. W. Chapman, The Transport Properties of Concentrated Electrolytic Solutions (Ph. D. Thesis), UCRL-17768, November 1967.

16. MIGRATION IN RAPID DOUBLE-LAYER CHARGING

John Newman

Potentials and charge movements are analyzed[1] for the rapid injection of a large surface charge into the interface between an ideally polarizable electrode and a dilute electrolytic solution. Under such conditions the concentrations and charge distributions are disturbed at distances much greater than the equilibrium thickness of the diffuse double layer. For example, if the electrode is charged from 0 to -10 $\mu C/cm^2$ in 0.001 M solutions of HCl, KCl, and KOH, the disturbance reaches to about 1860, 5280, and 7570 Å, respectively. The anions have been driven from this region, leaving the cations exposed and forming an extended region of charge. This large region of charge can lead to high, nonequilibrium electrode potentials, as indicated in Fig. 1. Experimental results[2] show longer decay times than those predicted here.

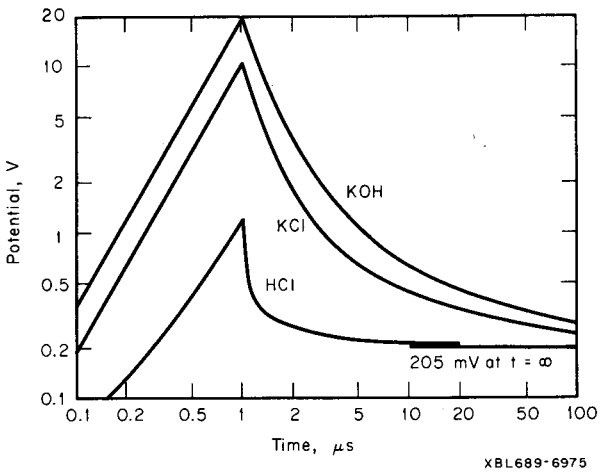

Fig. 1. Potential at inner limit of diffuse double layer. Charge produced in 1 millimolar solutions at 25° by passing 10 A/cm^2 for 1 μsec. During the charging period the potential is corrected for ohmic drop.

1. J. Newman, Migration in Rapid Double-Layer Charging, UCRL-18462, September 1968.
2. F. C. Anson and R. F. Martin, Creation of Non-equilibrium Diffuse Double Layers and Studies of Their Relaxation, J. Phys. Chem. (to be published).

17. THE GRAETZ PROBLEM

John Newman

The classical problem of heat transfer to a fluid in fully developed laminar flow in a tube was first treated by Graetz.[1] By treatment of his eigenvalue problem as a series of coupled, nonlinear, ordinary differential equations,[2] we have calculated[3] accurate values of the first five eigenvalues and coefficients as given in Table I. If the local transfer rate is divided by the concentration difference between the inlet and the downstream wall, multiplied by the tube diameter, and divided by the diffusion coefficient, the Nusselt number is formed. Then the eigenvalues and coefficients in Table I are used, for example, in the expression for the local Nusselt number at the wall of the tube:

$$Nu(\zeta) = \sum_{k=1}^{\infty} \frac{1}{2} \lambda_k^2 M_k e^{-\lambda_k^2 \zeta},$$

where $\zeta = zD/2\langle v_z \rangle R^2$, z is the axial distance, D is the diffusion coefficient, $\langle v_z \rangle$ is the average velocity in the pipe, and R is the radius of the pipe.

The work of Lauwerier[4] and of Sellars, Tribus, and Klein[5] has been extended to obtain improved asymptotic formulas for the eigenvalues and coefficients, formulas which hold in the asymptotic limit of large eigenvalues. With these improvements in the Graetz series, satisfactory agreement can now be obtained between the Graetz series and the Lévêque series.[6]

Axial diffusion is important at high Péclet numbers only in a small region at the beginning of the transfer section. Methods used for quite different problems[7, 8] have been used here to treat the region of axial diffusion, and the results are expressed in Fig. 1. In this figure, Θ is the dimensionless concentration, $X = (z/R)\,Pe^{1/2}$, $Y = (1-r/R)\,Pe^{1/2}$, r is the radial distance, and $Pe = 2R\langle v_z \rangle/D$

Table I. Eigenvalues and coefficients for the Graetz solution.

k	λ_k	$\frac{1}{8}\lambda_k^2 M_k$
1	2.70436443	0.74877456
2	6.67903145	0.54382796
3	10.6733795	0.46286106
4	14.6710785	0.41541845
5	18.6698719	0.38291919

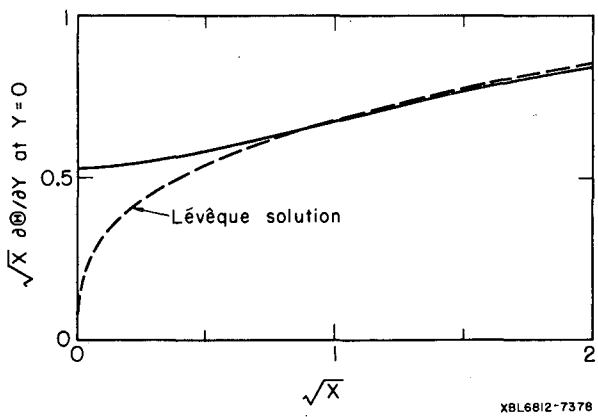

Fig. 1. Dimensionless transfer rate at the wall in the region of axial diffusion, with the Lévêque solution for comparison.

is the Péclet number. The figure thus shows a dimensionless transfer rate, with the Lévêque solution for comparison. With axial diffusion taken into account, the transfer rate at the wall is inversely proportional to the square root of the axial distance instead of the cube root.

1. L. Graetz, Ueber die Wärmeleitungsfähigkeit von Flüssigkeiten, Annalen der Physik und Chemie 18, 79-94 (1883); 25, 337-357 (1885).
2. J. Newman, Numerical Solution of Coupled, Ordinary Differential Equations, Ind. Eng. Chem. Fundamentals 7, 514-517 (1968).
3. J. Newman, The Graetz Problem, UCRL-18646, January 1969.
4. H. A. Lauwerier, The Use of Confluent Hypergeometric Functions in Mathematical Physics and the Solution of an Eigenvalue Problem, Appl. Sci. Res. A2, 184-204 (1950).
5. J. R. Sellars, Myron Tribus, and J. S. Klein, Heat Transfer to Laminar Flow in a Round Tube or Flat Conduit—The Graetz Problem Extended, Trans. ASME 78, 441-447 (1956).
6. J. Newman, Extension of the Lévêque Solution, UCRL-17600, June 1967.
7. P. H. Sih and J. Newman, Mass Transfer to the Rear of a Sphere in Stokes Flow, Intern. J. Heat and Mass Transfer 10, 1749-1756 (1967).
8. J. Newman, Mass Transfer to the Rear of a Cylinder at High Schmidt Numbers, UCRL-17599, June 1967.

18. RESEARCH PLANS FOR CALENDAR YEAR 1969

John Newman

This program is concerned with the development of the engineering treatment of electrochemical systems, and consequently most projects are related to the transport properties of electrolytic solutions, the prediction of system behavior, or the formulation of design methods.

Optical observation of restricted diffusion will be used to measure the diffusion coefficients of aqueous solutions of potassium hydroxide and to obtain additional values for aqueous solutions of nitric acid. The moving-boundary method will be used to obtain additional values of the transference numbers of aqueous solutions of ammonium nitrate. Measurement of the conductivities of aqueous solutions of calcium chloride would be desirable. Efforts for compilation, correlation, and interpretation of literature data will be continued.

Theoretical studies of free convection at vertical electrodes and of current distribution below the limiting current on plane electrodes in the wall of a flow channel should be completed. Experimental attempts to verify the theory of mass transfer to the rear of bluff objects in slow motion will be completed. Some intriguing theoretical studies along this line include the effect of streamwise diffusion at the downstream end of a diffusion layer and the asymptotic solution for large Reynolds numbers of the fluid flow near the trailing edge of a flat plate.

19. 1968 PUBLICATIONS

John Newman and Associates

Technical Journals

1. J. Newman, Engineering Design of Electrochemical Systems, Ind. Eng. Chem. 60 (no. 4), 12-27 (April 1968).
2. J. Newman, Numerical Solution of Coupled, Ordinary Differential Equations, Ind. Eng. Chem. Fundamentals 7, 514-517 (1968).
3. J. Newman, Book review: Electrochemistry by C. W. Davies, Ind. Eng. Chem. 60 (no. 8), 8 (August 1968).
4. W. H. Smyrl and J. Newman, Potentials of Cells with Liquid Junctions, J. Phys. Chem. 72, 4660-4671 (1968).

UCRL Reports

1. T. W. Chapman and J. Newman, A Compilation of Selected Thermodynamic and Transport Properties of Binary Electrolytes in Aqueous Solution, UCRL-17767, May 1968.
2. L. Hsueh, Diffusion and Migration in Electrochemical Systems (Ph. D. Thesis), UCRL-18597, December 1968.
3. V. Marathe, Current Distribution on a Rotating Disk Electrode (M. S. Thesis), UCRL-18264, June 1968.
4. P. Milios and J. Newman, Moving Boundary Measurement of Transference Numbers, UCRL-18105, February 1968.
5. J. Newman, Migration in Rapid Double-Layer Charging, UCRL-18462, September 1968.
6. W. R. Parrish and J. Newman, Current Distribution on a Plane Electrode below the Limiting Current, UCRL-18160, April 1968.

20. OPTICAL STUDIES OF INTERFACIAL PHENOMENA

a. Ellipsometer for Use with LEED Chamber*

Rolf H. Muller

Ellipsometry and low energy electron diffraction (LEED) have some complimentary properties which make the combination of both a powerful tool for the study of solid surfaces. The principal problems in combining the two types of instrumentation arise from the requirement for removing the optical components every time the bake-out shrouding is placed around the ultrahigh vacuum system, and the need for time-consuming alignment afterwards.

The optical elements of our ellipsometer have been mounted on a new base plate which can be moved on retractable casters and is rapidly placed over the frame of a LEED

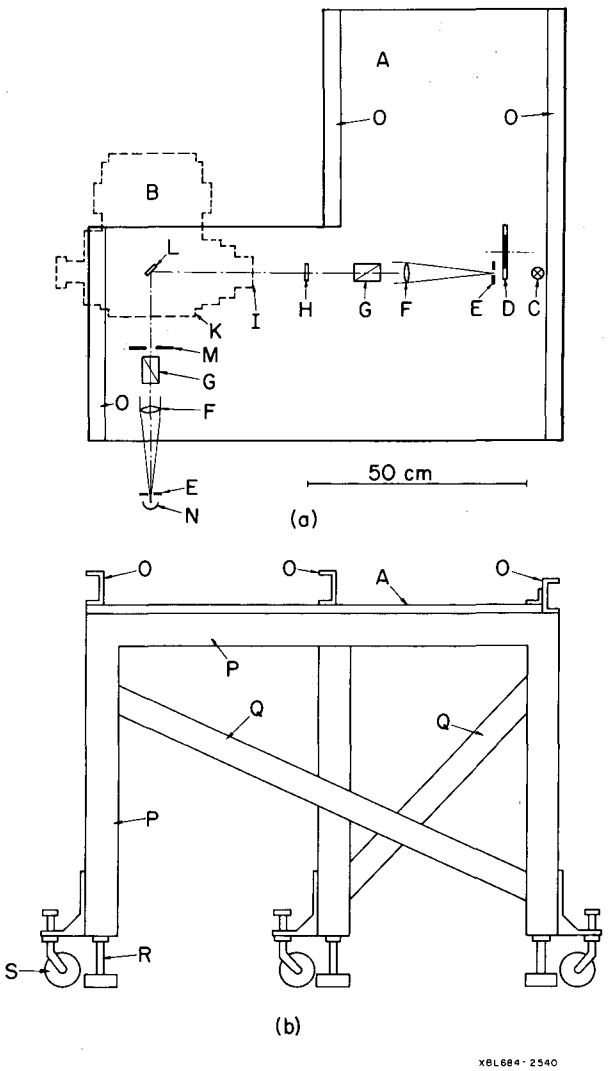

Fig. 1. Ellipsometer table for attachment to LEED equipment. (a) Plan view of table top A with outline of LEED chamber B and position of optical elements: C = monochromatic light source, D = light chopper, E = pinholes in focal plane of lenses F in collimator and telescope, G = Glan-Thompson polarizing prisms, H = quarter wave compensator, side window I, and optical viewport K on LEED chamber, L = crystal specimen, M = iris diaphragm, N = photomultiplier. (b) Side view of table. (LEED chamber and optical elements not shown) 0 = stiffening members on table top A, P = welded frame with braces Q, adjustable legs R, and swivel casters S.

apparatus. Reproducible positioning is achieved by means of spacers and tapered pins between both frames. The alignment of optic axis and azimuth circles can be performed with a test mirror in place of the specimen surface before the ellipsometer is connected to the vacuum system. Any changes found in the azimuth circle adjustment after the ellipsometer is connected to the vacuum chamber are indicative of birefringent or misaligned chamber windows. (See Fig. 1.)

The chief merits of the arrangement used are its simple construction and the application of a conventional LEED chamber. Only a major reconstruction of the latter would remove the principal shortcomings of the present design, namely, the 45° angle of incidence of the light on the specimen, which would preferably be 70-80°, and the need to rotate the specimen between LEED and ellipsometer observations.

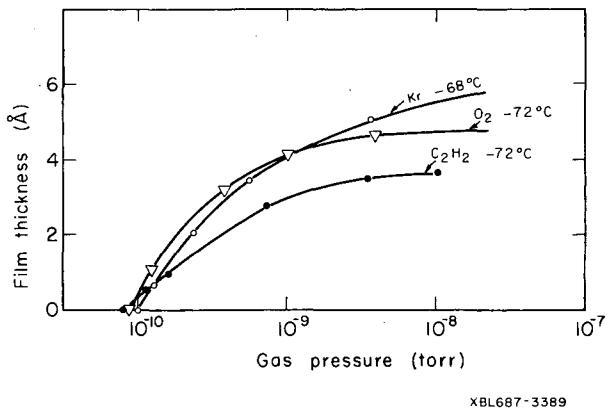

Fig. 1. Adsorption isotherms of krypton, oxygen, and acetylene on silver (110) in terms of film thickness determined by ellipsometry.

*Abstract from Rev. Sci. Instr. 39, 1593 (1968).

b. Gas Adsorption Studies by Ellipsometry in Combination with Low Energy Electron Diffraction and Mass Spectrometry

Rolf H. Muller, Gabor A. Somorjai, Rolf F. Steiger,* and Joseph M. Morabito†

For use in adsorption studies, ellipsometry is basically coverage-sensitive while LEED is structure-sensitive. The combination of the two techniques is therefore suitable for resolving some uncertainties inherent in either technique when employed separately. Problems in ellipsometry that may profit from such a combination of capabilities include (1) the question as to when a clean surface has been obtained and what its optical properties are, and (2) the question as to how well the classical theory of ellipsometry, which is based on a continuum model of matter and employs macroscopic material properties, applies to films of molecular dimensions.

The physical adsorption of Kr, Xe, CH_4, C_2H_2, C_2H_4, n-C_4H_{10} on the (110) and (100) faces of silver single crystals has been studied at temperatures of -196 to 0° and pressures of 10^{-10} to 10^{-6} torr. Adsorption isotherms have been determined from ellipsometer measurements in terms of optical film thickness. Examples are given in Fig. 1. Heats of adsorption, cross sectional areas of the adsorbed molecules, and molecular coverage ratios of substrate and adsorbate have been derived from the measurements. Selected results are shown in Table I. The low values of the heats of adsorption (extrapolated to zero coverage) confirm the weak interaction between substrate and adsorbate. The molecular cross sections, derived from the thickness of the monolayer and the bulk liquid density, compare well with literature data from volumetric adsorption work. This agreement confirms the classical electromagnetic theory of ellipsometry for the systems investigated at monolayer coverage.

A comparison of sub-monolayer coverages of adsorbed molecules as determined by ellipsometry and LEED has not yet been possible, because no ordered adsorptions have been observed and the LEED diffraction patterns are rather insensitive to disordered adsorption at beam voltages of 50-150 eV.

Basic to any adsorption studies are defined properties of the bare substrate. The ellipsometer measurements have shown that even in ultrahigh vacuum systems the preparation of clean surfaces is by no means trivial and great care is necessary to avoid the effect of contaminants in low temperature adsorption experiments. Surface topography may affect the optical constants of bare substrates determined by ellipsometry. Results indicate that ellipsometry is able to detect a precursor to the thermal faceting of the (110) surface of silver otherwise observed above 600°, after short heating to 140°. It may be possible to develop submicroscopic roughness measurements from such a dependence. For the same reason, ellipsometry now appears not to be a suitable technique for the precise determination of optical constants of solid materials, even if all the instrumental sources of error for absolute measurements were eliminated.

*Present address: CIBA Photochemical Ltd.,

Table I. Physical adsorption on a silver (110) surface, observed by ellipsometry.

Adsorbed gas	Heat of adsorption at zero coverage (kcal/mole)	Molecular cross section ($Å^2$/molecule)	Molecular coverage ratio at monolayer Ag: gas
Kr	1.4	25.6	2.2:1
Xe	6.1	19.6	1.7:1
O_2	1.8	26	2.2:1
C_2H_2	1.0	18.3	1.6:1
$n\text{-}C_4H_{10}$	-	42	3.5:1

Fribourg, Switzerland.
†Present address: Philips Research Laboratories, Eindhoven, Netherlands.

c. Definitions and Conventions in Ellipsometry*

Rolf H. Muller

The literature on ellipsometry contains a confusing multiplicity of definitions and conventions which arise from arbitrary choices which have to be made in the derivation of the basic equations from the electromagnetic theory. These choices are often not stated and their effect does not seem to be sufficiently recognized. Since some of them, although of profound consequence, are not recognizable from the results, the comparison of data from different sources may be impossible.

In an effort to untangle this situation, the effect of nine twofold alternatives of definitions and conventions and some of their multiply connected interactions have been analyzed. The results indicate that, although not all possible 512 combinations yield different results, the reflection from any given surface can be represented by eight numerically different combinations of ellipsometer parameters $\tan\psi$ and Δ. Conversely, from any measured set of ψ and Δ values 16 different combinations of optical constants can be derived.

Based on an extensive survey of literature usage, and discussions with an international group of workers in the field, a set of nine preferred definitions and conventions has been formulated. It is hoped that this set will be widely adopted. Thus, communication within a growing technical community would be greatly facilitated.

*Abstract from UCRL-18585.

d. Theory of Ellipsometry

Rolf H. Muller and Jonathan Z. Shoher

One of the still neglected basic problems of ellipsometry concerns the effect which surface roughness has on the state of polarization of reflected light. In the wake of our observations with clean silver single crystals, we have employed a model in which surface roughness is represented by a transitional layer with properties intermediate between bulk metal and vacuum. This model predicts ellipsometry to be sensitive to surface roughness in the Angstrom range. Under some restrictive assumptions, exact solutions for the optical reflection of polarized light from a surface with a saw-tooth profile have also been obtained. Numerical results from this treatment will show whether the physical basis for the much simpler transitional layer model is justified.

Adsorbed films of less than monomolecular coverage may be present in different forms of aggregation. Within certain limits the mean size of film patches should be measurable by ellipsometry with variable lateral coherence in the incident beam. While the complete relationship between a general patch size distribution and the partial polarization as a function of coherence appears very complex, the limiting cases of completely coherent and incoherent superposition of reflection from bare and film-covered areas have been derived. Numerical results will be analyzed to determine promising areas of application.

21. SURFACE CALORIMETRY

Rolf H. Muller and Charles G. Churchman

Techniques for the measurement of heat released on planar solid surfaces have been further developed.* The general equation

relating the electrical output of a thermopile to the time-dependent heat flux across its face has been revised and will be tested in new calibration experiments. The use of a new detector with lower inherent noise has increased the sensitivity of the system. The previously used thermopile with 27 soldered couples is being replaced by one with 210 welded couples, which are more precisely positioned in a plane and show a lower impedance. The improvements are expected to lower the detection limit by a factor of about 10. Thus, adsorption measurements appear possible in addition to the planned determination of electrochemical reaction enthalpies.

Vapor-deposited metal films have been investigated as an alternative approach to achieving a high packing density of thermocouples. This technique allows the use of material combinations with high thermoelectric coefficients. Most of these materials are not available in wire form. A sufficiently low electrical resistance of bismuth and antimony films, deposited on epoxy tape, has been difficult to achieve and subsequent ageing has resulted in deterioration of the deposits below acceptable levels.

*See IMRD Annual Report, 1967.

22. RESEARCH PLANS FOR CALENDAR YEAR 1969

Rolf H. Muller

Chemisorption of reactive vapors on metal single crystals in ultrahigh vacuum will be studied by ellipsometry in combination with low energy electron diffraction. The comparison of coverages derived by both methods will provide new insights into both techniques. Ellipsometry will also be used for the calibration of Auger electron spectroscopy.

Extensions of the theory of ellipsometry will be continued in the fields of rough surfaces and patch film coverage.

Enthalpies of single electrode electrochemical reactions and heats of immersion at controlled potential will be determined by surface calorimetry.

The force-and-energy balance in liquid films on metal surfaces will be investigated.

Studies in the field of high-current anodic metal dissolution will be continued. The combination of electrical, chemical, and optical observations is expected to yield new insights into the complex processes occurring. Of special interest will be the solid reaction products that are formed at the anode in the transpassive dissolution mode and reactions other than hydrogen evolution at the cathode.

Computational procedures to correct for errors due to light deflection will be employed to derive concentration profiles from interferograms of mass transfer boundary layers.

23. 1968 PUBLICATIONS

Rolf H. Muller and Associates

Journal Articles

1. R. H. Muller, Ellipsometer for Use with LEED Chamber, Rev. Sci. Instr. 39, 1593 (1968).

UCRL Reports

1. R. C. Gupta, Techniques for the Measurement of Small Amounts of Heat Released on Planar Surfaces (M.S. Thesis), UCRL-18089, February 1968.
2. K. W. Beach, A Laser Interferometer for Mass Transfer Studies (M.S. Thesis), UCRL-18037, February 1968.
3. J. M. Morabito, R. Steiger, R. Muller, and G. A. Somorjai, LEED and Ellipsometry Studies of Physical Adsorption on a (110) Silver Surface at Low Temperatures, UCRL-18334, June 1968.
4. R. F. Steiger, J. M. Morabito, G. A. Somorjai, and R. H. Muller, A Study of the Optical Properties and of the Physical Adsorption of Gases on Silver Single Crystal Surfaces by Low Energy Electron Diffraction and Ellipsometry, UCRL-18480, October 1968.
5. R. H. Muller, R. F. Steiger, G. A. Somorjai, and J. M. Morabito, Gas Adsorption Studies by Ellipsometry in Combination with Low Energy Electron Diffraction and Mass Spectrometry, UCRL-18132, October 1968.
6. R. H. Muller, Definitions and Conventions in Ellipsometry, UCRL-18585, November 1968.

E. PHYSICAL CHEMISTRY

1. DYNAMICS OF ION-MOLECULE REACTIONS*

Bruce H. Mahan

In recent experiments the energy and angular distributions of the products of ion-molecule collisions have been determined. It has proved possible to detect the results of inelastic collisions in which the projectile ion or the target atom becomes electronically excited, or in which dissociation of the target molecule is induced. In addition, the energy and angular distribution of the product ions of reactions such as $N_2^+ + D_2 \rightarrow N_2D^+ + D$ show that for exothermic hydrogen atom transfer reactions, most of the products are formed with very high internal excitation energy principally by grazing collisions. Very large isotope effects are found and can be understood, at least partially, in terms of product internal excitation and stability with respect to dissociation. More recent work shows that endothermic reactions such as $O_2^+ + H_2 \rightarrow O_2H^+ + H$ involve more nearly head-on collisions in which all atoms in the collision complex interact strongly. These results begin to give us a picture of the detailed dynamics of chemical reactions and inelastic collisions, and their relation to molecular structure.

*Abstracted from Accounts of Chemical Research 1, 217 (1968).

2. THE CHEMISTRY OF GASEOUS IONS

Bruce H. Mahan

Because gaseous ions can be accelerated and focused by electric fields and detected and identified by mass spectrometry, they are convenient objects with which to study reaction dynamics, and other molecular interaction phenomena. For example, detection of photochemical ionization in the system

$$Cs + h\alpha \rightarrow Cs^*(np)$$
$$Cs^*(np) + h\nu \rightarrow Cs_2^+ + e^-$$
$$Cs^*(np) + Cs \rightarrow Cs^+ + Cs^-$$

allowed us[1] to determine lower limits for the bond energy of Cs_2^+ and the electron affinity of Cs. The measurement of the rate of drift of Cs^+ and Cs_2^+ through gaseous Cs gave[2] a measurement of the long range interaction potential in Cs_2^+, and the polarizability of Cs.

From a mass spectrometric determination of the ion composition of photoionized ammonia and methyl amines,[3] we have deduced the equilibrium constants and thermodynamic properties of solvation reactions such as

$$NH_4^+(NH_3)_{n-1} + NH_3 = NH_4^+(NH_3)_n.$$

Complete, accurate, single ion thermodynamic properties will be determined in the not distant future.

Free electrons can be detected with great sensitivity through their effect on the dielectric constant of a gas at microwave frequencies. Using this technique, it has been possible to determine rate constants for dissociative recombination reactions like

$$e^- + NO^+ \rightarrow N + O$$

and electron capture and dissociative attachment reactions such as[4]

$$e + SF_6 \rightarrow (SF_6^-)^* \xrightarrow{M} SF_6^-$$
$$\rightarrow SF_5^- + F$$
$$\rightarrow SF_5 + F^-.$$

The mutual neutralization of gaseous ions is an ideal system from which to learn about three-body recombinations in general. By studying such processes as

$$NO^+ + NO_2^- \rightleftarrows (NO^+NO_2^-)^*$$
$$(NO^+NO_2^-)^* + M \rightarrow (NO^+NO_2^-) + M \rightarrow \text{neutrals}$$

we[5] have learned how to predict ion recombination rates. We have also learned that in stabilizing ion pairs, a multicollision "diffusional" process is important.

Finally, the study of metathetical ion-molecule reactions by using ion beam techniques has revealed important information about the nature of reactive collisions.[6] Exothermic hydrogen atom transfer reactions like $N_2^+ + H_2 \rightarrow N_2H^+ + H$ have been shown to involve principally grazing collisions, and to produce ion products which are very highly excited internally.

1. Y. Lee and B. H. Mahan, J. Chem. Phys. 42, 2893 (1965).
2. Y. Lee and B. H. Mahan, J. Chem. Phys. 43, 2016 (1965).

3. M. Mosesman (Ph. D. Thesis), University of California, UCRL-18459.
4. B. H. Mahan and C. E. Young, J. Chem. Phys. 44, 2192 (1966).
5. B. H. Mahan and J. C. Person, J. Chem. Phys. 40, 392 (1964).
6. B. H. Mahan, Accounts of Chemical Research 1, 217 (1968).

3. DYNAMICS OF THE REACTION OF N_2^+ WITH H_2, D_2, AND HD*

William R. Gentry, Eric A. Gislason, Bruce H. Mahan, and Chi-wing Tsao

Product velocity vector distributions have been determined for the reactive and inelastic scattering of N_2^+ by H_2, D_2, and HD. From these velocity vector distributions we learned that the reaction proceeds by a direct interaction mechanism, that the internal excitation energy of the products is a function of their scattering angle, and that most of the ionic products are scattered in the original direction of the N_2^+ projectile at a speed somewhat greater than that predicted from the ideal stripping model. Velocity ratio plots showed that the ideal knockout mechanism fails to give a quantitative explanation of the velocity or occurrence of backscattered products.

From the differential cross sections computed from the velocity vector distributions we drew further support for the direct interaction mechanism and the predominance of forward scattering. The isotopic variation of this differential cross section at three angles and its dependence on projectile energy showed that the degree to which the reaction product can be stabilized through recoil may in large measure account for observed isotope effects. The observations that the total reaction cross section falls with increasing projectile energy and is nearly the same for all isotopes at the same energy relative to the abstracted atom further reflect the importance of product stabilization through recoil at high collision energies.

From the studies of nonreactive scattering we found an inelastic process that increases in importance with increasing projectile energy. Together with charge transfer and dissociative charge transfer, collisional dissociation of H_2 is an important channel which competes with chemical reaction at high collisional energies.

*Abstracted from J. Chem. Phys. 49, 3058 (1968).

4. DYNAMICS OF THE REACTIONS OF N_2^+ WITH CH_4 AND CD_4*

Eric A. Gislason, Bruce H. Mahan, Chi-wing Tsao, and Arthur S. Werner

This study of the product velocity vector distributions has shown that over a wide range of projectile ion energies, the most probable reactive event is abstraction of a hydrogen or deuterium atom by the stripping process. Although little or no linear momentum is imparted to the methyl radical in such collisions, it is left with a substantial amount of internal energy, particularly when the projectile energy is large. Even for the highest projectile energies there is little forward recoil of the N_2H^+, in contrast to what was found for the N_2^+-H_2, D_2, and HD systems. In the relatively small range of angles where reactive scattering could be detected, Q was found to be a function of angle, with product internal excitation increasing with increasing scattering angle.

The nonreactive scattering was very weak at low projectile energies because of competition with reactive scattering. The disappearance of nonreactive scattering at all energies for angles greater than 30° indicates that small impact parameter collisions are overwhelmingly reactive or highly inelastic and spread the products very thinly over a large region of velocity space. At high projectile energies the nonreactive scattering is very inelastic, and there exists at $\theta = 0°$ and Q = -8.2 eV a feature which may be due to the electronic excitation of methane or of N_2^+: a very large isotope effect is observed in the reactive scattering, with the N_2D^+ product of much lower intensity and confined to smaller angles than the N_2H^+ ion.

*Abstracted from UCRL-18380 and a paper accepted for publication in the Journal of Chemical Physics.

5. DYNAMICS OF THE REACTION OF Ar^+ WITH D_2

Mervyn M. Chiang, Eric A. Gislason Bruce H. Mahan, Chi-wing Tsao, and Arthur S. Werner

We have studied the velocity vector distributions of Ar^+ and ArD^+ which result from Ar^+-D_2 collisions. Most ArD^+ is formed by grazing collisions and proceeds in a direction very near to that of the Ar^+ projectile. Forward recoil that stabilizes the product ion is found for the projectile energies above 50 eV in the laboratory system. The internal energy of ArD^+ scattered at small angles is usually very close to the dissociation energy of ArD^+. The product ArD^+ which is scattered through larger angles is also internally excited, but to a lesser degree.

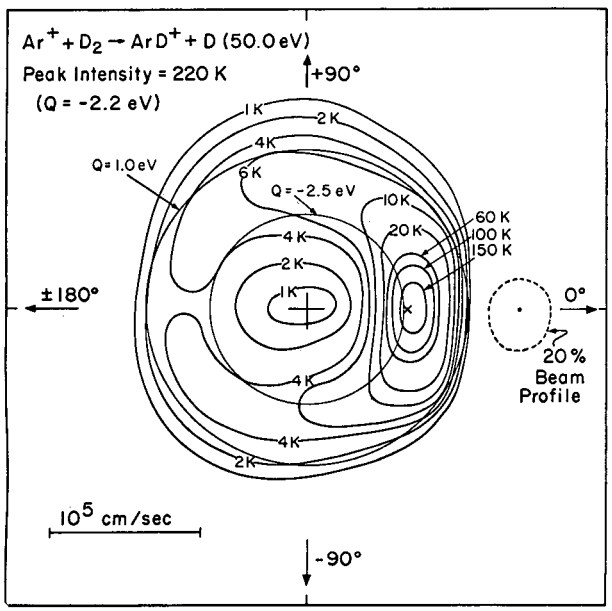

XBL 692-220

Fig. 1. A contour map of the intensity of ArD^+ product from the Ar^+-D_2 reaction plotted in the center of mass coordinate system. The direction of Ar^+ is taken to define zero degrees. The quantity Q is the relative energy of products minus that of reactants.

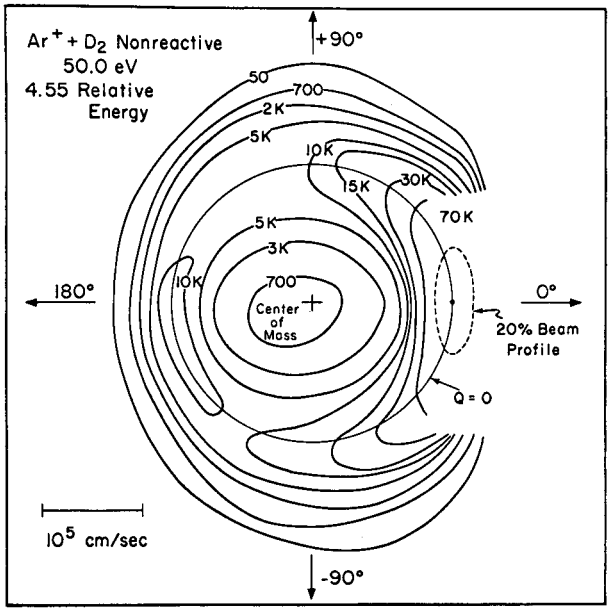

XBL 692-221

Fig. 2. A contour map of the intensity of Ar^+ scattered from D_2 without reaction. The circle labeled Q = 0 corresponds to elastic scattering of Ar^+ by D_2.

Figures 1 and 2 show contour maps of the intensity of ArD^+ and Ar^+ from Ar^+-D_2 collisions. In Fig. 3 we show the distribution of Ar^+ scattered by He. Comparison on these maps and similar ones for different projectile energies shows very strong similarities between reactive and nonreactive scattering from D_2 and scattering from He. One of the most important features is that the intensity of Ar^+ scattered by D_2 through 180° exceeds the intensity of ArD^+ at the same angle. This means that a significant fraction of the Ar^+-D_2 pairs that make head-on collisions fail to react, even though there is no activation energy barrier. From further analysis of the scattering of Ar^+ from He and D_2 we expect to be able to calculate a reaction probability as a function of scattering angles and to convert this to a reaction probability as a function of impact parameter. Preliminary analysis of Ar^+-D_2 collisions at 3 eV relative energy indicates that the reaction probability is approximately 0.3, and the nonreactive probability is 0.7 for angles greater than 60° in the center of mass system. At 7.5 eV relative energy the reaction probability falls to 0.15 or smaller, and again varies relatively slowly with angle.

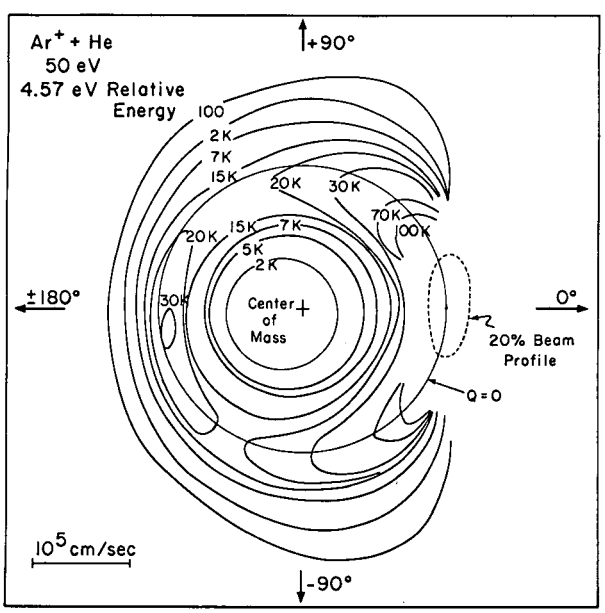

XBL 692-222

Fig. 3. A contour map of the intensity of Ar^+ scattered by helium. Note the similarity of this pattern to the reactive and nonreactive scattering of Ar^+ by D_2.

6. ISOTOPE EFFECTS IN THE REACTION OF N_2^+ WITH ISOTOPICALLY SUBSTITUTED METHANES

Mervyn Chiang, Mien Cheng, Eric A. Gislason, Bruce H. Mahan, Chi-wing Tsao, and Arthur S. Werner

We have determined the reaction cross sections per atom for N_2H^+ and N_2D^+ abstracted from CH_4, CH_3D, CH_2D_2, CHD_3, and CD_4. These cross sections are given in Table I for two projectile-target relative energies. The results have not yet been explained in detail, but some general observations are appropriate. First, the ratio of cross section for forming N_2D^+ from CH_3D and N_2H^+ from CH_4 is 29.6 at 8.8 eV relative energy and is 35.5 at 11.4 eV. Thus there can be a very large isotope effect associated with the mass of the atom transferred, even when the radical (CH_3 in this case) is the same for the two reactions. The magnitude of this effect does depend on the isotopic composition of the radical, since the cross-section ratios for N_2H^+ from CHD_3 and N_2D^+ from CD_4 are only 1.49 and 2.42 at 8.8 and 11.4 eV. Another demonstration that the radical composition matters is the fact that the cross-section ratios for N_2H^+ from CHD_3 and CH_4 are 0.15 and 0.17 at 8.8 and 11.4 eV. An attempt to explain these observations by using a minimum number of assumptions about the intermolecular potential is presently underway.

Table I. Reaction cross sections per isotopic atom.

E_{rel} (eV)	Product	σ_r (Å^2)
	$N_2^+ + CH_3D$	
8.8	N_2H^+	0.237
8.8	N_2D^+	0.059
11.4	N_2H^+	0.231
11.4	N_2D^+	0.042
	$N_2^+ + CH_2D_2$	
9.0	N_2H^+	0.275
9.0	N_2D^+	0.098
11.7	N_2H^+	0.194
11.7	N_2D^+	0.051
	$N_2^+ + CHD_3$	
9.4	N_2H^+	0.270
9.4	N_2D^+	0.123
12.2	N_2H^+	0.257
12.2	N_2D^+	0.069
	$N_2^+ + CH_4$ or CD_4	
8.7	N_2H^+	1.74
12.5	N_2D^+	0.181
8.7	N_2H^+	1.48
12.5	N_2D^+	0.106

7. DYNAMICS OF THE REACTIONS OF O_2^+ WITH H_2 AND D_2

Mervyn Chiang, Mien Cheng, Eric A. Gislason, Bruce H. Mahan, Chi-wing Tsao, and Arthur S. Werner

A collision between O_2^+ and H_2 has at low energies four possible channels:

$$O_2^+ + H_2 \rightarrow HO_2^+ + H \qquad \Delta E_0^0 = +1.99 \text{ eV}$$
$$\rightarrow OH^+ + OH \qquad \Delta E_0^0 = +1.98 \text{ eV}$$
$$\rightarrow O^+ + H_2O \qquad \Delta E_0^0 = 1.6 \text{ eV}$$
$$\rightarrow H_2O^+ + O \qquad \Delta E_0^0 = 0.6 \text{ eV}$$

In contrast to the reactions previously investigated in this laboratory, two of these processes are endothermic. Using a relative collision energy of 3 eV, we have determined the velocity vector distribution for all four ionic products. The distributions of OH^+ and of H_2O^+ are definitely isotropic in the center of mass system. The distribution of HO_2^+ is somewhat uncertain at present, due to interferences from the projectile O_2^+ at small angles, but appears either to be isotropic or backward peaked. These results suggest that HO_2^+, OH^+, and H_2O^+ all come from a common collision intermediate $H_2O_2^+$, which lives for several rotational periods. In contrast, the very weak O^+ signal appears to result from a stripping process. Study of the energy distributions of HO_2^+, OH^+, and H_2O^+ will show how the energy is shared among the dissociating products of a unimolecular decay process.

8. MASS SPECTROMETRIC STUDY OF PHOTOIONIZED GASES*

Michael Mosesman and Bruce H. Mahan

Ammonia, methyl-, dimethyl-, and trimethylamine were photoionized at pressures ranging from 0.03 to 10 mm Hg. The intensities of the many ions of the type $NH_4^+(NH_3)_n$ and $CH_3NH_3^+(CH_3NH_2)_n$, etc. were measured as a function of pressure and temperature; and equilibrium constants ΔH and ΔS for the various ion-solvent association reactions

were determined. The results indicate clearly that a closed solvation shell exists about $NH_4^+(NH_3)_n$ when n is equal to 4. Similarly, for $CH_3NH_3^+(CH_3NH_2)_n$, the equilibrium constants for formation of complexes fall when n is greater than 3. Apparently four massive groups about the central nitrogen atom complete the first solvation shell, as might be expected.

*Abstracted from UCRL-18459.

9. RESEARCH PLANS FOR CALENDAR YEAR 1969

Bruce H. Mahan

In 1969 we will concentrate on the dynamics of ion-molecule reactions as revealed by molecular and ion beam experiments. Extensive investigations of the reactions of O_2^+, OH^+, O^+, N^+, C^+, and F^+ with H_2, D_2, and hydrocarbons will be carried out. Experiments on the vibrational excitation of H_2 and D_2 by alkali ions will be performed.

10. 1968 PUBLICATIONS

Bruce H. Mahan and Associates

Technical Journals

1. W. R. Gentry, Y. Lee, and B. H. Mahan, Charge Transfer Between Positive Alkali Ions and Atoms, J. Chem. Phys. 49, 1758 (1968).
2. W. R. Gentry, E. A. Gislason, B. H. Mahan, and C.-W. Tsao, Dynamics of the Reaction of N_2^+ with H_2, D_2, and HD, J. Chem. Phys. 49, 3058 (1968).
3. B. H. Mahan, Dynamics of Ion-Molecule Reactions, Accounts of Chemical Research 1, 217 (1968).
4. B. H. Mahan, The Chemistry of Gaseous Ions, Vortex 29, 454 (1968).
5. B. H. Mahan, Gaseous Ion Recombination V, J. Chem. Phys. 48, 2629 (1968).
6. E. K. Parks, Capture Radius for Ion Recombination, J. Chem. Phys. 48, 1483 (1968).

UCRL Reports

1. E. A. Gislason, B. Mahan, C.-W. Tsao, and A. Werner, Dynamics of the Reaction of N_2^+ with CH_4 and CD_4, UCRL-18380, August 1968.
2. M. Mosesman, Mass Spectrometric Study of Photoionized Gases (Ph. D. Thesis), UCRL-18459, September 1968.

11. EPR SPECTRUM OF Co^{2+} IN α-$NiSO_4 \cdot 6H_2O$

W. Thomas Batchelder and Rollie J. Myers

The stable α phase of $NiSO_4 \cdot 6H_2O$ has some unusual properties. In this crystal each Ni^{2+} is surrounded by six water molecules. These waters form an octahedral coordination but with a tetragonal distortion. The $(3d)^8$ configuration of the Ni^{2+} forms a high-spin triplet but the spin-spin interaction parameter is close to 5 cm^{-1} in value. The ground state for each Ni^{2+} is nondegenerate and at helium temperatures there is no first-order paramagnetism. All the Ni^{2+} are identical except that they form a helix around the c axis of a tetragonal crystal; as a result, the crystal has some unusual electric and magnetic properties.[1] It is also possible to grow very large single crystals, and such crystals are commercially available.

At 1.3°K the most obvious features to the EPR spectrum of single crystals of α-$NiSO_4 \cdot 6H_2O$ are due to Co^{2+} impurity. The amount of this impurity is very difficult to establish but it is less than 0.01%. This spectrum is highly anisotropic and it is complicated by the eight hyperfine lines due to ^{59}Co. The angular dependence in the a-c and a-b planes are fit moderately well by an axial spin Hamiltonian with $A_{\parallel} = 322 \times 10^{-4}$ and $A_{\perp} = 27 \times 10^{-4}$ cm^{-1} and with $g_{\parallel} = 6.685$ and $g_{\perp} = 3.106$. These parameters indicate a high-spin Co^{2+} with a tetragonal distortion similar to the Ni^{2+}.

The Co^{2+} spectrum provides a very convenient method of identifying the a or b axis in the tetragonal α-$NiSO_4 \cdot 6H_2O$. The Co^{2+} appears to substitute exactly for the Ni^{2+} in the helix around the c axis. The spin parameters for the Co^{2+} indicate that their tetragonal, or z, axis is twisted by 61° away from alignment along the c axis. The magnetic evidence[2] for the Ni^{2+} gives this angle as closer to 39° for the Ni^{2+} sites. The source of this large difference is presently being investigated, for it is probably due to a fundamental problem associated with assignment of the z axis rather than to a difference caused by substitution.

Our work on the Co^{2+} spectrum is preliminary to the more important problem of the magnetic interactions between the Ni^{2+} in this lattice. The Co^{2+} is a convenient probe for the general problem of the Ni^{2+} sites in this interesting material.

1. S-L Hou, Paramagnetoelectric Effect in $NiSO_4 \cdot 6H_2O$, ONR Technical Report 458, Harvard University (1964).

2. J. W. Stout and W. B. Hadley, J. Chem. Phys. 40, 55 (1964); R. A. Fischer and E. W. Hornung, J. Chem. Phys. 48, 4284 (1968).

12. EPR SPECTRA OF MAGNETIC EXCITONS IN α-$NiSO_4 \cdot 6H_2O$ AT HELIUM TEMPERATURES

W. Thomas Batchelder and Rollie J. Myers

The magnetic susceptibility and heat capacity of single crystals of α-$NiSO_4 \cdot 6H_2O$ have been extensively studied.[1] These investigations have shown that these properties can be accurately predicted by the assumption of a noninteracting lattice of Ni^{2+} spins. These Ni^{2+} spins are triplets with a positive D value equal to 4.74 cm^{-1} and an E value equal to zero. The positive D value gives the Ni^{2+} a nondegenerate ground state, and at a few degrees Kelvin only a small fraction of the Ni^{2+} are populated in the excited state. With E = 0 this excited state is doubly degenerate in the absence of a magnetic field and interactions between the Ni^{2+} spins.

With a small amount of interaction between the Ni^{2+} spins the excited states can migrate from site to site. In this way these excited states should form a band structure and they should have the characteristics of magnetic excitons. The application of a magnetic field will split any magnetic degeneracy, so EPR spectra should be possible between these exciton states. We have observed such EPR spectra in α-$NiSO_4 \cdot 6H_2O$ over the range 1.2 to 4.2°K.

When H_1 is perpendicular to H_0 a strong EPR absorption can be observed. With single crystals and powdered samples we have shown that this absorption is most prominent when H_0 is perpendicular to the c axis of the crystals and pointed along the x axis of a Ni^{2+} site. With this orientation our measurements confirm the $g_\perp$ and D value previously obtained,[1] but they do require that $E \approx 0.03$ cm^{-1}. When H_0 is no longer along the x axis of a Ni^{2+} site then the position of the EPR absorption becomes temperature dependent. At the lowest temperature, a small rotation of H_0 away from the x axis will cause a very large decrease in the field for the absorption maximum. Such temperature dependence is good evidence for an exciton structure.

When H_1 is parallel to H_0 a strong EPR dispersion is observed. While we have used EPR quanta ranging from 0.3 to 1.2 cm^{-1} and H_0 values from 0 to 12,000 gauss, we have not been able to detect the absorption which is associated with this dispersion. One must assume that this dispersion is associated with the exciton structure since isolated Ni^{2+} spins should not have such an effect. Our investigation of this interesting type of exciton is continuing.

1. R. A. Fischer and E. W. Hornung, J. Chem. Phys. 48, 4284 (1968).

13. THE USE OF LEAST-SQUARES CURVE FITTING FOR THE DETECTING OF MINOR ISOTOPE STRUCTURE IN EPR SPECTRA

James J. Chang and Rollie J. Myers

With our data acquisition system and associated least-squares fitting programs[1] we are able to fit solution EPR spectra with great accuracy. This technique can be used both for a complex organic radical or for the more simple case of broad-line transition-metal spectra. Many EPR spectra contain hyperfine patterns that are caused by minor (0.1 to 10%) isotopes. In some cases these patterns are partially resolved and can be measured without interference from the main spectrum, but in many cases the main spectrum completely obscures the hyperfine pattern from the minor isotopes. This report is an attempt to detect a ^{33}S hyperfine pattern in a broad-line transition-metal complex. It illustrates the difficulties in this technique.

An attempt has been made to study the bis(maleonitriledithiolato) nickel (III) complex[2] with this technique. Observation of a hyperfine pattern due to the sulfur atoms coordinated to the nickel ion is of importance in the interpretation of the chemical bonding in the complex. However, a sulfur hyperfine pattern can only arise from interaction with ^{33}S isotope, which is only 0.74% abundant.

The EPR spectrum of the complex in solution has been measured at 9.2 GHz. At about -25° the spectrum consists of a single line with a derivative peak-to-peak line width of 6.2 gauss (see Fig. 1). A least-squares fit has been made to the main line to produce a difference spectrum (the theoretical minus the experimental spectrum). This is shown as the lower curve in Fig. 1 with a scale expansion of 40.38.

The difference spectrum shows two lines each about 7 gauss from the center of the main line. However, it has not been possible to assign these lines to ^{33}S splitting. It is more probable that these lines are due to hyperfine interaction with the 1.25% abundant ^{61}Ni isotope. The ^{61}Ni hyperfine lines have been observed in an isotopically enriched sample of the complex,[3] and were observed to occur in the same region as the two lines that we observe.

One of the difficulties in assigning the spectrum is due to the noise appearing in the center of the spectrum. The origin of the

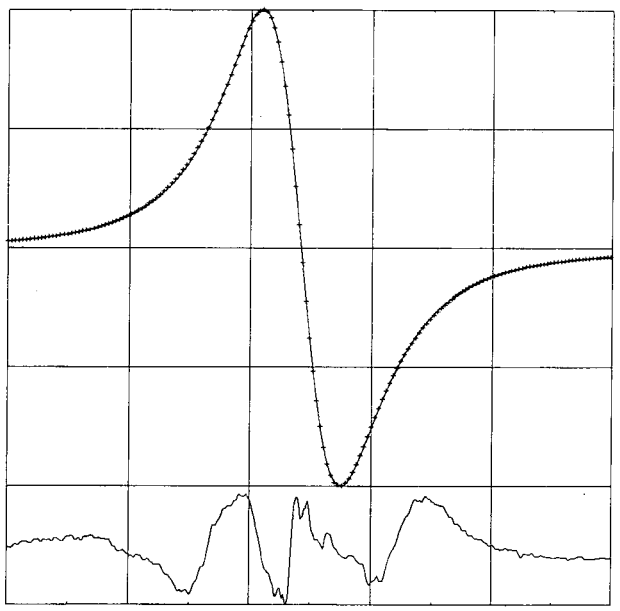

Fig. 1. A least-squares fit to a Ni^{3+} complex in solution. The experimental data from 10 EPR spectra were averaged and are given by the crosses in the figure. The best least-squares fit with a single Lorentz line is shown as the solid curve. The bottom error curve has a scale expansion of 40.38. Minor isotopes should appear in the error curve.

noise is not well understood, but it might possibly arise from an error in the magnetic field measurement by the data acquisition system. Another problem is that minor impurities can also give EPR signals which could be similar to those expected from minor isotopes. Work is in progress to improve the measurement and the analysis.

1. A. Bauder and R. J. Myers, J. Mol. Spectr. 27, 110 (1968).
2. We thank Professor A. Maki, Department of Chemistry, Riverside, for the sample.
3. A. H. Maki, N. Edelstein, A. Davison, and R. H. Holm, J. Am. Chem. Soc. 86, 4580 (1964).

14. AMINE RADICALS GENERATED IN LIQUID AMMONIA

Chia-tung Pao and Rollie J. Myers

Liquid ammonia has been shown to be an excellent medium for the electrolytic generation of radical anions. In the case of conjugated olefins[1] and aromatic nitrogen-heterocyclics,[2] the EPR spectra of many unstable radical anions can be examined in liquid ammonia. As part of our investigation of the usefulness of this solvent we have investigated the electrolytic reduction of arylamines in this solvent with EPR.

The anion radical of p-phenylene diamine has been prepared in liquid ammonia by electrolytic reduction at -50°. The radical anion is quite stable and its EPR spectrum shows a complex structure with more than 59 observed hyperfine components. Three isotropic coupling constants have been assigned to the aromatic ring protons, amine protons, and the ^{14}N nuclei. Our least-squares adjusted computer program and our data-reduction system will be used to obtain accurate assignments, and line width information.

A line width variation phenomenon is observed in this anion radical spectrum. Its total width between the centers of the outermost observed lines is considerably larger than that in the cation radical spectrum. The comparison between the radical anion parameters with the radical cation ones from previous work[3] can be used to obtain information about the hyperfine coupling mechanisms. In particular we want to know more about the importance of the sigma-pi interactions and conjugation effects between the amino group and aromatic ring.

A well resolved ESR spectrum has also been obtained from the electrolytic reduction of aniline. The radical spectrum appears to be that of a protonated neutral radical, which may be produced either from the direct reduction of protonated aniline at the cathode or from the protonation of aniline radical anion by ammonia.

1. D. H. Levy and R. J. Myers, J. Chem. Phys. 44, 4177 (1966).
2. C. Talcott and R. J. Myers, Mol. Phys. 12, 549 (1969).
3. M. T. Melchior and A. H. Maki, J. Chem. Phys. 34, 471 (1961).

15. RESEARCH PLANS FOR CALENDAR YEAR 1969

Rollie J. Myers

Our low temperature work on α-$NiSO_4 \cdot 6H_2O$ and related compounds will be continued. The effect of the exciton structure on its EPR spectrum will be further developed. We plan to try a proton NMR experiment on the waters of hydration to determine the rate of exciton

transfer. We also plan to examine several cases of dynamic Jahn-Teller distortions in transition-metal complexes.

The measurement of electron spin relaxation times will be extended to closed shell ions such as Cr^{3+}, Fe^{3+}, and Gd^{3+}. A study will be made of the EPR line shapes for these ions in solution and the spin relaxation mechanism which is important for these ions. This kind of problem is an ideal application of our digital data recording system and of our fitting programs.

The instrumentation phase of our gaseous radical spectrometer should be completed. Our present plans call for the use of photolysis in the vacuum ultraviolet region for the production of radicals and excited electronic states of atomic and molecular systems. If funds are available we would like to acquire a small digital computer for on-line digital data reduction to complement our present off-line system.

The use of our least-squares fitting programs and of our digital data recording system will be continued for transition-metal complexes in solution and for organic radical spectra.

16. 1968 PUBLICATIONS

Rollie J. Myers and Associates

Technical Journals

1. A. Bauder and R. J. Myers, Least Squares Curve Fitting of EPR Spectra, J. Mol. Spectr. 27, 110 (1968).
2. D. C. McCain and R. J. Myers, Electron Paramagnetic Resonance Studies of Complex Ion Formation Between Mn^{2+} and F^-, Cl^-, I^- or SO_4^{2-}, J. Phys. Chem. 72, 4115 (1968).

UCRL Reports

1. D. W. Pratt and R. J. Myers, The Nuclear Magnetic Resonance Spectrum of Liquid VCl_4, UCRL-18517, October 1968.

17. KINETICS OF NO_2 ELECTRONIC FLUORESCENCE

Stephen E. Schwartz and Harold S. Johnston

The fluorescence lifetime and intensity of gas phase nitrogen dioxide ($^2B_1$) have been measured as a function of excitation wavelength, fluorescence wavelength, and pressure. The phase-shift method was used; this technique allows lifetime measurements to be obtained with signal intensities of 100 counts per second and lower. The excitation source, tunable throughout the visible region, had a half-width bandpass as low as 15 Å. Fluorescence wavelength separation was accomplished with interference filters. The radiative lifetimes range from 55 to 90 μsec for excitation from 3980 to 6000 Å, and tend to increase with excitation wavelength; however, the lifetimes exhibit considerable variation within a narrow excitation region.

The fluorescence sample was contained in a 33 cm diameter spherical bulb; apparent fluorescence lifetimes in smaller cells were reduced because of migration of excited molecules (under collision-free conditions) and wall quenching. In order that the measured lifetime exhibit no more than 5% error, observation must be extended beyond the excitation region to a distance five times the product of the lifetime by the most probable velocity.

The phase-shift method gives both the lifetime and the intensity of the fluorescence. For excitation at 4800 Å or 20,830 cm^{-1} and for observation at three different wavelengths at lower energy, the fluorescence rate constant (reciprocal lifetime) is plotted against pressure in Fig. 1. A similar plot of inverse intensity is given by Fig. 2. By interpolation and extrapolation of such curves, the lifetime as a function of pressure and wavelength is given by Fig. 3 (for excitation at 4000 Å or 25,000 cm^{-1}). A similar plot of intensity is given by Fig. 4.

The Stern-Volmer analysis of fluorescence kinetics has been generalized to a multilevel system under conditions of modulated excitation and phase-sensitive detection. Analysis of fluorescence data in terms of this mechanism yields average values for energy transfer rate constants and efficiencies (amount of energy lost by the excited polyatomic molecule per effective collision). Energy transfer rate constants for excited NO_2 ($^2B_1$) with a ground state collision partner are approximately gas kinetic; efficiencies are approximately 2300 cm^{-1}.

---

1. P. Pringsheim, Fluorescence and Phosphorescence (Interscience, New York, 1949).
2. a) J. L. Steinfeld and W. Klemperer, J. Chem. Phys. 42, 3475 (1965); b) J. L. Steinfeld, J. Chem. Phys. 64, 17 (1967).
3. J. T. Yardley and C. B. Moore, Jr., J. Chem. Phys. 45, 1066 (1967).
4. D. Neuberger and A. B. F. Duncan, J. Chem. Phys. 22, 1693 (1954).
5. G. H. Myers, D. M. Silver, and F. Kaufman, J. Chem. Phys. 44, 718 (1966).
6. A. E. Douglas, J. Chem. Phys. 45, 1007 (1966).
7. P. N. Clough and B. A. Thrush, Trans.

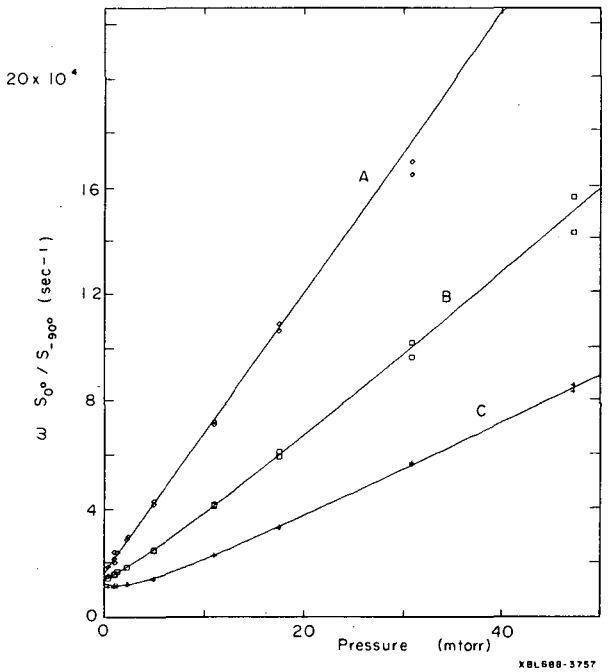

Fig. 1. Stern-Volmer graphs of lifetime data. Excitation energy: 4800 Å or 20,830 cm^{-1}. Observation energy: A, 19,960; B, 17,880; C, 14,270 cm^{-1}.

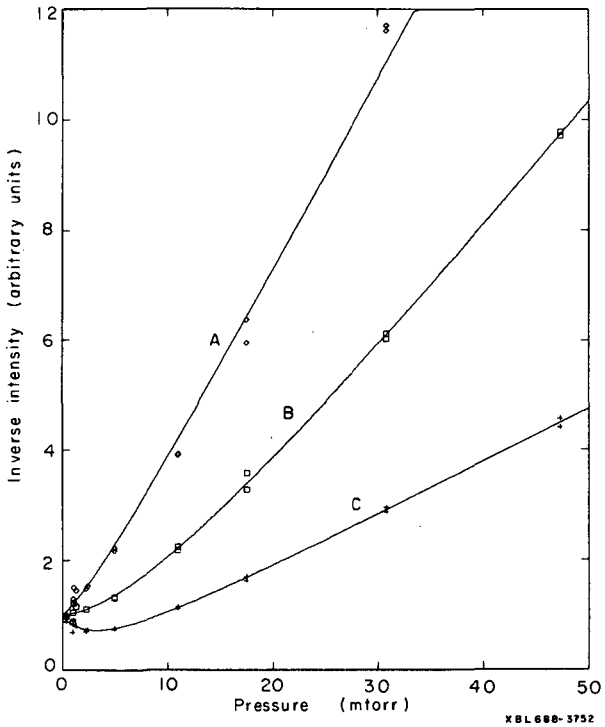

Fig. 2. Stern-Volmer graphs of intensity data. Excitation energy: 4800 Å or 20,830 cm^{-1}. Observation energy: A, 19,960; B, 17,880; C, 14,270 cm^{-1}.

Faraday Soc. 63, 915 (1967).
8. G. W. Robinson, J. Chem. Phys. 47, 1967 (1967).
9. J. Jortner and S. Berry, J. Chem. Phys. 48, 2757 (1968).

18. CHEMILUMINESCENCE FROM IF

Stephen D. Gabelnick* and Harold S. Johnston

Upon mixing fluorine and iodine (even at pressures around 10 to 50 mtorr), there is a fast reaction upon contact and a weak visible chemiluminescence (Fig. 1). The emission has been attributed to the $^3\Pi_{0+} \rightarrow {}^1\Sigma_{0+}$ transition of the chemically unstable molecule IF, which had previously been observed in a high-pressure fluorine-iodine flame by Durie.[1,2] This spectrum includes the calibration of our monochromator for wavelength and the calibration of the photomultiplier for spectral sensitivity.

The potential energy functions and vibrational levels of the two electronic states are given by Fig. 2. To go from the observed spectrum to relative populations in the excited electronic state, it was necessary to evaluate the electric transition moment for each

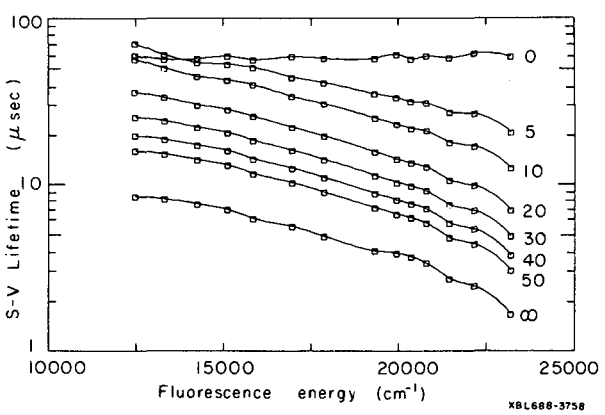

Fig. 3. Lifetime spectra as a function of pressure. Lifetimes were computed from fitted curves of R^{-1} by the Stern-Volmer relation $\tau = \omega^{-1} S_{-90°}/S_{0°}$. The running index gives the pressure in mtorr. The relative lifetime distribution obtained from the infinite pressure extrapolation is not scaled with respect to the ordinate. Excitation energy: 4000 Å or 25,000 cm^{-1}.

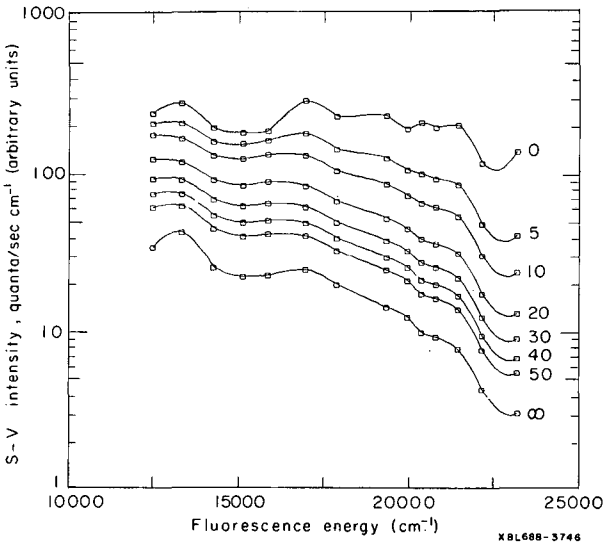

Fig. 4. Intensity spectra as a function of pressure. Intensities were computed from fitted curves of I^{-1}, where I is the Stern-Volmer intensity, $(S^2_{0°} + S^2_{90°})/S_{0°}$. The running index gives the pressure in mtorr. The spectral distribution obtained from the infinite pressure extrapolation is not scaled with respect to the other spectra. Excitation energy: 4000 Å or 25,000 cm^{-1}.

vibronic transition. The electric transition moment involves the Franck-Condon factors that are readily calculated from the potential energy curves and also the $\bar{r}$-centroid function.[3-5] The shape of the band envelope was calculated as a function of slit width and rotational temperature.

Evaluation of the transition moment function is accomplished through a semiempirical method that uses all of the data in a least-squares program, the Franck-Condon factors, and an assumed relation to the $\bar{r}$-centroid function, which was refined by successive approximations. From each of three complete spectra (such as Fig. 1) the transition moment was evaluated as a function of $\bar{r}$-centroid (Fig. 3). The curve shown in Fig. 1 was obtained in this way, and it agrees quite well with the observed intensities.

The radiative lifetime of the excited state is about 10^{-4} sec, which makes it competitive with the lifetime of vibrational deactivation at 10 to 100 mtorr. Thus this case is well suited to a study of collisional deactivation over a range vibrational state. From the rate of gas flow, heat release, and thermal conductivity, the translational temperature is calculated to be about 310-320°K. The width of the intense vibronic bands is a fairly sensitive function of the assumed rotational temperature, and these temperatures are between 500 and 700°K. Although light was detected from vibrational

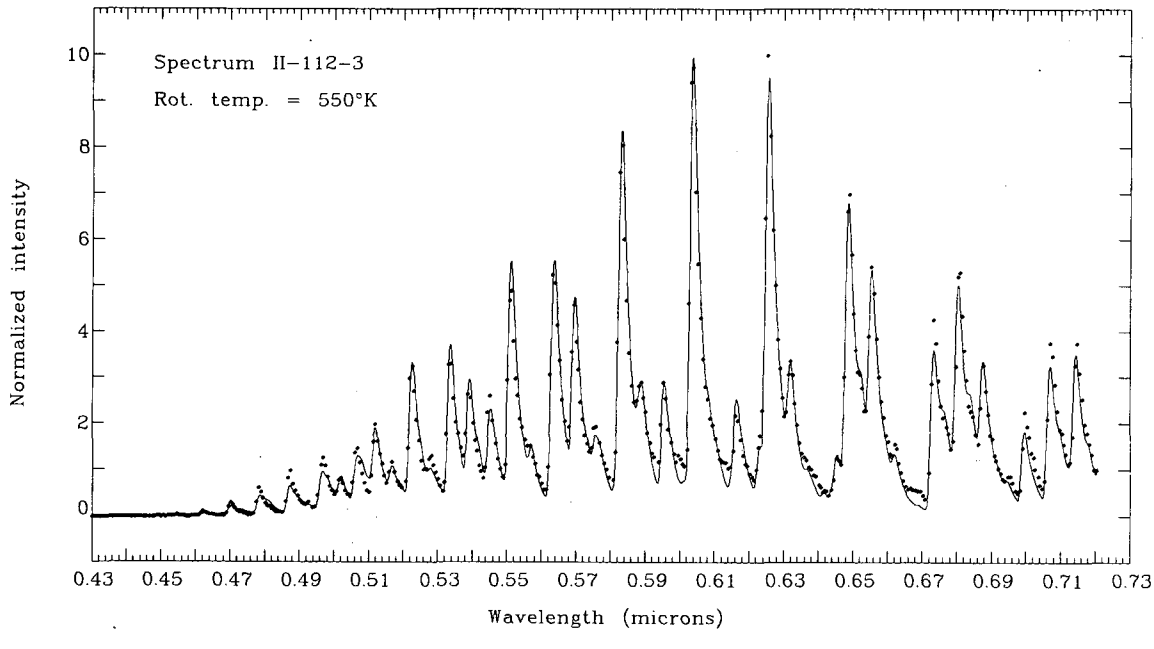

Fig. 1. Example of experimental data.

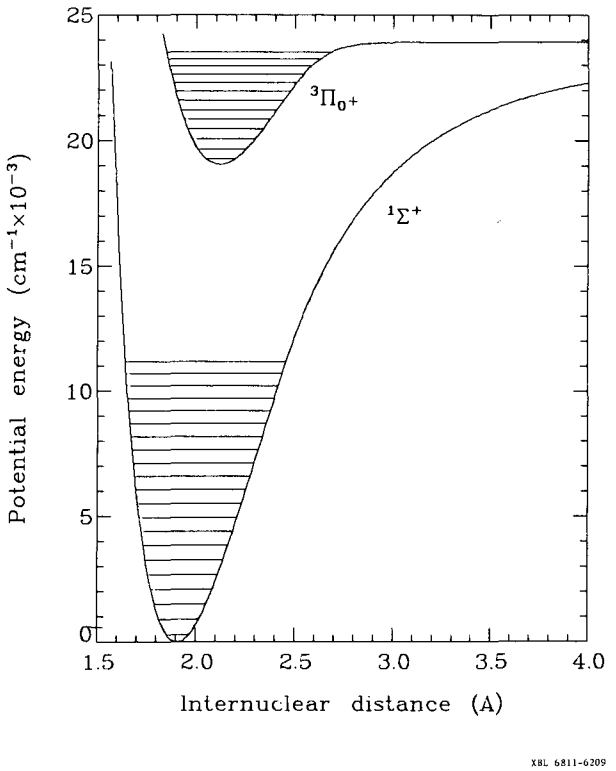

Fig. 2. Potential energy curves and vibrational energy levels of ground-state and excited-state IF.

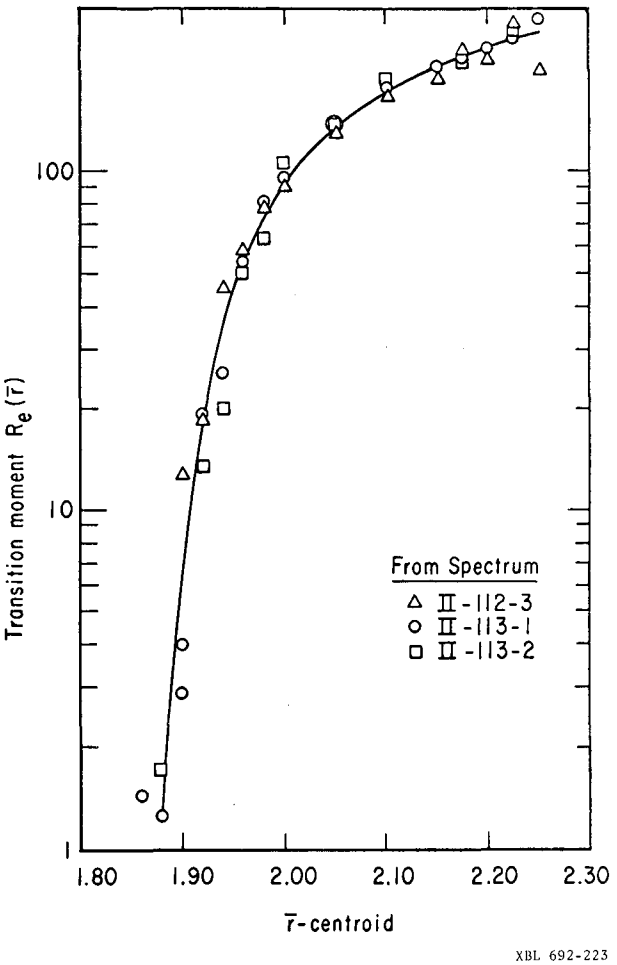

Fig. 3. Transition-moment function.

levels up to v = 11 of the upper electronic state, it is only for the first 5 or 6 levels that the populations are inferred with enough reliability to permit calculation of vibrational temperatures. For the first 5 or 6 levels the vibrational temperature is about 1200-1500°K.

The model for this system is chain reaction between F_2 and I_2 carried by the corresponding atoms. A chain terminating step is $I + F + M \rightarrow IF^* + M$, where IF^* is in a high vibrational state. Collisions of IF^* with inert molecules gives a stepwise deactivation of IF^* and presumably a much faster equilibrium of rotational states to the translational temperature. However, each step of vibrational deactivation, except for the vanishingly rare co-linear collision, would be expected to re-excite the rotations of IF^*, that is,

$$IF^*_{vJ} + M \rightarrow IF^*_{v-1,\, J+x} + M.$$

So far, only a limited amount of study has been carried out on the variation of total pressure and the addition of inert gases. However, enough study of this kind has been made to indicate that this system provides an exceptional opportunity for the study of molecular dynamics of highly vibrationally excited diatomic molecules.

---

*Present address: Argonne National Laboratory, Argonne, Illinois.

1. R. A. Durie, Proc. Roy. Soc. (London) A207, 388 (1951).
2. R. A. Durie, Canad. J. Phys. 44, 337 (1966).
3. P. A. Fraser, Canad. J. Phys. 32, 515 (1954).
4. R. G. Turner and R. W. Nicholls, Canad. J. Phys. 32, 457 (1954).
5. F. S. Ortenberg and E. J. Antropov, Sov. Phys. -Usp. 9, 717 (1967).

19. SPECTRA AND LIFETIMES OF GAS-PHASE FREE RADICALS AT VERY LOW CONCENTRATIONS

Harold S. Johnston, Edward D. Morris, Jr., Thomas T. Paukert, and Jack Van den Bogaerde

Utilizing the technique of chemical-modulation infrared spectrometry to study the gas phase photolysis of Cl_2 in the presence of O_2, an absorption spectrum attributable to the ClOO peroxy radical was detected and recorded. Spectroscopic evidence for the assignment lies in the near-coincidence of the peak band intensity, at 1443 cm^{-1}, with a fundamental vibrational frequency of matrix-isolated ClOO of 1441 cm^{-1} (Fig. 1). Phase-shift measurements of the modulated absorption signal over a wide range of reactant concentrations and ultraviolet excitation frequencies agreed well with expectation, providing kinetic confirmation for the identification of ClOO. The observed second-order decay of the ClOO radical was consistent with the generally accepted mechanism for the formation and disappearance of this species in Cl_2-O_2 mixtures:

$$Cl_2 + h\nu \rightarrow 2\ Cl$$

$$Cl + O_2 + M \underset{k_{-1}}{\overset{k_1}{\rightleftharpoons}} ClOO + M \qquad (1)$$

$$Cl + ClOO \underset{k_{-2}}{\overset{k_2}{\rightleftharpoons}} 2\ ClO \qquad (2)$$

$$Cl + ClOO \xrightarrow{k_3} Cl_2 + O_2. \qquad (3)$$

The kinetic measurements led to a value for $(k_1/k_{-1})(k_2+k_3)$ of 0.48×10^{-30} cm^6/molecule^2-sec, in close agreement with a reported value of 0.54×10^{-30} cm^6/molecule^2-sec.

Recent determinations by other investigators of pertinent molecular constants of the ClOO and ClO radicals have permitted a new evaluation of the absolute entropies of these species: S°_{298} (ClOO) = 63.0 cal/deg-mole, and S°_{298}(ClO) = 52.4 cal/deg-mole. The estimated thermodynamic properties of the participating species lead to the following values for the equilibrium constants, at 298°K, of reactions (1) and (2):

$$\frac{k_1}{k_{-1}} = 3.64\times10^{-21}\ cm^3/\text{molecule}$$

$$\frac{k_2}{k_{-2}} = 2.27\times10^{2}.$$

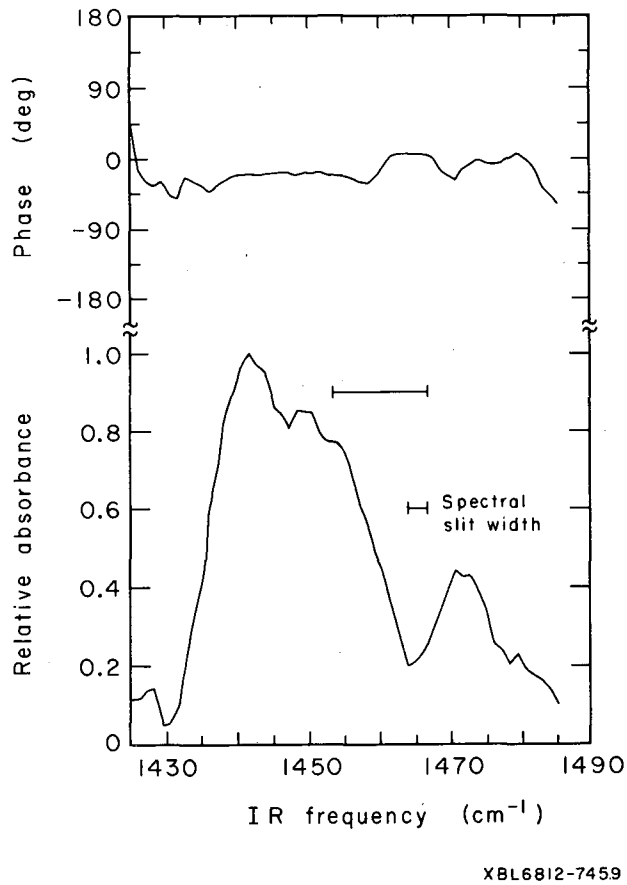

XBL6812-7459

Fig. 1. ClOO absorbance spectrum, based on smooth values of amplitude and phase from a total of 80 scans, taken in 4 mm Cl_2 + 199 mm O_2 + 567 mm He flashed at 2.0 Hz.

From reported values of the rate constants k_1 and k_{-2}, it may be inferred that $k_{-1} \leq 1.5\times10^{-13}$ cm^3/molecule-sec, $k_2 = 4.15\times10^{-12}$ cm^3/molecule-sec and $k_3 = 1.28\times10^{-10}$ cm^3/molecule-sec, using the presently measured value of $(k_1/k_{-1})(k_2+k_3)$.

The infrared absorption coefficient of the ClOO radical has been determined to be approximately 1.4×10^{-19} cm^2, from the observed degree of modulation of the infrared carrier signal. It is shown that failure to detect the modulated infrared absorption spectrum of the ClO radical in Cl_2-O_2 mixtures implies that the absorption coefficient of this species is probably less than 0.70×10^{-20} cm^2. A further implication of this observation is that the rate constant k_2 cannot be much larger than the estimated value given here.

Further attempts to observe the modulated infrared absorption spectrum of ClO by

the addition of CO to Cl_2-O_2 mixtures resulted in the detection of three, presently unidentifiable, modulated absorption bands of radical species. Of these, an intense band centered at 937 cm^{-1}, is shown conclusively not to be due to the ClO radical. Neither of the other two bands, centered at 1835 and 1905 cm^{-1} and of moderate intensity, can arise from the ClCO radical, on kinetic grounds.

1. G. Porter, Discussions Faraday Soc. 9, 60 (1950).
2. G. Porter and F. J. Wright, Discussions Faraday Soc. 14, 23 (1953).
3. M. A. A. Clyne and J. A. Coxon, Trans. Faraday Soc. 62, 1175 (1966).
4. A. Arkell and I. Schwager, J. Am. Chem. Soc. 89, 5999 (1967).
5. E. D. Morris, Jr. and H. S. Johnston, J. Am. Chem. Soc. 90, 1918 (1968).

20. HYDROGEN ATOM SPECTROMETER

Philip Dow and Harold S. Johnston

We have constructed a microwave Zeeman-modulated cavity-resonance spectrometer to measure hydrogen atom concentrations in a variety of kinetic and photochemical studies. We follow the 21-cm microwave, zero-field transition. This spectrometer resembles previous instruments built with Wittke[1] and the various hydrogen maser groups.[2] The requirements of high field and stringent homogeneity limit commercial ESR spectrometers to small sample volumes, with attendant problems of surface reactions at the low pressures required for these studies. By going to low fields (6 gauss maximum) we have been able to increase the sample volume to 1.6 liters.

Hydrogen atoms have been generated by a microwave discharge external to the cavity. A large hydrogen atom signal has been observed. The width of the signal is determined by the collision-induced "spin-flip" between two hydrogen atoms, and since this reaction is second order in atoms the width is proportional to hydrogen atom concentration so long as no other spin-flip mechanism is important. We have added small concentrations of nitric oxide or of oxygen to the system. Additional line broadening is observed, and this is a measure of the spin-flip rate as induced by the added paramagnetic gas. Further addition of nitric oxide leads to a decrease in total integrated absorption as the reaction

$$H + NO + M \rightarrow HNO + M$$

becomes important. The kinetics of this and related reactions is being studied in this spectrometer.

1. J. P. Wittke, A Redetermination of the Hyperfine Splitting in the Ground State of Atomic Hydrogen (Ph. D. Thesis), Princeton University, 1955.
2. D. Kleppner, H. C. Berg, S. B. Crampton, N. F. Ramsey, R. F. C. Vessott, H. E. Peters, and J. Vanier, Phys. Rev. 138A, 972 (1965); D. Kleppner, H. M. Goldenberg, and N. F. Ramsey, Phys. Rev. 126, 603 (1962).
3. K. W. Lamers, ESR Spectrometer for Gaseous Media, UCRL-17306, October 1967.

21. RESEARCH PLANS FOR CALENDAR YEAR 1969

Harold S. Johnston

Over the past 3 or 4 years, a major fraction of our effort has been devoted to developing several different methods of directly observing active intermediates in chemical and photochemical reactions. During 1968 the emphasis largely shifted to taking of data, but some further improvement of the methods is still underway. Components have been bought, and next year we will assemble what should be a great improvement on the infrared molecular modulation spectrometer. The IF chemiluminescence apparatus needs the relatively minor modification of changing the 1.4 liter stainless steel reaction bulb to a 400 liter stainless steel reaction tank, which has been procured for this purpose. The hydrogen-atom spectrometer needs some replacement parts to ensure better long-time stability. The molecular-modulation method using the mass spectrometer has not yet been put in operation, and work continues on it.

The experimental results on the NO_2 fluorescence and the IF chemiluminescence give detailed information about the effect of collisions on highly vibrationally excited molecules. In each case the work is being continued with a new graduate student. The fluorescence of NO_2 will give better information about the effect of collisions on very high vibrational states if excitation and emission at an adjacent wavelength is studied, pairwise, over a wide range of spectra, instead of the method so far used. Also at this time we want to study the effect of added inert gas on the redistribution of vibrational levels in the excited NO_2 molecules. The chemiluminescence of IF will be extended to much lower pressure, below 1 mtorr, and the effect of added inert gas will be studied in detail.

The study of molecular modulation of the Cl_2, O_2 system is drawing to a close, since we feel that this problem is essentially solved.

Further work will continue on the related system: Cl_2, O_2, CO. In this system we see a strong signal from an unidentified intermediate, and we'll try to find out what it is. The HOO radical is seen, but the signal-to-noise remains poor. For this radical, we hope to obtain much better results on the new infrared system. We plan to extend our study of peroxy radicals (ClOO and HOO, so far) to other members, especially CH_3OO and HCOOO.

The hydrogen atom spectrometer will be used to detect hydrogen atoms as side products in photolysis of simple aldehydes and ketones. The reactions of hydrogen atoms with atmospheric species, O_2, NO, and NO_2 will be continued. The rate of recombination of hydrogen atoms as a function of temperature will be followed to low temperatures. After the cavity is set up to work at low temperatures, we plan to take fast bimolecular reactions of hydrogen atoms to low temperatures, with special attention to possible quantum kinetic effects.

22. 1968 PUBLICATIONS

Harold Johnston and Associates

Technical Journals

1. H. S. Johnston and E. D. Morris, Jr., Ultraviolet Spectrum of the ClOO Radical, J. Am. Chem. Soc. 90, 1918 (1968).
2. H. S. Johnston and E. D. Morris, Digital Phase Sensitive Detector, Rev. Sci. Instr. 39, 620 (1968).
3. H. S. Johnston, Gas Phase Reaction Kinetics of Neutral Oxygen Species, U. S. Department of Commerce, National Bureau of Standards, NSRDS-NBS 20, p. 1 (1968).

UCRL Reports

1. Harold S. Johnston, Gas Phase Elementary Chemical Reactions, UCRL-18256, May 1968.
2. Stephen E. Schwartz, Kinetics of Nitrogen Dioxide Fluorescence (Ph. D. Thesis), UCRL-18431, September 1968.

23. MOLECULAR BEAM KINETICS: MAGNETIC DEFLECTION ANALYSIS OF THERMAL ENERGY Li ATOM REACTIONS

David D. Parrish and Ronald R. Herm

Laboratory angular distributions have been measured for both the non-reactive and reactive scattering of Li atoms from Cl_2, ICl, Br_2, $SnCl_4$, PCl_3, CH_3I, CCl_4, SF_6, CH_3NO_2, and NO_2. The two reactant beams, which crossed at an angle of 90°, were formed by thermal effusion (with full Maxwellian velocity distributions) from ovens mounted on a platform which could be rotated with respect to a stationary detector. Measurement of the scattered Li reactant and LiX reaction product intensities by two-filament differential surface ionization proved impractical. Instead, a heated oxygenated W filament was employed to ionize both the Li and LiX with comparable efficiencies; an inhomogeneous magnet, placed between the collision zone and detector, deflected aside a known fraction of the Li atoms when energized, thereby providing a measure of the scattered Li and LiX signals separately.

The transformations of the measured laboratory angular distributions into the center-of-mass (c. m.) coordinate system by the fixed velocity approximation[1] has been completed only for the data obtained with the first five reactants listed above. The derived total reaction cross sections, reactive attenuations of the wide angle elastic scattering, and product recoil energies correlate roughly with trends previously established in studies with the heavier alkali metals;[2] these observations suggest that qualitatively similar forces are operative in the reactions of all of the alkali metals. However, as Figs. 1 and 2 illustrate, the LiX product c. m. angular distributions are broader and more complex than those found in studies with the heavier alkali metals.

The origin of these "anomalous" LiX product distributions is not completely understood; nevertheless, they suggest an important mass effect in the overall alkali atom reaction dynamics. This effect might arise because the Li atom, by virtue of its lighter mass, is rapidly accelerated by the reactant gas; this may seriously influence the partitioning of momentum in the dissociating reactant. Moreover, if the Li is accelerated to within a close distance before this reactant has split off a product radical, many-body effects may become important, leading to much more complex collision trajectories and thereby producing a broadened product distribution. The qualitative difference between diatomic and polyatomic reactants observed in this study would then correlate with the expected rise in collision lifetime with increasing degrees of freedom in the reactant.

---

1. This is an approximate transformation procedure in which it is assumed that the incoming particles all possess their most probable source velocities and that all particles are scattered with one recoil energy; the product distributions are transformed by varying the recoil energy to obtain a consistent c. m. distribution. Details of this procedure are given in: E. A. Entemann, Ph. D. thesis, Harvard University, 1967.

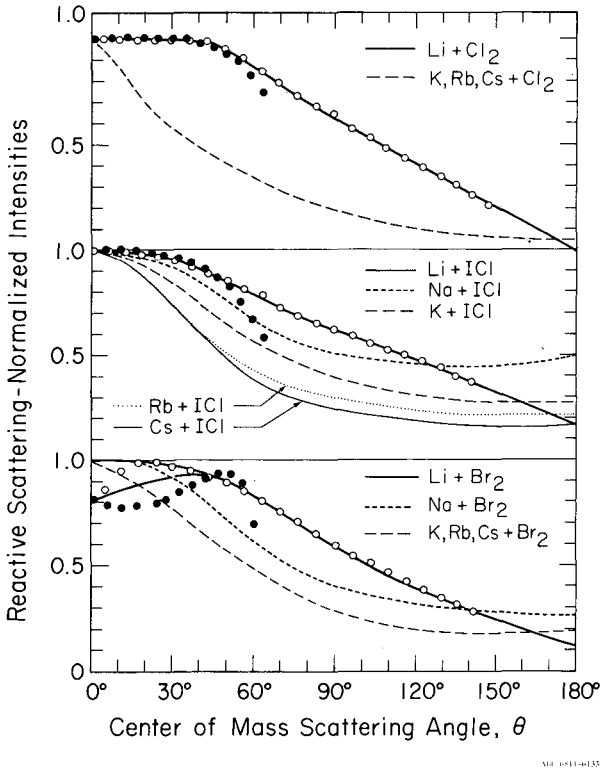

Fig. 1. Comparisons of c.m. alkali halide product angular distributions for reactions of the alkali metals with three diatomic halogen molecules; the results for Na, K, Rb, and Cs were taken from Ref. 2. The Li + Br_2 product distribution is uncertain at narrow angles, but is bounded by the two solid curves shown.

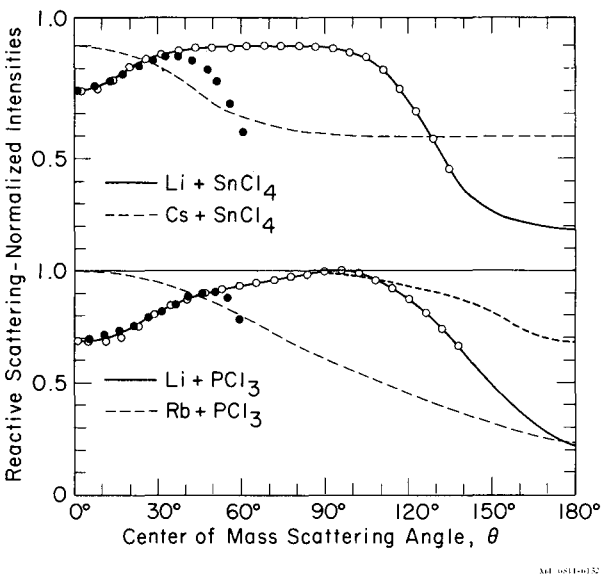

Fig. 2. Comparisons of c.m. alkali halide product angular distributions for reactions of the alkali metals with two polyhalide molecules; data for the heavier alkali metals were taken from Ref. 2. For Li + PCl_3, the solid curve provides the best fit to the measured laboratory distribution, although the totally symmetric distribution (heavy dashed curve) is considered to be within experimental uncertainty.

2. For K, Rb, Cs + Cl_2: R. Grice and P. B. Empedocles, J. Chem. Phys. 48, 5352 (1968); for K, Rb, Cs + ICl: G. H. Kwei, Ph.D. thesis, University of California, Berkeley, 1967; G. H. Kwei and D. R. Herschbach, J. Chem. Phys. (to be published); for K, Rb, Cs + Br_2: J. H. Birely, R. R. Herm, K. R. Wilson, and D. R. Herschbach, J. Chem. Phys. 47, 993 (1967); for Na + ICl, Br_2: J. H. Birely, E. A. Entemann, R. R. Herm, and K. R. Wilson, J. Chem. Phys. (to be published); for Cs + $SnCl_4$ and Rb + PCl_3: K. R. Wilson and D. R. Herschbach, J. Chem. Phys. 49, 2676 (1968).

24. MOLECULAR BEAM KINETICS: CONSTRUCTION OF A CROSSED BEAM APPARATUS TO STUDY REACTIONS OF NEUTRAL NON-ALKALI CONTAINING SPECIES

Shen-maw Lin, Charles A. Mims, and Ronald R. Herm

A crossed molecular beam apparatus has been assembled to make possible the determination of relative reaction cross sections, Q_r; activation energies, E_a; energy partitionings, E'; and reactant and product center-of-mass (c.m.) angular distributions for the reactions of thermal energy, non-alkali containing species. The apparatus consist of three differentially pumped vacuum chambers. The first two chambers, pumped by 10 inch oil diffusion pumps and provided with extensive liquid nitrogen baffling, provide for the preparation of the two crossed reactant beams with full thermal velocity distributions. The first chamber acts as the source chamber for a beam of non-condensible gas; this beam is crossed at 90° in the second chamber by a chopped beam of condensible gas. The third

chamber, housing a commercially purchased quadrupole residual gas analyzer detector with a phase sensitive amplifier locked in at the chopping frequency, is pumped by a combination ion pump and titanium sublimator unit; this entire chamber may be rotated through a full 360° with respect to the first two chambers. Thus, experimentally, reactant and product angular distributions will be measured in the laboratory coordinate system, as a function of reactant temperatures where possible; transformation of these data determine the c.m. angular distributions, Q_r, E_a, and E'.

Calibration experiments have indicated that a pressure of 10^{-9} torr will be maintained in the detection chamber under experimental conditions; this ambient background pressure should result in an acceptable contribution to the noise level in the detector. Initially, reactions of the type F + HR → HF + R and H + XR → HX + R will be studied. Resistance-heated nickel and tungsten tube furnaces have been built to provide the F and H atom beams respectively by thermal dissociation; a power supply providing up to 600 A and 10 V has been constructed to drive these furnaces.

25. PHOTODISSOCIATION OF THE ALKALI HALIDES AND THE QUENCHING OF EXCITED ALKALI ATOMS

Charles A. Mims, Shen-maw Lin, and Ronald R. Herm

During 1968 a program was initiated to extend previous studies[1] of the photodissociation of alkali halide molecules, $MX + h\nu_e \rightarrow M^* + X$. Since the shapes of the potential energy curves for the ground electronic states of the alkali halides are well known, measurements of the M^* fluorescence intensities as a function of excitation frequency, ν_e, will determine the dependences on internuclear separation of the potential energy for the excited states leading to dissociation. Once this is known, the velocity distribution of the M^* produced by the possible simultaneous photodissociation of a number of vibrational levels may be calculated as a function of ν_e. Subsequent measurements of the M^* fluorescence intensities as functions of foreign gas pressures will then be used to determine the velocity dependences of the M^* quenching cross sections.

A UV monochromator and light source, a high temperature cell to vaporize the alkali halides, and an interference filter-photomultiplier combination to monitor the M^* fluorescence have been assembled; experiments should commence early in 1969. Initially, experiments will be confined to the low excited states of the alkali metals and to quenching gases which react very rapidly with ground state alkali metal atoms. Diffusion flame and cross molecular beam determinations of the cross sections for reactions of ground state alkali metal atoms with these gases have been interpreted in terms of an "electron jump" mechanism; these experiments are intended to determine the role of this same mechanism in collisions which lead to quenching of the excited alkali atoms.

---

1. See, for example, the following: H. G. Hanson, J. Chem. Phys. 23, 1391 (1955); J. Gatzke, Z. Physik. Chem. 223, 321 (1963).

26. THE ENERGY DEPENDENCE OF THE CROSS SECTION FOR SENSITIZED FLUORESCENCE: Hg^* + Tl

Lambert C.-H. Loh, David D. Parrish, and Ronald R. Herm

Equipment has been assembled that will make possible the determination of the energy dependence of the total cross sections for the transfer of electronic excitation from the 6s6p $^3P_0$ and $^3P_2$ metastable levels of mercury to a Tl or a Na atom. The Hg^* atoms will be produced by electron bombardment and detected by Auger ejection of electrons from a continuously deposited potassium surface; this beam will be crossed by a velocity-selected beam of Tl or Na atoms, which will be detected by surface ionization. An interference filter-photomultiplier combination beneath the collision zone will measure the fluorescence from electronically excited Tl or Na produced by inelastic collisions.

A large fraction of our total effort on this project during 1968 was involved with the testing, modification, and calibration of the rotating disk velocity selector, which had been assembled during 1967. The selector can now be rotated at angular frequencies well in excess of 30,000 rpm for long periods of time with no detrimental effects, even while exposed to the temperature gradients prevailing during a beam experiment. As a final check, a transmitted beam of Li atoms is currently being analyzed in an inhomogeneous deflecting magnetic field in order to insure that no harmonics are transmitted by the velocity selector and to experimentally determine the resolution of the selector. These final tests are being run with a beam that is a mixture of Li and LiI. During these tests, a search is being made for the previously unreported molecule Li_2I which might be in equilibrium with the Li and LiI; the combination of magnetic and velocity dispersion employed in these tests should make possible the separation

of equilibrium mixtures of these three species. A crude model, based on ionic bonding of Li_2^+ to I^-, would suggest that this molecule might be quite stable.[1] In the event that no Li_2I is observed, it is hoped that an analysis of the noise level in the experiment will provide a useful limit to the equilibrium constant for the reaction $Li + LiI = Li_2I$.

1. A theoretical calculation based on an ionic model has predicted the existence of the molecule KNaCl; see: A. C. Roach and M. S. Child, Mol. Phys. 14, 1 (1968).

27. A STUDY IN PHOTOINDUCED ELECTRONIC CHEMILUMINESCENCE: THE $Hg^* + Cl_2$ REACTION†

R. Peter Frosch,‡ Lara A. Gundel, and Ronald R. Herm

Fluorescence has been observed from the $B^2\Sigma$ state of HgCl upon irradiation of a Hg-Cl_2-He flowing gas mixture by the 2537 Å Hg resonance line. Emission is observed only from vibrational levels in the $HgCl^*$ which could be populated by the exothermic reaction:

$$Hg^*(^3P_1) + Cl_2 \rightarrow HgCl^*(B^2\Sigma) + Cl(^2P). \quad (1)$$

Experience provided by diffusion flame and crossed beam studies of the reactions of alkali atoms with halogen molecules suggested that electronically excited atoms, by virtue of their relatively low ionization potentials, might undergo reactions of this type quite readily.

Work is continuing on this project with the investigation of the pressure dependences of the observed fluorescence and the determination of the quenching cross section for $Hg^*(^3P_1)$ by Cl_2. It is hoped that a knowledge of the pressure dependences will establish that the observed fluorescence is indeed chemiluminescence resulting from reaction (1). Once this is proven the vibrational energy level population distribution produced by this reaction will be determined by comparisons of the low pressure limit total emission intensities from the different vibrational levels in the $HgCl^*$. Subsequent measurements of the spectra band intensities as a function of foreign gas pressures should provide rate constants for vibrational energy relaxation in this state as well.

†This work is supported directly by the Lawrence Radiation Laboratory only to the extent of financial support for one of the investigators (LAG).

‡Not affiliated with LRL; assistant professor, Department of Chemistry, University of California, Berkeley.

28. RESEARCH PLANS FOR CALENDAR YEAR 1969

Ronald R. Herm

Work on the crossed beam investigation of F and H atom reactions, the photodissociation of alkali halides, the energy dependence of the sensitized fluorescence cross sections, and the mercurous chloride fluorescence will be continued.

The crossed molecular beam study of Li atom reactions begun two years ago is now complete, although analysis of the data collected will continue into 1969. During 1969, a new experimental investigation will be initiated, designed to determine more detailed features of these reactions. The existing inhomogeneous magnetic analyzing field will be replaced by a combination magnetic and electric deflecting field. Moreover, a low resolution slotted disk velocity selector will be inserted between the collision zone and detector as well. These modifications should make possible direct measurements of the distributions in lithium halide product recoil energies and rotation excitations.

29. 1968 PUBLICATIONS

Ronald R. Herm and Associates

1. R. J. Gordon, R. R. Herm, and D. R. Herschbach, Molecular Beam Kinetics: Magnetic Deflection Analysis of Scattering of Alkali Atoms from Polyhalide Molecules, J. Chem. Phys. 49, 2684 (1968).
2. D. D. Parrish and R. R. Herm, Possible Mass Effect in Alkali-Atom Reactions: Crossed Beam Studies of Li + Cl_2, ICl, Br_2, $SnCl_4$, and PCl_3, J. Chem. Phys. 49, 5544 (1968).

30. ELECTRON DELOCALIZATION IN TRANSITION METAL COMPLEXES

Charles B. Harris

The purpose of this experiment is to investigate the mechanisms of electron delocalization in some transition metals complexes, principally $Cu_2(CH_3CO_2)_4$.

A study of the ^{13}C line width and chemical shift as a function of concentration and temperature will be performed.

These data should give meaningful information about mechanisms of electron delocalization in transition metal organometallic complexes.

31. ELECTRON SPIN-SPIN INTERACTION IN TRANSITION METAL COMPOUNDS

Charles B. Harris

A current project is the synthesis, characterization, x-ray crystallographic structure, and electron spin resonance study of the octahedral cobalt (and other transition metals) complex of two organic ring nitroxide radicals:

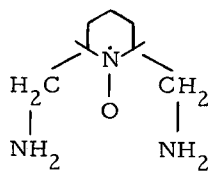

The oxygen (or possibly the ring nitrogen) will serve as one of the axial ligands, and the two amino groups will serve as two of the four equatorial ligands. (The metal should display C_{2h} point-group symmetry.) The steric hindrance of adjacent methyl groups should ensure great stability for the radical.

At present, the synthesis of the radical (a ten-step scheme, over-all) is underway. Materials being used are laboratory glassware and chemicals, instruments for characterization and synthesis (NMR, IR, VPC, pH meter, mass spectrometer, etc.). Following the proposed synthesis, x-ray diffraction equipment will be used to determine the actual structure of the metal-diradical complex. And finally, ESR equipment will be used to study the spin-coupling of the radicals through the central metal atom.

32. ELECTRONIC AND BONDING PROPERTIES OF ORGANO-RARE-EARTH COMPLEXES

Charles B. Harris

A study of a new group of organo-rare-earth sandwich complexes has been undertaken. The first of these, a complex of uranium (IV) with cyclooctatetraene dianion called uranocene, was prepared by Professor Andrew Streitweiser's research group. A complex of thorium has also been prepared and plans are being made to study other ligands. These compounds show a number of interesting and unusual properties. For example, uranocene is extremely stable to hydrolysis, which is unusual for compounds of uranium (IV). Also it is suspected that it may undergo stepwise oxidation, losing two electrons, one at a time.

The aims of this study will be to bring a number of physical methods to bear on the problem of illucidating the electronic structure and nature of the bonding in these compounds (i.e., the degree of covalency or ionicity). Methods used in the near future will be temperature-dependent measurements of the magnetic susceptibilities, NMR spectroscopy, and polarography.

33. NUCLEAR QUADRUPOLE RESONANCE (NQR) ZEEMAN STUDIES

Charles B. Harris

This project has been undertaken in order to gain information about the bonding in transition metal compounds, and resolve problems such as the unexplained large asymmetry parameter of Re_2CO_{10}, the cause of the trans effect, and the possibility of bent bonds.

By studying the angular dependence of the Zeeman splitting of a single crystal, information about the direction, magnitude, and asymmetry of the field gradient about a nucleus is obtained.

The interpretation of these data leads to experimental information regarding the electronic environment of the nuclei and consequently is used to resolve questions related to bonding.

34. TRANSITION METAL NQR

Charles B. Harris

Using a slow sweep super regenerative NQR spectrometer, approximately ten sets of resonances were found in organometallic compounds containing Co, Re, and Mn. The ^{59}Co NQR resonances in $MX_3Co(CO)_4$ (M = Si, Ge, Sn, Pb; X = Cl, Br, I, C_6H_5) were studied. Analysis of the data elucidated explicit features of the M-Co bond. In particular σ and π bond effects could be semiquantitatively evaluated.

A versatile frequency modulated marginal spectrometer capable of giving very accurate frequency measurements was developed. Using this instrument the temperature-dependent ^{55}Mn NQR of (pyrrole) $Mn(CO)_3$ and (cyclopentadienyl) $Mn(CO)_3$ was studied. The data suggest that the Mn-pyrrole anion bond is significantly distorted via a pyrrole slippage and might be described as a four electron metal-heterocyclic allyic and two electron metal-olefin bond rather than a six electron Π-cyclopentadienyl type bond. The crystal structure will be determined by using x-ray techniques.

35. PULSED NQR DOUBLE RESONANCE OF EXCITED ELECTRONIC STATES OF PYRAZINE

Charles B. Harris

This project has been undertaken in order to gain information about the electron distribution of the first excited triplet state of pyrazine. In particular we are interested in the spatial distribution of the wave functions.

In order to acquire this information a double resonance technique is being used which gives a sensitivity of 10^{16} nuclei/cc.

Paradichlorobenzene is used as a matrix for a 1 mole % concentration of pyrazine.

The Cl nucleus on the paradichlorobenzene is excited at its NQR frequency by short (1-10 μsec) pulses of rf energy in a 90-180° sequence. As a result of this an echo is produced as the magnetization regains phase coherence following the pulse sequence.

Double resonance is achieved when the nitrogen nucleus is excited at its NQR frequency between the 90 and 180° pulses. The experimental conditions are adjusted to give maximum dipolar coupling between the nuclei. When this is achieved it is detected by a decrease in the amplitudes of the echo produced by the paradichlorobenzene. The pyrazine is then excited to a long-lived triplet state (18 msec) and a search for the new nitrogen NQR frequency is made.

From the frequency of the nitrogen resonance the quadrupole coupling constant and asymmetry parameter are calculated directly. Using various models, information about the electronic structure is calculated.

36. 1968 PUBLICATIONS

Charles B. Harris and Associates

Technical Journals

1. C. B. Harris, Transition Metal Nuclear Quadrupole Resonance I, J. Inorg. Chem. 7, 1517 (1968).
2. C. B. Harris, Transition Metal Nuclear Quadrupole Resonance II, J. Inorg. Chem. 7, 1691 (1968).
3. C. B. Harris, An Evaluation of the Fe^{57} Nuclear Quadrupole Moment, J. Chem. Phys. 49, 4 (1968).

UCRL Reports

1. T. L. Brown, P. A. Edwards, C. B. Harris, and J. L. Kirsch, The Pure Nuclear Quadrupole Resonance Spectrum of Cobalt-59 in Adducts of Cobalt Tetracarbonyl, $MX_3Co(CO)_4$, UCRL-18515, October 1968.
2. F. A. Cotton and C. B. Harris, The Structure of Tetraphenylarsonium Bis-(N-Cyanodithiocarbimato) Nickelate (II), UCRL-18249, June 1968.

37. THERMODYNAMICS AND MOLECULAR STATE OF STRONG ACIDS

Otto Redlich, Richard W. Duerst, and André Merbach

The problem of the dissociation of strong electrolytes was first discussed in 1887. The first quantitative answer was presented in the first of a series of papers in 1943. The eleventh (last) paper of this series has now been published. It contains the interpretation of nuclear magnetic resonance measurements of the systems HNO_3-DNO_3-water and $HClO_4$-$DClO_4$-water. The work has been concluded.

38. THERMODYNAMIC CALCULATION METHODS

Victoria B. T. Ngo* and Otto Redlich

The demonstration of efficient methods in examples of thermodynamic calculations has been continued.

Optimum conditions in the synthesis of ammonia are considerably influenced by the fugacity coefficients of the components of the gaseous mixture. Sample computations have been prepared.

The use of automatic computers for the determination of the equilibrium in a complex system of simultaneous reactions has been repeatedly discussed in the literature. The method is based on finding the minimum of the total free energy of Gibbs under the prescribed conditions. The working of this method has been demonstrated in a simple example (cracking of methane) by computation of a sequence of steps leading to the minimum of the free energy.

The equation of state containing two parameters proposed by Redlich and Kwong 20 years ago has been frequently used. Various improvements have been suggested. On one hand, a two-parameter equation can never be satisfactory for all technical problems. On the other hand, the old equation has looked so promising that a really satisfactory relation has always been expected by introduction of one or two more individual parameters. This has been repeatedly attempted by several authors.

The most conspicuous shortcoming of the old equation is the inability to reproduce the individual variations of the critical compressibility factor Z_c, which is between about 0.29 to 0.25 for almost all substances. The old equation implies a fixed Z_c at 0.333 (van der Waals 0.375). It is at the critical isotherm and in the vicinity of the critical point that a new individual parameter should furnish a significant improvement.

The present work has been based on the observation that two useful functions, G and L, of the molal volume can be introduced into the old equation

$$P = RT(1-L)/(V-b) - a(1-G)/[T^{0.5}V(V-b)].$$

One can impose general conditions on the functions G and L which ensure that the equation will furnish the correct value Z_c at the critical point. This value is introduced as the third parameter. The principal conditions for G and L are (1) that they contain the volume V and the critical volume V_c through the intermediate variable

$$\Delta = 3V_c/V - 3(V_c/V)^2 + (V_c/V)^3,$$

(2) that G is zero at the critical point, and (3) that both are zero at zero pressure and infinite pressure.

The resulting equation represents the critical isotherm and reduced temperatures down to 0.8 very satisfactorily. For higher temperatures a further additional term has been introduced. The final results are satisfactory.

A program for the computation of the compressibility factor Z according to the new equation has been developed.

*Present address: Shell Development Company, Emeryville, California.

39. FUNDAMENTAL THERMODYNAMICS

Otto Redlich

The clarification of the basic concepts is believed to be completed in the essential points that precede a discussion of the two laws.

An important, though somewhat subtle, problem has been encountered. The definition of a quantity in the physical sciences is always based on a measuring procedure that enables us to compare the quantity being defined with a chosen standard. Such a procedure furnishes a Dedekind cut, i.e., a decision: smaller, or equal, or larger. In this decision the classical axiom of the excluded third is implied. Buchdahl has applied this method in an excellent, lucid definition of entropy. Later, however, he retracted his original method and loaded it with cumbersome complications on the grounds that a continuous variable is not exhaustible. The significance of this question goes far beyond the definition of entropy and will require further examination.

40. LEACHING OF CLAY WITH ACIDS

Irundi Edelweiss* and Otto Redlich

In the final tests clay was leached first with dilute sulfuric acid and the liquor was rejected. Subsequently the leach was continued with sulfurous acid. The results were in accord with the preceding ones. The first leach with sulfuric acid did remove some of the silica but the main extract, obtained with sulfurous acid, still contained unacceptable amounts of silica.

This work has clarified the role of silica in acid clay leachings to some extent. In dilute sulfuric acid (e.g., 0.01 mole/liter) amounts of silica and alumina extracted are of the same order of magnitude. In strong sulfuric acid (6 moles/liter) only alumina and no silica is extracted. In sulfurous acid the silica/alumina ratio is around 0.02. The technical requirement is 0.0002.

The practical result is negative. No combination of reasonable leaching steps appears to furnish alumina free of silica.

This investigation has been concluded.

*Present address: Salvador-Bahia, Brazil.

41. RESEARCH PLANS FOR CALENDAR YEAR 1969

Otto Redlich

Thermodynamic Calculation Methods

Extensive checking of the computer programs developed and preparation for publication.

Fundamental Thermodynamics

Investigation of special problems. Preparation of papers for didactic purposes.

42. 1968 PUBLICATIONS

Otto Redlich and Associates

Technical Journals

1. R. W. Duerst, Ionization of Strong Electrolytes X. Proton Magnetic Resonance of the Ternary System $HClO_4$-$DClO_4$-H_2O-D_2O, J. Chem. Phys. 48, 2275 (1968).
2. O. Redlich, R. W. Duerst, and A. Merbach, Ionization of Strong Electrolytes XI. The Molecular States of Nitric Acid and Perchloric Acid, J. Chem. Phys. 49, 2986 (1968).
3. O. Redlich, W. E. Gargrave, and W. D. Krostek, Thermodynamics of Solutions XIII. Consistency of Sparse Data. Activities of Nitric and Perchloric Acids, Ind. Eng. Chem. Fundamentals 7, 211 (1968).
4. O. Redlich and W. E. Gargrave, Reaction Rate and Dissociation of Sulfuric Acid, J. Phys. Chem. 72, 3045 (1968).
5. O. Redlich, Fundamental Thermodynamics Since Carathéodory, Rev. Mod. Phys. 40, 556 (1968).

UCRL Reports

1. I. S. Edelweiss, Clay Leachings With Acids (M.S. Thesis), University of California, Berkeley, UCRL-18099, February 1968.
2. V. B. T. Ngo, Calculation Methods in Chemical Thermodynamics (M.S. Thesis), University of California, Berkeley, UCRL-18510, December 1968.
3. O. Redlich and R. W. Missen, Some Relations for Vapor Liquid Equilibria and Critical Mixtures, UCRL-18520, October 1968.

F. NUCLEAR SCIENCE

MOLECULAR BEAM MASS SPECTROMETER

1. ANALYSIS OF GAS-SOLID SURFACE KINETIC MODELS USING LOCK-IN DETECTION OF MODULATED MOLECULAR BEAMS*

Donald R. Olander

The analytical techniques for extracting surface rate constants from the amplitudes and phase-shift data provided by the lock-in amplifier are developed for several types of gas-solid interactions. Based upon a particular model, the response of the surface emission rate of a particular reaction product or intermediate to the square wave input of the reactant gas molecular beam is calculated. The fundamental mode of the Fourier transform of the emission rate waveform is then determined. This mathematical step represents the operation of the lock-in detector on the output of the mass spectrometer. The analytical method is applied to the following processes:

(a) Slow, competitive first- and second-order surface reactions. The effect of the background gas on the response of the lock-in detector is described.

(b) Two slow competitive first order reactions each of which is followed by a slow desorption step. While data from a modulated beam experiment can in principle determine all four of the rate constants involved, the equivalent dc molecular beam experiment provides only the ratio of two of the rate constants.

(c) Competition between rapid first order desorption and solution and diffusion of the adsorbed atoms in the bulk solid. The balances appear as boundary conditions for the diffusion equation in the bulk medium.

(d) Competition between first order desorption and surface migration.

*Abstracted from paper presented at the Fourth International Materials Symposium, Berkeley, California, June 19-22 (1968).

2. ANGULAR DISTRIBUTIONS FROM MOLECULAR BEAM SOURCES*

Richard H. Jones, Valerie R. Kruger, and Donald R. Olander

An apparatus for measuring the leak rates and angular distributions of the molecular flux from multichannel sources was constructed. Four types of beam sources were tested: a single capillary, a crinkly foil stack, an electron beam milled quartz membrane, and two sources constructed by fiber optics techniques (Mosaic sources).

The conductances of the sources were compared with the predictions of Knudsen flow. The conductances of the Mosaic sources were 30-60% smaller than expected, possibly because of blockage of some of the channels. The conductances of the quartz membrane crinkly foil sources were considerably greater than the values predicted by Knudsen flow indicating the presence of leakage paths other than the observed channels. The conductance of the single capillary source was close to theory.

The angular distributions were characterized by a "peaking factor," defined as the ratio of the center-line beam intensity from the source to that from a cosine emitter of the same total flow rate. The data fell in the transition region between the limiting cases of free molecule flow at low source pressures and isentropic flow at high source pressures.

*Abstract of paper to be published in J. Appl. Phys.

3. GAS PHASE RADIATION CHEMISTRY

Valerie Kruger and Donald R. Olander

The apparatus for the analysis of radiation-induced gas phase reactions by molecular beam mass spectrometry has been constructed. The irradiation source is the 1 MeV proton beam from a Van de Graaff accelerator. A "chemistry cave" at the accelerator site has been constructed. The proton beam issues from the beam port terminated in the concrete shielding wall and enters the low pressure gas through a metal window. The gas flows through a long glass reactor tube at a pressure of 1 torr cocurrent with the proton beam. The end of the reaction tube contains a multi-

channel source for delivery of a molecular beam of the contents of the reaction tube directly to the ionizer of a mass spectrometer. In order to permit measurement of the low concentration of intermediate free radicals of the radiolysis, the proton beam is modulated and the mass spectrometer output is monitored by a lock-in detector at the modulation frequency.

The first system studied will be oxygen, since the only species expected are O, O_2, and O_3, the mass spectrum of which is simpler than any other radiolysis system. The mass spectrometer will be calibrated for O atoms by NO_2 titration of oxygen dissociated by a microwave discharge.

LIQUID METAL RESEARCH

4. VISCOSITIES OF LIQUID METALS

James Finucane and Donald R. Olander

The oscillating crucible viscometer for use with high temperature liquid metals is an absolute method which does not require calibration with liquids of known viscosity. Our apparatus was checked by measuring the viscosity of tin from its melting point at 1000°. The experimental viscosities agreed with literature values to within ±5%.

In attempting to operate the apparatus above 1000°, two problems associated with the passage of large currents (up to 800 A) through the heating element occur. First, significant transformer vibrations were transmitted through the connectors to cause noticeable movement of the pendulum. Second, induced magnetic fields due to the rectified ac heater current exert a force on the suspended crucible. Work on overcoming these difficulties is proceeding, and measurement of the viscosity of uranium will be made as soon as possible.

5. DIFFUSION IN LIQUID URANIUM

Donald R. Olander

Fabrication and initial testing of a system to measure the diffusion coefficients of selected fission product elements in molten uranium has been completed. The diffusion tube is a capillary 0.3 cm in diameter and 10 cm long. Because of the very reactive nature of uranium metal and many metallic fission products, measurements will be conducted in both beryllia and tantalum capillaries. Iodine, lanthanum, and barium are to be investigated. Experiments will be performed using these elements as they exist in minute concentrations directly from fission and also on macroscopic quantities introduced by contacting the molten uranium with large quantities of unirradiated solute. This comparison will indicate whether the small concentration of radioactive fission product solutes are gettered by impurities in the uranium.

The major problem that has been encountered is thermal convective mixing of the liquid in the capillary during melting, freezing, and thermal equilibration with the furnace.

ROTATING DISK STUDIES

6. ANALYTIC STUDY OF THE EFFECT OF CONDENSATION IN THE BOUNDARY LAYER ON MASS TRANSFER FROM A ROTATING DISK

Ronald P. Omberg and Donald R. Olander

The combined effect of convective-diffusion and homogeneous nucleation and condensation on mass transfer through a boundary layer of cold inert gas is described theoretically by a set of conservation equations for the diffusing vapor (termed the monomer) and drops of various sizes. These conservation equations of standard convective-diffusion theory are coupled by the phenomenon of condensation and evaporation exchange between the vapor and the drops. These rates are given by classical homogeneous nucleation theory, which heretofore has been applied only to infinite stationary media (i.e., a cloud chamber).

The combined process is described by a conservation equation for the vapor species:

$$\frac{d^2U}{dx^2} - ScH(x)\frac{dU}{dx} = -Sc\sum_{g=g_0}^{\infty} g(\beta^+_{g-1}V_{g-1} - \alpha^+_g V_g - \beta^+_g V_g + \alpha^+_{g+1}V_{g+1})$$

and a conservation equation for each drop size:

$$\frac{d^2V_g}{dx^2} - g^{2/3}ScH(x)\frac{dV_g}{dx} = -g^{2/3}Sc(\beta^+_{g-1}V_{g-1} - \alpha^+_g V_g - \beta^+_g\beta_g + \alpha^+_{g+1}V_{g+1}),$$

$$g = g_0, g_0+1, g_0+2\cdots.$$

In these equations, U is a dimensionless monomer concentration, V_g is a dimensionless

concentration for drops containing g atoms, x is a dimensionless axial velocity, and Sc is the Schmidt number (the ratio of the kinematic viscosity of the gas phase to the diffusion coefficient of the monomer in the inert species). The coefficients β_g^+ and α_g^+ are dimensionless condensation and evaporation rates for vapor atoms on drops of size g, obtained from classical nucleation theory.[1] Since β_g^+ depends upon U, the set of differential equations is coupled.

The infinite set of coupled differential equations is similar in many respects to the equations obtained by multigroup diffusion theory analysis of the neutron population in nuclear reactors. Consequently we have devised a multigroup scheme for the drops, which permits solution of the problem by machine computation. Preliminary results show that the enhanced vaporization rates reported for other systems[2] to be virtually nonexistent in the rotating disk system. This is primarily because the axial flow on the rotating disk is directed toward the hot surface rather than away from it, as in flow geometries previously considered. Thus drops which are formed by condensation in the highly supersaturated outer portion of the boundary layer are convected back towards the disk where they re-evaporate because of the reduced supersaturation. Drop diffusion also contributes to returning the evaporating species to the surface from which it originated. These return mechanisms act contrary to the tendency of diffusion to remove vapor from the boundary layer, and the net result is to keep the vaporization rate essentially unchanged.

1. R. M. Farley, Proc. Roy. Soc. (London) 212A, 530 (1952).
2. D. Rosner, Intern. J. Heat Mass Transfer 10, 1267 (1967).

7. REFRACTORY METAL OXIDATION

John S. Schofill and Donald R. Olander

Experimental work on the rotating disk oxidation of molybdenum has been completed and data analysis is in progress. Reaction temperatures were varied from 840 to 1700°. Within this range the reaction product (principally MoO_3, with a possible contribution from MoO_2 at the highest temperatures) is volatile, and the overall rate of the reaction is governed both by the surface kinetics and diffusion of reactant to the surface. Oxygen concentrations from 0.2 to 5.0% in inert gas were investigated. The total pressure was 1 atm for all experiments. The rotational speed of the disk was varied from 1000 to 15,000 rpm.

The oxidation rates were found to be surface kinetic limited at low temperatures and diffusion limited at high temperatures. The latter limit was temperature independent and conformed to the rate predicted for rotating disk convective-diffusion. The diffusion limitations become most significant about 1400°, but affect the overall rate even at lower temperatures. The most significant result of diffusion is to falsify the activation energy of the surface kinetic step. Preliminary analysis shows that the surface reaction is first order with respect to oxygen partial pressure at all temperatures.

8. RESEARCH PLANS FOR CALENDAR YEAR 1969

Donald R. Olander

The velocity distribution in molecular beams from multichannel sources will be investigated by comparing the phase lag and amplitude attenuation of the lock-in detector signal with that expected from a Maxwellian beam.

The effect of source diameter and various misalignments on the performance of highly peaked multichannel beam sources will be investigated in the molecular beam-mass spectrometer apparatus.

The apparatus for laser pulsing of solids and mass spectrometric analysis of the ejected vapor will begin.

The radiolysis of oxygen by proton irradiation will be examined.

A smaller heating element will be installed in the oscillating crucible viscometer to permit attainment of temperatures up to 3000° with the available power. An attempt will be made to measure the viscosity of liquid uranium dioxide sealed in tungsten crucibles.

The predicted effect of condensation on rotating disk vaporization will be verified experimentally with the chromium-helium system.

9. 1968 PUBLICATIONS

Donald Olander and Associates

Technical Journals

1. P. Concus and D. Olander, Transient Diffusion in a Composite Slab, Intern. J.

Heat Mass Transfer 11, 610 (1968).
2. R. A. Krakowski and D. R. Olander, Dissociation of Hydrogen on Tantalum Using a Modulated Molecular Beam Technique, J. Chem. Phys. 49, 5027 (1968).
3. A. Pasternak and D. R. Olander, Mass Transfer in Liquid Metal Systems, A. I. Ch. E. Journal 14, 235 (1968).
4. D. R. Olander, Drop Extraction Between Liquid Metals and Fused Salts, Nucl. Sci. Eng. 31, 1 (1968).
5. D. Olander and W. Waddel, Gas Analysis by Modulated Molecular Beam Mass Spectrometry, Anal. Chem. 40, 1687 (1968).
6. D. R. Olander and L. Ruby, The New Curriculum in Nuclear Engineering at UCB, Trans. Am. Nucl. Soc. 11, 44 (1968).

UCRL Reports

1. R. Jones, V. Kruger, and D. R. Olander, Characterization of Multichannel Sources and Design of Molecular Beam Systems for Their Utilization, UCRL-17859, December 1968.
2. D. R. Olander and W. Waddel, Gas Analysis by Modulated Molecular Beam Mass Spectrometry, UCRL-17866 Rev., February 1968.
3. D. R. Olander, Analysis of Gas-Solid Surface Kinetic Models Using Lock-In Detection of Modulated Molecular Beams, UCRL-18234, June 1968.

II. Metallurgy

A. CRYSTAL IMPERFECTIONS

1. PRE-YIELD PLASTIC DEFORMATION IN COPPER POLYCRYSTALS

Gopinathan Vellaikal and Jack Washburn

Pre-yield dislocation motion and multiplication were studied in large grained polycrystalline OFHC copper by the etch pit technique. Specimens were loaded in compression and dislocation arrangements were observed in both the stressed and unstressed conditions.

The following is a summary of the principle results of the investigation:

(a) The dislocation loops generated by the first active sources both on primary and secondary slip planes traversed the entire cross section of the grains and piled up at the grain boundaries. In single crystals this first operation of sources might be missed entirely because all the dislocation loops would have escaped at surfaces.

(b) At an applied stress level at which grain boundary pile-ups containing 10 or more dislocations were numerous in surface grains, none were found in interior grains.

(c) Preferential multiplication of dislocations near an external surface took place even when grown-in dislocations were immobile where they intersected the surface and extreme precautions had been taken not to introduce any fresh dislocations or permit any stress concentrations.

(d) Grown-in dislocations were relatively immobile where they intersected a {111} surface if extensive polishing was avoided following the last high temperature anneal. This was probably due to their tendency to lie at right angles to the {111} surface and therefore to have a high jog density.

(e) Pre-yield dislocation behavior did not appear to be significantly different in low dislocation density crystals of OFHC and 99.999% copper.

The above observations can be explained if it is assumed that all segments of the grown-in network contained jogs after a long anneal at high temperature.

Rapid multiplication of dislocations in interior grains probably becomes general only after a stress is reached that permits motion of dislocation segments of high jog density. At lower stresses most potential sources should generate only a single loop due to formation of a stable dipole.

2. THE FORMATION OF VOIDS AND DISLOCATION LOOPS IN QUENCHED ALUMINUM SINGLE CRYSTALS

Jean L. Strudel* and Jack Washburn

High purity aluminum single crystals were grown and shaped so as to facilitate resistivity measurements, high heating rates, and direct observation by electron transmission microscopy on the same specimen.

The samples were quenched from 425°, 475°, 525°, or 575° to -110° and then pulsed to aging temperatures ranging from -40 to +100°. Isothermal annealing curves were obtained by resistivity measurements at liquid helium temperature.

The apparent activation energy for the annealing was found to be $E_2^m = 0.27$ eV at low T_a, and $E_1^m = 0.48$ eV for $T_a > 20°$. Voids and dislocation loops were present in every case in different proportions with sizes ranging from 40 to 500 Å for the voids and 100 to 6000 Å for loops. The use of ⟨110⟩ single crystals facilitated the observation of very small voids.

The results suggest that a high concentration of divacancies favored the formation of loops.

The results also provided direct evidence that the stress field of a loop significantly increases its ability to collect vacancies: Under conditions where the concentration of secondary defects was small, the trapping efficiency of voids was comparable to that of loops. On the contrary, when the nucleation rate was high, as for instance in a more impure series of specimens or for low aging temperatures after quench from a high temperature, the growth ability was much higher for loops than for voids. In the most extreme case, T_Q = 575° and T_A = -40°, a typical loop collected 10 times as many vacancies as did a typical void.

In these cases a significant fraction of the total number of vacancies that eventually go to each defect come from short distances within which the greater stress fields associated with loops should be effective. Therefore the loops might be expected to attract greater total numbers of vacancies than voids. When defects are far apart, loops should still grow faster during the very early stages, but

most of the growth would occur by random walk of vacancies from greater distances where the stress field of the defect is unimportant. Under these conditions the total number of vacancies reaching a loop should not be greatly different from that reaching a void, as was observed.

---

*Present address: Centre des Materiaux de l'Ecole des Mines, Paris, France.

3. CLIMB OF 1/3 ⟨111⟩ DISLOCATIONS IN GOLD

Michael J. Yokota and Jack Washburn

Factors affecting the rate of climb of 1/3 ⟨111⟩ dislocations in gold have been studied by repeated transmission electron microscopy observations of the same areas during an interrupted anneal. Large 1/3 ⟨111⟩ stacking fault loops were obtained by quenching from 1000° and aging at 150°.

A new technique was devised that permitted measurement of the climb rate for each side of a polyhedral faulted loop independently. The following is a summary of the primary results of the study:

(a) Faulted loops in gold remained angular during shrinkage and did not tend to become round as do hexagonal 1/3 ⟨111⟩ loops in aluminum.

(b) The climb rate of a loop side is independent of its length above a critical length. The experimental observations made in the present investigation suggest that the critical length may be associated with the spacing between jogs.

(c) Within the temperature range studied the rate of climb of sides bounded exclusively by 60° corners was much less than that of sides terminated by at least one 120° corner (see Fig. 1). Jogs are probably nucleated more easily at 120° corners because in this case there must be a contraction of the Shockley partial and the stair-rod dislocation into which the 1/3 ⟨111⟩ dislocation is split.

(d) The distance to the foil surface did not affect the rate of shrinkage. Even sides cut by the surface climbed at normal rates, dependent on whether the other end terminated at a 60° or a 120° corner. This means that jogs were not easily nucleated where a Frank dislocation terminated at a surface.

(e) The apparent activation energy for climb of 1/3 ⟨111⟩ dislocations in gold was found to be 1.9 eV.

(f) Impurity pinning of jogs was suggested by some of the experimental observations.

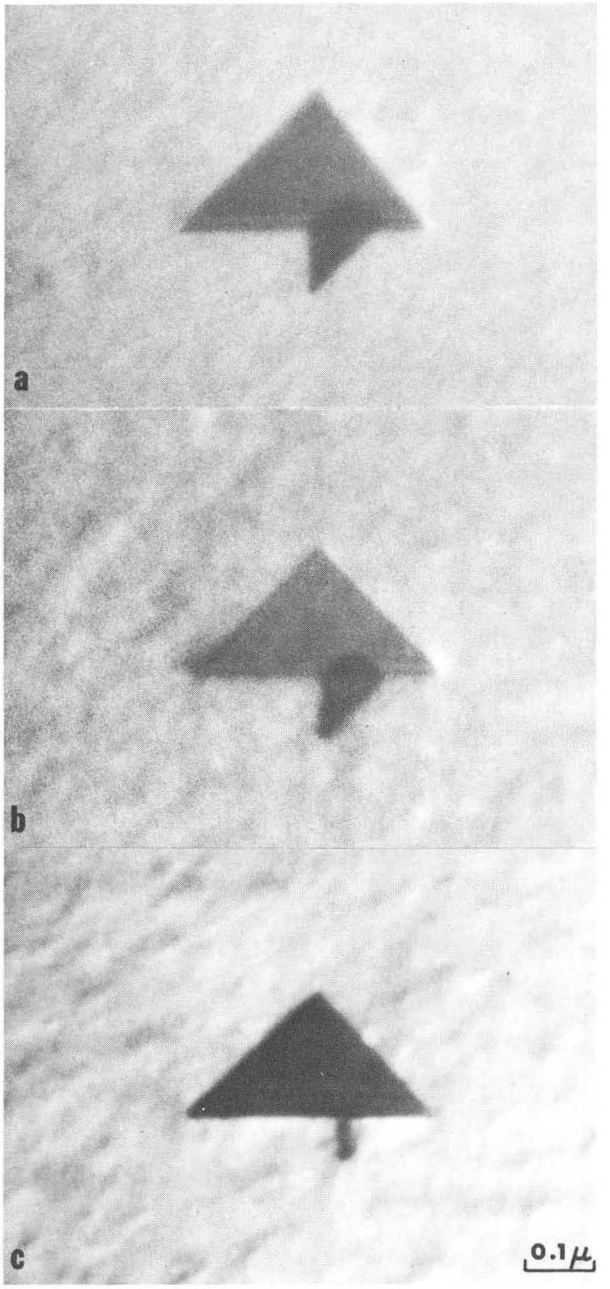

Fig. 1. Sequence showing rapid climb of a four-sided 1/3 ⟨111⟩ loop, three sides of which are bounded by 120° corners. During the same time period at the annealing temperature the triangular loop has hardly changed in size.
(XBB6711-6567)

4. MEASUREMENTS OF DISLOCATION VELOCITIES IN SILICON SINGLE CRYSTALS BY X-RAY TOPOGRAPHY

Vugranam C. Kannan and Jack Washburn

Measurements of glide velocities of isolated individual dislocations as a function of temperature in the range 775-920° were made in silicon single crystals by the x-ray Lang technique and the data were correlated with the orientation and appearance of the dislocation lines. The velocities were measured by recording an x-ray topograph before and after loading the specimen and then measuring the total distance traveled by the particular dislocation line. An example is shown in Fig. 1.

The apparent activation energy for dislocation motion was found to be 1.8 ± 0.3 eV for screw and 60° dislocations at a constant stress of 36 g/mm^2. Careful observation of the appearance of dislocation lines showed that they were not straight but were pinned fairly uniformly along their lengths. The distances between pinning points varied inversely with temperature. These pinning points were tentatively attributed to the presence of thermal jogs on the dislocation line.

Analysis of the velocity data led to the conclusions that the forward motion of jogs was not the rate-controlling process. However, their presence can account for the observed shapes of the dislocation lines. The activation energy for dislocation motion was identified with the energy required for kink-pair nucleation and migration. Formulation of forward velocity of a dislocation on this model shows the measured activation energy

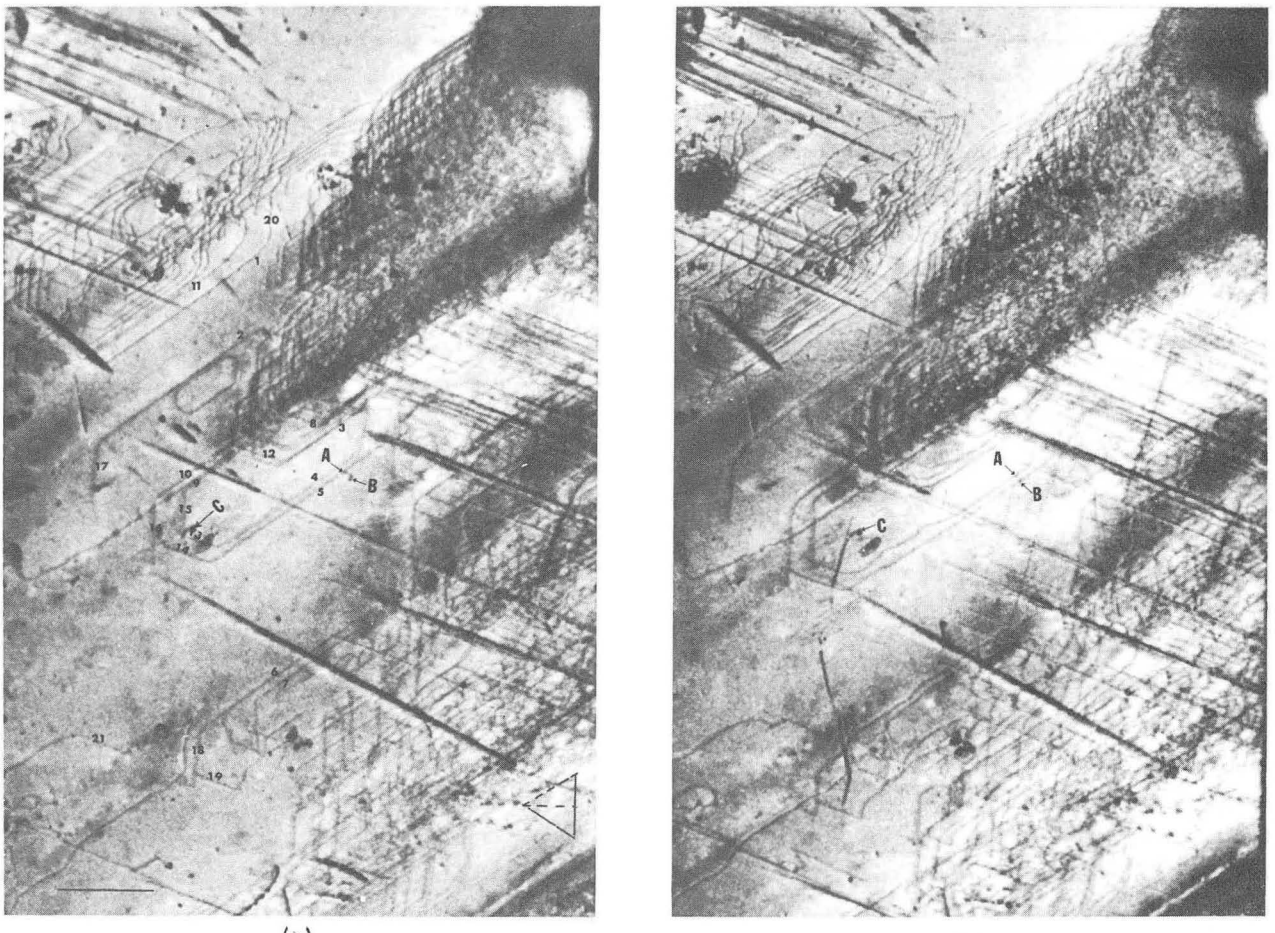

(a) (b)

Fig. 1. The positions of dislocations before (a) and after (b) the tensile test at 825°, under a resolved shear stress of 36 g/mm^2. (The solid black line represents 1 mm.)
(XBB6812-7419 and 7425)

of 1.8 ± 0.3 eV for dislocation motion should equal the arithmetic mean of the energies required for kink-pair nucleation and kink migration. Assuming a "quasi-parabolic" form of potential, the Peierls energy τ_p was computed from the pre-exponential term to be 1.76×10^{10} dynes/cm^2. Under small applied stresses, this leads to a velocity-stress dependence, $v \approx T^2$, which is in agreement with the observations of previous workers.

Other important conclusions that were made from the present investigation are:

(a) Under small stresses, dislocation generation took place at or near the surfaces; vacancy clusters or loops in a few quenched and aged specimens did not act as sources but rather were obstacles to the passage of dislocations.

(b) The propagation of screw dislocations at high temperatures (~1000°) always resulted in the development of pinning points, dipoles, and even large loops. An example of this is shown in Fig. 2.

(c) Dislocations generated at high temperatures or exposed to high temperatures (~1000°) were generally immobile at lower temperatures (~850°). Further motion of such dislocations always resulted in avalanche-like multiplication giving rise to bands of dislocations. Electron microscopic investigation of the detailed configuration of dislocations in these bands indicated that the damage left behind by the moving dislocations was exclusively in the form of dislocation pairs or dipoles of various sizes distributed on the main slip plane. These observations support the idea that dislocations at high temperatures develop large jogs possibly by local climb.

5. RESEARCH PLANS FOR CALENDAR YEAR 1969

Jack Washburn

A more sophisticated field ion microscope is being constructed which will permit a wide range of new experiments. The instrument will permit in situ ion bombardment of specimens and time-of-flight measurements to identify field-evaporated atoms. It is hoped that this instrument will become operational during 1969.

A 650 kV electron microscope is presently being installed which will permit observation of aluminum and silicon foils several microns in thickness. The dislocation climb studies in aluminum and gold will be continued, making use of this new instrument. Of particular interest is a further investigation of the effect of impurities on rates of dislocation climb and glide.

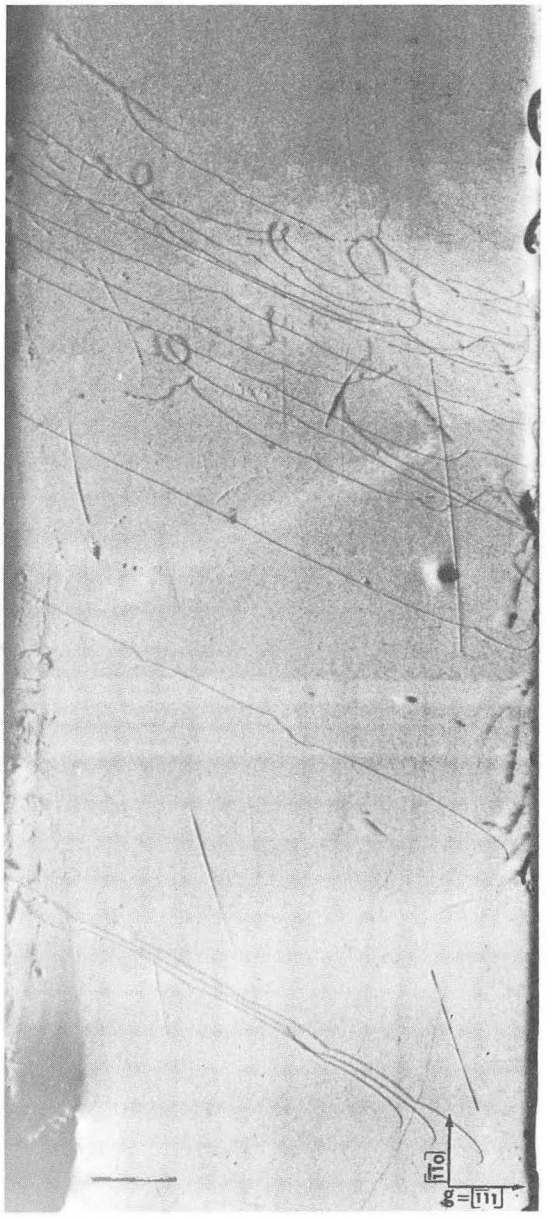

Fig. 2. Propagation of screw dislocations which developed cusps, long dipoles, and large loops while moving at 1025°. (The solid black line on this topograph is 2 mm long.)

XBB691-97

It has been discovered that under certain conditions vacancy defects are formed in silicon that are detectable by x-ray topography. An attempt to characterize these defects by using both x-ray and electron microscope techniques is continuing.

The early stages of vacancy clustering in nickel is being studied by resistivity measurements. Electron microscopy will be used to better characterize the specimens before and after quenching and annealing treatments.

A study of slip band formation in work hardened metals is continuing. Copper crystals deformed in multiple slip are being observed in the electron microscope after small amounts of additional deformation in single slip. This work is an extension of previous surface-replica studies of slip band growth in copper.

6. 1968 PUBLICATIONS

Jack Washburn and Associates

Technical Journals

1. G. Murty and J. Washburn, Effect of Initial Dislocation Density on Single Slip Strain Hardening of Copper, Trans. Japan Inst. Metals 9, 731 (1968).
2. P. Petroff and J. Washburn, A Liquid Helium Field Ion Microscope for Radiation Damage Investigations, Rev. Sci. Instr. 39, 317 (1968).
3. P. Petroff and J. Washburn, A Field Ion Microscope Investigation of 10 MeV Proton Damage in Iridium, presented at International Conference of Vacancies and Interstitials in Metals, Kernforschungsanlage Julich, Germany, Sept. 23-28, 1968; also UCRL-18260.
4. J. L. Strudel and J. Washburn, The Formation of Voids and Dislocation Loops in Quenched Aluminum Single Crystals, in Proceedings of Conference on Interactions Between Dislocations and Point Defects, Harwell, England, July, 1968.
5. G. Vagnard and J. Washburn, Plastic Deformation of Cuprous Oxide, J. Am. Ceram. Soc. 51, 2, 88 (1968).
6. J. Washburn, A Survey of Techniques for the Direct Observation of Structure and Crystal Imperfections, Chapter 1 in Techniques of Metals Research, Vol. 2, Part 1, R. Bunshah, ed. (John Wiley & Sons, Inc., New York, 1968).
7. J. Washburn, Dislocation Theory of Crystals, Chapter 5 in Modern Physics for the Engineer, David S. Saxon, ed. (Holt, Rinehart, and Winston, Inc., Delaware, 1968).

UCRL Reports

1. P. Petroff and J. Washburn, A Field Ion Microscope Investigation of 10 MeV Proton Damage in Iridium, UCRL-18521, October 1968.
2. J. L. Strudel, Precipitation of Vacancies in Quenched Aluminum (Ph. D. Thesis), UCRL-18407, University of California, Berkeley, September 1968.
3. J. Tartour and J. Washburn, Climb Kinetics of Dislocation Loops in Aluminum, UCRL-18019 Rev., May 1968.
4. G. Vellaikal and J. Washburn, Pre-Yield Plastic Deformation in Copper Polycrystals, UCRL-18524, December 1968.
5. G. Vellaikal, Some Observations on Microyielding in Copper Polycrystals, UCRL-18581, November 1968.
6. G. Vellaikal, Dislocation Motion, Multiplication, and Interactions in the Pre-yield Region of Copper Polycrystals (Ph. D. Thesis), UCRL-18435, University of California, Berkeley, November 1968.
7. M. Yokota, Hardening and Recovery of Quenched Gold (Ph. D. Thesis), UCRL-17785, University of California, Berkeley, August, 1968.

B. KINETICS OF DISLOCATION MECHANISMS

1. EXPERIMENTAL CORRELATIONS FOR HIGH TEMPERATURE CREEP

Amiya K. Mukherjee, James E. Bird, and John E. Dorn

The most important property of metals for high temperature service is their resistance to creep. Recent interest in this area has resulted in data that have not been well correlated with one another. This review and correlation was undertaken upon request by the "Committee for the Symposium on Creep" for presentation at the Fall 1968 ASM meeting.

A thorough search was made for reliable data on creep of metals over a range of stresses and at a series of high temperatures for cases where the auxiliary information on the self-diffusivity and the shear modulus of elasticity were also known. All the data could be correlated quite well with the semi-empirical dimensionless relationship

$$\frac{\epsilon_s kT}{DGb} = A\left(\frac{\sigma}{G}\right)^n ,$$

where ϵ_s is the secondary creep rate, kT is the Boltzmann constant times the absolute temperature, D is the diffusivity, G is the shear modulus of elasticity, b is the Burgers vector, σ is the applied stress, and A and n are constants. When the variation of G with temperature was taken into consideration, the above relationship gave an activation energy for creep that was in excellent agreement with that for self-diffusion. It is therefore firmly established that high temperature creep is diffusion controlled. Values of $\epsilon_s kT/DGb$ for the different metals varied over a band of less than 10^{-3} for the same values of σ/G. Although n had an average value of 5 it ranged from 4.3 for Al to 6.8 for α-Fe; A was also slightly different for the various metals. For the fcc metals, A or n appeared to vary somewhat systematically with the dimensionless quantity Gb/α, where α is the stacking-fault energy. The wider variation in these values for the bcc metals, however, could not be rationalized. The effect of grain size on the creep rate was small. Variations in the substructure were analyzed. The density of dislocations within the subgrains increased with $(\sigma/G)^2$ and the subgrain diameters increased with $(\sigma/G)^{-1}$. A major experimental and theoretical question concerns the origin of the observed variations in A and n.

2. THE ROLE OF CLIMB IN CREEP PROCESSES

Amiya K. Mukherjee, James E. Bird, and John E. Dorn

The attempt to systematize and rationalize the high temperature creep behavior of metals has resulted in a number of theories for this phenomenon. Few such theories have been examined in the light of recent experimental advances in terms of the validity of the model on which they are based, the rationale of their formulation, and the degree of their agreement with the experimental facts. This investigation was conducted upon invitation to present a survey of the present status of this subject at a Symposium on Interactions Between Dislocations and Point Defects at the British Atomic Energy Establishment at Harwell.

A careful correlation between the various creep theories and the experimental facts revealed the following:

(a) Only the Nabarro mechanism of creep by stress-directed diffusion of vacancies in polycrystalline aggregates is firmly established theoretically and in excellent agreement with experimental facts within the low stress and high temperature range of its applicability.

(b) Theories for creep at higher stresses, where dislocation mechanisms are known to predominate, fall into two major classes: glide theories based on the motion of jogged screw dislocation, and dislocation climb theories based on recovery of the substructure by climb of edge dislocations followed by glide.

(c) A careful and detailed analysis of the various theories based on the motion of jogged screw dislocations revealed that they cannot be improved so as to agree with the fact that the observed activation energy for creep is independent of the applied stress and agrees well with that for self-diffusion. Furthermore they cannot be improved to provide the observed fact that the creep rate increases as about the fifth power of the stress.

(d) None of the various dislocation climb theories agreed exactly with all of the experimental facts. The best agreements were obtained with Weertmann's theory for climb from piled-up arrays of dislocations and with Chang's theory based on dipole annihilation by climb. These agreed with the facts insofar as they were based on diffusion-controlled climb and this gave an activation energy equal to that for self diffusion. They did not, however, account accurately for the power of the stress with which the observed creep rate increases.

(e) Piled-up arrays of edge dislocations on which Weertmann's theory is based are not observed and have been shown theoretically to be unstable. Dipoles on which Chang's model is based are rarely observed. Neither model therefore is realistic.

(f) On the other hand it is inevitable that the dislocation-climb mechanism must play an important role in high temperature creep insofar as otherwise it becomes impossible to rationalize the attainment of a steady state.

(g) The development of better theories for high temperature creep seem to lie in building more realistic models based on observed substructural details such as density of dislocations, subgrain sizes, and misorientation of subgrains. The essential point concerns the sequence of events a single dislocation undertakes during creep from its origin, through its motions, to its annihilation.

3. HIGH TEMPERATURE DEFORMATION CHARACTERISTICS OF A DISPERSION STRENGTHENED MOLYBDENUM STEEL

Kamal Elsayed Amin and John E. Dorn

At present very little is known about the details of mechanisms of creep in the interesting class of dispersion strengthened engineering alloys. They frequently yield creep rates that are proportional to a power of the stress times an exponential of the negative of an activation energy divided by the gas constant times the absolute temperature. Whereas pure metals exhibit analogous correlations where the activation energy for creep equals that for self-diffusion, the activation energies for dispersion strengthened alloys are usually much greater than those for self-diffusion. For this reason it is not possible to ascertain whether diffusion plays any role whatsoever in their plastic behavior. Recently it was established that the apparent activation energy for creep electrolytic Fe agrees quantitatively with that for self-diffusion in Fe. Both exhibit the same pronounced unique peak at the magnetic Curie transformation. If creep in a dispersion strengthened steel were not diffusion controlled, such a peak in the apparent activation energy for creep would not be obtained. A series of creep and tension tests were therefore carried out on a rather stable dispersion, obtained by tempering martensite, of MoC_2 in a steel matrix.

The apparent activation energy for creep of this steel gave the expected hump in the Curie range. However, the apparent activation energy for creep was 13,000 cal/mole higher than that for self-diffusion. The data correlated well with the equation

$$\frac{\epsilon_s kT}{DGbe - H_c/RT} = A \frac{\sigma}{G} \qquad 6.8$$

This illustrates that the high temperature creep of this alloy is diffusion controlled but that activation involves the extra energy H_c of 13,000 cal/mole. The origin of the introduction of this extra activation energy is not presently known.

4. A MODIFIED PEIERLS MODEL FOR THERMALLY ACTIVATED DEFORMATION IN BODY CENTERED CUBIC METALS

John E. Dorn and Amiya K. Mukherjee*

Recent investigations have shown that single crystals of the technically important bcc metals exhibit some anomalous deformation characteristics at low temperatures:

(a) The generally applicable Schmid law fails insofar as the critical resolved shear stresses for slip are asymmetrically orientation sensitive.

(b) Slip band traces are also asymmetric.

(c) Compression tests have different critical resolved shear stresses from tension tests.

(d) The asymmetries of yielding and slip band formation reverses when tension is replaced by compression testing.

(e) The degree of asymmetric behavior increases as the test temperature is decreased.

A number of investigations have postulated that such anomalous behavior might arise from the splitting of $\alpha/2$ [111] screw dislocations to give partial dislocations on several planes of the zone of the screw dislocation. Such partial dislocations must then be constricted and recombined to permit their migration on a slip plane. Theories based on such models can agree roughly with critical resolved shear stress temperature relationship, the observed activation energies, and the observed activation volumes only over the higher temperature or lower stress ranges of low temperature deformation. The agreement is always poor at low temperatures or high stresses. Furthermore, this rather poor agreement can only be forced when the separation of the partial dislocations is assumed to be about one Burgers vector. If this were so, the entire basis of the analysis on which the theories have been based breaks down, because the cores of the partial dislocations overlap and it is no longer possible to assign meaning to stacking fault energies, interaction energies of partial dislocations, constriction energies, etc.

A new and better theory was formulated, based on the concept that the line energy of a screw dislocation decreases somewhat due to its tendency to dissociate. A dislocation can then be moved to the adjacent parallel row of atoms by surmounting the potential hill as a result of nucleation of a pair of kinks. The process is then analogous to the Peierls mechanism with the added feature that the Peierls stress is modified by the asymmetries in the core which are further dependent on the orientation of the applied stress. A theory based on these concepts seems to be able to account for the asymmetric behavior of the bcc metals. It checks quite well with the limited data now available on this phenomenon.

*Permanent address: Department of Mechanical Engineering, University of California, Davis.

5. ASYMMETRIC PLASTIC BEHAVIOR OF SINGLE CRYSTALS OF Mo

Sylvanus Lau and John E. Dorn

This investigation was initiated to determine in considerable detail the asymmetric plastic behavior in Mo single crystals. Up to the present, six different orientations of tensile axis in the unit standard triangle have been investigated relative to yield stress as function of temperature and slip band formation. From near the center of the triangle to the $[\bar{1}11]$ - $[011]$ line, slip takes place exclusively by the $[111]$ $(\bar{1}01)$ mode. As the $[001]$ corner of the unit triangle is approached, slip takes place principally by the $[111]$ $(\bar{1}\bar{1}2)$ mode and yet nearer the $[001]$ corner $[111]$ $(1\bar{1}2)$ mode. In the latter two cases some cross-slip is observed to planes of the form $\{101\}$ nearest the $(\bar{1}\bar{1}2)$ and $(1\bar{1}2)$ planes, respectively.

The data are being analyzed in terms of the predictions made by the Modified Peierls Mechanism discussed in the preceding subsection. The theory appears to account reasonably well for the observations. At least one more orientation will have to be investigated, however, to complete the picture.

6. ASYMMETRIC PLASTIC BEHAVIOR OF SINGLE CRYSTALS OF Mo + 10 AT. %Re

Chih-an Liu and John E. Dorn

The asymmetric behavior of bcc metals appears to be correlated with the ease with which atoms can be moved in the twinning direction. It was therefore thought that greater asymmetries could be obtained by alloying Mo with Re, which is known to promote twinning. Preliminary data have given extremely low yield stresses for tensile orientations near the [001] pole and high yield stresses near the [111] pole, thus confirming the correlation of asymmetric yielding with twinning.

A complete survey of the asymmetric plastic behavior of the highly asymmetric Mo + 10 at. %Re alloy has now been started.

7. ASYMMETRIC STRAIN HARDENING IN AgMg

Osama Abo-el-Fotoh, Jack B. Mitchell, and John E. Dorn

Low-temperature thermally activated deformation in AgMg single crystals is in good agreement with the dictates of the Peierls mechanism. Although it crystallizes in the CsCl type of lattice, it does not reveal the usual asymmetry of the thermally activated deformation with orientation common to bcc metals. In contrast, however, the athermal rate of strain hardening exhibits pronounced asymmetry. This asymmetry is being characterized in detail toward possible identification of its physical origin in terms of dislocation interactions.

8. THE ROLE OF DISLOCATION FLEXIBILITY IN THE STRENGTHENING OF METALS

Tibor Stefansky* and John E. Dorn

Fleischer's approximate theory for solid solution strengthening suggests that the yield strength should increase linearly with the square root of the solute-atom concentration. A more detailed analysis was made based on the interaction of a dislocation under stress with a regular array of strain centers appropriate to solute atoms. Whereas the yield stress was found to increase with concentration as suggested by Fleischer for very low concentrations, it reached a maximum value and then decreased as the concentration was further increased. The theory gave results in qualitative agreement with recent data by Suzuki.

*Present address: Physics International Company, San Leandro, California.

9. SOLUTE-ATOM LOCKING OF DISLOCATIONS

Loren A. Jacobson* and John E. Dorn

The energy required for thermally activated unpinning of a dislocation from a Cottrell atmosphere was calculated by a new and better approach than had heretofore been applied. It was based on variational principles for the minimum fluctuation in energy required to unlock a dislocation locally so as to release it from its atmosphere. It was found that this energy arises principally from the solute-atom atmosphere in the core region of the dislocation. The activation energy increased very rapidly with a decrease in the applied stress.

*Present address: Captain, USAF, Wright Patterson Air Force Base, Ohio.

10. DYNAMIC BEHAVIOR OF Al AND A 2% Cu ALLOY OF Al

Maximo P. Victoria, C. K. Hari Dharan,* Frank E. Hauser, and John E. Dorn

Impact tests were used to determine the dependence of the shear stress on the shear strain rate at strain rates from 0.5×10^4 to 2.2×10^4 per second in single crystals of pure Al, prestrained Al, and a 2% Cu alloy of Al. In all three cases a linear relationship was found between shear stress and shear strain rate, indicating the operation of a dislocation damping mechanism. The dependence of the damping on temperature was investigated between 10 and 293°K. The results were rationalized in terms of phonon and electron viscosities which provide the damping at high dislocation velocities. Greater increases in stress are needed to produce the same increase in strain rates for the alloy and for the cold-worked Al than for the annealed Al. Although this could be ascribed to higher damping constants arising from greater phonon and electron scattering, it is more likely due to a decrease in the mobile dislocation density.

*Present address: Ford Motor Company, Dearborn, Michigan.

11. DESIGN AND CONSTRUCTION OF A HIGH VELOCITY IMPACT MACHINE

C. K. Hari Dharan and Frank E. Hauser

In order to test materials at very high strain rates, an air-driven device capable of accelerating a 2 in. diameter, 6 in. long projectile to a velocity of 1000 ft/sec and the associated equipment was designed and built. The primary restrictions in the design were the space limitations, the operational safety requirements, and the alloted budget for the apparatus. The machine as built met these restrictions and was found to be reliable in generating experimental stress, strain, and strain rate data for materials at heretofore unachievable strain rates. For example, the flow stress of pure Al (S_y = 6 ksi) was found to be about 80 ksi at a strain rate of 10^5 per second. The impact machine is now ready to be used in investigations of very high strain-rate (impact) behavior of materials.

12. THE DYNAMIC BEHAVIOR OF Al AT HIGH STRAIN RATES

C. K. Hari Dharan, Frank E. Hauser, and John E. Dorn

The stress, strain, and strain rate behavior of pure polycrystalline Al at strain rates between 4000 and 120,000 per second was determined experimentally. These results have been rationalized in terms of damping mechanisms acting on dislocations moving at high velocities. A predicted decrease in phonon viscosity effect with increasing dislocation velocity which leads to a decrease in damping was confirmed and a new, as yet not fully understood, rapid increase in damping at still higher dislocation velocities was discovered. Whether this damping is a relativistic contraction effect or some new damping mechanism constitutes a new problem for a future investigation.

13. RESEARCH PLANS FOR CALENDAR YEAR 1969

John E. Dorn

Major emphasis will continue to be given to the experimental and theoretical rationalization of the mechanical behavior of metals and alloys in terms of dislocation mechanisms. Investigations in topics IIB-3, IIB-4, and IIB-5, described above, will be completed and those on items IIB-6 and IIB-7 will be pressed. In addition the following investigations and studies will be made:

(a) A detailed study of the quantitative relationship between microstructure and substructure on high temperature creep. The review and analysis are to be presented by special request at the International Symposium on Quantitative Metallography, August 1969, in Haifa.

(b) The effect of crystal orientation and polyslip on the high temperature creep of Al will be determined experimentally. Special

emphasis will be given to correlations of creep with the substructures that are developed.

(c) The newly developed high speed impact equipment will be applied to a study of the dynamic response of a series of fcc metals having different stacking fault energies. Attempts will be made to achieve dislocation velocities that approach their relativistic limit.

(d) The origin and nature of the serrated yielding previously observed in disordered and not in ordered Cu_3Au will be investigated. Special emphasis will be given to evaluations of strain rate and stress on the yield strength and on the serrated stress-strain behavior so as to obtain activation energies for this mechanism.

14. 1968 PUBLICATIONS

John E. Dorn and Associates

Technical Journals

1. C. Y. Cheng, A. Karim, T. G. Langdon, J. E. Dorn, Creep Mechanisms in Fe-4% Si Alloy, Trans. AIME 242, 890 (1968).
2. J. E. Dorn, Low-Temperature Dislocation Mechanisms, in Dislocation Dynamics (McGraw-Hill Book Company, New York, 1968), pp. 27-55.
3. J. Klepaczko, Strain Rate History Effects for Polycrystalline Aluminum and Theory of Intersections, J. Mech. Phys. Solids 16, 225 (1968).
4. A. Kumar, F. E. Hauser, and J. E. Dorn, Viscous Drag on Dislocations in Aluminum at High Strain Rates, Acta Met. 16, 1189 (Sept. 1968).
5. T. G. Langdon and J. E. Dorn, Low Temperature Dislocation Mechanisms in Ordered and Disordered Cu_3Au, Phil. Mag. 17, 999 (1968).
6. S. S. Lau, Response to Discussion by Evands and Flanagan on the Dorn-Rajnak Analysis, Trans. AIME 239, 921 (1967).
7. S. S. Lau and J. E. Dorn, Interstitial Impurity Effects on the Mechanical Properties of Molybdenum Single Crystals, Scripta Met. 2, 335 (1968).
8. A. K. Mukherjee, J. Bird, and J. Dorn, The Role of Climb in Creep Processes, Presented at the Conference at Harwell, England, July 1968.

UCRL Reports

1. C. K. H. Dharan, The Dynamic Behavior of Aluminum at High Strain Rates (Ph. D. Thesis), UCRL-18549, October 1968.
2. J. E. Dorn and A. K. Mukherjee, A Modified Peierls Model for Thermally Activated Deformation in Body Centered Cubic Metals, UCRL-18151, March 1968.
3. S. S. Lau and J. E. Dorn, Interstitial Impurity Effects on the Mechanical Properties of Molybdenum Single Crystals, UCRL-18195, April 1968.
4. C.-A. Liu, Orientation Effect on the Plastic Deformation Behavior of Molybdenum Single Crystals (M. S. Thesis), UCRL-18063, University of California, Berkeley, January 1968.
5. L. Jacobson, Solute Atom Locking of Dislocation (Ph. D. Thesis), UCRL-18310, University of California, Berkeley, August 1968.
6. A. K. Mukherjee, J. E. Bird, and J. E. Dorn, Experimental Correlations for High Temperature Creep, Presented at the 1968 A. S. M. Congress in Detroit, October 15, 1968; UCRL-18526, October 1968.
7. A. K. Mukherjee, J. Bird, and J. E. Dorn, The Role of Climb in Creep Processes, Presented at the Symposium on the Interaction Between Dislocations, Harwell, England, July, 1968; UCRL-18281, June 1968.
8. T. Stefansky, Strain Energy Interaction Between Solute Atoms and Dislocations (Ph. D. Thesis), UCRL-18332, University of California, Berkeley, July 1968.
9. T. Stefansky and J. E. Dorn, The Role of Dislocations Flexibility in the Strengthening of Metals, Accepted by Trans. AIME; UCRL-18405, August 1968.

C. RELATION OF STRUCTURE TO PROPERTIES IN CRYSTALS

1. STRUCTURE AND PROPERTIES OF DYNAMICALLY STRAIN AGED STEELS*

Eliot W. Page, † Patricio Mangonon, Jr., †
Gareth Thomas, and Victor Zackay

The introduction of small amounts of plastic deformation (2-5%) during the conventional heat treatment of tempered martensitic steels either between tempering stages (static strain aging) or during tempering (dynamic strain aging) can confer significant increases in strength without serious losses of ductility.

This investigation deals with the structure and properties obtained by dynamic strain aging of Fe/Cr/C and Fe/Mo/C steels. The structures were investigated using transmission electron microscopy and diffraction of foils and extraction replicas. Microprobe techniques were also employed.

After quenching, the structure consists of auto-tempered Widmanstatten cementite plates in a dislocated matrix (Fig. 1). After dynamic strain aging, there is evidence for an increase in dislocation density and also for plastic deformation of the carbide plates.

The results lead to the conclusion that dynamic strain aging provides an increase in strength that is limited by the ultimate tensile strength of the steel, i.e., by work hardening (Fig. 2). An increase in strength beyond this limit is only achieved in the Fe/Mo/C steel when dynamic strain aging produces secondary hardening through precipitation of an alloy carbide. Although chromium does not produce secondary hardening, the Fe/Cr/C steel is superior to the Fe/Mo/C steel regarding both strength and ductility.

Overaging of the Fe/Cr/C steel is due to recovery, recrystallization, and growth of cementite particles (Fig. 3). Recovery and recrystallization is not observed, at the same temperatures, in the Fe/Mo/C steel.

*Abstracted from UCRL-18386, September 1968.
†Present address: Inland Steel Company, East Chicago, Indiana.

2. STRUCTURE AND MECHANICAL PROPERTIES OF Fe-Ni-Co-C STEELS*

Santosh K. Das

The structure and mechanical properties of tempered martensite and bainite were investigated in a series of steels with varying C, Ni, and Co contents. At similar M_s temperatures, the martensite in the 0.24% carbon steels exhibited very small amounts of twinning compared with the 0.4% carbon steels. At equivalent yield and ultimate tensile strength levels the mainly untwinned martensite showed considerably higher toughness than the heavily twinned ones. The addition of cobalt promoted autotempering of martensite by raising the M_s temperature. But its addition in excess of 4% had a deleterious effect on toughness.

The structure of lower bainite showed laths or plates of ferrite with internal carbides but no internal twins. The strength and toughness of isothermally transformed lower bainite was found to decrease with increasing transformation temperature. This was associated with increased coarsening and grain boundary precipitation of the carbides at higher transformation temperatures. At similar strength levels the toughness of lower bainite was found to be superior to the heavily twinned martensite, but inferior to that of the mainly untwinned martensite. Thus, the role of microtwins in lowering the toughness has been demonstrated in two ways: firstly by comparison between the heavily twinned and mainly untwinned martensite and secondly by comparing the martensite with bainite.

*Abstracted from UCRL-18652, December 1968 (M. S. Thesis).

3. STRENGTHENING AND PHASE TRANSFORMATIONS IN 304 STAINLESS STEEL*

Patricio L. Mangonon, Jr. †

The α' martensite transformation in 304 stainless steel was induced only by deformation which resulted in very considerable increases in both yield and tensile strengths.

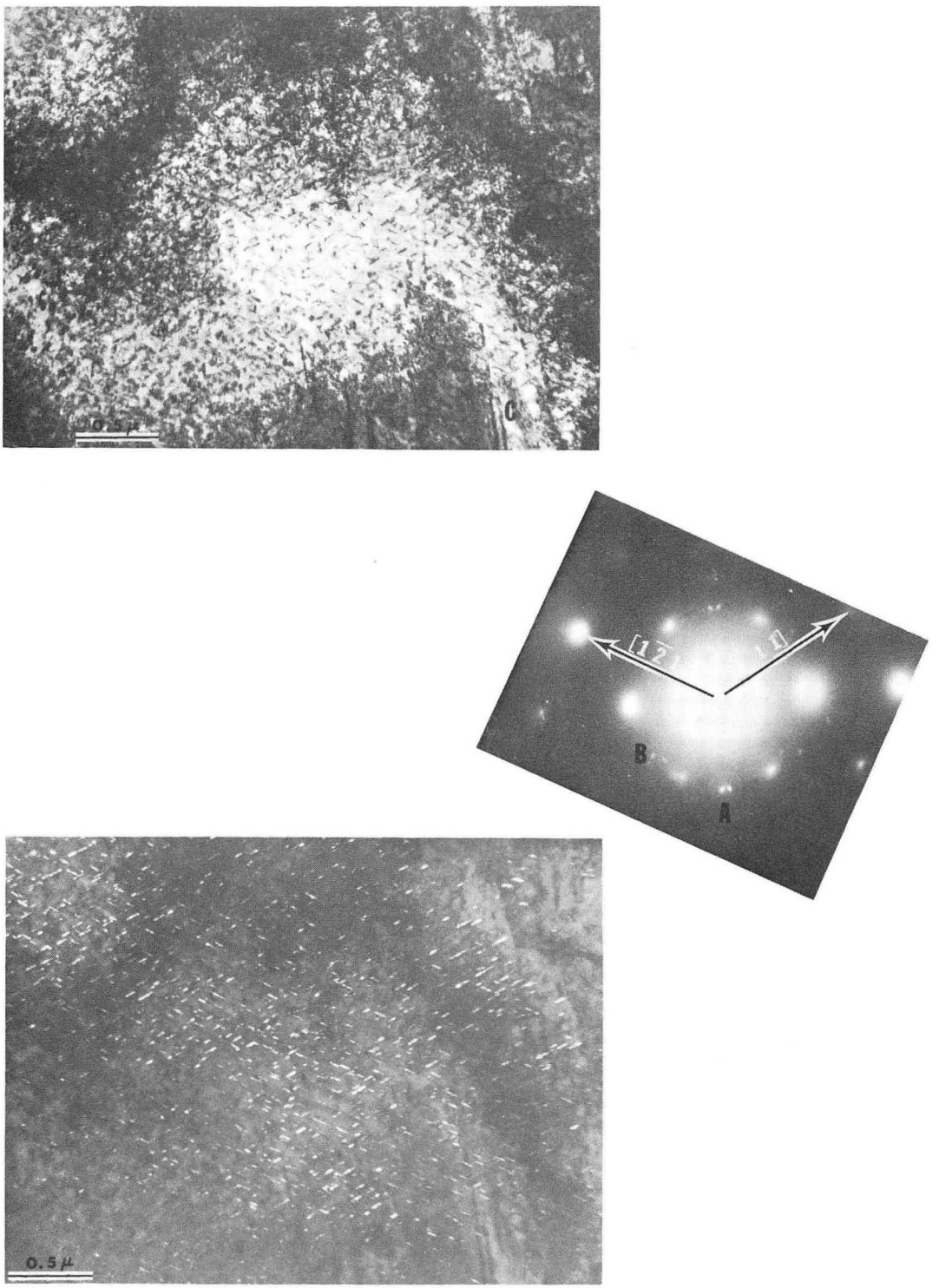

Fig. 1. Thin-foil micrographs of Fe/Cr/C steel after quenching; [111] orientation; a) bright field image revealing Widmanstatten precipitate pattern, high dislocation density, and twinning at "C"; b) dark field image of spots A in (C), showing only precipitate contrast is reversed; c) selected area diffraction; extra reflections are due only to Fe_3C.
(XBB685-3023)

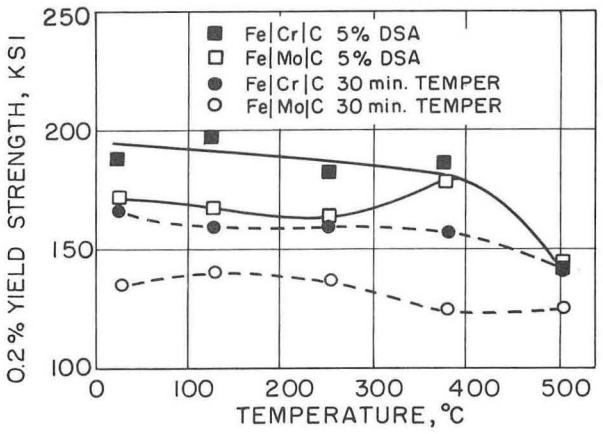

Fig. 2. Effect of DSA upon the yield strength of Fe/Cr/C and Fe/Mo/C steels as a function of processing temperature.

Further increases in these properties was achieved by aging the material deformed at -196° at temperatures from 200 to 400°. The latter increase in strength depended on the amount of prior deformation. Magnetic, x-ray, and transmission electron metallographic techniques revealed that the most probable cause of further strengthening upon aging is the formation of thermally nucleated martensite; i.e., the alloy is dispersion strengthened by α.

Detailed transmission electron microscopy revealed rather convincingly that the ϵ phase is indeed a phase and that the sequence in the transformation is $\gamma \rightarrow \epsilon \rightarrow \alpha'$. Formation of α' is favored at intersections of two ϵ bands. The orientation relationship between γ and α' was found to be predominantly the Nishiyama relationship at the start, which changes to the Kurdjumov-Sachs relationship on further deformation. A mechanism based on the most probable atom movements from the ϵ-hcp (faulted γ) structure to the bcc structure is proposed which predicts the habit plane, shear direction, and amount of shear.

---

*Abstracted from UCRL-18230 (Ph. D. Thesis), University of California, Berkeley, August 1968.

†Present address: Inland Steel Company, East Chicago, Indiana.

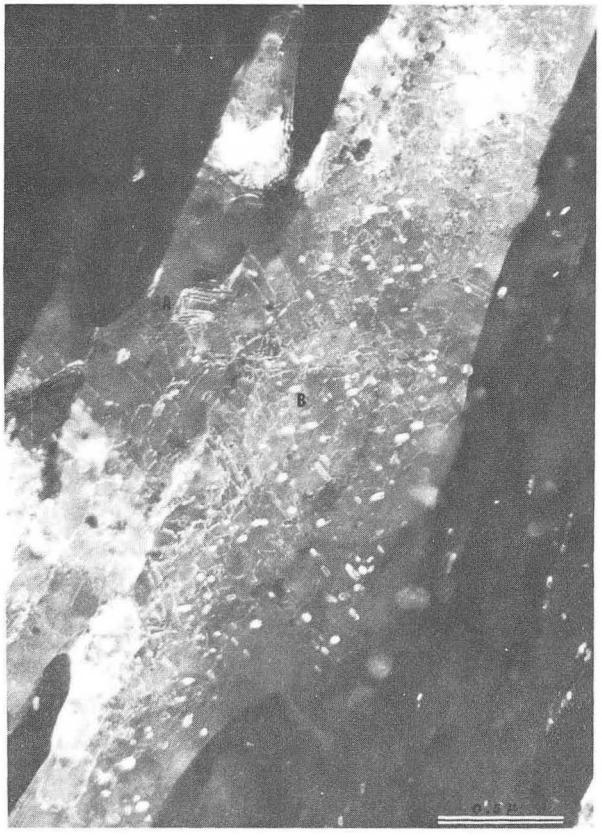

Fig. 3. Fe/Cr/C steel DSA at 600°; dark field image showing recrystallized structure with spheroidized precipitates (B) and recovered dislocations (A); orientation [311].
(XBB685-3028)

4. STRUCTURE OF YTTRIUM ALUMINUM GARNET (YAG)*

Kenneth H. G. Ashbee† and Gareth Thomas

The general chemical formula for garnet is $R'_3R''_2R'''_3O_{12}$. According to Menzer,[1] the crystal structure is cubic with space group Ia3d and the unit cell contains eight molecular formula units, i.e., 160 ions. The ionic positions are:

R'	in 16(a)	0	0	0
R''	in 24(c)	1/4	1/8	0
R'''	in 24(d)	1/4	3/8	0
O^{2-}	in 96(h)	x	y	z .

Each of the three R ion positions is surrounded by a different coordination polyhedron of oxygen ions. The polyhedron is an octahedron for R', a distorted cube for R'', and a tetrahedron for R'''. Although the oxygen ions in each case are equidistant or nearly equidistant from the central R ion, the edge lengths of any polyhedron are not equal.

In yttrium aluminum garnet (YAG), R' and R'' are both Al^{3+}, and R'' is Y^{3+}. Yoder and Keith[2] report that the lattice parameter of YAG is 12.01 ± 0.02 Å, and that the parameters x, y, z are 0.04, 0.055, and 0.64 respectively.

The dominant defects observed in the recrystallized grains are planar, as evidenced by the fringe patterns. Many of these defects are undoubtedly translation twins, i.e., surface defects terminated by partial dislocations. Several translation twins can be seen in Fig. 1. Three different fault planes are present in some grains, in which case their orientations can be deduced from their projected widths and the angles between their intersections with the foil surface. Thus, in Fig. 2, the translation twins labelled A, B, and C are found to lie on {110} planes.

To see if there are any obvious displacement vectors for translation twins on {110} planes, consider the garnet crystal structure. Since YAG is bcc, only one-quarter of the unit cell needs to be considered and, since the oxygen ions are the largest (the ionic radius of O^{2-} is 1.40 Å; cf. Y^{3+}, 0.93 Å and Al^{3+}, 0.50 Å) and the most numerous, it is instructive to focus attention on these. The oxygen ions are conveniently visualized in groups of six arranged as octahedra centered on the aluminum ions in 16(a); see Fig. 3. Although the total Burgers vector is probably 1/2 ⟨111⟩, it is evident from Fig. 3 that a very small rotation of an oxygen octahedron would allow it to settle at 1/4 ⟨111⟩. If the atomic displacements that constitute this small rotation can occur, a surface fault with low specific energy might be envisaged, since only yttrium and some aluminum [in 16(a)] ions would be misplaced. Such a defect might properly be called an antiphase boundary.

Electron diffraction suggests that some of the "fringe" boundaries may separate regions that differ by more than a rigid body translation. Splitting of Kukuchi lines indicates the presence of domains that are not exactly cubic.[4] Such a domain structure could be envisaged as a consequence of ordering of oxygen ions in such a way that the structure becomes very slightly tetragonal. One domain could then differ from the next by choosing a different cube axis for the tetragonal distortion.

In posturing the presence of a domain structure, it should be noted that, since none of the ions in YAG carries a magnetic moment, the domains cannot be attributed to ordering of magnetic spins. Any ordering must be purely crystallographic in nature.

---

*Abstracted from J. Appl. Phys. 39, 3778 (1968).

†Visiting scientist from University of Bristol in Summer 1967.

1. G. Menzer, Z. Krist. 69, 300 (1929).
2. H. S. Yoder and M. L. Keith, Am. Mineralogist 36, 519 (1951).
3. W. Class, H. R. Nesor, and G. T. Murray, in Crystal Growth, Proceedings of International Conference, Boston, 1966 (Pergamon Press, 1967), p. 75.
4. R. E. Villagrana and G. Thomas, Phys. Status Solidi 9, 499 (1965).

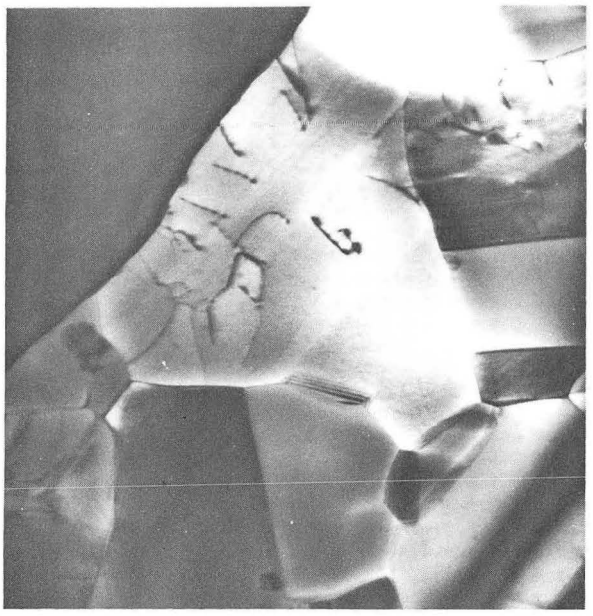

1μ

Fig. 1. Fringe patterns due to antiphase boundaries created by gliding dislocations. (XBB681-357)

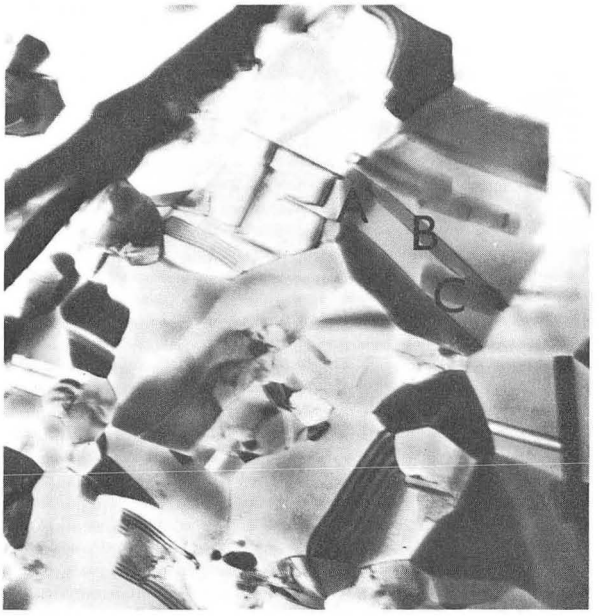

1μ

Fig. 2. Antiphase boundaries on {110} planes. (XBB681-355)

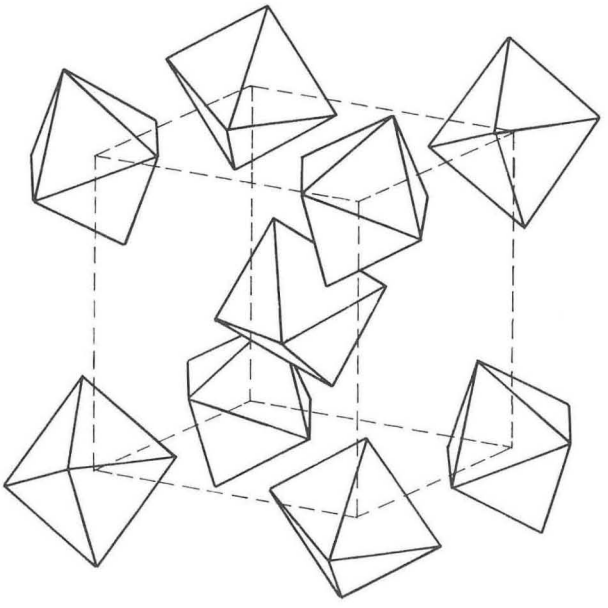

XBL678-5134

Fig. 3. Oxygen octahedron model of the garnet structure (see text).

D. ELECTRON MICROSCOPY

1. A METHOD FOR DETERMINING THE ANOMALOUS ABSORPTION PARAMETER OF A CRYSTAL*

Walter L. Bell and Gareth Thomas

The two-beam dynamical theory gives the intensity diffracted by a perfect wedge-shaped absorbing crystal at the Bragg angle for diffraction as:

$$I_s(t) = \frac{I_0 e^{-2At}}{2} (\cosh 2Bt - \cos 2\pi t), \quad (1)$$

where $A = \pi t_0/\xi_0'$, $B = \pi t_0/\xi_g'$, and $t = z/t_0$ are all dimensionless parameters of absorption and thickness. In common notation ξ_0' and ξ_g' are the mean and anomalous absorption distances, t_0 is the extinction distance, and z is the thickness of the foil; all are generally expressed in angstroms.

Values for the absorption parameters are obtained by using the extrema values from an intensity profile and determining the envelope for the intensity variations. The mean parameter is obtained from

$$I_\Delta(t) = I_{max}(t) - I_{min}(t) = I_0 e^{-2At} \quad (2)$$

and the anomalous parameter from

$$\frac{I_\Sigma(t)}{I_\Delta(t)} = \frac{I_{max}(t) + I_{min}(t)}{I_{max}(t) - I_{min}(t)} = \cosh 2Bt \rightarrow \frac{e^{2Bt}}{2} \quad (3)$$

in thick foils. If there is a diffuse or incoherent background intensity distribution, G(t), Eq. (2) will be independent of the background while Eq. (3) should contain twice the amount of background present in the image.

All previous methods[1-3] of obtaining the anomalous parameter have ignored background radiation and are therefore inherently inaccurate. By using background the following expression can be obtained:

$$\frac{I_\Sigma(t) - I_\Sigma(t+1)}{I_\Delta(t)} = \frac{I_\Sigma(t)}{I_\Delta(t)} - \left[\frac{I_\Delta(t+1)}{I_\Delta(t)} \frac{I_\Sigma(t+1)}{I_\Delta(t+1)}\right]$$

$$= \cosh 2Bt - e^{-2A} \cosh 2B(t+1) + \frac{\Delta G}{I_0 e^{-2At}}, \quad (4)$$

where $\Delta G = 2G(t) - 2G(t+1)$. Both the sign and the magnitude of ΔG will depend upon the shape of the background curve and the thicknesses used in Eq. (4). Using two thicknesses before the maximum in the background distribution curve, 2B calculated by Eq. (4), ignoring background (i.e., assuming $\Delta G = 0$), will be an overestimate; points used past this maximum will yield a value of 2B that is an underestimate when background is ignored. The simplest application is therefore to obtain the background distribution and determine its maximum. The interpolated value of the anomalous parameter at this thickness will be quite close to the real value. An alternative method would be to obtain two micrographs of the same wedge-shaped foil using different amounts of divergent radiation and hence different percentages of diffuse background intensities contributing to the images. The plots of the anomalous absorption parameters versus thickness obtained for the two cases will then cross at the correct value of the parameter and at a thickness approximately where the background exhibits a maximum.

Figure 1 shows the microphotometer traces obtained for two different amounts of defocusing the condenser lens on the Siemens I microscope, from an aluminum foil, and the intensity distribution at the (111) reciprocal lattice point when the angle of incident radiation is far from the Bragg angle. The values of the anomalous parameter determined by Eq. (4), ignoring background, are shown in Fig. 2, and it can be seen that the curves for different background distributions cross at thicknesses quite close to the observed maximum in the background distributions. Points on the plots are all relative to the (111) extinction distance and therefore these results show that the anomalous absorption length is not constant but varies with diffracting planes. However, these results indicate that the ratio of the imaginary part of the Fourier coefficient of the lattice potential to the real part is 0.431 for the (111) planes and 0.453 for the (200) planes in aluminum and that this ratio is fairly constant.

---

*Paper presented at Electron Microscopy Society of America, 26th Annual Meeting, New Orleans, Louisiana, September 1968; Proceedings published by Claitor, Baton Rouge, Louisiana (1968), p. 402.

1. H. Hashimoto, J. Appl Phys. 35, 277 (1964).

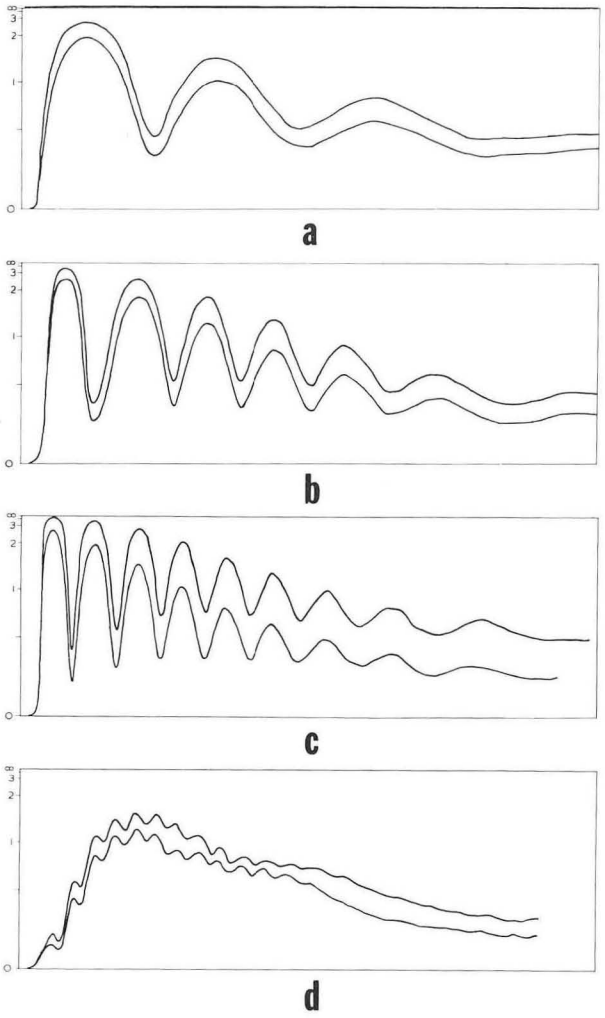

Fig. 1. Microphotometer traces for (a) (220), (b) (002), (c) (111) planes diffracting in aluminum and (d) the diffuse background distribution for the (111) reflection far from the Bragg angle.

2. A. J. F. Metherell and M. J. Whelan, Phil. Mag. 15, 755 (1967).
3. S. Amelinckx, Direct Observations of Dislocations (Academic Press, New York, 1964).

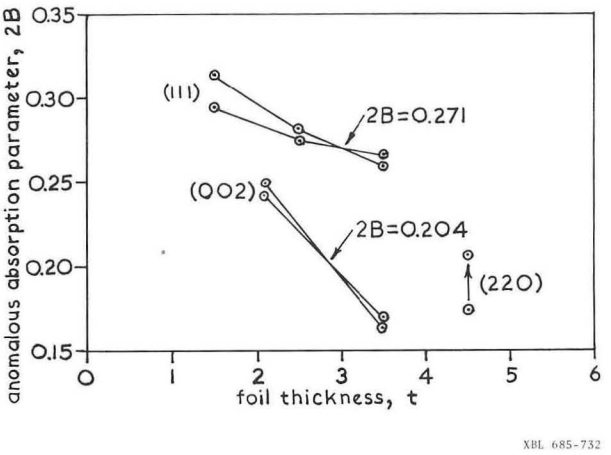

Fig. 2. Anomalous absorption parameters obtained from intensity profiles.

2. KIKUCHI DIFFRACTION CONTRIBUTIONS TO CONTRAST

Gareth Thomas and Walter L. Bell

It is now well known that incoherent and inelastic electrons can contribute to image contrast. Direct indications of this have come from the application of velocity analysis to mechanisms of image formation.[1-3]

In this paper we show that inelastic electrons subsequently rescattered coherently to form the Kikuchi pattern also contribute to image contrast, and furthermore, that the Kikuchi scattered beams behave dynamically in the foil.

Figure 1 shows a series of photographs: a) normal bright field, b) normal dark field, c) and d) images of Kikuchi electrons only, from points on the diffraction patterns shown by the objective aperture positions in e) and f), respectively. It can be seen from Fig. 1(c) that despite the fact that no normal Bragg reflection is contributing to the contrast (as evidenced from the aperture position and because the holes in the film are black) the fringes are quite well resolved. This result means that the Kikuchi electrons interact dynamically and oscillate periodically with depth in the crystal. Direct proof of this fact is shown in Fig. 2. In Fig. 2(a) a large selected area aperture is placed over a low-angle wedge-shaped foil of silicon such that both light and dark fringes contribute to the diffraction pattern. The normal Kikuchi pattern is obtained; i.e., black line through the transmitted spot and white line through the diffracted spot. In Fig. 2(b) a small selected area aperture is

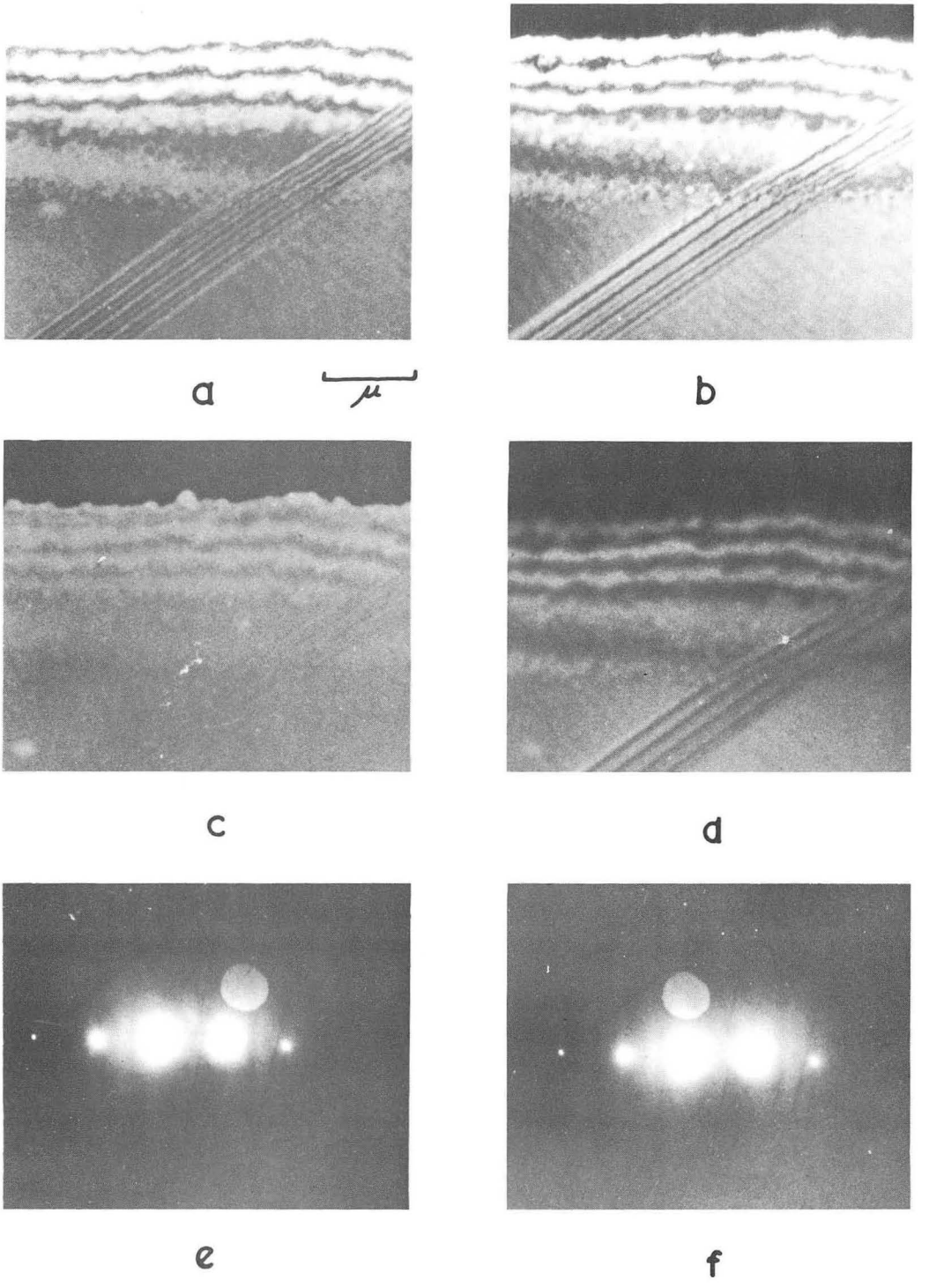

Fig. 1. Images of stacking faults in silicon: (a) normal bright field, (b) normal dark field, (c) and (d) images formed only of the Kikuchi lines shown by the objective aperture positions in (e) and (f). Note that the fringe contrast is retained in (c) and (d) and that the maxima and minima in (c) and (d) have shifted from the normal positions (a) and (b).
(XBB685-2981)

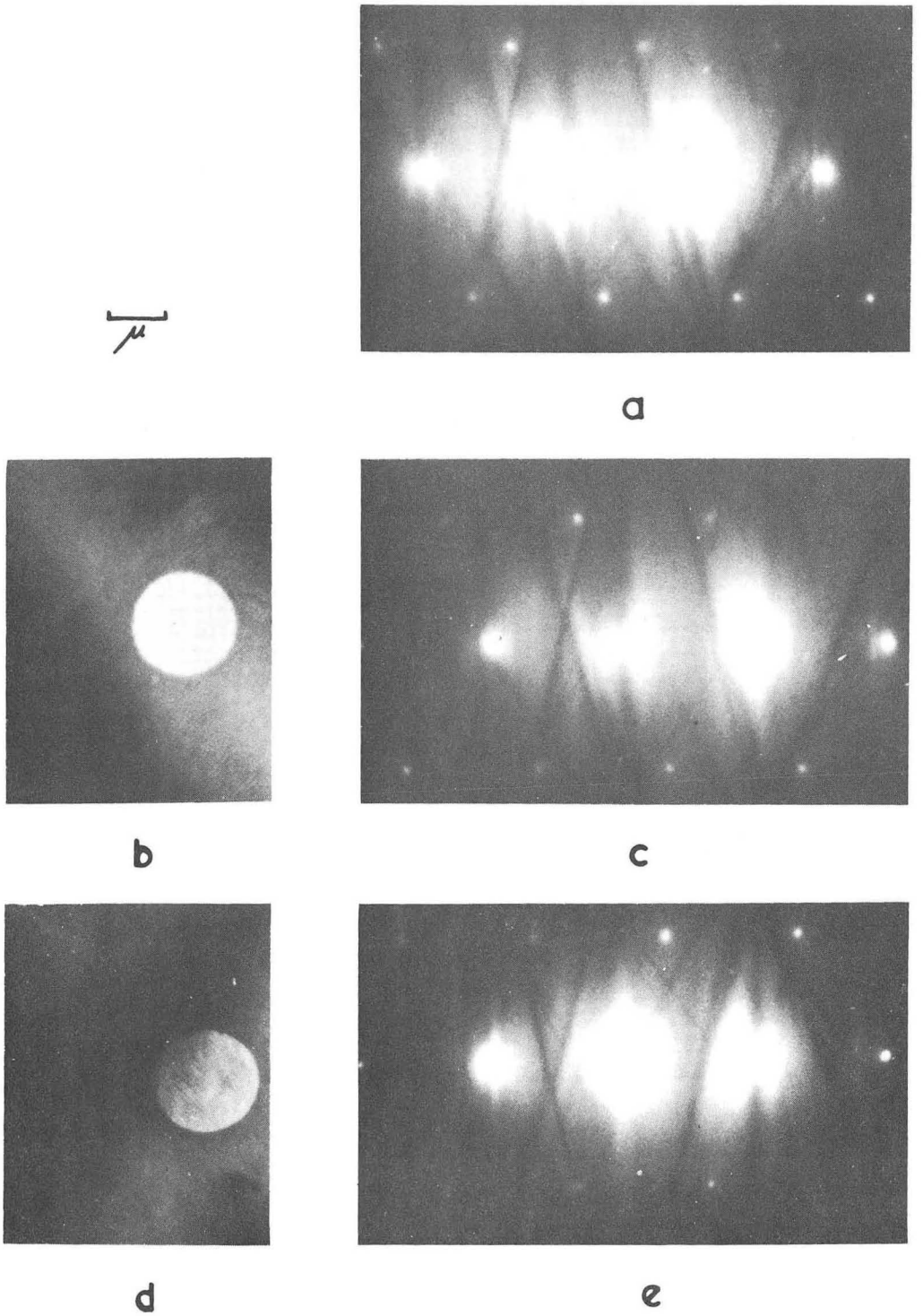

Fig. 2. Illustrations of the dynamic behavior of Kikuchi electrons: (a) normal SAD pattern of wedge foil, (b) selected area of white extinction fringe, (c) corresponding diffraction pattern, (d) selected area of foil at nt/4 (n = odd), (e) corresponding pattern. Note the reversal from the normal of Kikuchi intensity in (e).

(XBB685-2982)

used on a white fringe of the foil; the diffraction pattern in Fig. 2(c) is still normal. In Fig. 2(d) the aperture has been moved to a position to correspond roughly to a foil of thickness equal to an odd multiple of quarter extinction distances. It is seen that now the Kikuchi line intensity in the diffraction pattern reverses from the normal; i.e., the black line now passes through the diffracted spot and the white line through the transmitted spot. This means that the intensity oscillates with depth and that the color of the Kikuchi line depends on the thickness of the foil. Further experiments show that there is a small phase shift associated with the Kikuchi diffraction.

1. Y. Kamiya and R. Uyeda, J. Phys. Soc. Japan 16, 1361 (1961).
2. H. Watanabe and R. Uyeda, ibid. 17, 569 (1962).
3. S. L. Cundy, A. J. F. Metherell, and M. J. Whelan, Electron Microscopy 1966 (Maruzen Company, Tokyo), p. 87.

3. ANOMALOUS ABSORPTION OF ELECTRONS*

Walter L. Bell

The two-beam theory of electron diffraction in absorbing crystals is developed and its applicability to real diffracting media has been investigated by using electron micrographs, of wedge-shaped foils of silicon and aluminum, obtained in a 100,000 volt electron microscope. The anomalous absorption phenomenon believed to exist would be evidenced in electron micrographs by a significantly greater intensity of electrons being passed through a diffracting crystal than would be possible if only a simple mean linear absorption parameter were present. An anomalous absorption parameter is also predicted to exist, but the methods for measuring this parameter ignore the presence of diffuse background intensity which can simulate the effects of the anomalous parameter.

Using microphotometer traces obtained from the electron micrographs it is determined, by cancelling background contribu- to the intensity and by empirical methods, that the anomalous parameter exists and that the values obtained by conventional methods are usually wrong and influenced to a great extent by the magnitude and distribution of diffuse radiation, which in turn depends upon the diffracting material, the surface condition of the material, and the manner in which the electron microscope is operated to control inherent divergence in the incidence beam.

Evidence is presented that low-energy-loss electrons, assumed by the theory to be absorbed, actually re-enter the dynamical beams, effectively amplifying the information carried by these beams. Such re-entrainment of electrons makes the apparent incident intensity and the apparent mean parameter increase with foil thickness. However, the average mean parameter is found to be a crystal constant and independent of the diffracting planes.

The anomalous parameter is found not to be a crystal constant and depends upon the specific diffracting planes and, in addition, upon the structure of the diffracting crystal. In fcc aluminum the anomalous absorption length increases with higher-order diffracting planes in such a way that the ratio of the imaginary part of the Fourier coefficient of the lattice potential to the real part is fairly constant. In silicon, the irregularly spaced (111) diffracting planes exhibit less anomalous absorption than do the regularly spaced (220) planes.

In this investigation it is shown that the single most important influence upon measured absorption parameters is divergence in the incident beam, which can be lessened by defocusing the condenser lens of the microscope. Well-defocused incident illumination gives micrographs whose intensity profiles are very well developed and can be used to obtain consistent absorption parameter measurements.

*Abstracted from UCRL-18158, Ph. D. Thesis.

4. HIGH VOLTAGE ELECTRON MICROSCOPY

Walker L. Bell, M. Kodera, and Gareth Thomas

The installation of the 650 kV Hitachi electron microscope has been delayed several months, but the construction work is now well under way and it is anticipated that operations will commence in June or July 1969.

Meanwhile, theoretical work has been started to determine the new problems of diffraction and contrast that arise in high voltage work as a result of many beams that become excited. The two-beam dynamical theory must be modified to multiple-beam calculations. Computer programs for perfect crystals and crystals containing line and planar defects are being developed. One of the factors already investigated includes a determination of the time and cost involved in computations as a function of the number of beams

that must be considered in the dynamical equations. This is needed to find the minimum number of solutions that satisfy correct analysis.

Applications of high voltage microscopy will concentrate on observations of non-metallic crystals, involving cooperative programs with the ceramics group, continuation of determinations of useful penetration thickness vs. voltage, and studies of biological materials.

5. ELECTRON ENERGY ANALYZING MICROSCOPE

T. Tan, Walker L. Bell, and Gareth Thomas

An electron energy analyzing lens based on the design employed by Metherall and Whelan[1] at Cambridge University is now under construction for incorporation into one of our Siemens Elmiskop I microscopes. The lens is basically an electrostatic Mollenstedt type with a spectrum resolution of 1-2 eV. We anticipate installation by May 1969.

This instrument will be used to measure the characteristic plasmon energy losses in crystals both from the fundamental viewpoint of absorption and contrast, and towards utilizing the instrument for chemical analysis down to microscopy resolution limits (~20 Å), in applications such as grain boundary embrittlement, precipitation kinetics, and phase transformations in general.

---

1. J. F. Metherall and C. J. Whelan, Phil. Mag. 14, 1233 (1966).

6. RESEARCH PLANS FOR CALENDAR YEAR 1969

Gareth Thomas

a. Microstructural Factors in Strength and Embrittlement of Steels

Current research work in our group indicates that in order to avoid embrittlement in martensitic steels, one of the factors to be avoided is the formation of twinned martensite. Thus, control of composition is very important and the total alloy content in terms of, e.g., carbon and nickel, will be limited unless twinned martensite can be prevented by alloying and/or utilization of non-twinned lower bainite is effective. Research on the effects of cobalt and manganese on Fe/C, Fe/Ni/C, and Fe/Cr/C martensite steels is being carried out to this end, and to obtain better characterization of alloys through microstructural control.

Applications of strengthening mechanisms in thermal-mechanical processing will also be utilized in attempts to maximize the utilization of desirable microstructures. Cooperative efforts with Drs. Zackay and Parker will be continued.

b. Spinodal Alloys

Efforts are being directed to relate the mechanical properties of spinodally decomposed alloys in terms of compositional amplitudes and wavelengths and interphase interface structures. The latter will be determined by direct observation by using electron and field ion microscopy. Kinetics of aging will also be studied.

c. Structure of Ordered Alloys

The main interest here is in defining more precisely the nature of short range order in alloys. Field ion and electron microscope techniques are being used. Hot stage microscopy and diffraction at and near the critical temperature will give more direct information on the ordering reaction.

d. Interstitial Order and Ductile-Brittle Transition

Work will be continued on the Ta-C alloy system in which mechanical properties of Ta containing up to 3 at. % C will be correlated to microstructures. Preliminary results indicate that a transitional ordering phase (not $Ta_{64}C$) may be responsible for embrittlement.

e. Electron Microscopy and Diffraction

Continued research will be done on fundamentals of electron scattering, absorption, and contrast; applications to the study of interphase interfaces; high voltage microscopy; and velocity analysis; cooperation will continue with R. M. Glaeser (Donner Lab.) on biological applications (see UCRL-18347, p. 175).

f. Non-Metallic Systems

Continuation of research into precipitation in non-metallic alloy systems, e.g., spinels, and spinodal decomposition in oxide systems. This will be done mainly utilizing high voltage microscopy for microstructural characterization.

7. 1968 PUBLICATIONS

Gareth Thomas and Associates

Technical Journals

1. K. H. G. Ashbee and G. Thomas, Electron Microscopy of Yttrium Aluminum Garnet (YAG), J. Appl. Phys. 39, 3778 (1968).
2. W. L. Bell and G. Thomas, Kikuchi Diffraction Contributions to Contrast, in Fourth European Congress on Electron Microscopy, Rome, Sept. 1968, D. S. Bocciarelli, ed. (Tipografia Poliglotta Vaticana, Rome, 1968), p. 283.
3. W. L. Bell and G. Thomas, A Method for Determining the Anomalous Absorption Parameter in Diffracting Crystals, in Proceedings of the EMSA Conference, New Orleans, La., 1968, C. J. Arceneaux, ed. (Claitor's Publishing Division, Baton Rouge, 1968), p. 402.
4. I-Lin Cheng and G. Thomas, Structure and Properties of Fe-Ni-Co-Ti Maraging Steel, Trans. ASM 61, 14 (1968).
5. A. G. Fitzgerald and G. Thomas, Electron Microscope Observations of Twinning and Phase Transformations in Indium Sulfide Crystals, Phys. Status Solidi 25, 263 (1968).
6. R. M. Glaeser, R. Christensen, W. A. Brammer, and G. Thomas, Applications of Electron Diffraction to Problems in Biological Electron Microscopy, in Proceedings of the EMSA Conference, New Orleans, La., 1968, C. J. Arceneaux, ed. (Claitor's Publishing Division, Baton Rouge, La., 1968), p. 398.
7. P. R. Okamoto and G. Thomas, On the Four-Axis Hexagonal Reciprocal Lattice and Its Use in the Indexing of Transmission Electron Diffraction Patterns, Phys. Status Solidi 25, 81 (1968).
8. G. Thomas, Electron Microscopy at High Voltages, Phil. Mag. 17, 1097 (1968).

UCRL Reports

1. K. H. G. Ashbee, Electron Irradiation of Lanthanum Trifluoride, UCRL-18022, January 1968.
2. W. L. Bell, Analysis of Contrast From Lattice Defects, EMSA 26th Annual Meeting, New Orleans, La.; UCRL-18183, May 1968.
3. W. L. Bell, Anomalous Absorption of Electrons (Ph. D. Thesis), UCRL-18158, University of California, Berkeley, May 1968.
4. S. K. Das, Structure and Mechanical Properties of Fe-Ni-Co-C Steels (M. S. Thesis), UCRL-18652, University of California, Berkeley, December 1968.
5. R. M. Glaeser and G. Thomas, Experimental Systems for Digital Analysis and Improvement of Fourier Image Contrast in Biological Electron Microscopy, UCRL-18347, Spring 1968.
6. D. Maher and J. Strudel, Precision Circuitry for Conducting Joule Heating Experiments, UCRL-18033, February 1968.
7. P. L. Manganon, Strengthening and Phase Transformations in 304 Stainless Steel (Ph. D. Thesis), UCRL-18230, University of California, Berkeley, August 1968.
8. E. W. Page, P. L. Manganon, G. Thomas, and V. F. Zackay, Structure and Properties of Dynamically Strain Aged Steels, UCRL-18386, September 1968.
9. E. F. Sturcken, Performance of a Valdre Heating and Tilting Stage in the Siemens Electron Microscope, UCRL-17773, April 1968.

E. HIGH STRENGTH MATERIALS

Earl R. Parker, Victor F. Zackay,
and William W. Gerberich

High strength materials are often limited by their load-carrying capacity in the presence of a flaw. In this regard, the critical stress-intensity factor for unstable crack propagation is often a more important material parameter than the tensile strength. Because of this, increasing emphasis has been placed upon improving the strength-toughness relationship in high strength alloys. Unfortunately, strength and toughness are almost always inverse properties, and the possibility of drastically increasing both simultaneously in single phase systems is slim if not negligible. For this reason more novel approaches to increasing both strength and toughness must be found.

Currently, two lines of thought are being actively pursued. The first is to preferentially align a second phase within a matrix phase so as to obtain anisotropic properties that produce beneficial fracture characteristics in one orientation. This may be provided macroscopically as in fiber-reinforced composites or metallurgically as in unidirectional solidification. The second is to provide an internal mechanism such as twinning or a phase transformation that is occurring simultaneously with crack propagation so that it advantageously changes the energy balance at the crack tip. To gain insight into the first method, better understanding of fracture in two-phase materials on a macroscopic basis is being accomplished. To study the second method, detailed evaluations of fracture mechanisms in TRIP steels, which exhibit the strain-induced austenite to martensite transformation, has been made. Research to date indicates that both methods hold promise for extending the present limits of strength-toughness combinations in high strength materials.

1. FRACTURE OF TRIP STEELS

Peter L. Hemmings*
and William W. Gerberich

Previous work on uniaxial behavior had shown that strain-induced martensite may preferentially come out on habit planes nearest in line to macroscopic shear planes. It was assumed that this was to reduce the total energy of the system. Such a result is shown in Fig. 1 where "bracket" martensite has a

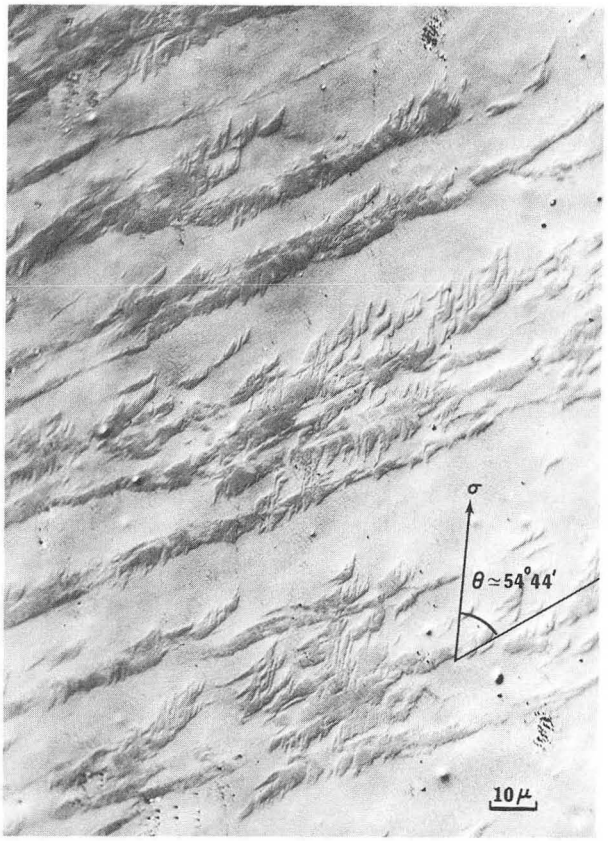

Fig. 1. Bracket martensite forming on tensile and shear axes of tensile specimen.

(XBB689-5384)

dual orientation–being lined up in the theoretical oblique shear angle, 54°44', and in the direction of the applied tensile stress. Based upon the premise that a similar effect would occur under triaxial stress conditions, an analysis was made with respect to crack propagation. Subsequent to this analysis it was found that the martensite is strain-induced in the direction of macroscopic shear, a typical result being shown in Fig. 2.

At the tip of a crack the transformation was looked upon as an energy-absorbing device. Based upon the crystallographic shear process taking place when fcc austenite (γ) transforms to bct martensite (α'), the energy contribution was determined to be

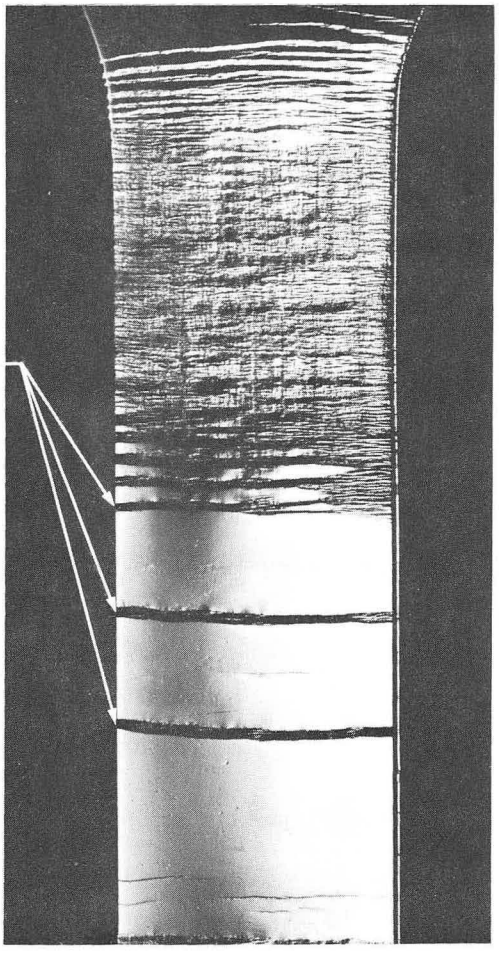

Fig. 2. Luder's band in tensile sample of metastable austenite. (XBB6811-6879)

$$U_{IS} = \frac{\pi}{8} t \int_0^{R_p} V_{\alpha'} \sigma_{\alpha'} \epsilon_{IS} r \, dr,$$

where t is the specimen thickness, R_p is the plastic zone size, $V_{\alpha'}$ is the volume fraction of martensite, ϵ_{IS} is the transformation shear and r is the distance from the crack tip. Observations of plastic zones and the distribution of strain-induced martensite within the zones provided an estimate of the plastic energy dissipation. This was then compared to the normal plastic energy dissipation as obtained from the deformation of austenite and martensite. One calculation gave the following results for a 0.20 carbon alloy tested at -196°:

$$U_{IS} = 2300 R_p^2,$$
$$U_{\alpha'} = 174 R_p^2 t,$$
$$U_{\gamma} = 314 R_p^2 t.$$

It is seen that the contribution to plastic energy dissipation from the strain-induced transformation was approximately 4 times as great as the sum of the normal plastic deformation processes. This was reflected in the critical stress intensity at fracture. For this alloy, which exhibited a 327,000 psi ultimate strength at -196°, the critical stress intensity factor was about 280,000 psi-in$^{1/2}$. This high degree of toughness was also exhibited in thick sections where a comparison of TRIP steel with conventional low-alloy steels is given in Fig. 3. The expected decrease in toughness with increasing thickness was much less in TRIP steel than with conventional steels of the same general strength level.

Although the theoretical energy estimates and experimental measurements attest to the unusual strength-toughness combinations attainable with this steel, further insight to

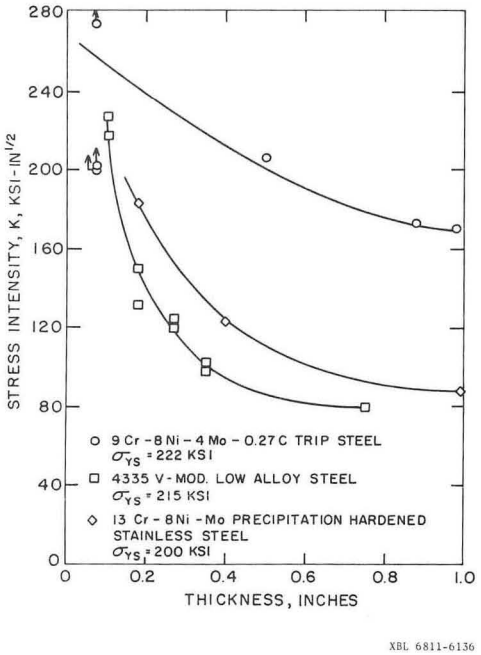

Fig. 3. Effect of thickness on toughness transition of TRIP steel and two conventional steels.

Fig. 4. Typical fractograph taken from a thick sample of B-450 materials tested at -196°. (XBB689-5385)

the actual crack growth mechanism was desired. This was attainable with the aid of electron fractography. It was found that the crack growth process was microscopically ductile. Three types of morphology were observed on the fracture surfaces, typical regions being shown in Fig. 4. Both wavy slip (center) and dimpled rupture (upper left) are noted along with an almost featureless stretched region (lower right). It was found that the martensite fractures first by wavy slip, a stretched region forms at the austenite-martensite interface, and then the austenite fractures by dimpled rupture. The process is such that in between martensite regions the austenite tears in a direction which is microscopically perpendicular to the macroscopic crack growth direction. This results in a macroscopic flat structure mode even though the toughness is very high.

*Present address: Boeing Commercial Airplane Division, Seattle, Washington.

2. FRACTURE OF COMPOSITE MATERIALS

William W. Gerberich

Crack propagation in an age-hardenable aluminum alloy reinforced with stainless steel wires has been studied to determine the energy dissipation mechanisms for both longitudinal and transverse fracture. A cross section showing aluminum around a single fiber of 450,000 psi strength steel is shown in Fig. 1. It is seen that there is a flow pattern in the aluminum about the fiber; this deformation resulted from diffusion bonding of alternate layers about the fibers at 500°. The strength characteristics followed the rule of mixtures, which means that the strength increases with the volume fraction of the reinforcement according to

$$\sigma_c = V_m \sigma_m + V_f \sigma_f,$$

where σ_m, σ_f are strengths of the matrix and fiber and V_m, V_f are the respective volume fractions. Uniaxial strengths as high as 220,000 psi for the 40% volume fraction material were obtained, which is equivalent to a 360,000 psi strength steel on a strength-to-weight basis.

An analysis of the crack propagation process was made, considering that the work to fracture is a function of the plastic energy dissipation in each wire or matrix bundle as the crack progresses. This work may be described by

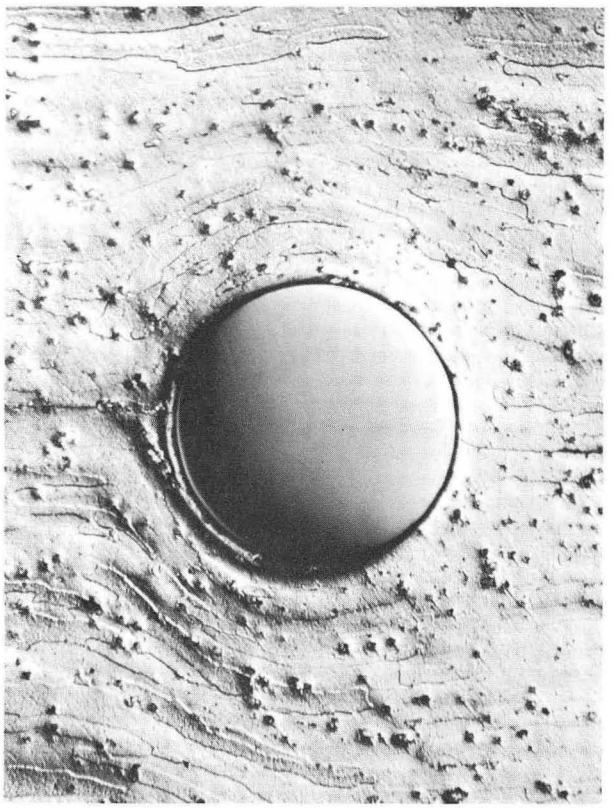

10μ

Fig. 1. Single stainless steel fiber in an aluminum alloy matrix.
(XBB686-3414A)

$$W = f(V_f, h) \int_0^{\epsilon_f} \sigma d\epsilon,$$

where V_f is the volume fraction of the fiber, h is the height of the severely deformed region around the advancing crack, and the integral represents the strain energy density in terms of the stress and strain to fracture. For fracture across high strength ductile fibers, the major energy dissipation process is in the fibers and the work to fracture is a function of the volume fraction and height of the plastic strip, which is necking down as indicated in Fig. 2. For crack propagation parallel to the unidirectional reinforcement, the only energy-dissipation mechanism is the matrix. Here, the work to fracture is controlled by the spacing between fibers, which limits the region of severe plastic deformation in the matrix. In both cases the work per unit fracture area may be equated to the strain energy release rate, G, which in terms of the stress intensity, K, is

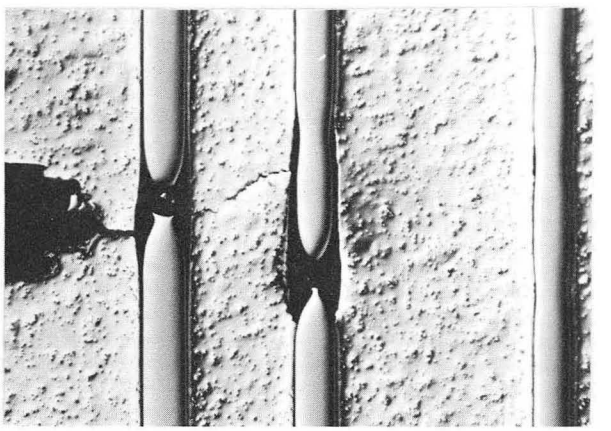

V_f = 0.05 100μ

Fig. 2. Micrograph showing ductile fiber breaks in 5% volume fraction composite.
(XBB686-3417A)

$$K = (E'G)^{1/2} = (E'\frac{W}{A})^{1/2},$$

where E' is the secondary modulus of elasticity.

These considerations led to a description of the critical stress intensity factor for fracture across (longitudinal) and between (transverse) unidirectional fibers as given by

$$\text{Longitudinal:} \quad K \approx \left[E' \frac{d(1-V_f)^2}{V_f} \sigma_m \epsilon_m + \sigma_f \epsilon \cdot 2dV_f \right]^{1/2},$$

$$\text{Transverse:} \quad K \approx \left\{ E' \sigma_m \epsilon_m \left[\frac{d}{2} \left(\frac{\pi}{V_f} \right)^{1/2} - d \right] \right\}^{1/2}.$$

Here d is the fiber diameter. These two equations, as shown in Figs. 3 and 4, are seen to describe the experimental data reasonably well.

3. FRACTURE OF CRACKED TUNGSTEN SINGLE CRYSTALS

P. Leland Key*

The fracture of tungsten single crystals containing cracks of a known size and shape was investigated both analytically and experimentally. Analytically, the methods of linear elastic fracture mechanics have been applied to establish several possible criteria for the fracture of cracked crystals, including both

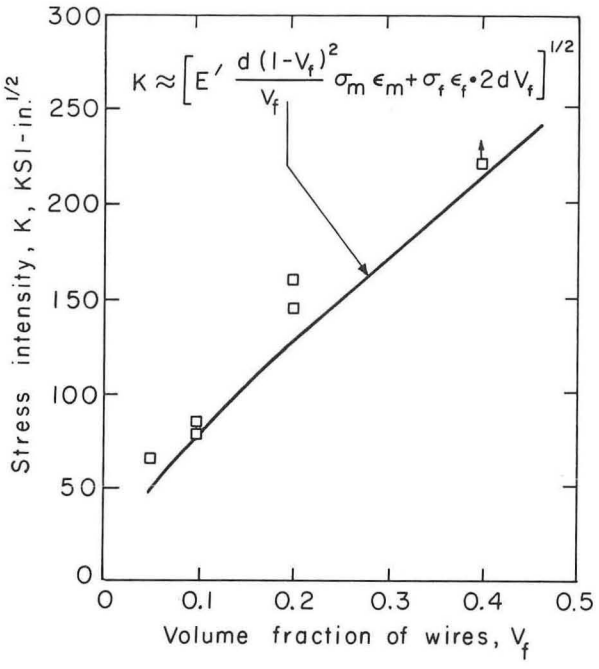

XBL686-972-A

Fig. 3. Effect of volume fraction on the longitudinal toughness of an aluminum alloy composite.

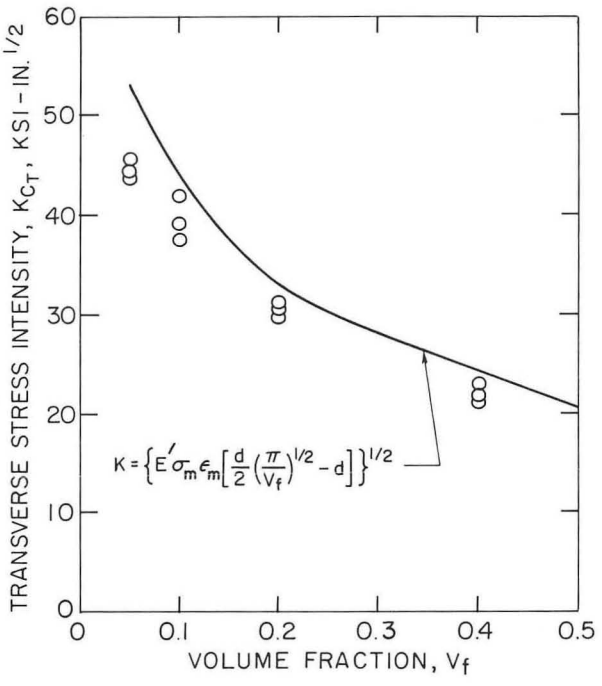

XBL692-2053

Fig. 4. Effect of volume fraction on the transverse toughness of an aluminum alloy composite.

critical local stress and critical strain energy release rate criteria. Experimentally, small cracks (about 150 μ deep) were introduced into tungsten single crystals of various crystallographic orientations by a spark discharge technique (see Fig. 1). The tensile fracture behavior of these cracked crystals was then evaluated at room temperature for both unannealed crystals and for crystals annealed in the range 1200 to 2400°.

All cracked crystals fractured in a brittle fashion at both room temperature and at liquid nitrogen temperature. The fracture of many of the cracked crystals required a sharp crack to be nucleated from the spark-induced crack prior to fracture. The fracture behavior of these crystals was controlled by the crack nucleation processes. For other crystals the spark crack could be directly propagated, and a crack propagation criterion based on either a local or total strain energy release rate appeared to best describe the data. The fracture surface energy of tungsten determined from these results was 6200 ergs/cm^2 at liquid nitrogen temperature and 26,000 ergs/cm^2 at room temperature. The liquid nitrogen temperature value is close to the value of the thermodynamic surface energy.

The fracture behavior of cracked tungsten crystals was significantly affected by annealing. At room temperature the fracture surface energy decreased, then increased as the annealing temperature was increased, and the opposite effect was observed at liquid nitrogen temperature as shown in Fig. 2.

---

*Present address: Bell Telephone Laboratories, Murray Hill, New Jersey.

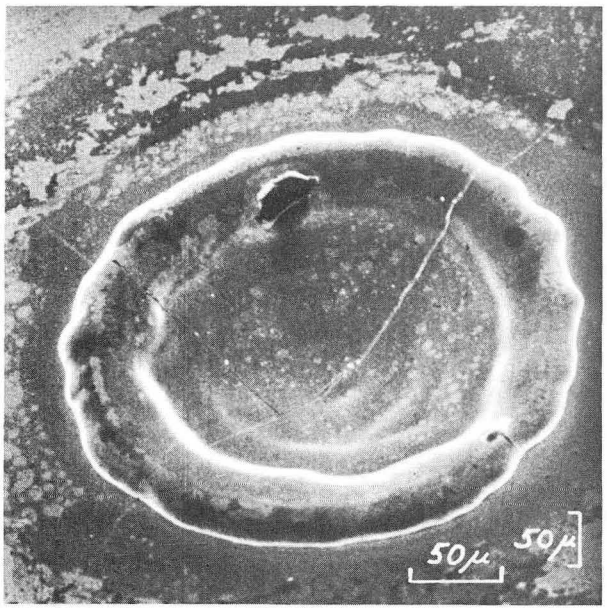

Fig. 1. Scanning electron micrograph of a spark cavity on the surface of a tungsten single crystal.
(XBB6812-7306)

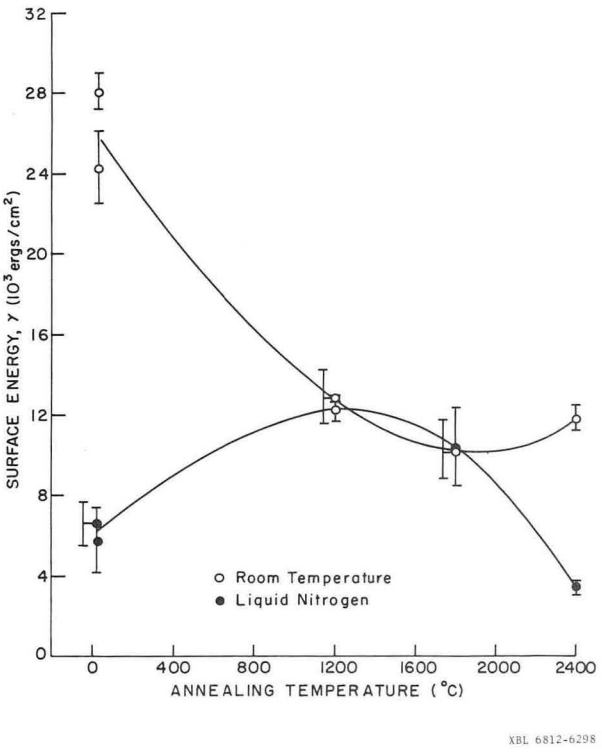

Fig. 2. Effect of annealing on the fracture surface energy of (001) tungsten crystals.

4. STRESS-CORROSION CRACKING OF TITANIUM ALLOYS

Yosef Katz

Stress corrosion is a complex phenomenon involving both mechanics and electrochemistry and also the interaction of these processes. To obtain reproducible information on stress

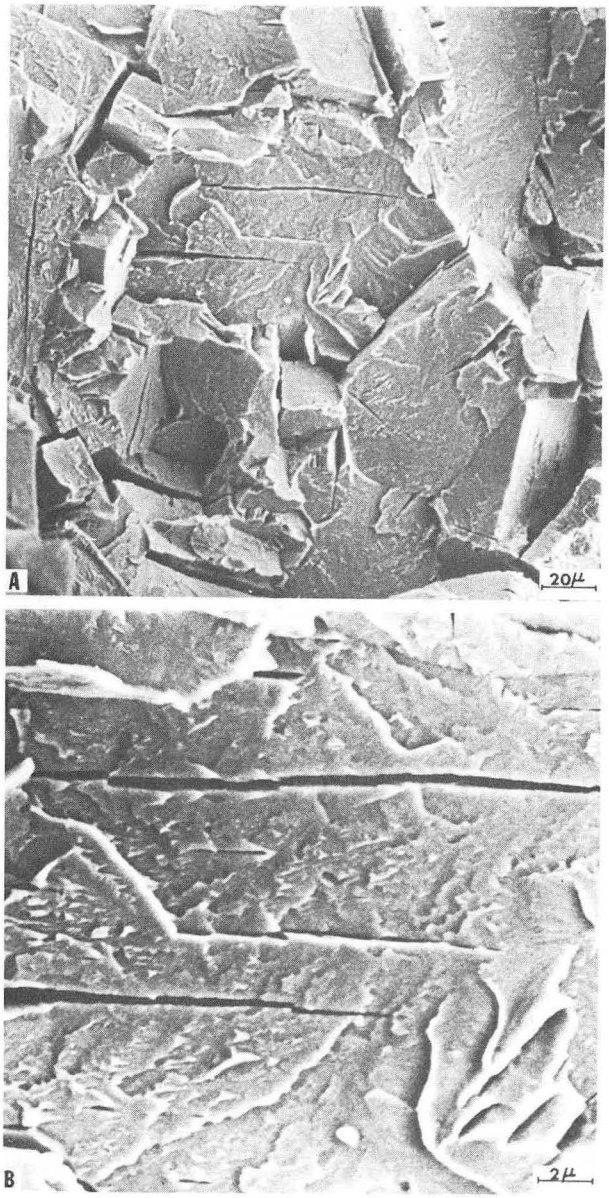

Fig. 1. Electron scanning micrographs of fracture surface and secondary cleavage cracks resulting from stress-corrosion cracking of all beta alloys.
(XBB6812-7713)

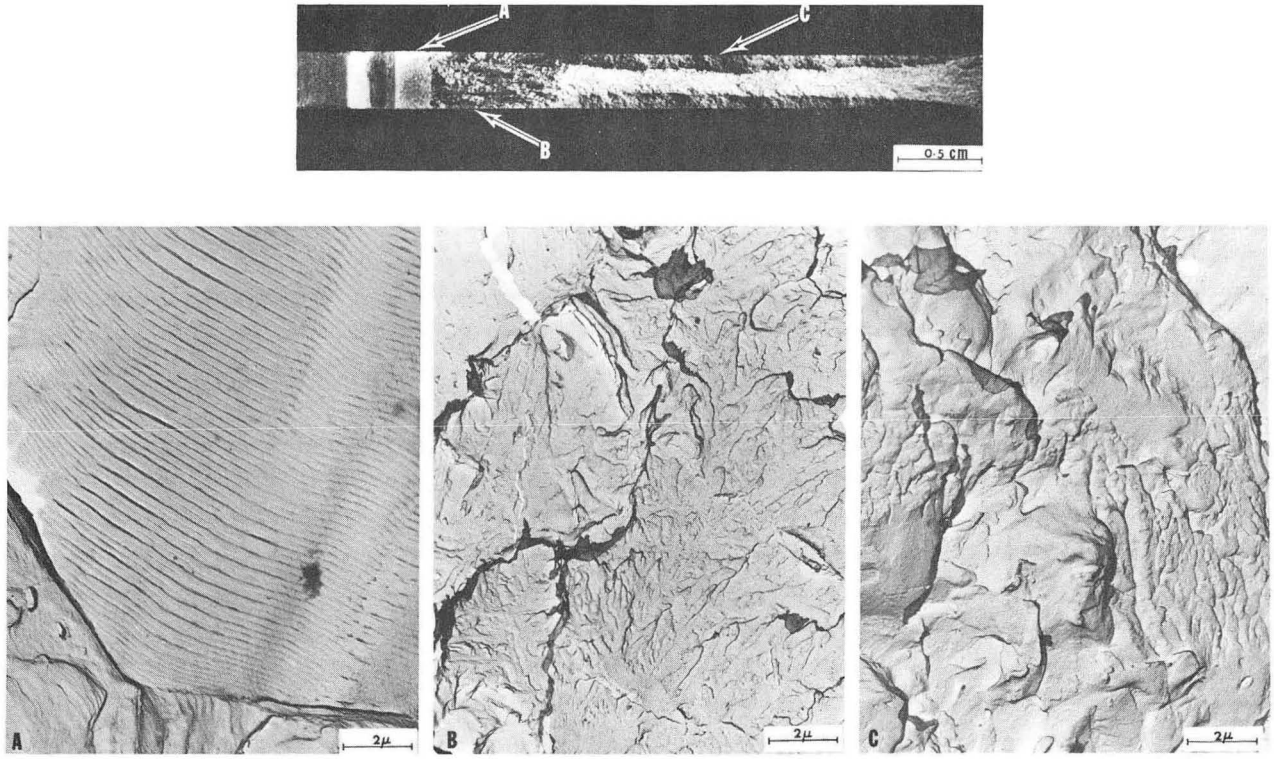

Fig. 2. Electron scanning micrographs of fracture surface and secondary cleavage cracks resulting from stress-corrosion cracking of all beta alloys.

(XBB6812-7705)

corrosion processes, the experimental conditions must be carefully defined. In this investigation, fracture mechanics is used to define the state of stress existing at the tip of a crack in a corrosive environment. Titanium alloys were chosen because of their current technological importance. The specific alloys chosen for study are: Ti (commercial purity), Ti-8Al-1Mo-1V, Ti-5Al-2.5Sn, and Ti-13V-11Cr-3Al. These alloys were chosen because each has a different microstructure; namely, alpha, alpha plus a small amount of beta, alpha plus beta, and beta. The environments selected were distilled water and salt water (3-1/2% NaCl); some tests were conducted in air to obtain base-line data.

The information being obtained includes the influence of microstructure on the mode and crystallographic nature of the fracture, and the effect of varying stress fields and environment on the crack propagation rate and time to failure. Figure 1 illustrates the crystallographic nature of a stress corrosion crack in the Ti-13V-11Cr-3Al alloy. These are scanning electron micrographs showing cleavage of large grains and the orientation of secondary cracks within these grains.

From deformation bands around a microhardness indenter put into a polished grain containing one of the secondary cracks, a trace analysis showed that the cracks had a {100} habit. Single edge notch fracture specimens are being used for the fracture mode studies; tapered crackline-loaded specimens are being used for measurement of crack propagation and time to failure. Both scanning electron microscopy and electron fractography (replica) are used for observation of the fracture surfaces. A typical fractograph from a stress corrosion crack in the Ti-5Al-2.5Sn alloy is shown in Fig. 2. The stress wave emission technique of monitoring crack growth is being used to investigate the nature of the crack extension process.

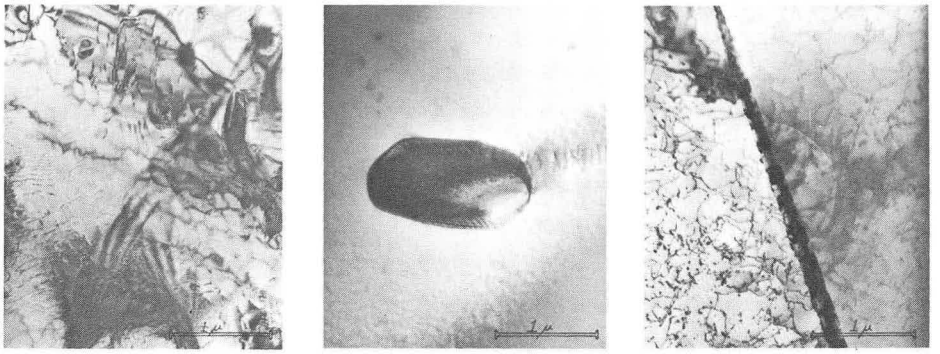

(a) (b) (c)

Fig. 1. α-phase titanium-aluminum alloy in (a) as received, (b) annealed, and (c) 10% cold-rolled condition. (XBB691-620)

5. HIGH-STRAIN-RATE STUDIES OF Ti-Al BINARY ALLOYS

Charles J. Bruggemann

A series of binary titanium-aluminum alloys have been subjected to an inert atmosphere grain growth anneal to produce comparable grain sizes as well as to creep-flatten the as-received slabs. Techniques for spark-cutting flat sections from bulk material for electron microscopy studies have been improved and a small jet pump for use in preferential thinning of foil blanks at -50° has been constructed. Characterization of materials has involved electron microscopy of the as-received, annealed, and 10% rolled materials, shown respectively in Figs. 1(a), (b), and (c) at 20,000 magnifications. Figure 1(b) shows a particle of retained high temperature β phase and Fig. 1(c) includes a $\{1\bar{2}14\}$ deformation twin. Stereographic projection twin analysis was made, based upon the work of Bullough and Wayman. [1]

1. R. Bullough and C. M. Wayman, Twinning and Some Associated Diffraction Effects in Cubic and Hexagonal Metals, Part I, Trans. AIME 236, 1704 (1966).

6. CORROSION OF TRIP STEELS

Jean-Francois Challande

Studies of 17 different alloys have indicated that TRIP steels may be quite resistant to corrosion. Eleven steels that were totally austenitic and six that had been partially transformed to austenite-martensite mixtures were evaluated using a potentiostatic technique. Potential/current density curves were obtained in a 10% by weight solution of sulfuric acid. Current densities in the passive range were then compared as a function of alloy content. Assuming the reaction

$$Fe \rightarrow Fe^{2+} + 2e^{-}$$

is the major contributing dissolution reaction, a current density of 1 $\mu A/cm^2$ compares to about 0.5 mils per year of corrosion.

Results showed that chromium content was of importance but, surprisingly, that manganese content was even more critical. The effect of manganese was only noted for alloy contents between 2 and 4%. The other large alloy factor was carbon, which with increasing amounts increased the corrosion rate. An alloy parameter that grouped the experimental data about a single curve is given by

$$\text{Alloy parameter} = 1\,Cr - 3(2 < Mn < 4) - 10C,$$

where the alloy contents are in weight percent. For each specimen the alloy parameter was calculated and plotted in Fig. 1 as a function of current density. Of course there is a basic difference between corrosion behavior of austenite and martensite and so two separate groups of data result. It is obvious that with an increase in the alloy parameter there is a decrease in current density or corrosion rate.

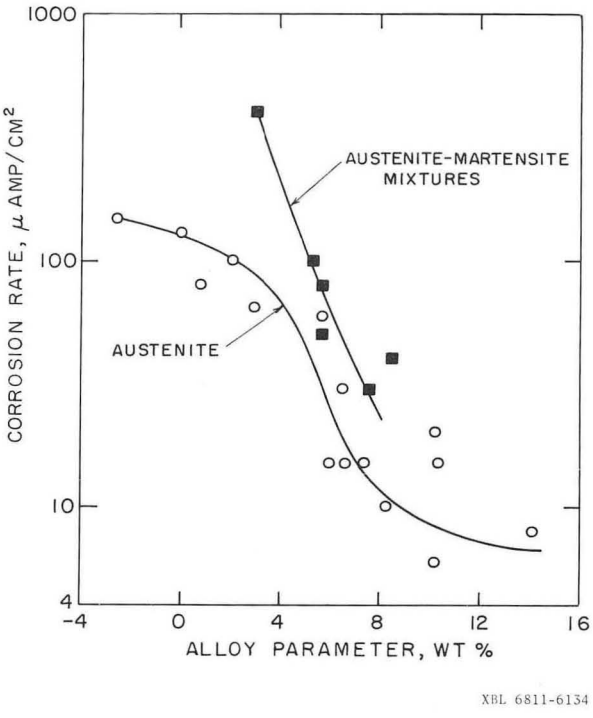

Fig. 1. Effect of alloy content on corrosion behavior of TRIP steel.

For comparison, type 316 stainless steel corrodes at a rate between 2 and 20 mils per year in a 10% sulfuric acid solution. Thus, the better TRIP steels, which appear to corrode at a rate near 5 mils per year, are commensurate with austenitic stainless steels.

7. THE EFFECT OF STACKING FAULT ENERGY ON THE STRAIN-INDUCED MARTENSITE TRANSFORMATION

John Dunning

Two series of Fe-Cr-Ni-Mo alloys, one with and one without carbon, were designed such that in each series the S. F. E. varied in a regular manner. The alloys were austenitized and then deformed by varying amounts at 450°, prior to being subjected to tensile straining. The temperature at which tensile straining was carried out was progressively lowered until transformation to martensite occurred during tensile straining to failure. The degree of transformation occurring during straining to fracture was observed in all cases.

A number of factors were observed in the two series:

(a) The effect of S. F. E. on the amount of transformation
(b) Mechanical stabilization effects
(c) The effect of the strain-induced transformation onductility as represented by elongation in the case of carbon containing alloys.

This work is being extended with single crystal studies of a number of Fe-Cr-Ni alloys.

Three single crystals are being utilized:
(a) Fe-34.5Ni
(b) Fe-18.5Ni-10Cr
(c) Fe-15Ni-15Cr.

The crystals, which exhibit a wide variation in S. F. E. (Ni raises the S. F. E. of Fe, Cr lowers the S. F. E.), have been grown in the [001] orientation and will be large enough for a number of varying orientations to be cut from one crystal. Single crystal tensile specimens will be cut with the tensile axis being [001], [011], [135], or [123].

In two orientations (the tensile axis being the [001] or [011] direction) multiple slip occurs directly after tensile testing is started. However, when the tensile axis is close to (135) or (123) a region of single slip occurs. During the course of the test in the latter case, the specimen rotates until the orientation is such that double slip commences. It is important that the longitudinal axis of these specimens be close to the center of the stereographic triangle to allow enough single slip to occur before double slip starts. It is anticipated that the strain-induced martensite transformation will not occur in the easy glide region, and it is hoped that nucleation sites can be detected when double slip starts. The size of tensile specimens will be such that transmission electron microscopy can be used effectively.

8. INTERGRANULAR FRACTURE OF PRECIPITATION HARDENING ALUMINUM ALLOYS

David Porter

The fracture path in polycrystalline materials may be either transgranular or intergranular. Since most engineering failures occur by some form of transgranular fracture, this mode of fracture is more widely studied and perhaps better understood than intergranular fracture. Intergranular fracture is, however, an important fracture mode in such engineering areas as stress-corrosion cracking, creep, and the development of high strength precipitation hardening alloys. In regard to the latter area, precipitation hardening aluminum alloys are known for intergranular failure at peak strength.[1]

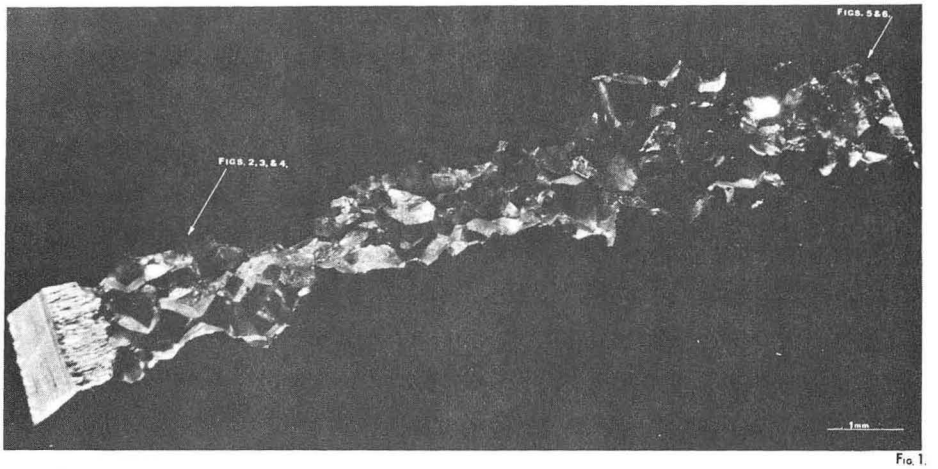

FIG. 1.

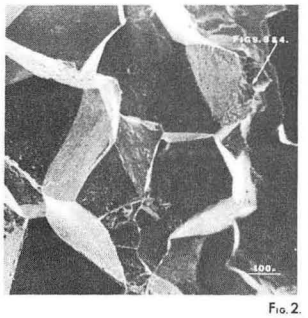

FIG. 2.

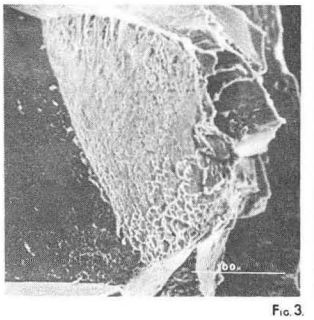

FIG. 3.

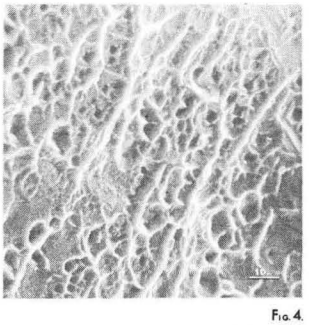

FIG. 4.

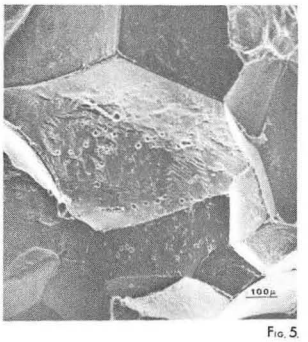

FIG. 5.

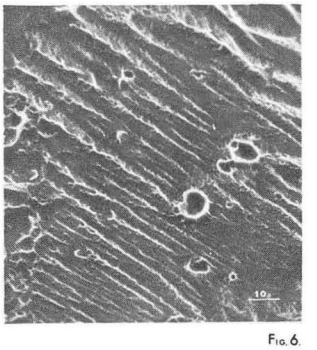

FIG. 6.

Figs. 1-6. Two modes of intergranular fracture in a single-edge-notched sample of solution treated and quenched aluminum, 26 wt % zinc. Figure 1* shows the general appearance of the fracture surface and the areas from which the scanning electron micrographs come. The first series of scanning electron micrographs, Figs. 2, 3, and 4, were taken from the slow crack region. This series of micrographs shows that fracture is occurring by microvoid coalescence in the grain boundaries. After the crack grows slowly for a while there is a transition to fast crack growth, and fracture occurs by cleavage in the grain boundaries. This is shown in the second series of micrographs, Figs. 5 and 6.

*Figure 1 is a scanning optical micrograph. It was taken by scanning the sample along the optical axis of a microscope with respect to a highly collimated beam of light that is fixed at the focal point of the microscope. Only that portion of the sample that is in focus is illuminated and recorded.

(XBB6812-7538)

The literature of intergranular fracture has mainly been limited to the area of creep.[2] The present investigation has endeavored to understand intergranular fracture in non-creep conditions by applying the concepts of fracture mechanics to high purity aluminum alloys showing intergranular failure. Several binary alloys of aluminum-zinc and aluminum-silver were studied because they show very distinct intergranular fracture characteristic over a wide range of heat treatments and strength levels. One of the most interesting results of this study is shown in Figs. 1-6. Certain compositions in an aluminum-zinc system (approximately 20-40% Zn) can be made to fracture intergranularly in a two-stage process. Under these conditions the crack starts growing slowly at a low stress intensity level to a point where the crack becomes unstable. At this point the specimen fails catastrophically by "intergranular cleavage" (not true cleavage, due to the lack of crystallographic character). This cleavage occurs at approximately the maximum load and if one does not consider the slow crack growth that has taken place up to this point, the stress intensity to yield strength ratio is greater than one. The alloys appear to have good toughness from standard fracture tests because such tests are not always sensitive to slow crack growth. The use of stress-wave emission has shown clearly that the fracture process starts at a very low stress intensity level and that these alloys have poor resistance to crack growth.

---

1. D. A. Ryder and A. C. Smale, Fracture of Solids, D. C. Drucker and J. J. Gilman, eds. (John Wiley & Sons, New York, 1963), p. 237.
2. H. C. Chang and N. J. Grant, Trans. AIME 206, 544 (1956).

9. RESEARCH PLANS FOR CALENDAR YEAR 1969

William W. Gerberich, Earl R. Parker, and Victor F. Zackay

Stress-Corrosion Cracking of Titanium Alloys

Analysis of crack growth rate, stress-wave emission, and fractographic evidence will be made on four titanium alloys. First, the relative importance of electrochemical versus mechanical processes at various stages of the growth process will be attempted. Secondly, an interpretation of the growth rate will be inserted into the appropriate fracture mechanics framework to allow analysis of the time to failure in a stress-corrosion cracking test.

Acoustic Emission Studies of Dislocation Mobility

In conjunction with the acoustic emission group at Livermore, considerable information has been obtained with respect to relative dislocation mobilities in an aluminum alloy. Particularly, it has enabled a prediction of a region of plastic instability at the tip of a crack, which is the micro-step involved in the slow crack growth process. Extension of this analysis to TRIP steels will be made since the simultaneous occurrence of a transformation with a growing crack will drastically affect the dislocation mobility and hence the region of fracture instability.

High-Strain-Rate Studies of Ti-Al Binary Alloys

The high-strain-rate study will employ uniaxial stress measurements at strain rates of 10^3-10^5 sec^{-1} and uniaxial strain plate impact tests in the range of 50 kbar. An attempt will be made to prevent reverse plastic flow in the uniaxial strain tests in order to investigate the microstructure produced by the passage of a single plastic shock wave. The effect of substructure produced by quasistatic deformation and by high-strain-rate deformation on the resulting mechanical properties of these deformation twinning materials will also be investigated.

Fracture of Two-Phase Materials

Continued investigation of fracture in unidirectional composite systems will include the analysis of fatigue-crack propagation data. There has already been some success with describing crack growth rates in aluminum reinforced with stainless steel wire. This analysis will be extended to the aluminum-boron system. A description of the fracture process will then be attempted for microsystems. The first system will be various pearlitic structures with carbon content, lamellae size, and interlamellar spacing as the variables. Macroscopic observation of crack growth in crack-line loaded samples will be made with a crack-opening displacement gage. Electron fractography, scanning electron microscopy, and acoustic emission techniques will be utilized to analyze the microscopic growth process.

Environmental Effects on TRIP Steels

Further investigation of the mechanism of corrosion in TRIP steels will be made on a series of Cr-Ni-Mo-Mn-C steels. Besides potentiodynamic corrosion test data, experiments to evaluate the resistance to crack propagation and stress-corrosion cracking characteristics will be run. Alloy optimization

with respect to strength, toughness, and corrosion characteristics will be attempted. Future work on hydrogen embrittlement effects will consist of evaluating specimens that have been cadmium-plated, cathodically-charged, and then baked at 300°F to insure a homogeneous distribution of hydrogen. Various baking times will be utilized to attain concentration levels in the range of 1 to 10 ppm. Fatigue-crack growth rate studies will also be made to determine the relationship between stress intensity and crack growth rate. Continuum fatigue-crack propagation theories will be evaluated with respect to the interaction of a fatigue crack and the austenite-martensite mixtures resulting from the strain-induced transformation.

10. 1968 PUBLICATIONS

Earl Parker, Victor F. Zackay, and Associates

Technical Journals

1. W. W. Gerberich and V. F. Zackay, On the Plane Stress Plastic Zone Correction in Fracture Mechanics, Weld. J. Res. Supp. 47, [8], 3785 (1968).
2. W. W. Gerberich and G. S. Baker, The Toughness of Two-Phase 6Al-4V Titanium Microstructures, in Applications Related Phenomena in Titanium Alloys (ASTM STP 432, American Society for Testing and Materials, 1968), p. 80.
3. W. W. Gerberich and C. E. Hartbower, Some Observations on Dimple Size in Cyclic-Load-Induced Plane-Stress Fracture, Trans. Quart. ASM 61, 184 (1968).
4. W. W. Gerberich, P. L. Hemmings, M. D. Merz, and V. F. Zackay, Preliminary Toughness Results on TRIP Steel, Trans. Quart. ASM 61, No. 4 (1968).
5. W. W. Gerberich, C. E. Hartbower, and P. P. Crimmins, Spontaneous Strain-Aging as a Mechanism of Slow Crack Growth, Weld. J. Res. Supp. 47, 4335 (1968).
6. W. W. Gerberich, Metastable Austenitic Steels with Ultra-High Strength and Toughness, Society of Automotive Engineers, Paper No. 690262, Dec. 1968.
7. C. E. Hartbower, W. W. Gerberich, and P. P. Crimmins, Monitoring Subcritical Crack Growth by Detection of Elastic Stress Waves, Weld. J. Res. Supp. 47, 1S (1968).
8. C. E. Hartbower, W. W. Gerberich, and H. Liebowitz, Investigation of Crack-Growth Stress-Wave Relationships, Eng. Frac. Mechanics 1, 291 (1968).
9. C. E. Hartbower, W. W. Gerberich, and P. P. Crimmins, Monitoring Subcritical Crack Growth by an Acoustic Technique, in Weld Imperfections, F. Pfluger and R. E. Lewis, eds. (Addison-Wesley Publishing Co., Reading, Mass., 1968), p. 371.
10. Y. Katz, P. L. Key, and E. R. Parker, Dimensionless Fracture Toughness Parameters, J. Basic Eng., Trans. ASME 90, 622 (1968).
11. E. R. Parker and V. F. Zackay, Strong and Ductile Steels, Scientific American 219, 36 (1968).

UCRL Reports

1. J. Challande, Corrosion Resistance of Metastable Austenitic Steels (M.S. Thesis), UCRL-18475, September 1968.
2. Y. Chung, The Effect of Strain Aging on the Fracture Toughness of Steel (M.S. Thesis), UCRL-18116, March 1968.
3. W. W. Gerberich, P. L. Key, and E. R. Parker, A Semi-Quantitative Model of Pop-in Behavior, UCRL-18184, April 1968. Presented at National Symposium on Fracture Mechanics, Lehigh University, June 1968.
4. W. W. Gerberich, P. L. Hemmings, and V. F. Zackay, Observations of Strain-Induced Martensite Around a Crack, UCRL-18534, October 1968.
5. W. W. Gerberich and P. L. Hemmings, Fractographic Observations of Stretched Regions in Front of Fatigue Cracks, UCRL-18622, November 1968.
6. W. W. Gerberich, Metastable Austenitic Steels with Ultra-High Strength and Toughness, UCRL-18609, November 1968.
7. W. W. Gerberich, P. L. Hemmings, V. F. Zackay, and E. R. Parker, Interactions Between Crack Growth and Strain-Induced Transformation, UCRL-18467, September 1968.
8. J. Hall, Structural Observations in a Metastable Austenitic Steel (M.S. Thesis), UCRL-18282, June 1968.
9. P. Hemmings, The Influence of Strain-Induced Transformation on Fracture of Steels (M.S. Thesis), UCRL-18458, September 1968.
10. Y. Katz and M. D. Merz, Notch Toughness Variations in Steels with the Same Tensile Properties, UCRL-18015, January 1968.
11. P. L. Key, Y. Katz, and E. R. Parker, An Application of Fracture Mechanics to Glassy Plastics, UCRL-17911, February 1968.
12. P. L. Key and Y. Katz, On the Pop-in Mode of Fracture, UCRL-17898, February 1968.
13. P. L. Key, The Effect of Yielding on the Strain Energy Release Rate, UCRL-18299, June 1968.
14. P. L. Key, A Relation Between Crack Surface Displacements and the Strain Energy Release Rate, UCRL-18065, June 1968.
15. P. L. Key, An Investigation of the Factors Affecting the Fracture Characteristics of Cracked Tungsten Crystals (Ph.D. Thesis), UCRL-18620, December 1968.
16. E. W. Page, Structure and Properties of Dynamically Strain Aged Steels (M.S. Thesis), UCRL-18244, June 1968.

17. E. W. Page, P. Mangonon, G. Thomas, and V. Zackay, Structure and Properties of Dynamically Strain Aged Steels, UCRL-18386, September 1968.

F. HIGH FIELD SUPERCONDUCTIVITY

Leo Brewer, Earl R. Parker,
and Victor F. Zackay

The program is directed towards increasing our understanding of the factors that increase the ability of high field superconductors to carry large transport currents in the presence of magnetic fields and to find new methods of making such materials.

1. EFFECT OF FINE PRECIPITATES ON CRITICAL CURRENT DENSITIES OF SUPERCONDUCTING NIOBIUM 1% ZIRCONIUM

Masaki Suenaga

In Type II superconductors, magnetic fields penetrate in a form of a quantized flux lattice when the applied field, H, exceeds the lower critical field, H_{c_1}. In a homogeneous superconductor, the flux lines are forced to move because of the Lorentz force. Flux movement produces a voltage drop across a sample when a transport current, which is not parallel to H, is present. It is well known that the motion of flux lines can be prevented or retarded to much higher current densities when crystal lattice defects, such as dislocations and precipitates, are present to pin flux lines. Numerous papers have been published on the qualitative relationship between the critical current densities and the nature of defects in superconductors, but practically no quantitative investigations of the subject have been reported. In the present investigation a simple model for flux pinning by non-superconducting precipitates was developed, and the model was compared with the experimental results on Nb 1% Zr alloy. The model developed is very similar to Orowan's theory of the yield strengths of metals containing non-deformable precipitated particles. Since Orowan's theory has been very successful in spite of its simplicity, and because there is a great deal of similarity between dislocations and flux lines, as has been pointed out by Goodman and Matricon, a similar pinning mechanism approach was employed to treat the variation of critical current densities with precipitate size and spacing.

With simplifying assumptions,* which were used in the model, the dependence of critical current densities, J_c, of the alloy on the interprecipitate spacing, 2δ, the precipitate sizes, $2b$, and applied field, H, were expressed as

$$J_c \approx m\left(\frac{b}{\delta}\right)^{3/2}\left(\frac{\mathcal{J}}{2k^2-1}\right)^{1/2}\left(\frac{H_{c_2}-H}{H}\right) \quad \text{for } \frac{\delta}{R} \ll 1,$$

where $\mathcal{J}$ is the flux line energy per unit length, H_{c_2} is the critical field at 4.2°K, m is a multiplicity factor that takes into account the fact that all flux lines would not be released from pinning sites at the same instance, and R is the radius of the curvature of a flux line between a pair of pinning sites.

This expression was compared with experimental results of the heat treated Nb 1% Zr alloys with regard to critical current densities and microstructural variations of the alloys.

(1) The model developed predicts that critical current densities vary with applied fields as $J_c(H) \approx (H_{c_2} - H)/H$. Experimental results showed that such variation of J_c with H was in good agreement for alloys with intermediate pinning strength (Fig. 1). However, the agreement became poorer for alloys with much stronger or very weak pinning strength. Those discrepancies were thought to be due to the effects that were not accounted for in the simplified model.

(2) The model also predicted that critical current densities vary with precipitate size, $2b$, and interparticle spacings, 2δ as $J_c \approx (b/\delta)^{3/2}$. The experimental results were plotted as $\ln J_c/b^{3/2}$ vs. $\ln \delta$ (Fig. 2). It was observed that slopes of the plots were approximately -3/2. Although it was difficult to determine the exact slope of $\ln J_c/b^{3/2}$ vs. $\ln \delta$ plots, due to the scattering of experimental points, the experimental results were reasonably consistent with the model in spite of simplifing assumptions made in developing the model.

H_{c_2} (4.2°K) and J_c were measured with use of a superconducting magnet. H_{c_2} of the homogenized alloys were 5.2_0 kG (alloy A) and 5.0_5 kG (alloy B), and H_{c_2} did not change more than 0.7 kG after the required heat treatments at 1000°. Critical temperatures, T_c, of the alloys were also measured, and it was found that T_c were 9.1_8°K (alloy A) and 9.2_2°K (alloy B) in the homogenized condition and changed less than 0.2°K after the heat treatments.

*Details of the assumptions and calculations can be found in UCRL-18536 (Ph. D. Thesis, M. Suenaga), Jan. 1969.

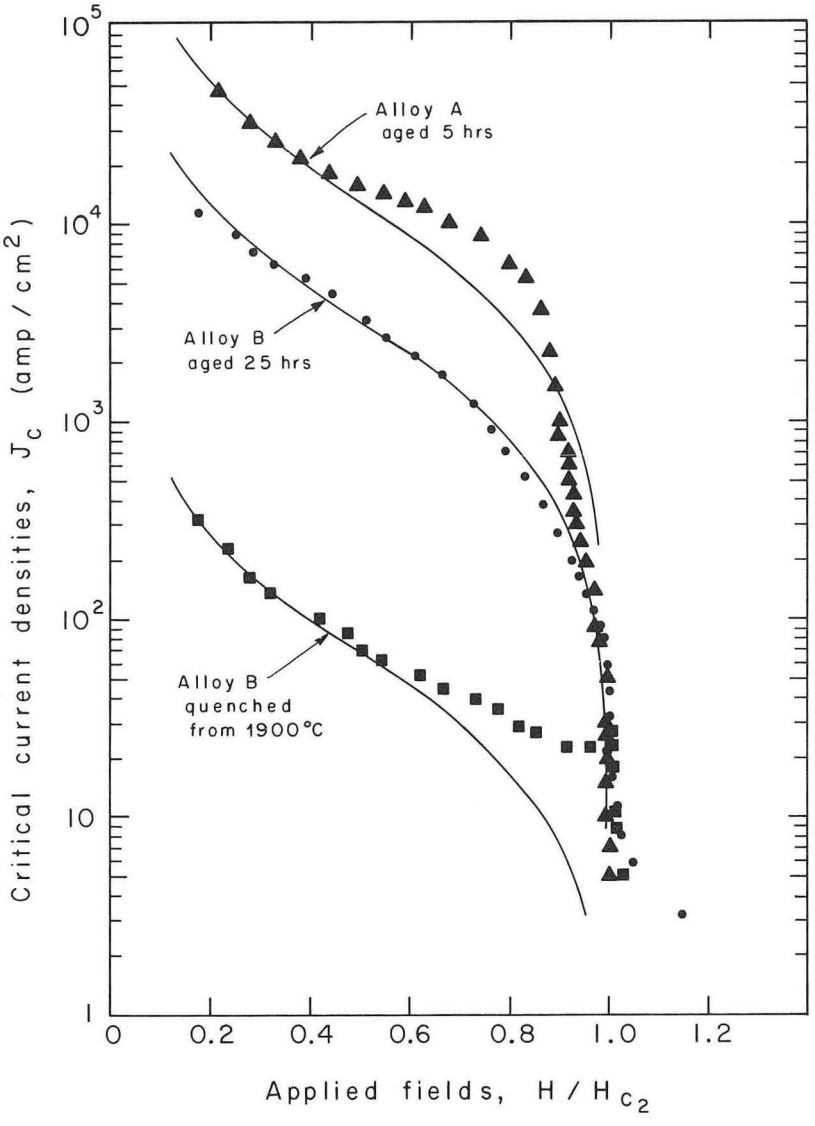

Fig. 1. Comparison of the experimental J_c vs. H/H_{c_2} curves with the expression (1).

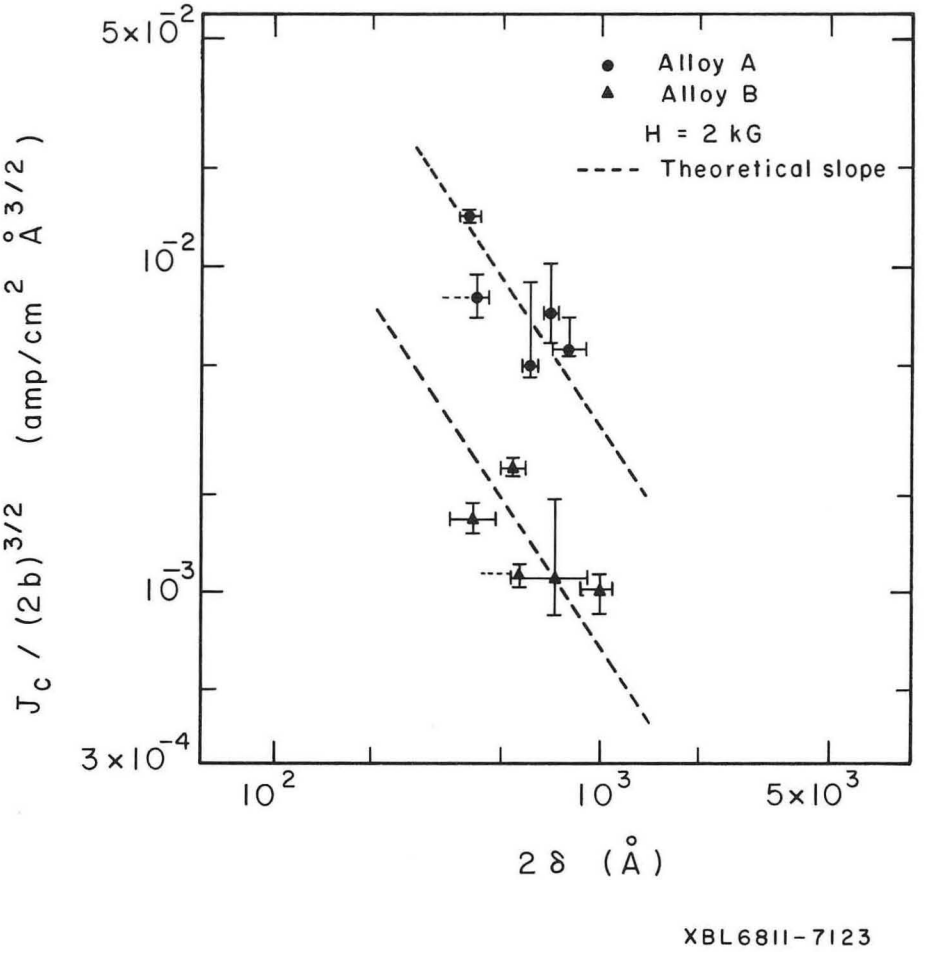

Fig. 2. Plots of $J_c/b^{3/2}$ vs. 2δ for the alloys A and B.

For measurements of b and δ of precipitates, ZrO_2, a carbon extraction replica method was employed. Figure 3 shows representative electron micrographs of the alloy B. Variation in sizes and distribution of precipitates with aging time is clearly shown.

Figure 4 shows details of structures of the precipitates at a higher magnification.

Transmission electron and optical microscopies were also used to investigate the precipitates.

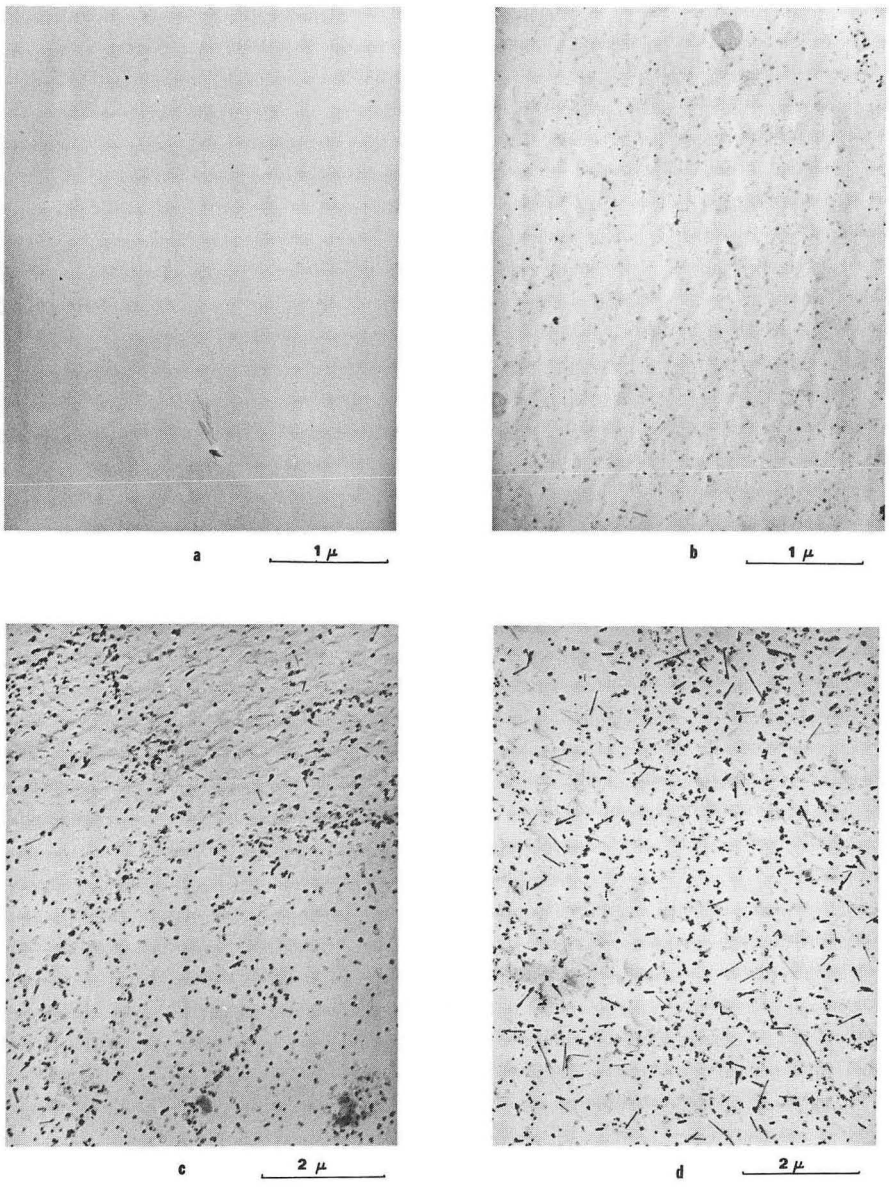

Fig. 3. Carbon replication micrographs of the alloy B. (a) As quenched from 1900°, and aged at 1000° for (b) 10 hours, (c) 25 hours, and (d) 50 hours.

(XBB6811-6838)

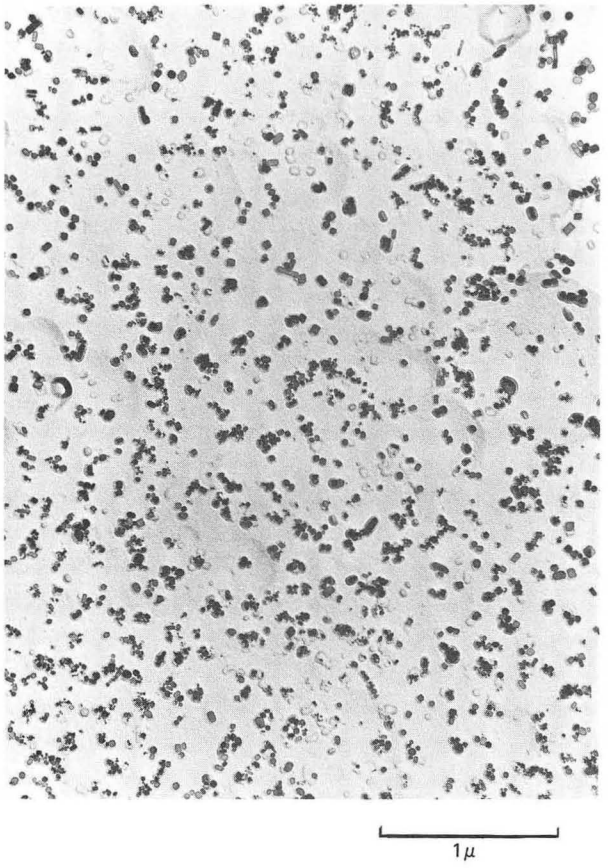

Fig. 4. Carbon replication micrographs of the alloy A quenched from 1800° and aged for 27 hours, showing details of precipitates.

(XBB6811-6832)

2. THE SUPERCONDUCTING CRITICAL CURRENT AND CRITICAL FIELDS OF Nb_3Sn-NbC AND Nb_3Sn-Nb COMPOSITES*

Russell Jones

The critical currents and critical fields of a Type II superconductor are dependent on certain microstructural aspects. These properties have been studied using composite samples with Nb_3Sn surrounding grains of NbC and niobium. Two types of processing treatments have been examined, resulting in desirable composite microstructures with good critical current and field values.

Films of Nb_3Sn surrounding NbC grains were obtained by hot-pressing powders of niobium, tin, and graphite. Films of Nb_3Sn surrounding niobium grains were obtained with presintered porous niobium impregnated with tin. Metallography, x-ray diffraction, and electron beam microprobe were used in the examination of the samples. The critical temperatures were measured and the field properties were determined using the pulsed-field technique. The highest critical current (J_{cN}) obtained was 53,700 A/cm^2. The highest critical temperature was 17.8°K, and the best upper critical field (H_{c_2}) was 234 kG (Fig. 1).

Two types of processing were used. In one, sintering resulted in grains of NbC coated with Nb_3Sn; in the other, impregnation of presintered porous niobium by tin resulted in niobium grains coated with Nb_3Sn.

Sintered Type

The sintered samples were shown to obey the relationship $H_{c_2} \propto \rho_n \gamma T_c$. The best properties obtained are as follows:

(a) J_{cN} = 3000 A/cm^2 (composite)
(b) J_{cN} = 53,700 A/cm^2 (Nb_3Sn only)
(c) T_c = 17.8°K sintered at 1600°C
(d) H_{c_2} = 234 kG.

The critical temperature of 17.8°K corresponded to an Nb_3Sn composition of 75.3 at. % Nb.

The critical current (J_{cN}) was highest when large amounts of tin were present; it did not vary with T_c or Nb_3Sn composition. The low critical current (J_{cS}) of these samples is attributed to phases that separate the Nb_3Sn and are not superconducting or have lower field properties.

The percentage of Nb_3Sn in the composite was dependent on the sintering temperature T_1. The higher this temperature, the less Nb_3Sn. The distribution of Nb_3Sn was greatly enhanced by lowering T_1 to about 1050°C. The resistivity of these samples is a measure of the composite resistivity and was lowest when excess tin was present.

Impregnated Type

The impregnated samples had a good distribution of Nb_3Sn. The properties of this series were:

(a) J_{cN} = 3400 A/cm^2 (composite)
(b) T_c = 17.6°K
(c) H_{c_2} = 225 kG.

The achievement of a thin continuous network of Nb_3Sn is dependent on the tin wetting the niobium powders; this is true for both the sintered and the impregnated samples. A suggestion for further work is the addition of a wetting agent to the tin. Both samples S1050 and IMP 1 could be improved with this technique.

*Abstracted from UCRL-18437, September 1968.

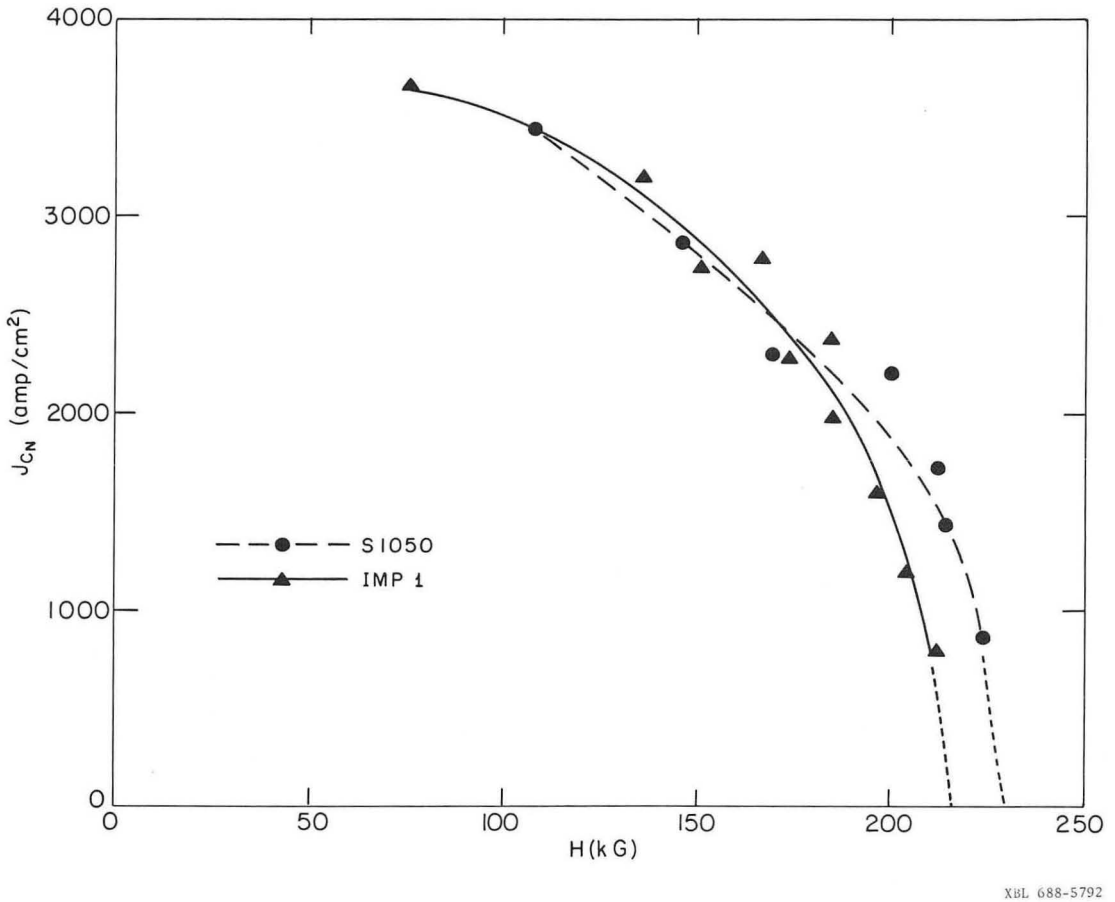

Fig. 1. J_{c_N} vs. H. Comparison of sintered Type B with impregnated type. J_{c_N} is transition to normal state. H is applied magnetic field. H ⊥ J.

3. THE CRITICAL TEMPERATURE OF Nb_3Sn IN VARIOUS MICROSTRUCTURES*

Roger Goolsby

The effects of process variables on the microstructural distribution and critical temperature (T_c) of Nb_3Sn were studied. By utilizing two preparation techniques it was possible to prepare samples whose microstructures consisted of a Nb_3Sn film network surrounding a second phase of either niobium or NbC. The critical temperature of a sample with such a network was approximately the same as that for bulk Nb_3Sn.

One preparation technique consisted of sintering niobium, tin, and carbon powders; the other technique consisted of impregnating a porous niobium powder compact with liquid tin, reacting to form a Nb_3Sn film network at the niobium-tin interface. The critical temperatures of the samples were varied systematically by change of process variables, with T_c values ranging from 15.9 to 17.8°K. For samples prepared by the sintering process, a linear relationship was observed between upper critical field and critical temperature as shown in Fig. 1. Efforts were made to refine the microstructure by obtaining a very thin (< 1000 Å) Nb_3Sn film network, because it was anticipated that thin film superconducting effects would result if sufficiently thin films were obtained.

*Abstracted from UCRL-18452, September 1968.

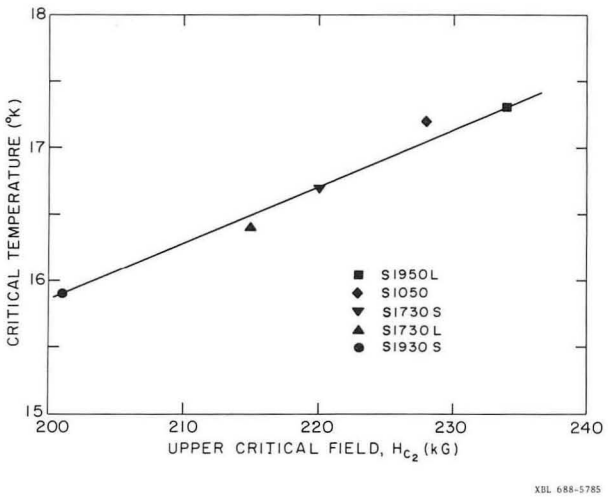

Fig. 1. Variation of critical temperature with upper critical field for sintered samples.

4. EFFECT OF SUBSTITUTIONAL VANADIUM AND TANTALUM ON THE CRITICAL TEMPERATURE OF $Nb_3(Al_xGe_{1-x})$

Larry Hartsough

A study of the superconducting properties of the intermetallic compound $Nb_3(Al_xGe_{1-x})$, was reported in the 1967 IMRD Annual Report, UCRL-18043. Additional investigations to determine the influence on the critical temperature by the substitution of other transition elements in place of the Nb atom were made. The compounds $Nb_{.75-x}V_x(Al_{.75}Ge_{.25})_{.25}$ were prepared with up to 16 at. % V. The critical temperature decreased nearly linearly from about 19.8°K (midpoint of transition) to 16°K for 9.8 at. % V. Likewise the addition of Ta caused a nearly linear decrease in T_c, reaching 16°K at 16 at. % Ta.

5. 1968 PUBLICATIONS

Leo Brewer, Earl R. Parker, Victor F. Zackay, and Associates

Technical Journals

1. L. Hartsough, V. F. Zackay, and E. R. Parker, High Field Characteristics of $Nb_3(Al, Ge)$, Appl. Phys. Letters 13, 2 (1968).
2. K. M. Ralls, E. R. Parker, and V. F. Zackay, Superconductivity of Ceramic Compounds, in Ceramic Microstructures (John Wiley & Sons, New York, 1968), p. 489.

UCRL Reports

1. R. Goolsby, The Critical Temperature on Nb_3Sn in Various Microstructures (M. S. Thesis), UCRL-18452, September 1968.
2. R. Jones, The Superconducting Critical Current and Critical Fields of Nb_3Sb-NbC and Nb_3Sn-Nb Composites (M. S. Thesis), UCRL-18437, September 1968.
3. M. Suenaga and K. Ralls, Some Superconducting Properties of the Ti-Nb-Ta Alloys, UCRL-18276, May 1968.
3. V. F. Zackay, M. Merriam, and K. Ralls, Superconductivity and Phase Diagrams, UCRL-18362, August 1968.

6. SUPERCONDUCTING TRANSITION TEMPERATURES OF LEAD-THALLIUM ALLOYS*

Eckhard Nembach†

It has been reported by Claeson[1] that the alloy system lead-thallium shows a dip in the superconducting transition temperature T_c in the composition range 47-53 at. % Tl. The change in T_c is from 0.1 to 0.2°K lower than one would expect by interpolating T_c's of specimens with higher or lower thallium concentrations (see Fig. 1.). Moreover, these specimens show two different T_c's. An explanation, based on the electron structure of pure lead and the rigid-band model, suggested that a lead-thallium alloy with a composition of roughly 50 at. % Tl should have a very high density of electron states at the Fermi surface because at the electron concentration of these alloys electrons start entering the third band. It was also noted that a phase change, such as ordering, could also result in the dip of T_c.

In order to check these results samples were made in the same way as Claeson's, but instead of slowly cooling from the melt, these samples were quenched in ice water. They were then annealed for at least 21 days at 295°C, then quenched again in ice water.

The superconducting transition was detected by the change of the mutual inductance of two coaxial coils, as described in previous reports (see the 1967 IMRD Annual Report, UCRL-18043, or Ref. 2). The results of this investigation together with the results of Claeson are shown in Fig. 1. Within the absolute accuracy of 0.1°K of his temperature measurements, our T_c's and his coincide, except for specimens with thallium contents between 49 and 50 at. %, for which Claeson had found a deviation from a smooth curve. From our measurements it is clear that this special

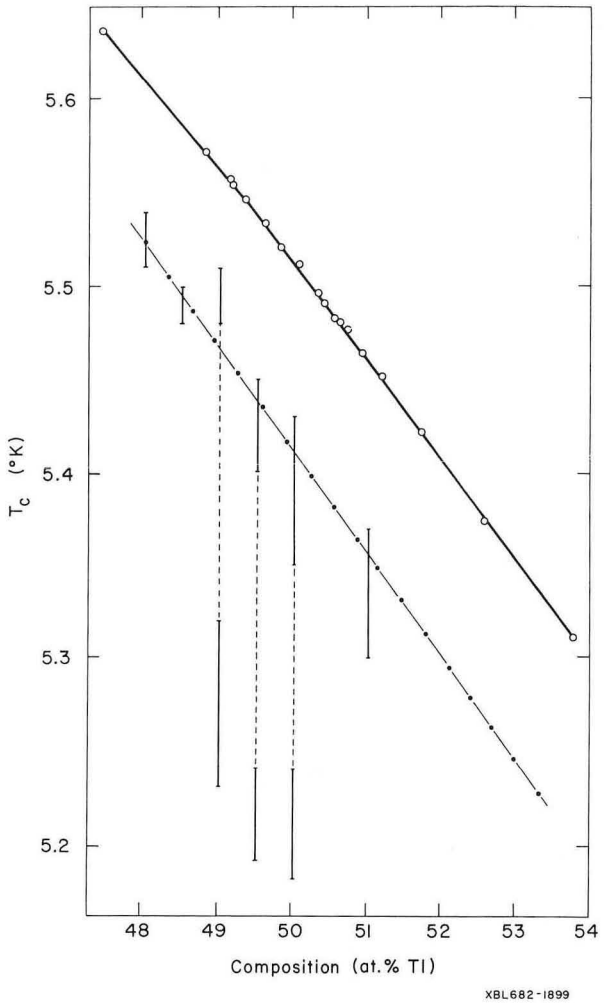

Fig. 1. Critical temperature as a function of the Tl concentration.

O This investigation

T. Claeson's transitions

Links the two transitions of a specimen

---- Interpolation of T. Claeson's T_c values for Tl contents lower than 49 or higher than 51 at. %.

behavior does not exist. Claeson's findings are probably due to inhomogeneity of his specimens, because they are slowly cooled from the melt, which results in regions of various thallium contents in a sample. As the solidus and liquidus lines in the lead-thallium phase diagram make only a rather small angle with the concentration axis, cooling a specimen slowly through the two-phase region may bring about a great scatter in the composition, even though the solidus and liquidus lines are rather close together.

In order to prove this idea five samples were melted once more, but, instead of being quenched from the melt, they were cooled at rates between 1.0 and 2.5°C/min through the two-phase region and then treated as before. This slow cooling increased Δ_{10} on an average by a factor of 2, showing that the specimen had become inhomogeneous.

Therefore the conclusions drawn by Claeson from his measurements are no longer valid. Either the high density of states does not exist, or its influence on the superconducting transition temperature is counterbalanced by some other effect.

---

*Abstracted from Phys. Rev. 172, 425 (1968).
†Present address: National Research Institute for Metals, Tokyo, Japan.

1. T. Claeson, Phys. Rev. 147, 340 (1966).
2. E. Nembach, J. Phys. Chem. Solids 29, 1205 (1968).

7. THE LOW TEMPERATURE REGION OF THE LEAD-INDIUM PHASE DIAGRAM*

Eckhard Nembach

The phase diagram of the system lead-indium has been the subject of extensive investigations,[1,2] but recently T. Heumann and B. Predel[3] concluded from their thermodynamic data that a new feature should occur below room temperature. The maximum values for the enthalpy and entropy of mixing are reached at a composition of 50 at. % Pb and are +400 cal/g-atom and +1.7 cal/g-atom degree, respectively. From this the authors estimated that a miscibility gap should occur below 30°C, centered at 50 at. % Pb. Resistivity measurements seemed to support this view. These authors proposed the phase diagram outlined in Fig. 1. Three phases exist at 30°C: the tetragonal In phase with $c/a > 1$, the tetragonal intermediate phase α_1 with $c/a < 1$, and the face-centered cubic Pb phase. We observed,[4] during an investigation of the superconducting properties of Pb-In alloys, that aging a specimen with 50 at. % Pb for 14 days at -18°C decreased the superconducting transition temperature about 0.13°K and tripled the transition width. Following this, it seemed desirable to investigate the low temperature portion of the Pb-In phase diagram with use of superconductivity and x-ray diffraction.

The samples were prepared by quenching in ice water from the melt, followed by homogenization at 20-30°C below the solidus line, established by T. Heumann and B. Predel.

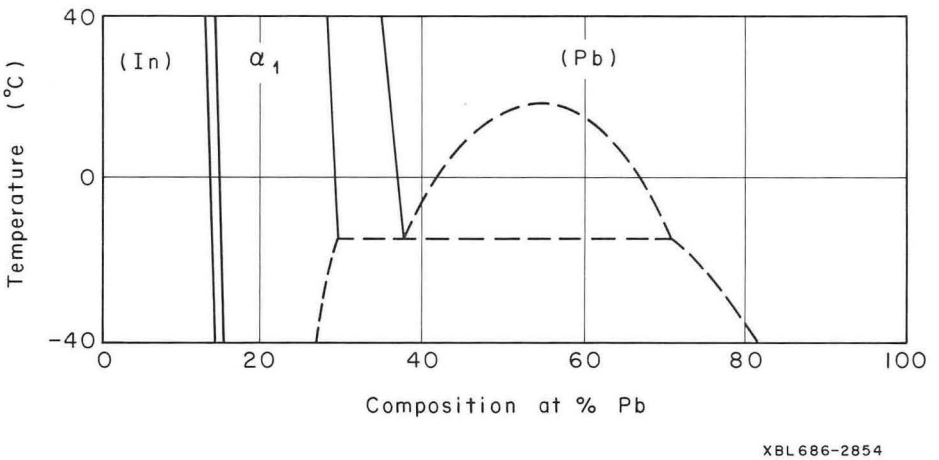

Fig. 1. The low temperature region of the In-Pb phase diagram as outlined by T. Heumann and B. Predel. (In) tetragonal, c/a > 1; α_1 tetragonal, c/a < 1; (Pb) fcc. The miscibility gap is dashed.

The annealing times were 144 hr for specimens containing less than 30 at. % Pb and 36 hr for the remainder. The specimens were then quenched into ice water.

The critical temperatures were measured using the change in inductance, as described previously. Then the specimens with lead content between 38 and 75 at. % were aged for 7 days at temperatures between -30 and 40°C. If this treatment caused T_c to change by more than 0.005°K or the width of the transition to increase by more than 0.002°K, it was concluded that the specimen had undergone a phase change and no longer consisted only of the fcc Pb phase, as it did immediately after homogenizing. The result is shown in Fig. 2. From this one can estimate the extension of the fcc phase. The x-ray measurements were based on these preliminary results.

X-ray patterns were taken with use of 75 μ diameter powder, after annealing for 30 minutes at temperatures between 120 and 160°C, followed by an ice-water quench. The x-ray measurements were made at -178°C, using a Picker diffractometer, model 3488K. In this way the relation $a = 4.6970 + 0.002469\ C$, for $40 \leq C \leq 7.5$, where a is the lattice constant (Å) and C is the at. % of Pb, was obtained, which is very similar to one found by Heumann and Predel at room temperature.

Following this, homogenized specimens with compositions between 15 and 56 at. % Pb were aged for at least 10 days at temperatures between -27 and +25°C. The aging temperatures were chosen in accordance with the superconductivity results. Since an aging time of only 7 days gave the same results, obviously the aging time of 10 days was sufficient to produce the equilibrium phases. Then the x-ray patterns were again taken at -178°C. Three types of x-ray patterns were found: (a) those containing only lines of the tetragonal α_1 phase, (b) those containing only lines of the fcc Pb phase, or (c) those containing lines of the α_1 and the fcc Pb phase. However, lines belonging to two fcc phases, differing only in lattice constant, have never been observed in a sample. This shows that the miscibility gap, proposed by Heumann and Predel, does not exist.

The boundary between [only Pb phase] and [Pb phase + α_1] was established by calculating the concentration of the fcc phase from its lattice constant, using Eq. (1). This procedure was not possible for the phase boundary between [only α_1] and [α_1 + Pb phase], because the lattice constant of α_1 could not be measured accurately enough. Low intensity made it impossible to use lines with $\theta > 34°$.

Therefore another method has been used. Specimens with lead contents between 15 and 28 at. % Pb were first annealed above 100°C. This treatment produced specimens containing only the α_1 phase. If the subsequent aging below room temperature resulted in the formation of the fcc phase, the (111)-x-ray-line of this phase could be observed as well as the (111)-line of the tetragonal α_1 phase. The limit of detection of the former line was about 0.3% of the intensity of the latter. The results are again plotted in Fig. 2, together with the suggested phase diagram.

No attempt has been made to investigate the range of stability of the α_1 phase in the

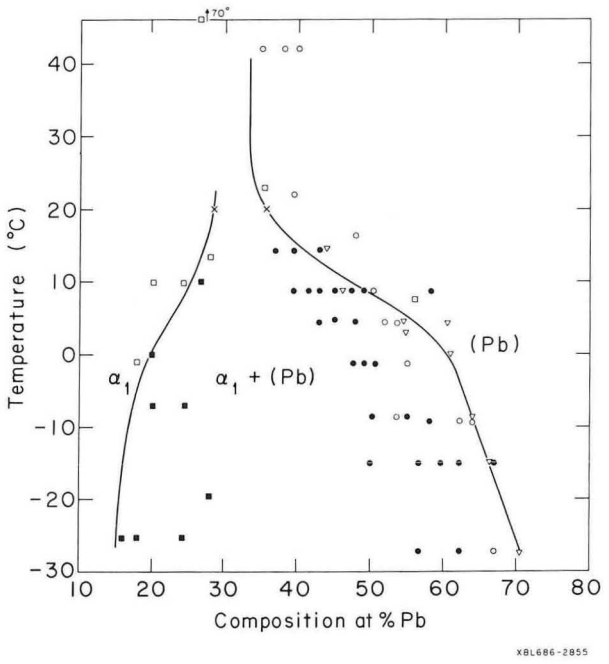

Fig. 2. Results of the superconductivity and x-ray measurements:

low temperature aging did change ● } the superconducting properties
did not change ○ }

phase boundary from lattice constant measurements ▽

x-ray lines of two ■ } phase detectable
of only one □ }

× Points on the phase boundaries given by T. Heumann and B. Predel

— Phase boundaries based on this investigation.

low concentration region, as previous work[5-7] has shown that it is very difficult to establish equilibrium even above room temperature.

The results of this x-ray study show that a narrowing of the stability ranges of the α_1 and the fcc phases in the Pb-In system occurs below room temperature. This is in agreement with Heumann and Predel's thermodynamic data, which suggested a segregation of lead and indium because of the high positive enthalpy of mixing. However, the miscibility gap, proposed by these authors, does not exist.

*Abstracted from UCRL-18284, June 1968.

1. M. Hansen and K. Anderko, Constitution of Binary Alloys (McGraw-Hill Book Company, New York, 1958).
2. R. P. Elliott, Constitution of Binary Alloys, 1st Supplement (McGraw-Hill Book Company, New York, 1965).
3. T. Heumann and B. Predel, Z. Metallk. 57, 50 (1966).
4. E. Nembach, J. Phys. Chem. Solids 29, 1205 (1968).
5. C. Tyzack and G. V. Raynor, Trans. Faraday Soc. 50, 675 (1954).
6. A. Moore, J. Graham, G. K. Williamson, and G. V. Raynor, Acta Met. 3, 579 (1955).
7. G. V. Raynor and J. Graham, Trans. Faraday Soc. 54, 161 (1958).

8. A LOW TEMPERATURE STAGE FOR THE PICKER THETA-THETA X-RAY DIFFRACTOMETER

Eckhard Nembach

During an investigation of the low temperature region of the Pb-In phase diagram[1] it became necessary to determine the crystal structures of the various phases by x-ray diffraction. The powdered specimens were quenched from the aging temperature in liquid nitrogen and their x-ray patterns taken at liquid nitrogen temperatures.

An important feature of this diffractometer is that the x-ray tube and the counter rotate, whereas the specimen remains stationary, with its surface horizontal.

The cold stage is shown schematically in Fig. 1. The powder sample Sp is placed under a 6 μ thick Mylar foil M1 in a disk-shaped cavity of the copper block B, which is attached to the copper rod R (diam. 32 mm). The lower end of this rod is placed in liquid nitrogen to cool the specimen by heat conduction. In order to prevent condensation of water and air on the specimen, it is enclosed in a vacuum chamber consisting of the stainless steel tube T, the flange F, and the cover plate. The x rays reach the specimen through a rectangular Mylar window M2 (25 μ thick, 16×25 mm^2). The chamber is evacuated to about 10^{-3} torr by a mechanical pump. The temperature of the specimen is measured with a copper-constantan thermocouple which is clamped to the copper block B.

The cold stage is connected to the Picker diffractometer via brackets supporting the flange F. Because the copper rod R shrinks more than the steel tube T during the cooling process, the height of the specimen changes with temperature. Therefore the stage has to be aligned after it has cooled to liquid nitrogen temperature. The alignment is achieved by moving the whole stage vertically

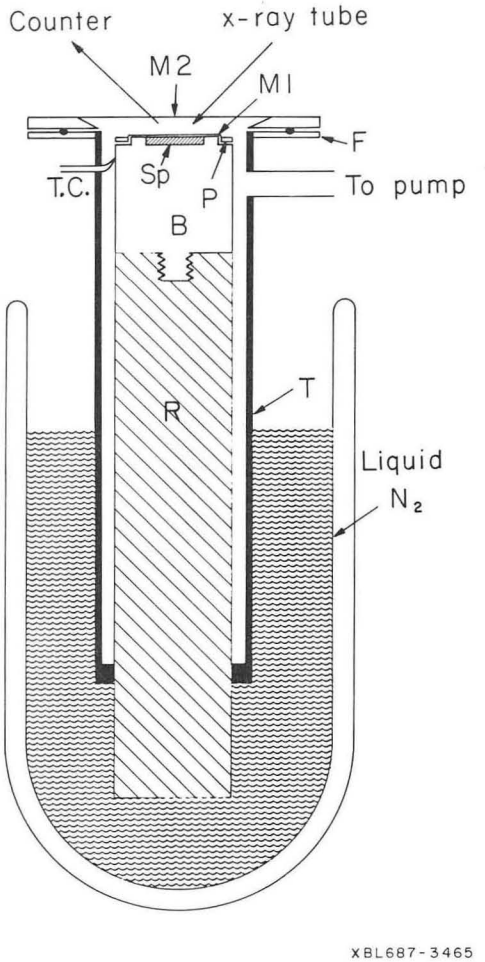

Fig. 1. Cold stage. B, copper block; R, copper block; T, stainless steel tube; M1, M2, Mylar foils; P, brass ring for clamping M1; F, flange; Sp, powder specimen; T.C., thermocouple.

until an x-ray line of a standard specimen occurs at the correct Bragg angle. In order to get a good alignment it is advisable to use a line with a Bragg angle of not more than 15°. For precise work the liquid nitrogen level must be kept constant, otherwise the alignment might deteriorate. If the humidity of the air is high it is necessary to blow dry air over the Mylar window M2 in the cover plate in order to prevent water from condensing on it.

*Abstracted from UCRL-18410, August 1968.
1. E. Nembach, The Low Temperature Region of the Lead-Indium Phase Diagram, UCRL-18284, June 1968

9. 1968 PUBLICATIONS

Eckhard Nembach

Technical Journals

1. E. Nembach, Superconducting Transition Temperatures of Lead-Thallium Alloys, Phys. Rev. 172, 425 (1968).
2. E. Nembach, Superconducting Transition Temperatures of Various Lead-Based Alloys, J. Phys. Chem. Solids 29, 1205 (1968).

UCRL Journals

1. E. Nembach, Superconducting Transition Temperatures of Lead-Thallium Alloys, UCRL-18090, February 1968.
2. E. Nembach, The Low Temperature Region of the Lead-Indium Phase Diagram, UCRL-18284, June 1968.
3. E. Nembach, A Low Temperature Stage for the Picker Theta-Theta X-ray Diffractometer, UCRL-18410, August 1968.

G. THERMODYNAMICS OF METAL SYSTEMS

1. EVALUATION OF THERMODYNAMIC DATA

Ralph Hultgren, Molly Gleiser, Kenneth K. Kelley, and Pramod D. Desai

The project for the evaluation of Thermodynamic Data of Metallic Systems, the first phase of which was published in book form,[1] has been continued. Current evaluations as they are completed are distributed in loose-leaf form to all those requesting them. During 1968 selected values were distributed for these systems: Ag, Al, Ba, Be, Bi, Ca, Ce, Cu, La, Pd, Sb, Ag-Cu, Ag-Pd, Al-Ti, Be-Ce, Be-Gd, Be-La, Be-Mo, Be-Nb, Be-Ta, Be-Ti, Be-U, Be-Y, C-U, Cd-Mg, Cr-Mo, Cr-Re, Cr-Ti, Cu-Fe, Fe-Mo, H-Zr, Hf-Ta, Ir-Mo, Ir-Nb, Mo-Nb, Mo-Ni, Mo-Os, Mo-Pd, Mo-Re, Mo-Ru, Mo-Si, Mo-Tc, Nb-Os, Nb-Pd, Nb-Pt, Nb-Re, Nb-Rh, Nb-Ru, Nb-Sn, Ni-Ti, Re-W, Si-Ta, Ta-W.

The reference file and associated Termatrex system by which pertinent literature searches are carried out is being overhauled and modernized, and a microfiche system is being installed.

1. R. Hultgren, R. L. Orr, P. D. Anderson, and K. K. Kelley, Selected Values of Thermodynamic Properties of Metals and Alloys (John Wiley & Sons, Inc., New York, 1963).

2. THERMODYNAMIC PROPERTIES OF INDIUM-TIN ALLOYS

Hong-il Yoon and Ralph Hultgren

Heats of formation of solid indium-lead alloys were determined in the liquid tin solution calorimeter. From these measurements various thermodynamic properties of the system were calculated.

3. LOW TEMPERATURE HEAT CAPACITY OF AuCu

Donald T. Hawkins and Ralph Hultgren

Work has been continued on the effect of ordering on the low temperature heat capacity of AuCu. Measurements have been made on the heat capacities of the elements and further improvements have been made on the calorimeter.

Measurements will be made on the highly ordered alloy and on an alloy quenched from the disordered temperature region. From these measurements the effect of alloying and the effect of ordering on the lattice heat capacity will be determined as well as the entropies of formation at 0°K.

4. RESEARCH PLANS FOR CALENDAR YEAR 1969

Ralph Hultgren

Revision of the low temperature (liquid hydrogen) calorimeter will be completed and measurements made of the low temperature heat capacities of ordered and disordered AuCu alloys. From these and other data, entropies of formation at 0°K can be calculated and the effects of ordering and heats of formation on lattice vibrational heat capacities determined.

Attempts will be made to determine heats of decomposition of austenite by drop calorimetry into a tin bath at elevated temperature, thus avoiding the martensite reaction.

Evaluation of published data will be continued. Evaluations are now in progress for Cu-Sb, Cu-Pb, Cu-Sn, Cu-Al, Cu-Cd, Cu-Zn, Cu-Mn, Cu-Tl, Cu-Cr, Cu-Co, B-Ti, N-Ti, Py-Mg, Lu-Mg, Ag-Gd, and other systems.

5. 1968 PUBLICATIONS

Ralph Hultgren and Associates

Technical Journals

1. P. J. Desre, D. T. Hawkins, and Ralph Hultgren, Vapor Pressure of Thallium and Activity Measurements on Liquid Silver-Thallium Alloys by the Torsion-Effusion Method, Trans. Met. Soc. AIME 242, 1231 (1968).
2. D. T. Hawkins and P. D. Desai, Thermodynamic Properties of Cerium Gas, J. Chem. Eng. Data 13, 497 (1968).

UCRL Reports

1. J. P. Chan and R. Hultgren, The Thermodynamic Properties of Silver-Palladium

Alloys, UCRL-18273, June 1968.
2. H-I. Yoon, Thermodynamic Properties of Indium-Lead Alloys (M.S. Thesis), UCRL-18402, University of California, Berkeley, September 1968.

III. Ceramic Science

A. HIGH TEMPERATURE REACTIONS

1. MULTIPLICITY OF ELECTRONIC GROUND STATES OF HIGH TEMPERATURE VAPOR SPECIES

David J. Meschi and Alan W. Searcy

A molecular beam apparatus that utilizes an inhomogeneous field magnet is now being used to determine the magnetic moment and hence the multiplicity of the electronic ground state of diatomic molecules. This apparatus is shown schematically in Fig. 1.

The mechanics of the experiment are quite simple. A molecular beam emanating from the Knudsen cell is collimated and then passed between the poles of the inhomogeneous-field magnet. Detection of the beam is done by means of a quadrupole mass spectrometer. Sweeping the movable slit across the detector gives a profile of the beam. If the species in the beam have a magnetic moment, the beam profile will change when the magnet is on because the beam will be deflected somewhat.

Following initial tests with bismuth, the diatomic species S_2 and Te_2 were run to determine whether or not they had magnetic moments indicative of a triplet ground state. The beam profiles of these two species are shown in Figs. 2(a) and (b).

As expected, S_2 did show a magnetic moment. Te_2, on the other hand, showed no evidence of a magnetic moment. Considering the sensitivity of the present apparatus, this means that the average magnetic moment of the Te_2 molecules is at least one and perhaps two orders of magnitude less than that of S_2. Either Te_2 is in a singlet ground state or one component of the triplet state has split away and is considerably lower in energy than the other two.[1] If we assume in the latter case that these upper states together have less than one-tenth the population of the low lying state, then, since the beam temperature was about 800°, the low lying state must be at least 2000 kaysers below the others.

Preliminary results on Se_2 indicate that it is much like Te_2 in that no significant fraction of the Se_2 molecules have a magnetic moment at 800°. This appears to be at variance with the results of other experimenters which are consistent with a closely spaced triplet ground state.[2]

We hope that further experiments on such mixed species as S-Te and S-Se will provide more information about the nature and magnitude of this splitting.

---

1. R. F. Barrow, G. G. Chandler, and C. B. Meyers, Phil. Trans. Roy. Soc. (London), Ser. A260, 395 (1966).
2. C. H. Massen, A. G. L. M. Weijts, and J. A. Poulis, Trans. Faraday Soc. 60, 317 (1964).

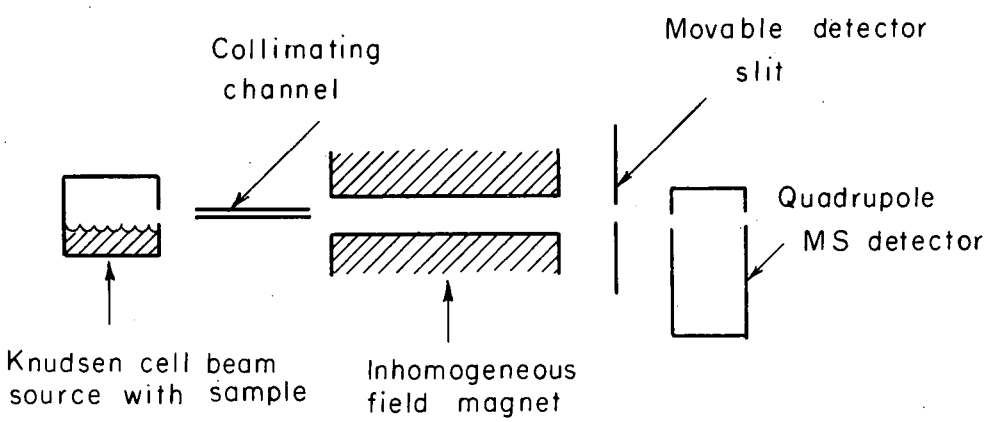

XBL 692-2054

Fig. 1. Schematic of apparatus.

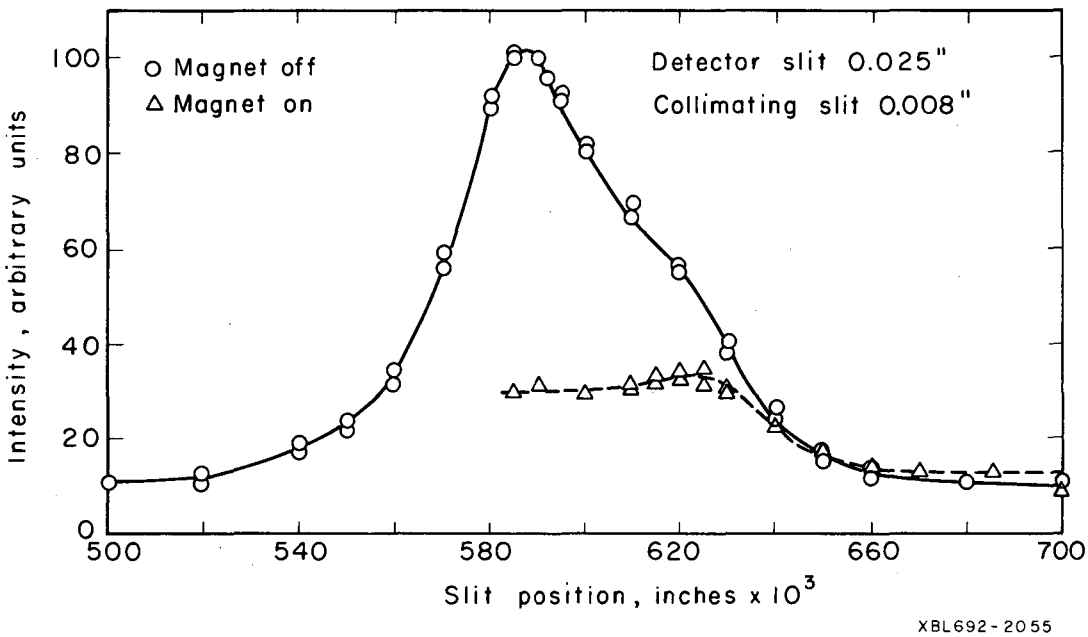

Fig. 2(a). Beam profile of S_2.

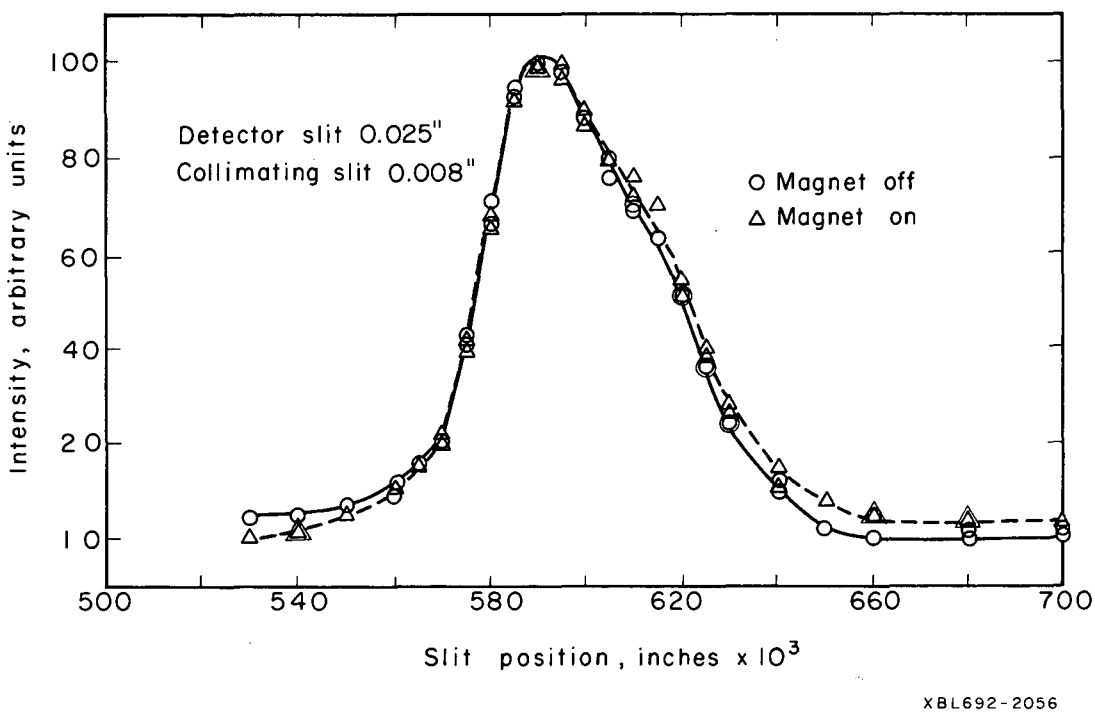

Fig. 2(b). Beam profile of Te_2.

2. A MASS SPECTROMETER STUDY OF SUBLIMATION OF CHROMIUM TRIOXIDE

Charles Washburn* and Alan W. Searcy

$CrO_{3(s)}$ is metastable, even at room temperature, relative to decomposition to $Cr_2O_{3(s)}$ $O_{2(g)}$. However, the decomposition reaction is strongly kinetically suppressed. The oxygen partial pressure in a Knudsen cell containing 0.5 gram $CrO_{3(s)}$ and fitted with a 1 mm diameter orifice is less than 10^{-10} times the pressure expected from thermodynamics, and, in fact, $CrO_{3(s)}$ sublimes congruently or nearly congruently below its melting point (196°).

The species Cr_nO_{3n} where n = 3, 4, and 5 were reported as neutral molecule components of CrO_3 vapor in investigations published while this work was in progress. Appearance potential cell exhaustion and double oven experiments in the present study show neutral species in CrO_3 vapor to include in addition to O_2, Cr_nO_{3n}, n = 3, 4, 5, and 6; Cr_nO_{3n-2}, n = 3, 4, and 5. Small concentrations of Cr_4O_{11} and Cr_3O_8 are probably also present in the vapor.

In addition to ions corresponding to the molecules mentioned above, ions of the following compositions were detected in the mass spectrum resulting from the sublimation of $CrO_{3(s)}$ but were determined to be fragments of heavier molecules: $Cr_4O_9^+$, $Cr_4O_8^+$, $Cr_4O_7^+$, $Cr_3O_6^+$, $Cr_3O_5^+$, $Cr_3O_4^+$, $Cr_2O_5^+$, $Cr_2O_4^+$, and $Cr_2O_3^+$.

Considerable evidence was found that the chromium-containing molecules, unlike oxygen, evaporate with evaporation coefficients near unity and that the gaseous chromium-containing molecules are in equilibrium among themselves but not with oxygen. The partial pressures of the six most important chromium-containing species are given by the following equations between 415.1°K and 468.1°K:

$$\log P_{(CrO_3)_5}\,(\text{atm}) = -\frac{(7.943 \pm 0.240)\times 10^3}{T} + (15.02 \pm 0.54)$$

$$\log P_{Cr_5O_{13}}\,(\text{atm}) = -\frac{(9.373 \pm 0.154)\times 10^3}{T} + (19.13 \pm 0.35)$$

$$\log P_{(CrO_3)_4}\,(\text{atm}) = -\frac{(6.849 \pm 0.150)\times 10^3}{T} + (13.70 \pm 0.34)$$

$$\log P_{Cr_4O_{10}}\,(\text{atm}) = -\frac{(7.983 \pm 0.124)\times 10^3}{T} + (17.17 \pm 0.28)$$

$$\log P_{(CrO_3)_3}\,(\text{atm}) = -\frac{(6.836 \pm 0.152)\times 10^3}{T} + (13.08 \pm 0.34)$$

$$\log P_{Cr_3O_7}\,(\text{atm}) = -\frac{(7.465 \pm 0.095)\times 10^3}{T} + (15.09 \pm 0.22).$$

---

*Present address: Department of Mechanical Engineering, Sacramento State College, Sacramento, Calif.

3. THE MELTING POINT, VAPOR PRESSURE, AND HEAT OF VAPORIZATION OF STANNOUS FLUORIDE

James J. Dudash and Alan W. Searcy

The melting point of stannous fluoride was determined to be 488.2 ± 0.5°K. The total vapor pressure of stannous fluoride, measured in the temperature range 532 to 670°K by the torsion effusion method, is represented by the expression

$$\log_{10} P_{atm} = -(6.951 \pm 0.033)\,\frac{10^3}{T} + 6.726 \pm 0.055,$$

where the quoted errors are the standard deviations from the least-squares fit. With use of this expression for the total pressure and the relative pressures measured by Zmbov, Hastie, and Margrave, heats of vaporization at 600°K for the monomer, dimer, and trimer were found to be 31.8 ± 3, 30.3 ± 3, and 42.0 ± 5 kcal/mole, respectively.

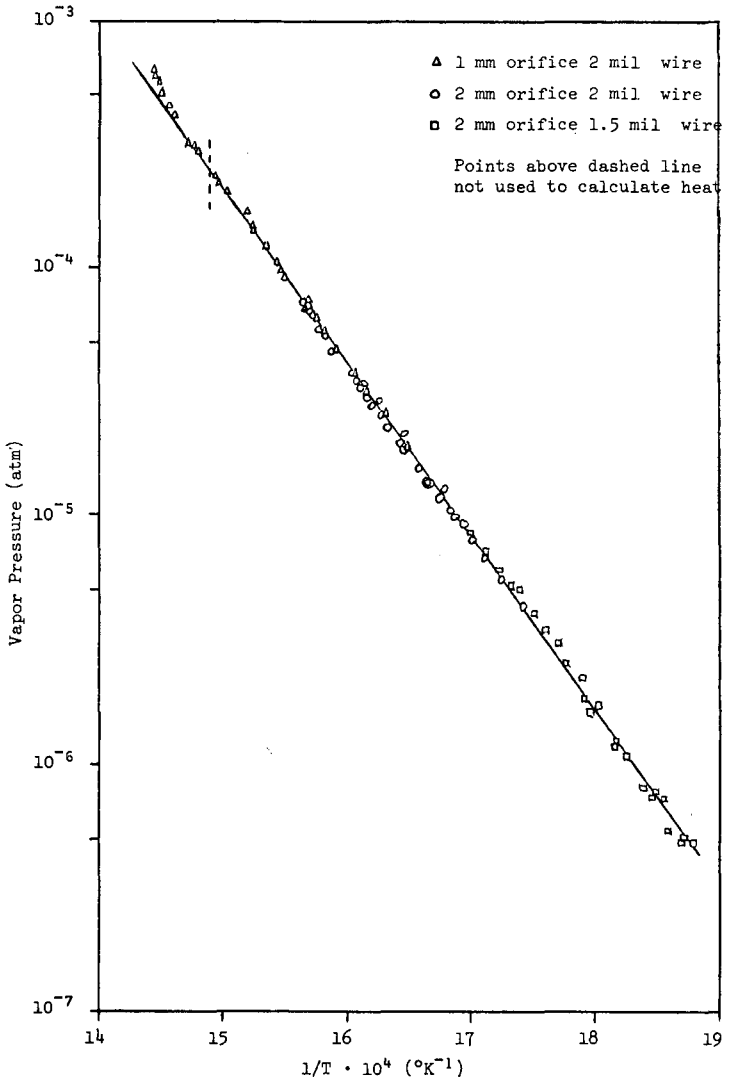

XBL 6810-6013

Fig. 1. Vaporization data for $SnF_2(\ell)$.

4. THE VARIATION OF SUBLIMATION RATES AND STRUCTURE OF THE (0001) ZINC SURFACE WITH TIME

Raymond W. Mar* and Alan W. Searcy

Zinc single crystal rods were cleaved on (0001) planes at liquid nitrogen temperatures, transferred to a methyl alcohol bath in an inert atmosphere, warmed to room temperature, dried in a stream of air, and stored in a dessicator until introduced into a vacuum system for vaporization rate studies by the torsion-Langmuir method. Rates of sublimation were measured as functions of time at constant temperatures near 600°K. Some runs were interrupted after various periods of time so that the surfaces that developed could be examined by optical microscopy and by a scanning electron microscope.

Although apparently no previous experiments have been reported in which variations of sublimation rates of more than about a factor of 3 with time have been observed, in the present study rates were observed to increase by as much as a factor of 100. Exposure of surfaces that had once achieved their steady state sublimation rates to various reagents such as air or methyl alcohol caused some delay in achievement of the steady state sublimation rates on reheating, but the slowest approach to steady state was found for freshly cleaved samples.

The rate of sublimation was directly proportional to the area of that part of the sample surface that was covered by thermal etch pits. These pits nucleated upon initial heating, and the steady state rate was achieved when they had spread to cover the entire exposed surface.

Studies of patterns of pit development in the mirror-image surfaces formed by a single cleavage operation showed clearly that the thermal pits were formed at crystal imperfections, probably at some kinds of dislocations. But the concentration of thermal etch pits, while varying from sample to sample, was clearly shown to be about an order of magnitude lower than the concentrations of chemical etch pits, about 10^4 thermal pits per cm^2 compared with about 10^5 chemical pits per cm^2. Chemical and thermal etching experiments on the same surfaces and on mirror-image surfaces showed that the nucleation sites for thermal etching are probably not even a sub-set of the chemical pit sites.

The importance of pits formed at crystal imperfections as sources for sublimation and the inertness of the freshly cleaved surfaces are predicted by mechanistic theories of stepwise sublimation. The poor correlation of thermal and chemical pitting is not expected from the theories.

*Present address: University of Leeds, Leeds, England.

5. THE KINETICS OF STEADY STATE SUBLIMATION OF ZINC SINGLE CRYSTALS

Raymond W. Mar* and Alan W. Searcy

A widely accepted theory[1] predicts that the rate of sublimation from low index crystallographic planes of metal single crystals for which the dislocation density is less than 10^5 dislocations per cm^2 will be one-third the rate predicted from the equilibrium vapor pressures by use of the Langmuir equation. This prediction has never been rigorously tested by experimental measurement, and the purpose of this study was to determine whether or not it is correct.

Zinc was chosen for study because it is available as high purity single crystals and has a relatively high vapor pressure at its melting point. Torsion-Langmuir experiments were conducted with (0001) surfaces of zinc single crystals from two sources and with $(10\bar{1}0)$ surfaces from a single crystal source.

To insure against systematic error, the vapor pressure of zinc was measured by the torsion effusion method in the same apparatus used for the rate studies. The measurements yielded $\Delta H_{298} = 31.29 \pm 0.075$ kcal compared with 31.245 ± 0.050 reported by Hultgren, Orr, Anderson, and Kelley from evaluation of 15 separate studies.[2]

Those crystals that were used for both (0001) and $(10\bar{1}0)$ surface studies were prepared in our laboratory. The only spectroscopically detectable impurities that they contained were copper and silver, both at less than 0.001 at.%. For these laboratory-grown crystals the ratio of the measured rates of sublimation to the predictions from equilibrium pressure data (the ratio is called the evaporation coefficient) were at 540 to 640°K for the (0001) surface 0.73 ± 0.08, and for the $(10\bar{1}0)$ surface 1.02 ± 0.09, where the uncertainties are standard deviations. An experiment in which the flux from two (0001) surfaces was oriented to impart a twist to the torsion fiber of the Torsion-Langmuir cell that was opposed to the flux from two $(10\bar{1}0)$ surfaces yielded, when the $(10\bar{1}0)$ flux was assumed equal to the predictions of the Langmuir equation, 0.71 ± 0.04 as the evaporation coefficient for the basal plane, in excellent

agreement with the directly measured value. The $(10\bar{1}0)$ surface is jagged so the true evaporation coefficients for the exposed planes may be a little less than the measured value.

Zinc from a second source showed no spectroscopically measurable impurities. The evaporation coefficient measured for the (0001) planes of this zinc was 1.10 ± 0.08. Chemical etch pit measurements for three samples of this high purity zinc showed dislocation counts from $10^4/cm^2$ to $6 \times 10^5/cm^2$, but the high counts were in distorted areas near crystal edges. Furthermore, the thermal etch pits which form during non-steady state early stages of sublimation (see previous abstract) are present at only about 1/10 the concentration of the chemical pits.

Since during steady state sublimation of the high purity (0001) surface of zinc the surface is generally smooth when viewed at some 10,000 magnifications, since the count of active imperfections is less than $10^5/cm^2$, and yet the evaporation coefficient is found to be unity to within 10% estimated error, quantitative prediction of the Hirth and Pound theory appears to be disproved.

---

*Present address: University of Leeds, Leeds, England.

1. J. P. Hirth and G. M. Pound, J. Chem. Phys. 26, 1216 (1957).
2. R. Hultgren, R. L. Orr, P. D. Anderson, and K. K. Kelley, Selected Values of Thermodynamic Properties of Metals and Alloys (John Wiley & Sons, New York, 1963).

6. THE KINETICS OF EVAPORATION AND CONDENSATION REACTIONS

Alan W. Searcy

In the paper with this title[1] the author derives the complete temperature dependent rate expression for an evaporation reaction that is assumed to consist of two consecutive steps, a surface step and a desorption step. He shows that comparison of experimentally measured rates of evaporation and condensation as functions of temperature to thermodynamically calculatable maximum possible rates through use of the model leads to several important conclusions about the possible nature of the rate-determining step, the frequency factor, the enthalpy of evaporation or condensation, and the entropy of activation or condensation in specific experimental studies. In particular for reactions for which free surface evaporation occurs at the same rate as evaporation through the orifice of an effusion cell (that is for reactions for which the evaporation coefficient is unity), desorption must be rate-determining, the activated complex as normally defined in kinetic studies must be the vapor molecule, and the frequency factor in the rate expression, when expressed in moles of vapor per unit time per unit area of surface is $(2\pi MRT)^{-1/2}$. This result confirms assumptions of reaction kinetics that have previously been considered unverified, and perhaps even unverifiable.[2,3]

For evaporation reactions for which the apparent activation enthalpies are less than 90% of the enthalpy of the equilibrium reaction (after possible experimental error has been allowed for), the desorption step cannot be rate determining. For reactions for which the apparent activation entropies, calculated on the assumption that desorption is rate determining, are nearly identical with entropies of the equilibrium reaction, the desorption step is probably usually rate determining.

The paper demonstrates fallacies in assumptions about the stabilities of various surface sites, in particular the kink sites in ledges, which have previously been presumed to play critical roles in determining the kinetics of sublimation.[4]

The paper reviews experimental variables that influence the rates of evaporation and summarizes the generalizations that can be made about the rates of evaporation of various chemical classes.

---

1. Abstracted from UCRL-18631, December 1968; to appear as Chapter 6 in Chemical and Mechanical Behavior of Inorganic Materials (Proceedings of the First International Conference on Materials Science, sponsored by the National Academy of Lincei, Italy), A. W. Searcy, D. V. Ragone, and U. Colombo, eds. (Interscience Publishers, New York).
2. See, for example, I. Amdur and G. G. Hammes, Chemical Kinetics (McGraw-Hill Book Company, New York, 1966).
3. The conclusions to be drawn for reactions with unit evaporation coefficient are also briefly summarized by H. Skinner and A. W. Searcy, in J. Phys. Chem. 72, 3375 (1968).
4. See, for example, W. Hirschwald and I. N. Stranski, in Condensation and Evaporation of Solids, E. Rutner, P. Goldfinger, and J. P. Hirth, eds. (Gordon and Breach, New York, 1964), p. 59.

7. A COMPARISON OF THE INTERNAL ENERGY STATES OF P_4 MOLECULES PRODUCED BY FREE SURFACE SUBLIMATION AND BY EFFUSION

Raymond W. Mar* and Alan W. Searcy

When the apparent activation enthalpy for free surface sublimation of a substance is greater than the equilibrium enthalpy of the sublimation reaction, there is reason to expect that the vapor molecules that leave the surface may be in excited internal energy states.[1] It may be possible to demonstrate the existence of the excitation by comparing the intensities of the ions produced in a mass spectrometer as a function of electron beam energy with the intensities produced for the same ions when an equilibrium vapor beam is used; if the excitation energies are high enough, the excited molecules may show significantly different fragmentation patterns from those of the related equilibrium vapors. Even if the vapor molecules are internally excited when they evaporate, a difference in fragmentation patterns can be expected only if the lifetime for the excited state is long compared with the time of travel of the beam from the surface of evaporation to the ionization chamber, about 10^{-4} sec. Depending on the nature of the internal excitation and on the energy spectrum of the excited molecule, the half-lives for de-excitation by radiation may be long enough for detection or may be as short as $\sim 10^{-8}$ sec.[2]

Red phosphorus was chosen for study because it is known to sublime almost exclusively as P_4 molecules in the temperature range convenient for molecular beam studies and to have an apparent enthalpy of activation for the free surface sublimation process of 52 kcal compared with 28 kcal for the equilibrium process.

Red phosphorus of 99.999% purity was heated in a graphite cell to temperatures near 620°K.

Free surface sublimation was achieved by supporting a lump of phosphorus flush against the lower surface of the lid, which was pierced by a conical orifice. The geometry was such that most P_4 molecules would reach the ionization chamber without undergoing collisions with any surface.

The same cell and orifice were used for Knudsen effusion runs in which phosphorus powder was placed in the bottom of the cell. A number of molybdenum inserts with eccentrically placed holes were placed in the cell between the powder and the orifice to insure that each vapor molecule would make a number of collisions with the cell walls, the molybdenum inserts, and with other P_4 molecules before effusing through the orifice. The multiple collisions should deactivate any excited vapor molecules.

Four different runs were made in an Atlas mass spectrometer with each type of experimental arrangement. The variation of P_3^+, P_2^+, and P^+ intensities relative to P_4^+ intensities was not significantly different between free surface and effusion experiments when electron energies were varied from below the threshold of measurable intensities at about 10 to 70 eV.

It is concluded that either P_4 molecules that leave the surface during free surface sublimation are not internally excited or that the lifetime for loss of excitation energy by emission is less than 10^{-4} sec.

---

*Present address: University of Leeds, Leeds, England.

1. A. W. Searcy, The Kinetics of Evaporation and Condensation Reactions, abstracted from UCRL-18631, December 1968; to appear as Chapter 5 in Chemical and Mechanical Behavior of Inorganic Materials (Proceedings of the First International Conference on Materials Science, sponsored by the National Academy of Lincei, Italy), A. W. Searcy, D. V. Ragone, and U. Colombo, eds. (Interscience Publishers, New York).

2. W. H. Flygare, Accounts of Chemical Research 1, 121 (1968).

8. RESEARCH PLANS FOR CALENDAR YEAR 1969

Alan W. Searcy

Studies of the effect of atmospheres of various gases on the kinetics of effusion and free surface sublimation of magnesium nitride by the torsion-effusion method, the torsion-Langmuir method, and by quadrupole mass spectrometry will be completed. The measurements will probably be extended to an oxide such as cadmium oxide.

A mass spectrometer and microscopic study of the kinetics of free surface sublimation of magnesium oxide will continue and should be completed in 1969.

During 1968, studies of the weight loss and surface structure of zinc oxide during sublimation established characteristic differences in sublimation kinetics for the (0001) and ($000\bar{1}$) surfaces. Studies of the effects on sublimation rates and surface structure of variables such as composition and furnace atmospheres should be completed in 1969.

A mass spectrometric investigation of gaseous AlOH was not conducted as planned for 1968 because an investigation of the kind we intended has been reported by others. A mass spectrometer investigation of the composition and stabilities of gaseous rhenium oxides and of their stabilities, which was instituted in place of the AlOH study, will be continued.

The apparatus for detection of low lying molecular energy states that have unpaired electrons will be modified to give improved collimation of the beams. A double-oven heating chamber probably also will be introduced. Both modifications are designed to make feasible at least semi-quantitative measurements of the relative concentrations of molecules with paired and unpaired electrons and, in consequence, measurements of the approximate energy separations of the molecular states. Probable substances for study are alkaline earth oxides and sulphides for which conflicting information on electronic ground states has been reported.

Studies of non-steady state sublimation, such as were completed in the past year with zinc single crystals, will be conducted for (0001) planes of magnesium. Either the altered c/a crystallographic axial ratio or a difference in morphology of surface oxides formed by reaction with the residual oxygen of the vacuum system may cause very different results from those obtained for zinc.

9. 1968 PUBLICATIONS

Alan W. Searcy and Associates

Technical Journals

1. B. A. H. Blank and A. W. Searcy, The Rate of Sublimation of Magnesium Nitride from Effusion Cells and From Free Surfaces in Vacuo and in Argon and Nitrogen Gases, J. Phys. Chem. 72, 2241 (1968).
2. R. W. Mar and A. W. Searcy, Kinetic Energy of Molecules that Traverse an Excess-Energy Barrier During Sublimation, J. Chem. Phys. 49, 182 (1968).
3. R. S. Newbury, G. W. Barton, and A. W. Searcy, Vapor Species of the Barium Oxygen System, J. Chem. Phys. 48, 793 (1968).
4. H. B. Skinner and A. W. Searcy, The Vapor Pressure, The Heat of Sublimation and the Evaporation Coefficient of Praeseodymium Trifluoride, J. Phys. Chem. 72, 3375 (1968).

UCRL Reports

1. J. J. Dudash, The Melting Point, Vapor Pressure and Heat of Vaporization of Stannous Fluoride (M.S. Thesis), UCRL-18164, University of California, Berkeley, May 1968.
2. O. Herstad and A. W. Searcy, The Free Energy and Enthalpy of Formation of Aluminum Sesquisulfide, UCRL-18004, January 1968.
3. R. W. Mar, Sublimation Kinetics of Zinc Single Crystals (Ph. D. Thesis), UCRL-18257, University of California, Berkeley, June 1968.
4. A. W. Searcy, The Kinetics of Evaporation and Condensation Reactions, UCRL-18631, December 1968.

B. MICROSTRUCTURE AND BEHAVIOR OF CERAMIC MATERIALS; GLASS AND CERAMIC-METAL SYSTEMS

Joseph A. Pask

An objective of this program is to contribute to the development of a fundamental understanding of the factors involved in obtaining ceramic materials with controlled character, which includes microstructure, and of the relationship of character to mechanical behavior at room and high temperatures. This objective involves studies on the kinetics and mechanisms of solid state reactions, which in general play a part in the development of microstructure. It also involves studies on the mechanisms responsible for the mechanical behavior of single crystals, and on the application of such knowledge to the understanding of the behavior of polycrystalline ceramic materials.

A second objective of this program is concerned with structural, thermodynamic, and electrochemical studies of glass, glass-metal, and ceramic-metal systems. It deals with studies related to wetting, bonding, and the nature of the interfaces between such phases; to the thermodynamics and kinetics of chemical reactions at such interfaces; and to the kinetics and mechanisms of dissolution and diffusion in glasses.

1. INTERDIFFUSION IN NiO, CaO, AND MgO SINGLE CRYSTALS*

Marvin Appel† and Joseph A. Pask

Cation interdiffusion in single crystals of NiO, CaO, and MgO was investigated from 1300 to 1700° using NiO-CaO, NiO-MgO, and MgO-CaO diffusion couples. In air, NiO is non-stoichiometric and has a concentration of chemically created cation vacancies proportional to $P_{O_2}^{1/6}$. These excess cation vacancies allow diffusion to proceed more rapidly in NiO than in either CaO or MgO. This condition causes the phase boundary in the NiO-MgO or the NiO-CaO diffusion couple to move, the NiO growing at the expense of the other crystal. When the two crystals are of different crystallographic orientation, the orientation of the volume swept out transforms to that of the growing crystal. Figure 1 shows typical diffusion profiles for a NiO-MgO couple.

In air, the diffusivity in the NiO-CaO and the NiO-MgO systems was found to be exponentially dependent on the Ni concentration. In vacuum, where NiO, CaO, and MgO are all stoichiometric, there was no concentration dependence of the diffusivity and no measurable phase boundary motion was observed.

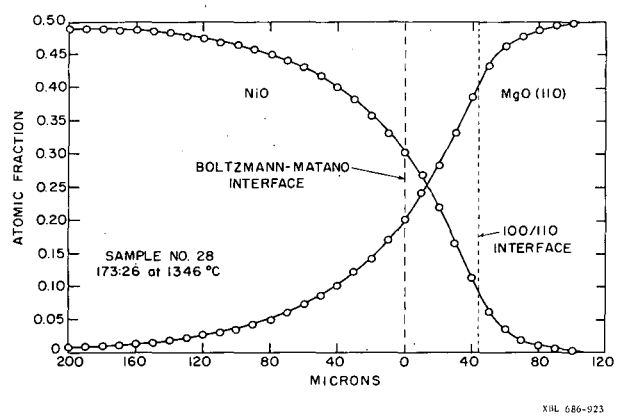

Fig. 1. Diffusion profiles for NiO-MgO couple (100 NiO face is contact with 110 MgO face) after 173 hours at 1346°.

The chemical diffusivities for NiO-CaO interdiffusion in air were found to be

$$\tilde{D}_{\substack{NiO \\ matrix}} = 0.231^{+.395}_{-.145} \exp\left(\frac{-72{,}090 \pm 3380}{RT}\right) \text{ cm}^2/\text{sec},$$

$$\tilde{D}_{\substack{CaO \\ matrix}} = 13.9^{+162}_{-12.7} \exp\left(\frac{-93{,}800 \pm 8630}{RT}\right) \text{ cm}^2/\text{sec}.$$

The intrinsic diffusivities were also determined by using Darken's equations. Current theoretical and experimental attacks on the validity of Darken's analysis were considered.

---

*Abstract from Marvin Appel, UCRL-18258, June 1968.

†Present address: Materials Division, Research and Development Dept., Central Electricity Research Labs., Cleeve Road, Leatherhead, Surrey, England.

2. DENSIFICATION MECHANISMS IN HOT-PRESSING MAGNESIA WITH A FUGITIVE LIQUID*

Patrick E. Hart,† Robert B. Atkin, and Joseph A. Pask

The densification of MgO powder with LiF additions into transparent polycrystalline MgO was shown to occur in three stages. During hot pressing, an adherent LiF-rich liquid film on MgO particles provides lubrication for the first or rearrangement stage. Pressure-flow-enhanced liquid phase sintering is the dominant densification mechanism during the second stage, which occurs towards the end of the hot-pressing step. The kinetics of this stage were controlled by flow of the LiF-rich liquid film as indicated by a density-$(\text{time})^{-2/5}$ relationship which corresponds to a densification rate-$(\text{porosity})^{7/2}$ dependence. During the third or annealing stage the remaining liquid film is vaporized, resulting in fully transparent polycrystalline MgO.

*Abstracted from UCRL-18279, July 1968.
†Present address: Battelle Northwest, Richland, Washington.

3. FACTORS CONTROLLING THE WETTING OF MgO BY SILICATES*

Ilhan A. Aksay and Joseph A. Pask

In the presence of a liquid phase, the spatial distribution of phases in a multiphase system is determined by the relative values of grain-boundary and solid-liquid interfacial energies. Thus the microstructure of liquid-containing systems can be controlled if the factors controlling the interfacial energies are understood. In this study the MgO (solid) $CaO \cdot MgO \cdot SiO_2$ (liquid) system has been selected as the basic system. The effect of Al_2O_3, Cr_2O_3, Fe_2O_3, and TiO_2 additions to the liquid are being determined. Emphasis has been placed on the use of sessile drop experiments as a means of studying the changes taking place in the solid-liquid interface and interfacial energy.

The effect of Al_2O_3, Cr_2O_3, Fe_2O_3, and TiO_2 additions to the CMS liquid on the contact angle of the resulting liquid when placed on [100] faces of MgO at 1550° is shown in Fig. 1. In sessile drop experiments in the absence of reactions, a change in contact angle is due to changes in interfacial energies because of the adsorption of additives either at the solid-liquid interface or the liquid surface. If a reaction takes place between the liquid and the solid, however, a redistribution of components involving both the substrate and the liquid will take place. In these systems, although CMS is in chemical equilibrium with MgO at 1550°, Al_2O_3, Cr_2O_3, Fe_2O_3, and TiO_2 additions disturb this equilibrium. The kinetics of the interaction that then takes place affect the contact angle.

Electron microprobe investigations, and existing phase equilibria and diffusion data indicate that, with Al_2O_3 and Fe_2O_3 additions, the interface appears to approach an equilibrium composition state rapidly resulting in finite contact angles. With Cr_2O_3 additions, a high free energy of interface reaction exists, resulting in a spreading of the liquid of MgO or a zero contact angle. Analysis of the experiments by use of CMS liquid with TiO_2 additions is continuing.

*These studies are a continuation of those initiated by Abbaraju P. Raju and Joseph A. Pask in 1966.

4. REACTIONS BETWEEN Al_2O_3 AND SiO_2

Robert F. Davis* and Joseph A. Pask

An objective of this study program is to determine the reaction and diffusion characteristics of Al_2O_3 single crystal (sapphire) and fused silica diffusion couples. Time was spent in developing techniques to produce usable and reproducible diffusion couples and to determine suitable temperatures and times for these experiments. Diffusion experiments are now being conducted at temperatures of 1600 to 1800° in a tantalum element furnace Experiments are also being conducted using cristobalite (SiO_2)-alumina and 15% Al_2O_3-85% silica glass-alumina couples to provide an understanding of the mechanisms involved in the reaction to form mullite ($3\,Al_2O_3 \cdot 2\,SiO_2$).

A second objective is to develop a dense mullite body with a controlled microstructure. Techniques of mullite formation such as precipitation from gels, mixtures of $SiCl_4$ and $AlCl_3$, and sintering of different types of alumina and silica powders have been explored in an effort to produce mullite free of glass and corundum. Repeated sinterings of the oxides with intermediate grindings has produced the most complete reaction to form mullite. Studies on densification of such powders by hot-pressing techniques are continuing.

*Edward Orton, Jr. Ceramic Foundation Fellow.

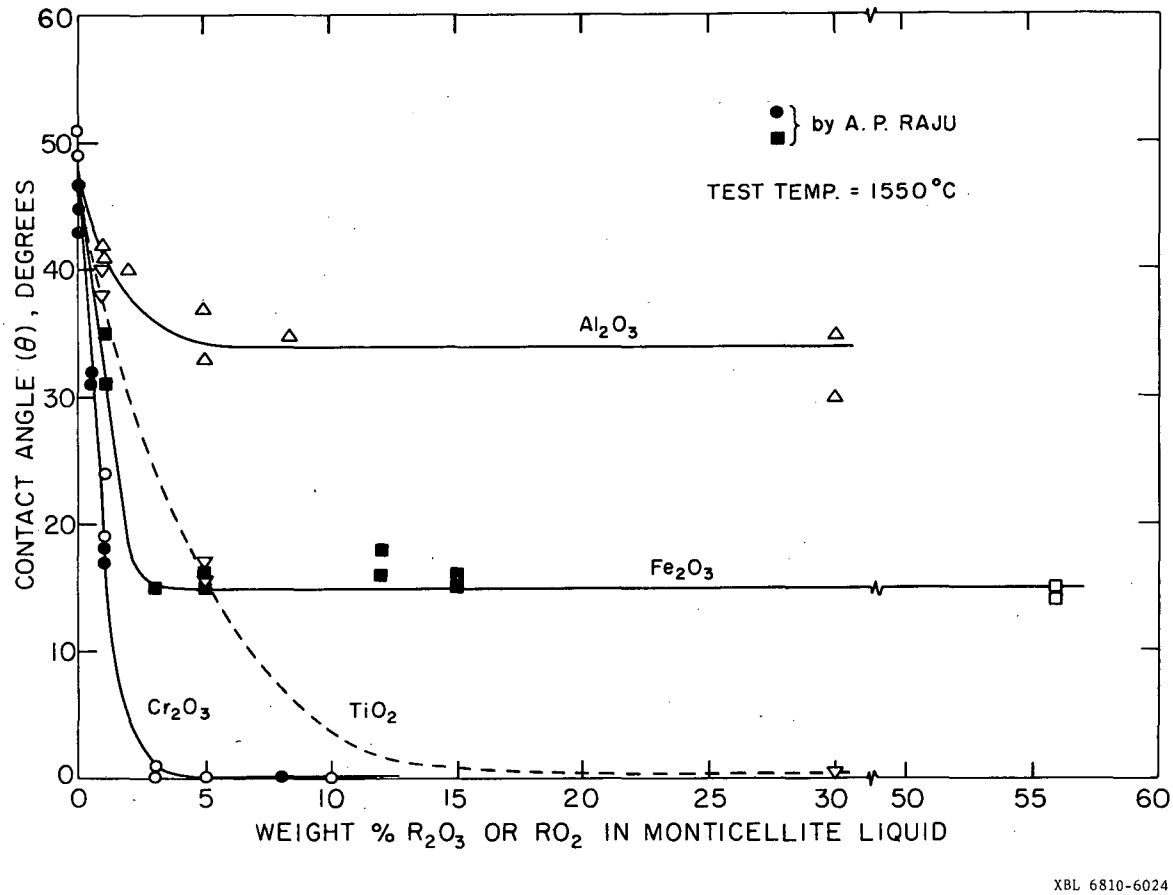

Fig. 1. Effect of Al_2O_3, Cr_2O_3, Fe_2O_3, and TiO_2 additions to $CaO \cdot MgO \cdot SiO_2$ liquid on wetting of MgO at 1550°.

5. CREEP OF POLYCRYSTALLINE LiF*

Donald R. Cropper and Terence G. Langdon†

The creep behavior of polycrystalline LiF under conditions of constant stress was investigated over the temperature range from 300 to 550° and found to be essentially similar to that observed in pure metals. The relationship between the creep strain rate and the applied stress was found to be of power law form, i.e., $\dot{\epsilon} \propto \sigma^n$, where n is approximately 6.6. The measured activation energy for steady-state creep was of the anticipated magnitude for diffusion of the fluorine ion. Thus, at temperatures above 300° the steady-state creep rate obeys a relationship of the form for Weertman's dislocation climb model:

$$\dot{\epsilon} = A \frac{\sigma^{6.6}}{TG^{5.6}} \exp\left(\frac{-50.1 \text{ kcal/mole}}{RT}\right),$$

where $\dot{\epsilon}$ is the steady-state creep rate, σ is the applied stress, T is the absolute temperature, G is the shear modulus, and R is the gas constant.

*Abstracted from UCRL-17856, April 1968; also, Phil. Mag. 18, 1181 (1968).

†Present address: Department of Surface Physics, Cavendish Laboratory, University of Cambridge, Cambridge, England.

6. EFFECT OF PLASTIC INSTABILITY ON COMPRESSIVE DEFORMATION*

Donald R. Cropper and Joseph A. Pask

Mechanical-property measurements obtained from compression tests may be affected by the occurrence of plastic buckling. Analytical expressions obtained from considerations of continuum mechanics were shown to accurately predict the compressive load at which a plastically deforming column becomes unstable. Experiments verified that the application of suitable end constraints and careful choice of specimen geometry can eliminate the possibility of buckling.

*Abstracted from UCRL-17105 Rev., February 1968.

7. CREEP OF MgO SINGLE CRYSTALS

Donald R. Cropper and Joseph A. Pask

Work has continued on the compressive creep behavior of MgO single crystals above 1300°. Specimens approximately 1/4 in. square and 1/2 in. long were loaded parallel to ⟨100⟩. Differential stress tests were performed to determine the stress dependence of the creep strain rate. These have shown that the relationship between the creep strain rate and the applied stress is a power law similar to that found for polycrystalline LiF; i.e., $\dot{\epsilon} \propto \sigma^n$ with the value of n about 7.6.

Attempts were made to determine the temperature dependence of the strain rate by deforming crystals at a constant stress while the temperature was changed by increments of about 20° at intervals of about 0.03-0.04 strain. There does not appear to be a single activation energy characteristic of creep between 1100 and 1400°, however, as values ranging from 151 to 349 kcal/mole have been obtained. These rather high and widely scattered values suggest that, despite the relatively high temperature (~0.55 Tm), a nondiffusional process may still be rate controlling. Investigation of the causes for this variability is continuing.

8. KINETICS OF THE DISSOLUTION AND DIFFUSION OF THE OXIDES OF IRON IN SODIUM DISILICATE GLASS*

Marcus P. Borom† and Joseph A. Pask

The dissolution and diffusion of the three oxides of iron in sodium disilicate glass from 900 to 1100° were shown to be controlled by diffusion in the molten glass. Concentration profiles were determined with an electron microprobe. Diffusion kinetics were applied on the basis of an ideal binary couple with concentration-independent interdiffusivities. Concentration dependence of the interdiffusivities was determined by the Boltzmann-Matano method, and the resulting interdiffusivities were interpreted in terms of a ternary diffusion model. The relation among the self-diffusion coefficients was

$$D^*_{Na^+} \gg D^*_{Fe^{2+}} > D^*_{Fe^{3+}} \geq D^*_{Si^{4+}}.$$

The activation energy for the interdiffusion process for all the iron oxide-sodium disilicate couples was 30 kcal.

*Abstract from J. Am. Ceram. Soc. 51, 490 (1968).

†Present address: Research and Development Center, General Electric Co., Schenectady, N. Y.

9. CONDUCTIVITY AND ELECTRODE POLARIZATION IN MOLTEN SODIUM DISILICATE GLASS WITH IRON OXIDE ADDITIONS*

Richard N. Schweinberg† and Joseph A. Pask

Electrical conductivity and polarization measurements were performed for the system $FeO\text{-}Na_2O\cdot 2SiO_2$, ranging from 0 to 20%. Arrangements using parallel plate electrodes of Fe-Fe, Au-Au, and Pt-Pt were studied under constant dc and ac potential at 0.2 and 0.4 volts.

The drops in current with a dc potential were recorded with Fe-Fe electrodes and concentration profiles were analyzed using the electron microprobe. Iron ions entered the glass at the anode by replacing sodium ions that migrated toward the cathode, and a cloud of metallic sodium formed near the cathode. Iron dendrites were observed to grow out from the cathode in experiments with glasses containing iron oxide. The cathode material did not affect the current-vs.-time curves. Efforts were made to separate ionic and electronic current contributions to the conductivity. Total current readings were obtained by investigating alternating current frequency ranges of 0.5-50 kHz and the initial dc peak currents. Blocking electrodes (only slight reaction of glass and electrode) such as Au and Pt were used as anodes to obtain the electronic current. Increase of FeO content increased both the ionic and electronic contributions to the conductivity.

Since electroneutrality must be maintained, the steady-state composition of the glass at the anode and the mobility of the anode cation appear to be the controlling factors in determining the nature of polarization and conduction in molten glasses.

---

*Abstracted from UCRL-18200, April 1968.
†Present address: U.S. Atomic Energy Commission, Washington, D.C. 20545.

10. THERMODYNAMIC ACTIVITIES OF NiO, CoO, AND Fe_xO IN SODIUM DISILICATE GLASS

Alton M. Lacy and Joseph A. Pask

A solid state electrochemical cell using calcia-stabilized zirconia was developed in order to obtain thermodynamic activities of NiO in a solution of sodium disilicate glass in the temperature range 750-1150°C. A standard oxygen pressure is maintained at temperature by the equilibrium between Ni metal and NiO, while a lesser oxygen pressure is established by Ni metal and the NiO contained in the glass at a reduced activity (relative to solid NiO powder). The generated emf of the cell is directly related to the activity of the NiO in the glass by the expression $a_{NiO} = \exp(-nFE/RT)$, where n, F, R, and T are constants and E is the emf in volts generated by the cell.

Preliminary results show an approximate maximum solubility of NiO in sodium disilicate as 7.5% at 1000°. NiO appears to form a nearly ideal dilute solution in the sodium disilicate and there appears to be a slight tendency toward negative deviations from ideality at higher temperatures (1100°).

Work is continuing on CoO-sodium disilicate and Fe_xO-sodium disilicate glass solutions.

11. EFFECT OF NATURE OF SURFACES ON WETTING OF SAPPHIRE BY LIQUID ALUMINUM*

John J. Brennan and Joseph A. Pask

Contact angles of aluminum drops on sapphire measured under vacuum conditions, from 660 to 1250°, generally fell into three ranges. Large obtuse contact angles indicating interfacial energies greater than either of the two surface energies were obtained up to about 900°; Van der Waals bonding then existed at a compound interface. In the intermediate range, contact angles were 90 deg or slightly greater, indicating a common interface with an energy ($_s\gamma_\ell$) greater than $_s\gamma_g$ but less than $_\ell\gamma_g$. Acute contact angles indicating a $_s\gamma_\ell$ less than $_s\gamma_g$ and greater than $_\ell\gamma_g$ occurred above about 950° because of the formation of a high temperature complex surface structure with a $_s\gamma_g > {}_\ell\gamma_g$. A hydroxylated sapphire surface has a lower $_s\gamma_g$, which increases with gradual dehydroxylation and conversion to the high temperature surface structure with a corresponding change in contact angle through the three ranges. Chemical bonding existed in the latter two ranges. Reactions occurred between Al and the sapphire surface to form volatile species at contact angles less than 90 deg. Molten Al normally has an oxide coating whose effect appears to be removed at about 870°.

---

*Abstract from J. Am. Ceram. Soc. 51, 569 (1968).

12. RESEARCH PLANS FOR CALENDAR YEAR 1969

Joseph A. Pask

Solid State Reactions

Studies are continuing on the mechanism and kinetics of diffusion, using single crystals in the diffusion couples. The relationship between phase boundary movement and the stoichiometry of the constituents in the diffusion couple will be further clarified using NiO-MgO and NiO-CaO couples. Additional studies will also be made with diffusion couples involving systems in which a compound forms, such as the $MgO\text{-}Al_2O_3$ system.

Diffusion experiments are continuing on couples consisting of fused SiO_2-sapphire, fused aluminum silicate-sapphire, and cristobalite-sapphire. These studies will provide kinetic data as well as information on mechanisms of formation of mullite. Such data will then be utilized in an effort to develop a fully dense polycrystalline mullite body.

Development of Microstructures

Studies of the factors that play a role in the development of microstructure, or the distribution of phases, in two- and three-phase systems are continuing. The systems being used are $CaO \cdot MgO \cdot SiO_2$ liquids with Al_2O_3, Cr_2O_3, Fe_2O_3, and TiO_2 additions and MgO as well as $MgO \cdot R_2O_3$ spinals. These data will be applied to the study of the kinetics of sintering in similar systems.

Mechanical Behavior

Constant-load tests in compression will continue to be made on single crystal specimens of MgO oriented for flow on a conjugate pair of slip systems. The nature of the deformation process will be studied. Creep data on LiF single crystals over a wide temperature range will also be obtained.

Glass Studies

Measurements of thermodynamic activities of CoO and Fe_xO in a solution of sodium disilicate glass will be made in the temperature range 750-1150°. Relationships of these data to the activities of NiO in this glass will be explored.

Electrical conductivity studies will continue in the system $NiO\text{-}Na_2O\cdot 2SiO_2$ with NiO varying from 0% up to the saturation amount. The total conductivity in this system should have a small electronic conductivity contribution because of the small amount of Ni^{3+}. Electrodes of different compositions will be used.

Ceramic-Metal Interfaces

Studies are being undertaken to further verify the theory that a chemical bond occurs at a glass-metal interface when the thermodynamic activity of the low valent metal oxide in the glass and metal at the interface is one. The substrates included are Fe, Ni, Co, Pt, and Ti metals and FeNi, FeCo, and NiCo alloys. The included oxides are NiO, FeO, CoO, and TiO_2.

13. 1968 PUBLICATIONS

Joseph A. Pask and Associates

Technical Journals

1. M. P. Borom and J. A. Pask, Kinetics of the Dissolution and Diffusion of the Oxides of Iron in Sodium Disilicate Glass, J. Am. Ceram. Soc. 51, (9), 490 (1968).
2. J. J. Brennan and J. A. Pask, Effect of Nature of Surfaces on Wetting of Sapphire by Liquid Aluminum, J. Am. Ceram. Soc. 51, (10), 569 (1968).
3. D. R. Cropper and T. G. Langdon, Creep of Polycrystalline Lithium Fluoride, Phil. Mag. 18, 1181 (1968).
4. R. M. Fulrath and J. A. Pask, eds., Ceramic Microstructures: Their Analysis, Significance and Production (John Wiley & Sons, Inc., New York, 1968), p. 1008.
5. Ibid., T. G. Langdon and J. A. Pask, The Examination of Polycrystalline MgO by Transmission Electron Microscopy, pp. 594-602.
6. R. M. Langston and J. A. Pask, The Nature of Anauxite, Clays and Clay Minerals 16, (6) (1968).
7. J. A. Pask, Chairman of Ad Hoc Committee on Ceramic Processing of Materials Advisory Board, Ceramic Processing (Publ. 1576, Nat. Acad. of Sciences, 1968), p. 298; also, Report MAB-233, Nat. Res. Council, April 1968.

UCRL Reports

1. M. Appel, Interdiffusion in NiO, CaO and MgO Single Crystal (Ph. D. Thesis), UCRL-18258, University of California, Berkeley, June 1968.
2. D. R. Cropper and T. G. Langdon, Creep of Polycrystalline Lithium Fluoride, UCRL-17856, April 1968.
3. D. R. Cropper and J. A. Pask, Effect of Plastic Instability on Compressive Deformation, UCRL-17105 Rev., April 1968.
4. P. E. Hart, R. B. Atkin, and J. A. Pask, Densification Mechanisms in Hot-Pressing Magnesia with a Fugitive Liquid, UCRL-18279, July 1968.
5. T. G. Langdon and J. A. Pask, Mechanical Behavior of Single Crystal and Polycrystalline MgO, UCRL-18250, June 1968.
6. R. N. Schweinberg, Conductivity and Electrode Polarization in Molten Sodium Disilicate Glass (M. S. Thesis), UCRL-18200, University of California, Berkeley, April 1968.

C. RELATION OF MICROSTRUCTURE TO PROPERTIES IN CERAMICS

Richard M. Fulrath

The principal objective of this research is to develop a quantitative relation between the microstructure developed in a ceramic material during processing and its physical and mechanical properties. Microstructure is broadly used to include the geometric arrangement of phases and the chemical composition of each phase present.

The principal areas of research are: (1) the mechanical properties of brittle glass matrix composite systems, (2) the permeation of gas through glass and ceramic materials, and (3) the processing and properties of piezoelectric and ferroelectric ceramics. In each area the effect of microstructure changes are related to changes in the properties measured. Both conventional and unique fabrication techniques are used to provide the microstructures desired for study.

1. LIMITATION OF GRIFFITH FLAWS IN GLASS MATRIX COMPOSITES*

Yogesh Nivas and Richard M. Fulrath

Hasselman and Fulrath[1] proposed a fracture theory for brittle matrix composite systems. This theory was experimentally verified by dispersing alumina microspheres in a glass matrix and calculating the mean free path in the glass matrix by Fullman's equation.[2] This study was undertaken to (1) extend the experimental verification of the Hasselman-Fulrath postulate to smaller mean free paths and (2) develop experimental techniques to measure the mean free path in the matrix. Reduction of the mean free path in the glass matrix and consequent limitation of Griffith flaw length in the abraded composite surface was achieved by using two sizes of tungsten microspheres or a wide distribution about one average size. The measurement of the mean free path in the glass matrix was made by using statistical techniques.

Three glass compositions (Ny, D, and N4) were used. All were in the soda borosilicate system and were chosen because of their thermal expansion coefficients. Tungsten microspheres, commercially available in wide size ranges, were chosen for the dispersed phase. Composites of glasses and tungsten microspheres were fabricated by vacuum hot-pressing. D glass-tungsten and N4 glass-tungsten composites were made using only single size with varying volume fraction of tungsten. Strength measurement of these composites showed the effect of internal stresses present due to mismatch of thermal expansion of two phases. Ny glass that had a thermal expansion matching tungsten was used to fabricate a series of composites varying in volume fraction of tungsten. The tungsten dispersions used were of a single particle size, two particle sizes with size ratio 1:7 (72% coarse + 28% fine), and a wide distribution about one average size.

The mean free path was measured by statistical techniques for a single particle size dispersion and was in good agreement with that calculated by Fullman's equation. Hence this technique was successfully used when the dispersed phase had two particle sizes or a wide particle size distribution.

The strengths of Ny glass and tungsten composites plotted against reciprocal square root of measured mean free path are shown in Fig. 1. The results agree very well with Hasselman and Fulrath's proposed fracture theory and extend the theory to smaller sizes of Griffith flaws.

---

*Abstracted from Yogesh Nivas, Limitation of Griffith Flaws in Glass Matrix Composites, UCRL-18586, November 1968.

1. D. P. H. Hasselman and R. M. Fulrath, Proposed Fracture Theory of a Dispersion-strengthened Glass Matrix, J. Am. Ceram. Soc. 49, 68 (1966).

2. R. L. Fullman, Measurement of Particle Sizes in Opaque Bodies, Trans. AIME 197, 447 (1953).

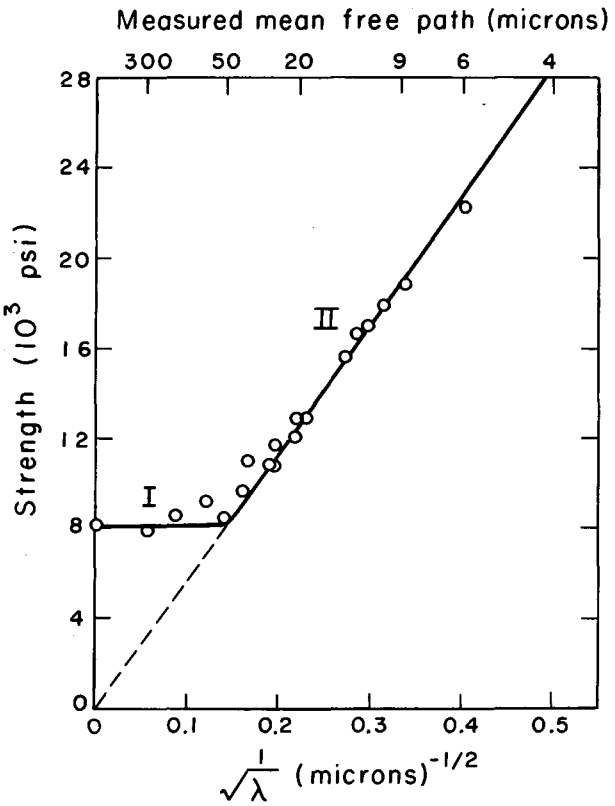

Fig. 1. Experimental data for the strength of Ny glass and tungsten composites plotted against reciprocal square root of measured mean free path.

2. STRENGTHENING BY CHEMICAL BONDING IN BRITTLE MATRIX COMPOSITE*

Mark A. Stett and Richard M. Fulrath

Bertolotti and Fulrath[1] reported that nickel microspheres did not bond to a glass of low thermal expansion relative to nickel and used the nickel-glass composite to study the effects of porosity on the strength of glass. Small microspheres, however, indicated that some bonding could be present.

Following the hypothesis of Pask and Fulrath[2] on interfacial bonding, nickel microspheres were oxidized to varying oxide thicknesses and hot-pressed into a glass matrix to enhance interfacial bonding. The strength of the composite and fracture surface appearance were used to evaluate the interfacial bonding achieved.

Figure 1, where the composite strength as a function of weight gain during oxidation or oxide thickness is plotted shows that for this particular fabrication process the composite strength is a function of the interfacial bonding. Scanning electron micrographs of the non-bonded, Fig. 2, and bonded, Fig. 3, composite fracture surfaces also confirm that interfacial bonding was achieved and affects the fracture path. In the composite where the interface between the nickel microspheres and the glass was not bonded the fracture path tends to bisect the glass volume around the nickel microsphere. Where bonding had occurred at the interface the fracture through the composite tends to remain in the glass matrix and leave a glass coating around each nickel inclusion.

---

*Abstracted from M. A. Stett and R. M. Fulrath, J. Am. Ceram. Soc. 51 (10), 599 (1968).

1. R. L. Bertolotti and R. M. Fulrath, Effect of Micromechanical Stress Concentrations on Strength of Porous Glass, J. Am. Ceram. Soc. 50, 558 (1967).
2. J. A. Pask and R. M. Fulrath, Fundamentals of Glass-to-Metal Bonding: VII, J. Am. Ceram. Soc. 45, 592 (1962).

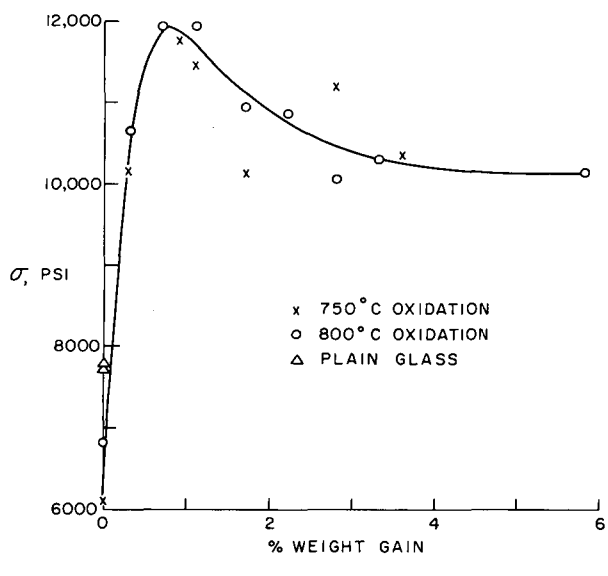

Fig. 1. Composite strength as a function of weight gain during oxidation.

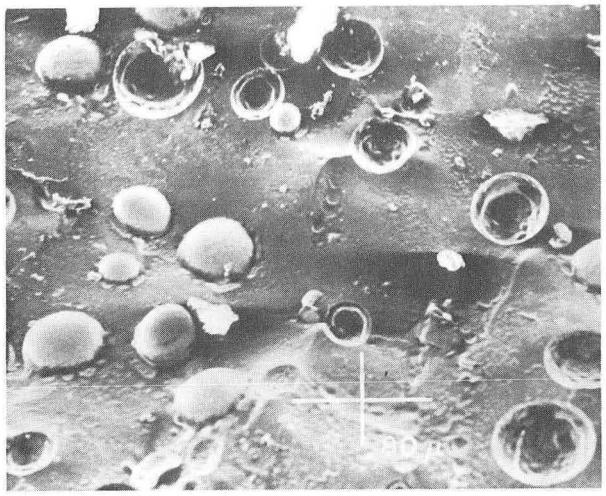

Fig. 2. Scanning electron microscope photograph of fracture surface of nickel-D glass (non-bonded) composite.
XBB 685-2984

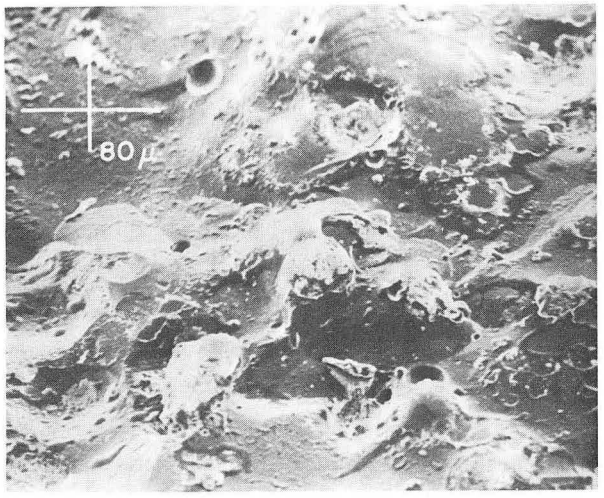

Fig. 3. Scanning electron microscope photograph of fracture surface of oxidized nickel-D glass (bonded) composite.
XBB 685-2983

3. PERMEATION IN FUSED SILICA*

Joseph S. Masaryk† and Richard M. Fulrath

Since the turn of the century, many publications have given the permeability, diffusivity, and solubility of gases in fused silica and other silicate-based glasses.[1-6] It is a well known fact that the structure at room temperature of fused silica depends on its fictive temperature. In all previous studies on helium and hydrogen permeation through fused silica, permeation specimens were not characterized according to the fictive temperature. Recently it was noted that different fused silicas had different hydroxyl ion contents. Depending upon its method of manufacture, fused silica may contain from 10 to 3000 ppm of hydroxyl ions.[7] At the temperatures used in the fabrication of a permeation membrane it can be calculated that the entry and removal of hydroxyl ions would be fairly rapid. It is possible that if the membrane were made by using an oxy-hydrogen flame, the glass could become saturated with hydroxyl ions. The purpose of this study was to investigate the effects of fictive temperature and hydroxyl ion content on the permeation of helium and hydrogen through fused silica.

Permeation specimens were fabricated by drawing down fused silica tubing to a size approximately 0.020 in. outside diameter and with a wall thickness of 0.003 inch. This very fine tubing was wound on a mandrel to form a helix 1 in. in diameter. One end of this permeation coil was inserted in a fused silica support tube and sealed with a bead of sealing glass. The other end of the coil was sealed by flame fusion. A cage of fused silica was built around the helix to protect it during handling (see Fig. 1). The permeation assembly was inserted in a fused silica protection tube, which in turn was inserted in a furnace. The pressure on the outside of the sample was kept at either 1 atm of helium or hydrogen. The inside of the sample was evacuated to 1×10^{-6} mm Hg. This pressure differential of 1 atm caused the gas around the sample to permeate from the high pressure to the low pressure side. The flow rates through the wall were measured with a mass spectrometer which was calibrated to give absolute values with the use of a standard leak. The permeation constant K, atoms/cm-sec-atm was calculated by using Darcy's law:

$$F = \frac{K A \Delta P}{d} ,$$

where F = flow rate, A = area, d = thickness, ΔP = pressure difference across d, K = permeation constant.

Given fictive temperatures and hydroxyl ion contents were established by holding the specimen at 1000 or 1100 ° in 0 or 1 atm water vapor pressure. Water concentrations were determined by including a fused silica disk of similar thickness with the permeation coil in the treatment apparatus and then measuring the intensity of the 2.7 μ OH stretching vibration of the silica disks.[8] The density of each disk after a specific treatment was measured with the aid of a density gradient column

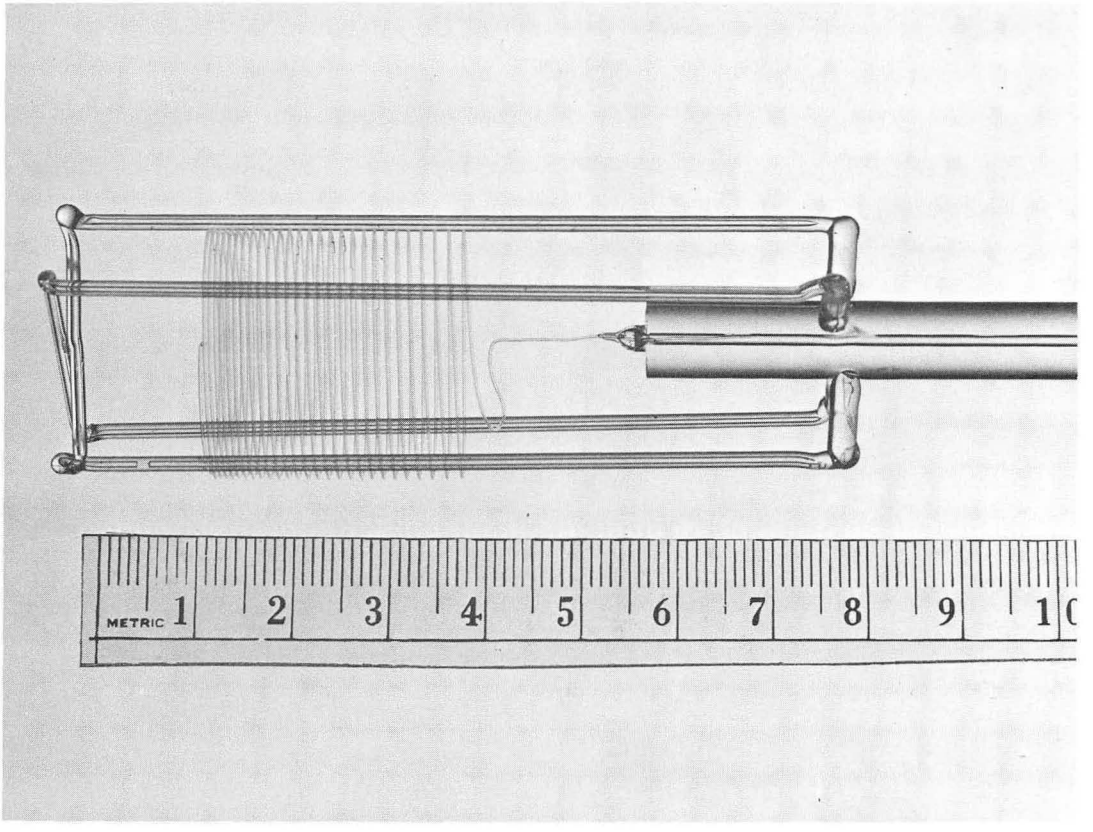

Fig. 1. Fused silica permeation assembly. XBB 670-5959

Table I. Permeation of He.

Treatment	T (°C)	Permeation constant K $\left(\frac{\text{atoms}}{\text{cm-sec-atm}}\right)$	Activation energy ΔH (cal/mole)	wt % OH	Density (g/cc) ±0.0002
As received	14	8.25×10^{9}	5115.0 ± 33.5	0.0097	2.2049
Desaturated 1100°	14	8.20×10^{9}	5095.6 ± 58.6	0.0105	2.2029
Saturated 1100°	14	6.95×10^{9}	5120.4 ± 53.3	0.186	2.2011
Desaturated 1000°	15	7.35×10^{9}	5107.5 ± 34.1	0.0193	2.2013
Saturated 1000°	15	6.30×10^{9}	5215.5 ± 69.5	0.106	2.2006

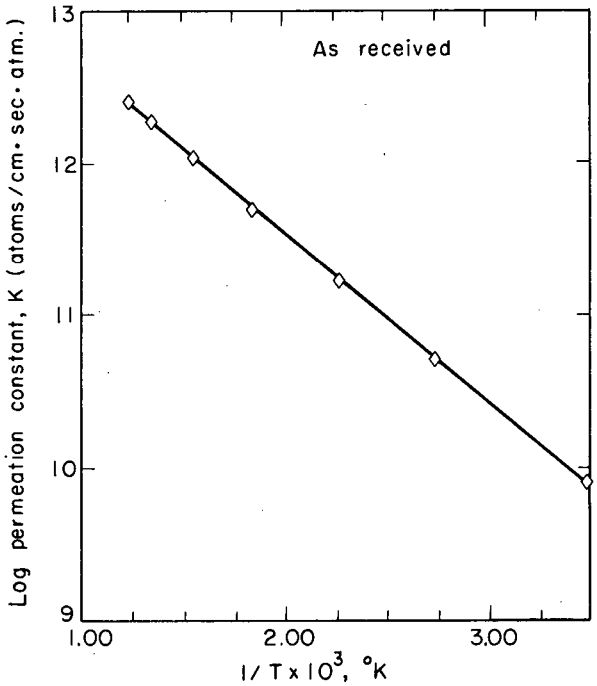

XBL692-2057

Fig. 2. Helium permeation through fused silica.

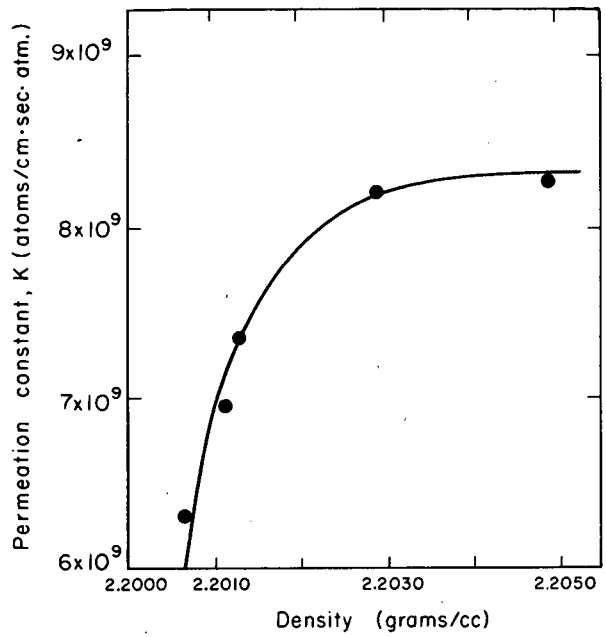

XBL692-2058

Fig. 3. Change in helium permeation through fused silica with density at 14 to 15°.

Table II. Permeation of H_2.

Treatment	T (°C)	Permeation constant K $\left(\frac{\text{atoms}}{\text{cm-sec-atm}}\right)$	Activation energy ΔH (cal/mole)	wt % OH	Density (g/cc) ±0.0002
As received	188	3.45×10^{9}	8264.1 ± 92.8	0.0097	2.2049
Desaturated 1100°	196	3.57×10^{9}	8234.4 ± 73.5	0.0105	2.2029
Saturated 1100°	196	3.65×10^{9}	8214.5 ± 131.8	0.186	2.2011
Saturated 1000°	194	3.57×10^{9}	8282.3 ± 151.0	0.106	2.2006
Desaturated 1000°	195	3.59×10^{9}	8498.7 ± 200.2	0.0193	2.2013

accurate to ±0.0002 g/cc.

The permeation constants as a function of temperature were calculated in the range of 14 to 530° for helium and 200 to 600° for hydrogen. A computer program was used to determine a least-squares fit of the log permeation constant versus 1/T°K (see Fig. 2) with a confidence level of 95%. The activation energy was then determined from the slope of this line (see Tables I and II). The permeabilities and activation energies for different thermal treatments lie within a narrow range. Therefore, helium and hydrogen permeation through fused silica are not significantly affected by hydroxyl content or fictive temperature in the range studied.

Although no significant changes in the permeation constant, K, of helium or in activation energy for permeation were observed, there is a definite trend indicated in the permeation constant. If the permeation constant (Fig. 3) for helium at 14 to 15° is plotted against the room temperature density, there appears to be a direct relationship of decreasing helium permeation with decreasing density. This would indicate that either the fictive temperature or hydroxyl ion content, which both affect the density of fused silica, is related to the permeation characteristics. It is apparent, however, that much more precise measurements of the permeation constant are necessary to fully substantiate this observation.

It can be concluded that the method of manufacture of fused silica does not significantly affect its permeation characteristics for hydrogen or helium.

---

*Abstracted from J. S. Masaryk, Permeation in Fused Silica, UCRL-18393, August 1968.

†Present address: U. S. Army, Fort Bragg, North Carolina.

1. P. Villard On the Permeability of Fused Silica to Hydrogen, Compt. Rend. Acad. Sci. 130, 1752 (1900).
2. R. M. Barrer, The Mechanism of Activated Diffusion through Silica Glass, J. Chem. Soc. 136, 378 (1934).
3. F. J. Norton, Helium Diffusion through Glass, J. Am. Ceram. Soc. 36 (3), 90 (1953).
4. V. O. Altemose, Helium Diffusion through Glass, J. Appl. Phys. 32 (7), 1309 (1961).
5. D. E. Swets, R. W. Lee, and R. C. Frank, Diffusion Coefficients of Helium in Fused Quarts, J. Chem. Phys. 34 (1), 17 (1961).
6. R. W. Lee, R. C. Frank, and D. E. Swets, Diffusion of Hydrogen and Deuterium in Fused Quartz, J. Chem. Phys. 36 (4), 1062 (1962).
7. R. W. Lee, Diffusion of Hydrogen in Natural and Synthetic Fused Quartz, J. Chem. Phys. 38 (2), 449 (1963).
8. I. Burn, A Study of Diffusion and Exchange of Water in Silica Glass Using Radioactive Isotopes (Ph. D. Thesis), Leeds University, 1966.

4. DENSIFICATION AND ELECTRICAL PROPERTIES OF LEAD ZIRCONIUM TITANATE*

Bruce F. Semans† and Richard M. Fulrath

Lead zirconate titanate solid solutions (PZT) are currently finding varied commercial applications because of their piezoelectric properties. With its relatively high Curie temperature and excellent piezoelectric constants, this material is found to be superior to other materials. The applications for piezoelectric materials range from sonar, ultrasonic cleaning devices, strain gages, phonograph pickups, and many other transducer applications. Haertling,[1] as well as others, has reported the effect of Bi_2O_3 additives on the electrical properties of PZT. All investigations to date have been complicated because porosity has varied. Therefore a direct effect of the doping material on measured properties is difficult at best.

This study was to investigate the effect of 0.5 wt % Al_2O_3 and 0.5 wt % Bi_2O_3 on densification and electrical properties of PZT. The former impurity simulates a similar amount of pickup during regular ceramic processing as observed in this laboratory, while the later is comparable to the amount of dopant previously reported.

Densification was investigated by monitoring sample compaction under constant pressure while a linear rate of temperature increase was maintained. When deflection is then plotted against temperature it is possible to observe at what temperature an increased rate of densification occurs as shown in Fig. 1. (This temperature is designated $T_{inc.}$) It was found that Al_2O_3 had a minimal effect on time while Bi_2O_3 lowered the temperature at which the rate of densification increased by 80°. Final densities, obtained by applying pressure just about T_{inc} and holding for 2 hours, showed no variation with doping agent.

It is felt two mechanisms might be operating in this system to explain the variation in densification. Bi_2O_3 forms a low melting liquid (730°) with PbO. During heating PbO is lost to the atmosphere. If the vapor were

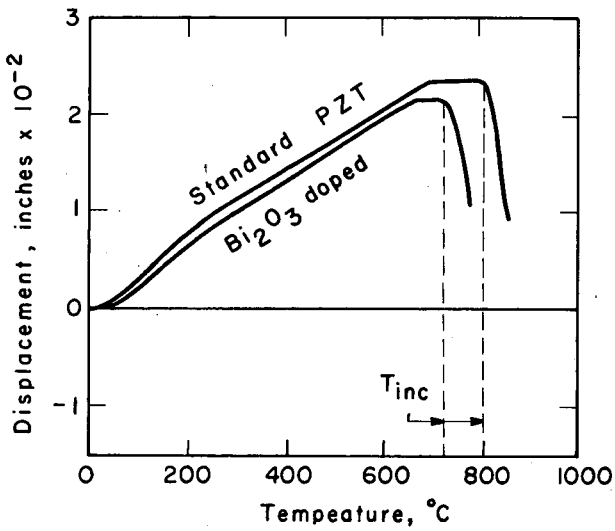

Fig. 1. Displacement vs. temperature for standard and Bi_2O_3 doped PZT under constant pressure of 1000 psi.

to form a second phase with the Bi_2O_3 impurity, a reactive liquid would be formed at the grain boundaries that would aid densification. A second mechanism could be operative in this system. Considering ionic radii and valance state, it seems reasonable to assume the Bi^{3+} may be substituting for Pb^{2+}, thus causing an increased number of cation vacancies. This situation would enhance solid state diffusion that would explain the effect on densification rate that was noted.

The microstructure of the samples doped with Al_2O_3 is changed with the appearance of a second phase. This is possible only by the formation of the lead aluminate liquid that is predicted by the PbO-Al_2O_3 phase diagram. Microprobe analysis indicated the second phase pockets were high in aluminum and lead concentration.

Coercive field, remnant polarization, and saturation polarization were lowered by the Bi_2O_3 additive as compared to the undoped and Al_2O_3 doped materials. The values obtained for the Bi_2O_3 doped samples agreed well with Haertling's findings.

---

*Abstracted from B. F. Semans, Densification and Electrical Properties of Lead Zirconium Titanate (M. S. Thesis), UCRL-18126, March 1968.

†Currently serving with the U. S. Army.

1. G. H. Haertling, Hot Pressed Lead Zirconate-Lead Titanate Ceramics, Am. Ceram. Soc. Bull. 43, 12 (1964).

5. IMPURITY EFFECTS IN SINTERING LEAD ZIRCONATE TITANATE*

Garet A. Pryor† and Richard M. Fulrath

Research efforts on lead zirconate titanate (PZT) have concentrated on its electrical properties. Many investigators primarily studying electrical properties of PZT have indicated that higher densities and mechanical strength were obtained from sintering PZT with impurities added. Additives have long been known to give favorable electrical properties to PZT so that additives are universally employed in commercial production of PZT.

This evidence that impurities may contribute significantly to the sintering of PZT led to the present investigation. Impurities may be added to a material by intentional doping, or unintentionally during processing steps, such as ball milling. The purpose of this investigation was to study the effect of impurities normally encountered in processing on the sintering behavior and mechanism in the PZT system.

High purity PZT powder was obtained by calcination of a mixture of PbO, ZrO_2, and TiO_2 at 800°. No sintering occurred for compacts made from this powder unless a ball milling treatment was used. Equal batches of PZT were ball milled in high Al_2O_3 mills: (1) dry, (2) in water, and (3) in isopropyl alcohol. The powders thus obtained were characterized as to particle size and impurity level. Impurities picked up were Al_2O_3 and a lesser amount of SiO_2. Average particle sizes of wet milled powders were slightly less than 2 μ.

Pressed samples of the powders having the highest impurity levels and smallest particle sizes (H_2O and isopropyl alcohol milled) sintered to the highest densities, nearly 92% of theoretical (8.0 g/cc). Dry milled powder having a larger particle size and less impurities gave densities between those for the sintered wet milled powders and the unmilled powder which did not sinter.

Investigation of the above PZT powders indicated an optimum temperature range of approximately 1200-1260° for sintering in air at constant times of 1-1/2 hours.

Sintering in atmospheres of argon and oxygen in addition to air indicated that gas

entrapment in closed pores during sintering may occur and lead to lower densities. Approximately a 3% density difference was observed between the less dense argon-fired samples and the oxygen-fired samples.

The above investigations indicated that impurities introduced in ball milling may have contributed significantly to the sintering of PZT. The fact that particle size, another important variable in sintering, was also changed in the powder treatment steps made definite conclusions impossible. Therefore, a high purity, fine particle size powder was obtained by milling, using organic materials as container and grinding media. This material was then used as a standard material to which varying amounts of the principal ball milling impurities, Al_2O_3 and SiO_2, were added.

The effect of the impurity level alone on the sintered density of this PZT powder of fine particle size is shown in Fig. 1. The Al_2O_3 and SiO_2 additives increase density by 10 and 5% respectively when added in optimum amounts of 0.4 and 0.6 wt %.

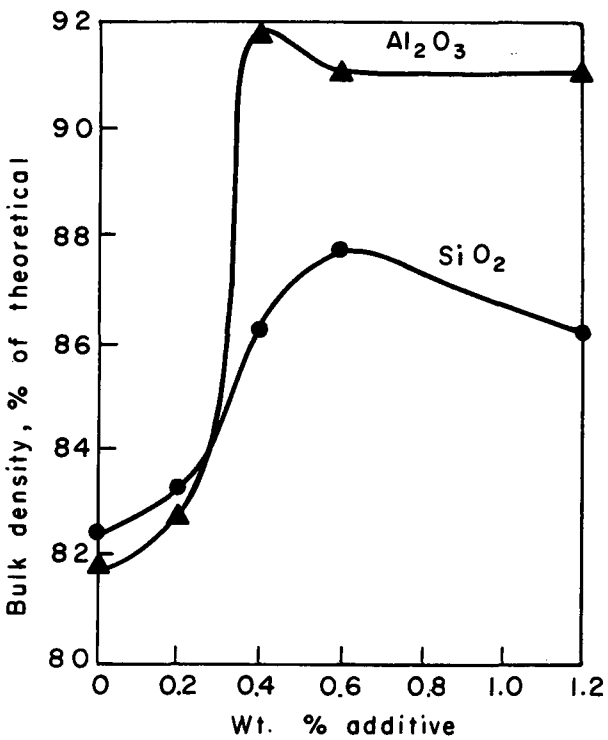

Fig. 1. Effect of Al_2O_3 and SiO_2 additives to high purity PZT on sintered density.

Observations were made on a number of the Al_2O_3 and SiO_2 additive samples, using the optical microscope, electron microprobe, and scanning electron microscope.

Microprobe analysis indicated aluminum concentration occurred in isolated pockets. The beam diameter was too large, however, to detect concentrations at grain boundaries.

Microprobe data for the SiO_2 additive samples indicated possible reaction of the SiO_2 with ZrO_2 and PbO.

Comparison of the microstructures of the samples by optical and scanning electron microscopy indicated that the grain size for the Al_2O_3 additive sample is much smaller than for the SiO_2 or no additive samples (Figs. 17, 19, and 27 in UCRL-18191).

The evidence obtained strongly suggests the contribution of a liquid phase in the sintering process of PZT. This contribution appears to be greater for Al_2O_3. Further, the liquid aluminate inhibits grain growth. SiO_2 as additive appears to form a reactive liquid with PbO and ZrO_2 but does not reduce grain growth and has less effect on sintering.

It is concluded that liquid phases make a major contribution to the sintering of lead zirconate titanate prepared and processed by conventional methods.

---

*Abstracted from G. A. Pryor, Impurity Effects in Sintering Lead Zirconate Titanate (M. S. Thesis), UCRL-18191, May 1968.

†Present address: U. S. Marine Corps Recruit Depot, San Diego, California.

6. MICROSTRUCTURE DEVELOPMENT OF LEAD ZIRCONATE TITANATE

Robert B. Atkin and Richard M. Fulrath

The study of the effect of impurities on the sintering of lead zirconate titanate has been extended to a composition with optimum ferroelectric properties. The material has the base composition $Pb(Zr_{0.53}Ti_{0.47})O_3$. Doping with bismuth and niobium is known to improve the electrical character of lead zirconate titanate so these impurities were also considered (as well as alumina and silica).

A technique* was developed to accurately control the composition during sintering. Suitable materials were prepared by mixing,

---

*Patent disclosure filed.

calcining, and grinding in organic mills, high purity oxides. The "impurities" (Al, Bi, Nb, and Si) were introduced by either additions of their oxide before calcining (Bi and Nb) or as an aqueous solution after the plastic milling operation (Al and Si). Pellets were cold-pressed and buried in pure unground lead zirconate titanate powder for sintering. This burial provides the equilibrium vapor pressure around the specimen so evaporation of lead oxide is prevented. Sintering experiments were conducted for various times at 1170 and 1200°. The specimens were used to determine the sintering kinetics, as well as microstructure developed and ferroelectric properties. The scanning electron microscope was used for microstructure observation.

Ionic size and valance predicted very limited solubility of aluminum and silicon in the lead zirconate titanate lattice, but bismuth and niobium solubility was expected to be relatively large. Bismuth and niobium should substitute for lead and titanium, respectively, and create cation vacancies. Alumina and silica additions were expected to result in secondary phases. These secondary phases should react with lead oxide from the primary phase to form liquids. These predictions were confirmed with experimental findings.

Liquid phase sintering kinetics were observed when alumina or silica was present. The rate of solid state sintering was increased by bismuth and/or niobium doping. The materials without alumina or silica sintered according to the relation

$$\rho = \rho_0 + \alpha\ (\text{time})^{1/2},$$

where ρ is the relative density and ρ_0 is the relative density at the start of isothermal sintering, α is a constant. The values of ρ_0 and α increased with temperature and doping concentration. This behavior is interpreted as solid state sintering with the lattice defects increasing the diffusivity. Additions of alumina or silica changed the sintering relation to

$$\rho = \rho_0 + \beta\ (\text{time})^{1/3};$$

again ρ_0 and the constant, β, were composition and temperature dependent. These kinetics are identified as the solution-precipitation stage of liquid phase sintering. Material transport across interfacial boundaries (for grain growth) was usually enhanced by the presence of the liquid phase. Niobium and bismuth apparently provide an impurity drag effect that reduces grain boundary mobility.

Ferroelectric measurements and microstructure observations were used to support and extend the above explanation of the sintering behavior. The following information was obtained in this study: (1) niobium and bismuth enter the lattice and create cation vacancies, (2) silica is not appreciably soluble in the lattice so it is retained as a second phase at grain boundaries, (3) alumina, alone, has a solubility of less than 1 at. % and lead zirconate titanate saturated with aluminum is anti-ferroelectric, (4) trivalent aluminum and pentavalent niobium enter adjacent titanium (tetravalent) sites and thereby compensate for one another, and (5) a tendency for compensation of aluminum by trivalent bismuth in a divalent site is observed.

This study has definitely established the effect of these impurities on the sintering of lead zirconate titanate. Liquid phase sintering occurred at relatively low concentrations (only 0.4 wt %) of alumina and silica. Similarily only 2 at. % bismuth or niobium was sufficient to greatly enhance solid state sintering. Ferroelectric property measurements have been used to supplement densification and microstructural observations.

7. RESEARCH PLANS FOR CALENDAR YEAR 1968

Richard M. Fulrath

Composite Materials with Ceramic Matrices

The many factors that dictate the strength of brittle matrix composites can best be studied with simple model systems. The work in this laboratory has concentrated on using glass as the matrix and metallic or crystalline oxide microspheres as the dispersed phase. Previous studies have demonstrated the dependence of the composites strength on volume fraction and size of the dispersed phase, volume and size of pores, and to a limited degree the interfacial bonding between the dispersed phase and the matrix. During the past year it has been shown that experimental methods to determine an important parameter, the average mean free path in the matrix phase, can be successfully employed.

During 1969 further investigation into the interfacial bonding characteristics and the relation of this to strength and fracture propagation paths will be made.

Work has been initiated and will continue on establishing the relation of internal stresses due to thermal expansion differences between the matrix phase and dispersed phase.

Gas Permeation Through Ceramics

Permeation of gases through ceramics is of practical importance in high temperature devices. Studies of permeation characteristics can further the understanding of microstructural features such as interfacial boundaries in polycrystalline materials. Previous work in this laboratory has indicated that in polycrystalline commercial aluminum oxide helium permeation is through grain boundaries or secondary glassy phases. As a result of this study, a program on permeation through fused silica and silicate-based glasses was initiated in 1967. The first problem studied was whether the fictive temperature or hydroxyl ion content of fused silica significantly affected permeation of helium or hydrogen. An effect of density that is related to both fictive temperature and hydroxyl ion content was found.

A study is now under way to identify the density dependence on these two variables. During the past year techniques and equipment were developed to change both these variables independently. Following this study it is planned to extend the previous work and obtain both permeation and diffusion data by dynamic techniques.

Studt[1] theoretically predicted that the solubility coefficient temperature dependence of helium in fused silica was related to the solute site geometry. Equipment to determine solubility directly was constructed in 1968, and it is planned to measure solubility of both helium and hydrogen in fused silica this year. The results will be analyzed according to Studt's model.

---

1. P. L. Studt, Mechanism of Gaseous Permeation through Glass, Single Crystal Silicon, and Germanium; and Stress-Enhanced Gaseous Permeation through Alumina Bodies (Ph. D. Thesis), UCRL-10466, September 1962.

Electrical and Magnetic Ceramics

The research in this area during the past year has resulted in the development of new and unique sintering procedures for the production of polycrystalline ferroelectric ceramics. These techniques allow the fabrication of high density ceramics of controlled purity with regard to both doping additions and impurities normally encountered in processing. Studies are now planned to develop a structural model for electrical properties with regard to lattice substitional solid solutions and compare these to real polycrystalline systems.

Studies on grain boundaries using the scanning electron microscope were initiated in 1968 and will be continued.

Further studies in the ferroelectric area are planned using the differential thermal calorimeter to obtain the paraelectric-ferroelectric transition heat for compositions in the lead titanate-lead zirconate system.

In mid-1969 it is planned to apply the techniques developed in sintering perovskite structures to spinel type materials that have ferromagnetic characteristics.

8. 1968 PUBLICATIONS

Richard M. Fulrath and Associates

Book and Technical Journal

1. R. M. Fulrath and J. A. Pask, eds., Ceramic Microstructures: Their Analysis, Significance, and Production (John Wiley & Sons, Inc., New York 1968).
2. Ibid., D. P. H. Hasselman and R. M. Fulrath, chapter on Mechnical Properties of Continuous Matrix, Dispersed Phase Ceramic Systems.
3. M. A. Stett and R. M. Fulrath, Strengthening by Chemical Bonding in Brittle Matrix Composite, J. Am. Ceram. Soc. 51 (10), 599 (1968).

UCRL Reports

1. J. S. Masaryk, Permeation in Fused Silica (M. S. Thesis), UCRL-18393, August 1968.
2. Y. Nivas, Limitation of Griffith Flaws in Glass Matrix Composites (M. S. Thesis), UCRL-18586, November 1968.
3. G. A. Pryor, Impurity Effects in Sintering Lead Zirconate Titanate (M. S. Thesis), UCRL-18191, May 1968.
4. B. F. Semans, Densification and Electrical Properties of Lead Zirconium Titanate (M. S. Thesis), UCRL-18126, March 1968.

IV. Solid-State Physics

A. THEORETICAL SOLID STATE PHYSICS

1. ELECTRONIC STRUCTURE OF SOLIDS

Marvin L. Cohen

We have analyzed the optical properties and electronic structure of several semiconductors and insulators using the empirical pseudopotential method (EPM). The EPM has resulted in more accurate band structures than all other methods combined. The optical spectra, effective masses, electron-lattice couplings, photoemission spectra, superconducting properties, photoabsorption and various other properties of solids have been analyzed using the results of this method. Pseudopotentials for metals and semimetals were extracted from the optical properties of semiconductor compounds. It became possible to use the results of optical experiments on InSb to compute the Fermi surface of In and Sb, and to calculate the superconducting transition temperature of In.

2. SUPERCONDUCTIVITY IN DEGENERATE SEMICONDUCTORS AND IN METALS

Marvin L. Cohen

We have examined the problem of calculating superconducting transition temperatures and electron-phonon renormalizations in metals and degenerate semiconductors. We have successfully calculated the electron-phonon mass enhancement for Be, Mg, Zn, and Cd, and the superconducting transition temperatures of Be, Zn, and Cd. Using the same theory we have predicted the superconducting transition temperature of Mg. Mg has not yet been found to be superconducting, but a search at low temperatures has been started. The carrier concentration dependence of the superconducting properties of degenerate semiconductors has also been calculated and found to be in agreement with experiment.

Another main project is to use a dilution refrigerator to explore superconductors at ultralow temperatures. We hope that a close collaboration between theory and experiment will result in a deeper knowledge of the mechanisms of superconductivity. In this way it may become possible to predict which materials will be superconducting and to learn more about maximizing the superconducting transition temperature.

A dilution refrigerator was built during the past year and is now being tested.

3. RESEARCH PLANS FOR CALENDAR YEAR 1969

Marvin L. Cohen

We plan to extend our work using the EPM to other crystals and to attempt new types of calculations.

Previous theoretical calculations indicate that Mg may be a superconductor in a measurable temperature range. Pure Mg has been obtained and these tests will be made.

Work on the dilution refrigerator is being completed and further tests on the properties of low transition temperature superconductors will follow.

A close relation between experimental and theoretical work will be continued to measure the properties of superconductors to the lowest available temperature, at least 0.02°K or possibly lower.

4. 1968 PUBLICATIONS

Marvin L. Cohen and Associates

Technical Journals

1. M. Y. Au-Yang and M. L. Cohen, Meson Captures in Solids, Phys. Rev. 174, 468 (1968).
2. M. L. Cohen, Recent Pseudopotential Calculations in Solids, Proc. Nat. Acad. Sci. 61, 6 (1968).
3. M. Y. Au-Yang and M. L. Cohen, Electronic Structure and Dielectric Function of Mg_2Si, Solid State Commun. 6, 855 (1968).
4. C. Y. Fong, W. Saslow, and M. L. Cohen, Pseudopotential Calculation of the Optical Constants of MgO from 7-28 eV, Phys. Rev. 168, 992 (1968).
5. C. Y. Fong and M. L. Cohen, Band Structure and Ultraviolet Optical Properties of Sodium Chloride, Phys. Rev. Letters 21, 22 (1968).

UCRL Reports

1. C. Y. Fong, Empirical Pseudopotential Method for Electronic Band Structure Calculations in Insulators (Ph. D. Thesis), UCRL-18356, July 1968.

B. MAGNETIC PROPERTIES OF SOLIDS

1. NUCLEAR RESONANCE IN ANTIFERROMAGNETIC INSULATORS

Weston J. Sandle* and Alan M. Portis

The nuclear magnetic resonance absorption of ^{19}F has been studied in $KMnF_3$ from 4.2°K up to 300°K. In the ideal perovskite structure the ^{19}F nucleus would be midway between a pair of oppositely magnetized Mn^{2+} ions and there would be no hyperfine field. The actual structure is slightly distorted, leading to a detectable hyperfine interaction with the ^{19}F nuclear spins. A study of the hyperfine interaction as a function of the magnitude and direction of an externally applied field establishes the character of the deviation from the ideal perovskite structure. In addition the ^{19}F nuclear resonance may be used as a probe of the response of the Mn^{2+} ion spin orientation to the applied field. Results that are not directly interpretable in terms of the conventional single ion anisotropy model are obtained. It is suggested that an unsuspected source of antisymmetric exchange may be operating.

*Present address: Department of Physics, University of Otago, Dunedin, New Zealand.

2. ANTIFERROMAGNETIC RESONANCE

Jerome F. Siebert* and Alan M. Portis

A study has been made of magnetic relaxation in the three antiferromagnets, $CsMnF_3$, $RbMnF_3$, and $KMnF_3$ as a function of temperature with special emphasis on the critical region just above the ordering temperature. $CsMnF_3$, which crystallizes in the hexagonal perovskite structure, shows a large line width maximum in the vicinity of the transition. The other two materials, which crystallize in the cubic perovskite structure, failed to show any additional line broadening near the transition. This difference in behavior is not consistent with existing theories of spin relaxation based on the conventional theory of critical fluctuations. It is possible that by considering the effect of collective oscillations in isotropic and anisotropic media that a qualitative difference can be expected as indicated from the experimental results.

*Present address: Department of Physics, Cornell University, Ithaca, New York.

3. SPIN WAVE RESONANCE IN MAGNETIC FILMS

William C. Holzer* and Alan M. Portis

Standing spin wave resonance has been observed as a function of temperature in evaporated films of permalloy and of nickel. The permalloy studies were performed by measuring the microwave power transmitted through the film as a function of applied dc magnetic field. A previously unpredicted interference effect between the propagating electromagnetic wave and the spin waves was observed and explained. The emphasis in the studies of the nickel films was on the high temperature behavior of the exchange stiffness constant. It was found that at temperatures above 0.8 of the transition temperature of 627°K the exchange stiffness varies linearly with temperature. This observation seems to be consistent with predictions based on general arguments which invoke a thermal screening length. [1]

*Present address: Service de Physique des Solides, Universite de Paris, Orsay, France.

1. L. P. Horwitz and D. C. Mattis, Phys. Rev. Letters 10, 511 (1963).

4. NUCLEAR RELAXATION IN FERROMAGNETIC ALLOYS

Michael H. Bancroft,*† Boris Chornik,‡ and Alan M. Portis

Nuclear magnetic relaxation of ^{63}Cu in dilute nickel-based copper alloys has been measured in the temperature range from 2.1 to 300°K. The relaxation is inferred from the strength of the nuclear spin echo. This echo comes from nuclei in the wings of domain walls in zero applied field and from nuclei in the saturated bulk in large external fields. The observed lattice relaxation rate for copper in nickel is if anything slower than for copper in metallic copper. It is concluded that there is little if any contribution to the relaxation from holes in the d band. This suggests, in agreement with screening arguments, that Cu in nickel has no atomic magnetic moment. In the liquid helium range spin-spin interaction may be observed between ^{63}Cu nuclei at concentrations as low as 1%.

*Present address: Department of Physics, Imperial College, University of London,

London, England.
†NSF Predoctoral Fellow.
‡California-Chile Predoctoral Fellow.

5. DOMAIN WALL EXCITATION OF NUCLEAR RESONANCE

Jean-Noel Aubrun* and Alan M. Portis

Coherent wall switching has been observed in micron-sized particles of fcc cobalt through the saturation of the ^{59}Co nuclear resonance. Walls driven at a fundamental frequency in the megacycle range evidently are capable of generating harmonics into the hundreds of megacycles as may be concluded from the saturation of the nuclear resonance at 213 MHz. Our interpretation of this observation is that discontinuous jumps in wall displacement, coherent from cycle to cycle, must be occurring. The fact that these jumps take place for applied fields as small as 10 Oe is surprising. We are not entirely satisfied with this situation and are exploring other possibilities. We have also investigated the non-resonance relaxation of ^{59}Co nuclei with applied audio-frequency fields. An unexpectedly large effect is obtained and is explained as resulting from frequency modulation of the ^{59}Co resonance. A comparison between theory and experiment should give a measure of the microscopic inhomogeneity in the hyperfine field.

*Present address: Stanford University, Stanford, California.

6. ELECTRON RESONANCE IN NEARLY FERROMAGNETIC METALS

Eric R. Katz* and Alan M. Portis

A study of the magnetization of nickel-rhodium alloys as a function of composition and temperature and of electronic relaxation as a function of temperature is in progress. For uncorrelated localized moments, there is a simple theoretical connection between magnetization and relaxation.[1] In the case of pure nickel[2] it was found that for temperatures more than 20°K above the Curie temperature the theory was confirmed, suggesting that nickel does support localized moments above T_c. Near the Curie temperature, deviations were observed that were consistent with the existence of oscillatory spin correlations—paramagnons. Similar studies for the alloy system at concentrations near the critical concentration should indicate the extent of spin correlation and localization in this complex region.

*NSF Predoctoral Fellow.

1. P. G. de Gennes, C. Kittel, and A. M. Portis, Phys. Rev. 116, 327 (1959).
2. M. B. Salamon, Phys. Rev. 155, 224 (1967).

7. NUCLEAR SPIN DIFFUSION IN FERROMAGNETIC METALS

Earl D. Shaw and Alan M. Portis

A careful study is being performed on the diffusion of spin excitation through the ^{59}Co absorption spectrum in both single and multidomain ferromagnetic particles. The stimulated echo technique is being used to produce an alternation in spin orientation through the spectrum. Spin-lattice, incoherent spin-spin, and diffusion processes all act to wash out the alternation. By varying the periodicity of the alternation it is possible to sort out the diffusion process. An effort is being made to determine the effect of domain wall excitations on spin diffusion. Incoherent spin-spin processes are also being studied and an effort is being made to determine the effectiveness of wall displacements. These observations are being compared with the corresponding spin-spin processes in bulk cobalt. Both single domain particles in low magnetic fields and multidomain particles in large saturating fields are being investigated.

8. RESEARCH PLANS FOR CALENDAR YEAR 1969

Alan M. Portis and Associates

Nuclear Relaxation in Ferromagnetic Alloys

The initial measurements on copper in nickel are being extended to a wide range of alloys. We believe that longitudinal relaxation provides a much better indication of the presence of a local magnetic moment than does the hyperfine interaction, which is relatively insensitive to whether the moment is local or dispersed. By examining various nuclei in a wide range of alloys we hope to establish some of the systematics of local moment formation in alloys.

Electron Resonance in Nearly Ferromagnetic Metals

Experiments are now in progress. We anticipate that the interpretation of the experimental results, even in phenomenological

terms, will be difficult. In order to establish the difference between local moment formation and spin correlation, it may be desirable to investigate magnetization and resonance absorption in a series of rare earth alloys, where local moments are clearly established.

Nuclear Spin Diffusion in Ferromagnetic Metals

The study of nuclear spin diffusion, as described above, is in progress. It is planned to perform these measurements on a wide range of samples of pure cobalt, prepared in various ways. In addition to establishing the contribution of wall excitations to spin-spin coupling, it is hoped that the effect of local defects on spin diffusion can be measured so that the diffusion rate can be used as a measure of local interactions.

9. 1968 PUBLICATIONS

Alan M. Portis and Associates

Technical Journals

1. W. Bindloss, Anisotropic Spin-Disorder Resistivity of AuMn, Phys. Rev. 165, 725 (1968).
2. W. Bindloss, The Magnetic Structure of AuMn, J. Phys. Chem. Solids 29, 225 (1968).
3. R. H. Lindquist, G. Contstabaris, Walter Kundig, and A. M. Portis, Mossbauer Spectra of Fe^{57} in Superparamagnetic Nickel, J. Appl. Phys. 39, 1001 (1968).

UCRL Reports

1. M. H. Bancroft, Nuclear Relaxation of Cu^{63} in Ni-Cu (Ph. D. Thesis), University of California, Berkeley, UCRL-18461, September 1968.
2. W. C. Holzer, Standing Spin Wave Resonance in Magnetic Thin Films (Ph. D. Thesis), University of California, Berkeley, UCRL-18311, June 1968.
3. J. F. Siebert, Electron Resonance Studies of Critical Fluctuations in Antiferromagnets (Ph. D. Thesis), University of California, Berkeley, UCRL-18119, March 1968.

C. FAR INFRARED PROPERTIES OF SOLIDS

1. TUNEABLE FAR INFRARED RADIATION GENERATED FROM THE DIFFERENCE FREQUENCY BETWEEN TWO RUBY LASERS

Dillard W. Faries, Karl A. Gehring, Paul L. Richards, and Y. R. Shen

Far infrared radiation has beam generated in the frequency range from 1.2 to 38 cm^{-1} by beating two Q-switched ruby lasers in the non-linear optical materials quartz and $LiNbO_3$. The difference frequency was tuned by adjusting the temperature difference between the lasers. The expected spectral content and frequency of the far infrared radiation has been verified using a Fabry-Perot interferometer (Fig. 1). The importance of phase matching was also verified (Fig. 2). Difference frequency signals as large as 2×10^{-2} W in a 3×10^{-8} sec pulse were observed. Experiments involving three other laser sources are in progress and show promise of providing a practical tuneable far infrared source.

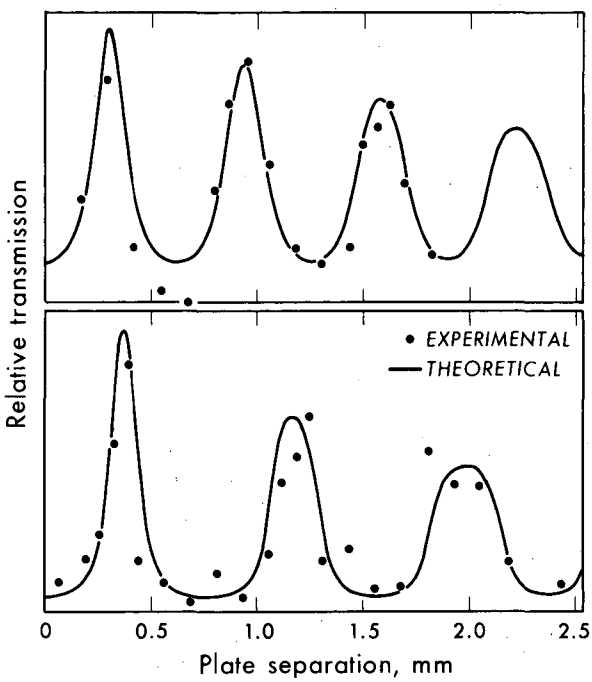

Fig. 1. Fabry-Perot scan of the difference-frequency output. The upper scan (a) is for a temperature difference $\Delta T = 60°$ of the two lasers. For the lower scan (b), $\Delta T = 47°$. The theoretical curves are Airy functions, calculated from the geometrical properties of the Fabry-Perot reflectors and averaged to account for the 30 deg collection half-angle.

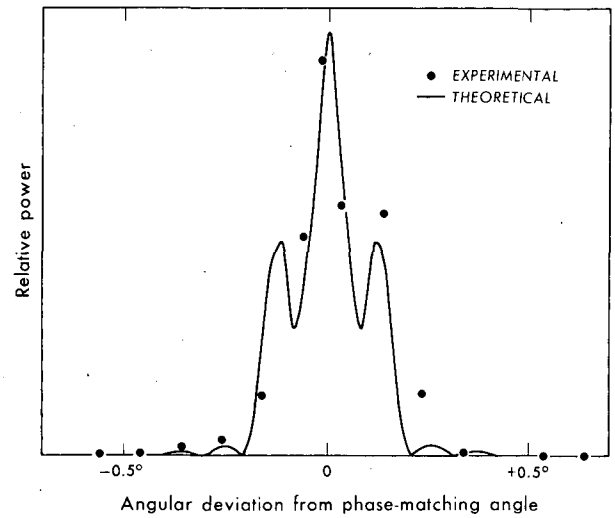

Fig. 2. Variation of the power of the difference-frequency signal as a function of the angular deviation from the phase-matched angle. The angles refer to the inside of the 1.5 cm $LiNbO_3$ crystal used.

2. LOW LYING ENERGY LEVELS OF INTERMEDIATE AND HIGH SPIN Fe^{3+} IN MATERIALS OF BIOLOGICAL INTEREST

George C. Brackett and Paul L. Richards

The low lying energy levels of the ferric (Fe^{3+}) ion in compounds with a large axial crystalline field are described by the spin Hamiltonian $\mathcal{H} = \beta \underline{H}.\underline{g}.\underline{S} + D[S_z^2 - 1/3\ S\ (S+1)]$. The magnetic dipole transitions between these levels have been studied by the methods of far infrared Fourier transform spectroscopy in compounds with S = 3/2 and S = 5/2 for both positive and negative D (Fig. 1). This work on model compounds has been extended to some intact heme-proteins (Fig. 2). A computer program has been prepared to predict from the spin Hamiltonian the absorption

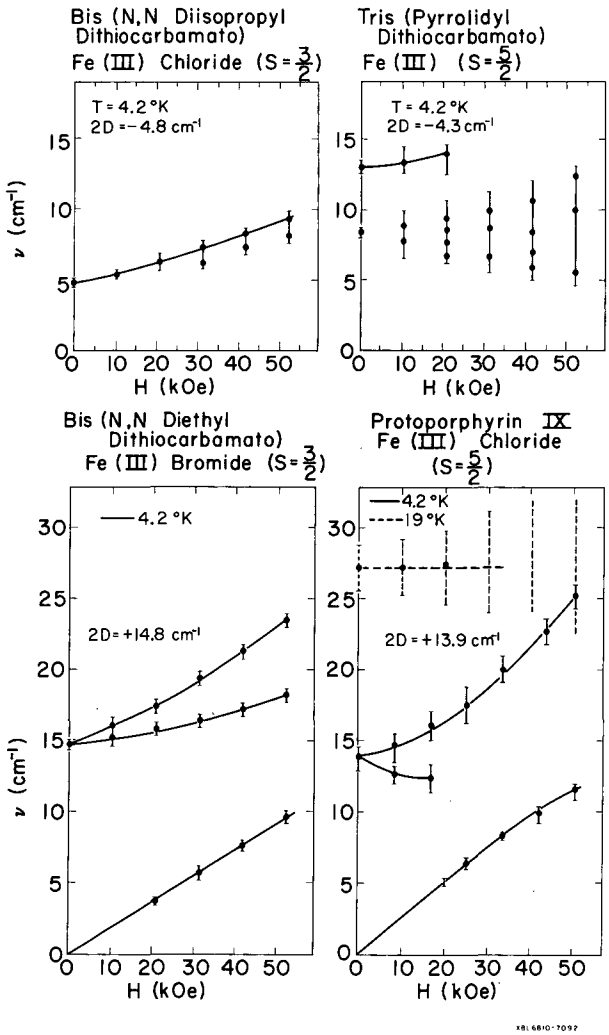

Fig. 1. Frequencies of far infrared absorption lines as a function of magnetic field for organic compounds with S = 3/2 and S = 5/2 and both positive and negative axial crystalline field.

coefficient for powder specimens as a function of frequency and magnetic field. It is planned to extend these measurements to a number of proteins containing high spin Fe^{2+} and Fe^{3+}.

Electric dipole absorption due to molecular vibrations is also seen in the far infrared. Sharp structure on this absorption is seen for some proteins which we hope to correlate to the conformation of the protein.

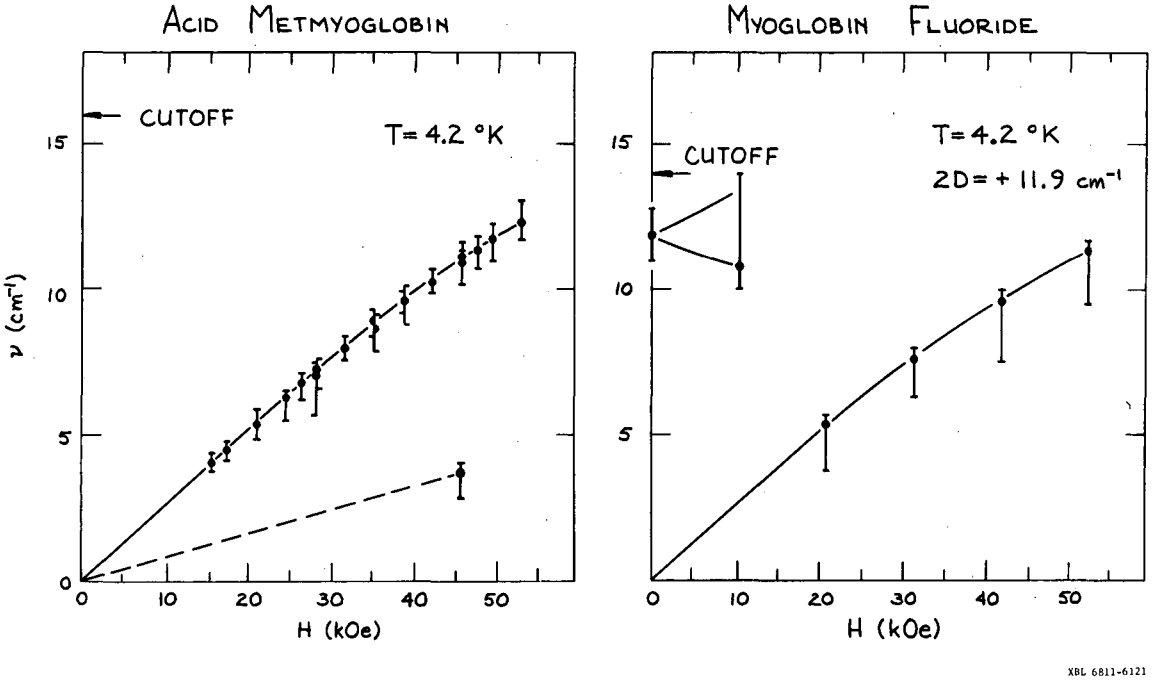

Fig. 2. Data for met-myoglobin and myoglobin fluoride similar to that shown in Fig. 1 for $S = 5/2$ and $D > 0$.

3. FAR INFRARED REGENERATIVE RECEIVER USING JOSEPHSON JUNCTION

Paul L. Richards and Steward A. Sterling

Experimental evidence has been found (Fig. 1) for the feedback-narrowed far infrared response of a point contact Josephson junction that is strongly coupled to a resonant cavity. The observed response shows high sensitivity (NEP $< 10^{-14}$ W/$\sqrt{\text{Hz}}$) and frequency selectivity ($Q \gtrsim 10^3$). It occurs at the frequency of a strongly coupled resonant cavity mode with low Q (~10) when the junction is biased to the high differential resistance point created by the cavity mode. The non-linear differential equation governing the detection mechanism has been set up and solved analytically by suitable approximations. The predicted line narrowing (Fig. 2) as a function of feedback parameter Γ is in good agreement with experiment. Further experiments are in progress to obtain a more useful receiver configuration.

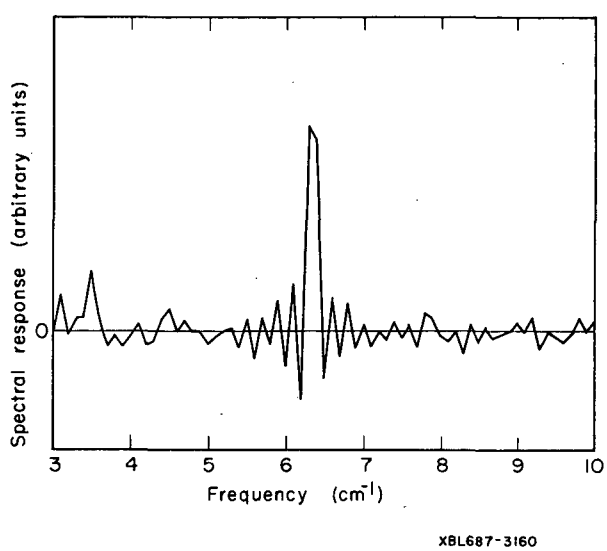

Fig. 1. Spectral response of regenerative receiver measured by using Fourier spectroscopy. Peak shape is proportional to $(\sin \nu)/\nu$ finite resolution of spectrometer.

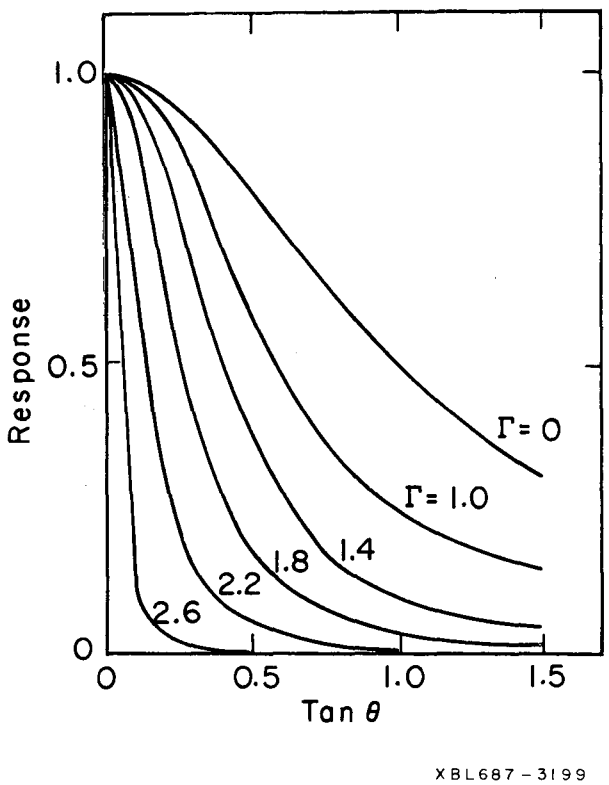

Fig. 2. Calculated dependence of response width on feedback parameter Γ.

4. GAP IMPURITY MODES IN ANTIFERROMAGNETS

Bernd Enders and Paul L. Richards

Two novel impurity modes lying within the spin wave energy gap of antiferromagnetic CoF_2 have been studied using Fourier spectroscopy. The strength of this mode is correlated with the concentration of oxygen in the COF_2. It is intended to interpret this observation by using the developing theory of impurity modes in one- and three-dimensional antiferromagnets.

5. FAR INFRARED CYCLOTRON RESONANCE IN Pb

Richard R. Joyce and Paul L. Richards

Apparatus is being constructed to measure Azbel-Kaner cyclotron resonance in Pb, using various laser lines in the 30-60 cm^{-1} frequency range. Our pulse laser has been converted to cw operation. A cryostat has been constructed that includes a large-bore 60 kOe superconducting magnet plus field modulation coils. It is anticipated that we will be able to observe changes in the effective mass and the relaxation time as the resonance frequency nears the phonon frequencies.

6. 1968 PUBLICATIONS

Paul L. Richards and Associates

Technical Journals

1. G. C. Brackett, P. L. Richards, A. M. Trozzolo, and H. H. Wickmann, Far Infrared Absorption of Fe^{3+} in Several Organic Compounds, Bull. Am. Phys. Soc. (Ser. II) 13, 436 (1968).
2. C. C. Grimes, P. L. Richards, and Sidney Shapiro, Josephson Effect Far-Infrared Detector, J. Appl. Phys. 39, 3905 (1968).
3. R. R. Joyce and P. L. Richards, Far Infrared Spectra of $Al_2O_3:Ti^{3+}$ and $Al_2O_3:V^{4+}$, Bull. Am. Phys. Soc. (Ser. II) 13, 435 (1968).
4. P. L. Richards, Analog of the ac Josephson Effect in Superfluid Helium, Bull. Am. Phys. Soc. (Ser. II) 13, 506 (1968).
5. P. L. Richards, Sidney Shapiro, and C. C. Grimes, Student Laboratory Demonstration of Flux Quantization and the Josephson Effect in Superconductors, Am. J. Phys. 36, 690 (1968).
6. S. A. Sterling and P. L. Richards, Far Infrared Response of Superconducting Point Contacts, Bull. Am. Phys. Soc. (Ser. II) 13, 476 (1968).

UCRL Reports

1. D. W. Faries, K. A. Gehring, P. L. Richards, and Y. R. Shen, Tunable Far Infrared Radiation Generated from the Difference Frequency Between Two Ruby Lasers, UCRL-18525, October 1968.
2. P. L. Richards and R. R. Joyce, Far-Infrared Spectra of Al_2O_3 Doped with Ti, V, and Cr, UCRL-18229, June 1968.
3. P. L. Richards and S. Sterling, Resonant Non-Linear Response of Point Contact Josephson Juncations, UCRL-18635, December 1968.

D. SUPERCONDUCTIVITY

1. FLUX JUMPING IN TYPE II SUPERCONDUCTORS*

Gene I. Rochlin

The size distribution of flux jumps in cylindrical specimens of Pb + 2 at. % In alloys has been measured as a function of magnetic field at 4.2°K for samples with varying surface preparation. The distribution was found to be of the form

$$N(\phi) = N(0) \exp(-\phi/\overline{\phi}),$$

where N is the number of jumps at a given flux value ϕ. The mean bundle size $\overline{\phi}$ was found to be of the order of 10^2 to 10^4 times the elemental flux quantum $\phi_0 \approx 2\times10^{-7}$ g-cm^2. By comparing the total flux count in the jumps with the area of the magnetization curve, the fraction of flux entering in these large bundles was also determined, and was found to have essentially the same magnetic field dependences as the mean bundle size. This indicates that the average number of bundles entering per unit time at a given field sweep rate is almost independent of field, while the number of fluxoids per bundle varies quite markedly.

Figure 1 illustrates the type of data obtained on a polished sample exhibiting surface superconductivity. The most interesting fracture is the occurrence of jumping in the surface superconductivity regime above H_{c_2}. That the behavior above H_{c_2} is determined by the surface is strikingly demonstrated by the behavior of the Ni-plated sample shown in Fig. 2. As the shape of our curves is independent of field sweep rate over the wide range available to us, these jumps appear to be quite distinct from the thermal runaway "catastrophic" jumps often observed, and should, therefore, probe directly the pinning forces in the sample.

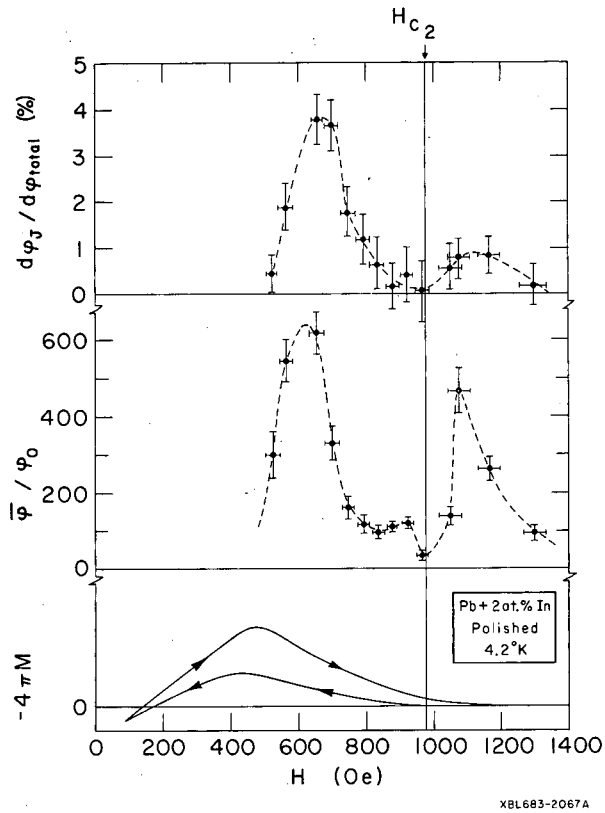

Fig. 1. The magnetization, M, mean number of fluxoids per bundle, $\phi/\overline{\phi}_0$, and the fraction of flux entering the sample via jumps, $d\phi_J/d\phi_T$, as a function of magnetic field for an unannealed sample exhibiting surface superconductivity.

*Abstracted from Phys. Rev. Letters 21, 691 (1968); UCRL-18262, May 1968.

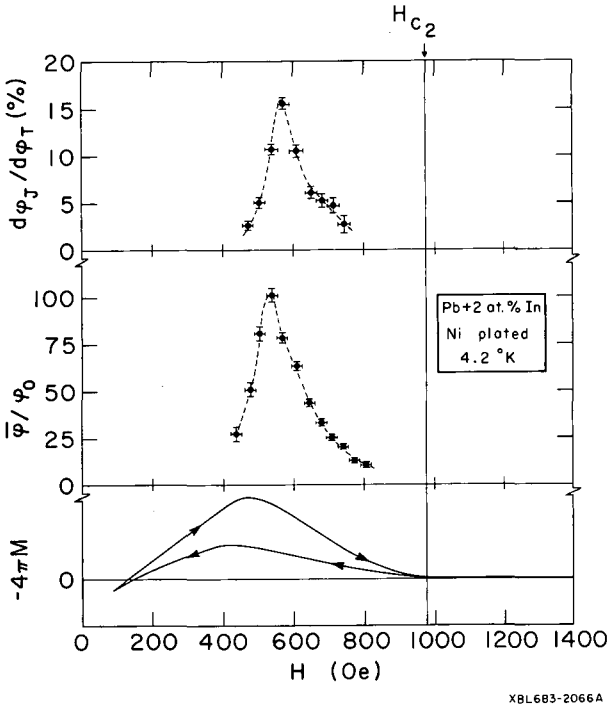

Fig. 2. M, $\bar{\phi}/\phi_0$, and $d\phi_J/d\phi_T$ when the sample has been plated with $\sim$ 1000 Å of Ni.

2. THE JOSEPHSON EFFECT IN GAPLESS SUPERCONDUCTORS

Michael Jack and Gene I. Rochlin

We have revamped a ^{3}He refrigeration dewar that is set up for "quenched" evaporation of thin films onto ^{4}He-cooled substrates at 4.2°K. This will allow us to deposit alloy films composed of metals that have little or no mutual solid solubility without aggregation. We intend to study systems with paramagnetic impurities such as Pb-Gd, as well as amorphous films of substances such as Pb or Bi. Preliminary data have been taken on ordinary Pb-I-Al junctions to check the system out, and we expect to obtain significant data in a few months.

3. MICROWAVE COUPLING TO TUNNEL JUNCTIONS

Gene I. Rochlin and James N. Sweet

Using a re-entrant coaxial cavity, we have been studying the effect of 4 kMHz radiation on both the Josephson effect and the quasiparticle tunneling current in thin film tunnel junctions. For our rather unique field coupling geometry there are apparently large discrepancies between our observations and the theoretical predictions extrapolated from other experiments. We are presently investigating this effect further to determine the precise reason why our geometry yields results so much at variance with the reported behavior of junctions in other geometries.

4. FLUCTUATIONS IN SUPERCONDUCTING MICROBRIDGES JUST BELOW T_c

Gene I. Rochlin

The power spectrum of fluctuation noise in thin film microbridges near T_c has been studied for thin aluminum bridges approximately 10 μ by 50 μ by 100 Å thick. The I-V characteristics show definite steplike structure as shown in Fig. 1. When biased on a step at constant current, there is a rapid switching between two or more discrete voltage levels; the symmetry of the switching can be varied by varying the drive current. The power level involved is very far below the nucleate boiling threshold for superfluid helium. Figure 2 shows the noise power spectrum of a typical switching pattern. The

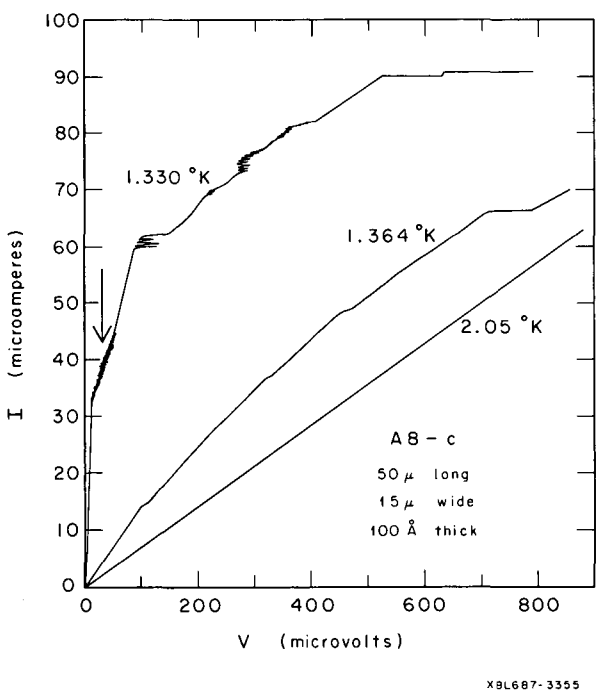

Fig. 1. I-V curve of a typical aluminum microbridge at several temperatures. The arrow indicates the point at which the noise power spectrum of Figs. 2 and 3 was taken.

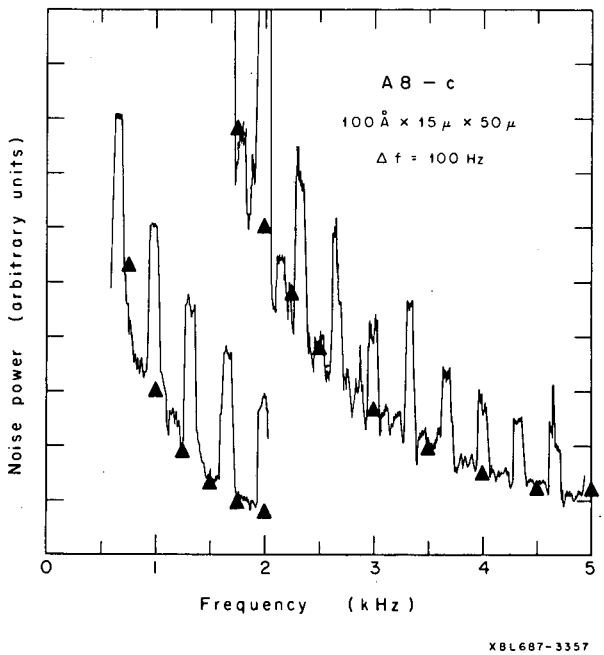

Fig. 2. The noise power spectrum of the e.c. aluminum microbridge of Fig. 1 at the point indicated by the arrow. The triangles are the best fit to an F^{-2} dependence for the smooth part of the spectrum.

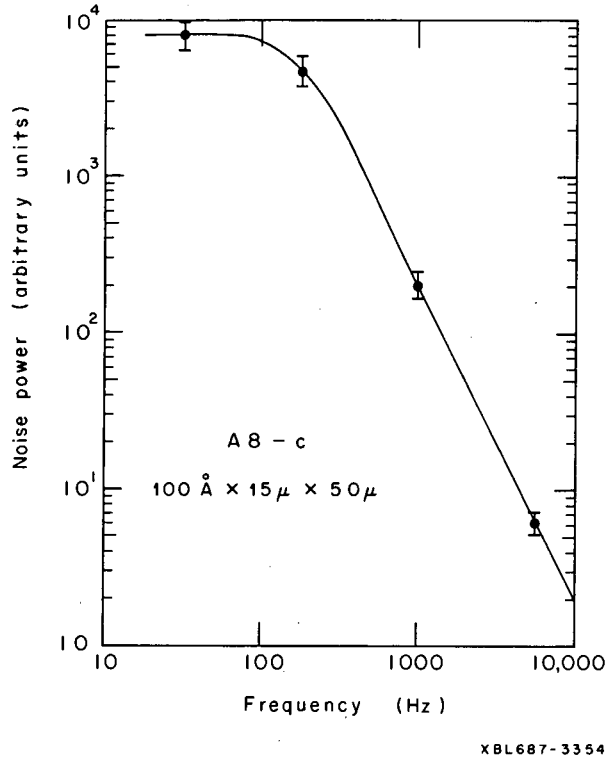

Fig. 3. The frequency dependence of the smooth part of the spectrum for the microbridge of Fig. 1 at the point indicated by the arrow. The curve is a plot of a Poisson spectrum $S_0(w) = 4\lambda/(\lambda^2 + w^2)$. Only a few typical data points are shown to illustrate errors. The fit is equally good at all other points checked.

spikes in the spectrum occur at all harmonics of 335 Hz up to at least the fiftieth at remarkably constant power per harmonic. We believe that the switching is usually triggered by external noise, as 120 Hz is a usual frequency for the spikes, but observations such as this at 335 Hz indicate that there may be an internal mechanism for the switching that tends to synchronize with external noise. The background or "smooth" part of the power spectrum has the characteristic shape of a semirandom telegraph signal, with a power spectrum

$$S_0(w) = \frac{4\lambda}{\lambda^2 + w^2} .$$

Figure 3 illustrates how well our data fit this formula. We have constructed a model by using a synchronized repetitive autocorrelation function with Poisson statistics and derived a theoretical spectrum of the form

$$S(w) = S_0(w)[(1 - a) + a \sum_{1a=\alpha}^{\alpha} F[\mu, (\mu + \frac{2\pi k}{\tau_0})]],$$

where τ_0 is the synchronization period and μ is the decay of the correlation between successive synchronization signals. There are three possible solutions for F that are physically reasonable, but μ is so long that the width of the spikes ($\sim 1/\mu$) generated by F is far less than the experimental resolution of our apparatus at present. In addition the shape of our I-V curves explains the steplike structure seen in the V vs. temperature plots at constant current, which are measured with these bridges to study fluctuation phenomena near the critical point (T_c).

5. WEAKLY COUPLED SUPERCONDUCTORS*

John Clarke

Studies have been made of the current-voltage characteristics at lead-copper-lead junctions at temperatures of 4.2°K and below. It has been shown that the junctions will sustain a supercurrent up to a certain critical value above which a voltage appears, rising smoothly from zero as the current is increased (Fig. 1). The critical current rises as the temperature is lowered, decreases exponentially with increasing thickness of copper, and increases with increase of the mean path of the copper. It has been demonstrated that the junctions behave phenomenologically as Josephson junctions. A new type of self-induced oscillation on the I-V characteristic has been discovered and investigated.

The effect of electromagnetic radiation of frequency v is to induce steady currents at voltages $V = (n/m)(hv/23)$, where m and n are integers (Fig. 2). These steps, unlike those observed with other types of junction, are true supercurrents. By comparing junctions of different materials we have shown that the frequency-voltage relation is independent of the superconductors used or the experimental conditions to 1 part in 10^8. This result has wide implications to fundamental constants, standards of emf, and quantum electrodynamics.

*Abstracted from UCRL-18159 and Phys. Rev. Letters 21, 1566 (1968).

6. RESEARCH PLANS FOR CALENDAR YEAR 1969

Gene I. Rochlin

The experiments on paramagnetic impurities, gapless superconductors, and the Josephson effect using the quenched evaporator will be continued. We also intend to investigate the phonon spectrum both in these cases and in the case of amorphous films using our newly developed all-dc technique for taking derivatives.

The problem of the coupling of microwave radiation to tunneling junctions, particularly with respect to the ac Josephson effect, will be studied further by varying the coupling and junction parameters. We shall also extend this study further to include the investigation of the film-bridge geometry which also shows an ac-Josephson-like effect, but where the coupling to external fields can be more easily varied.

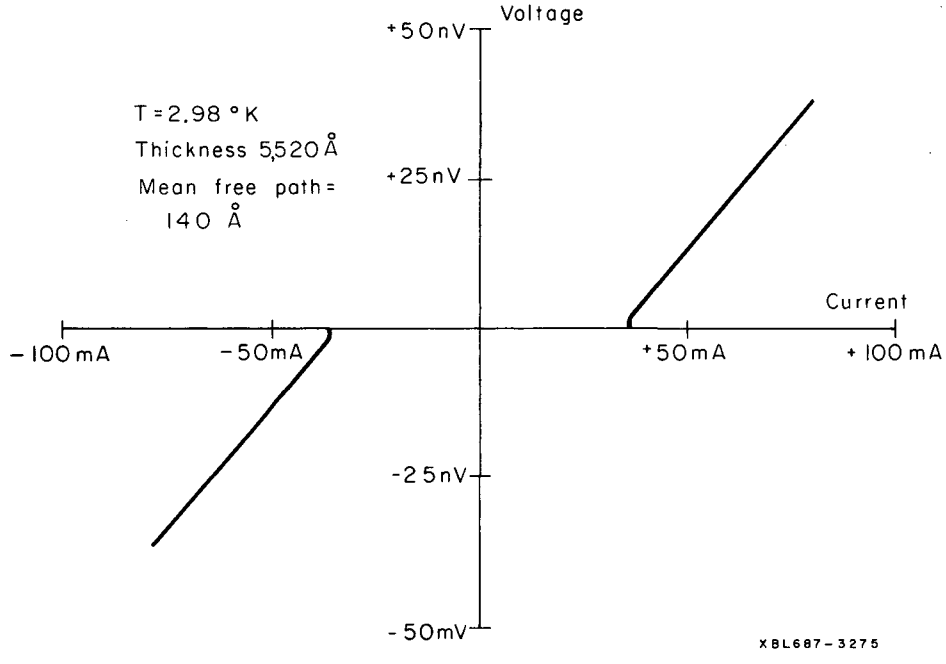

Fig. 1. The I-V characteristic of a typical SNS junction.

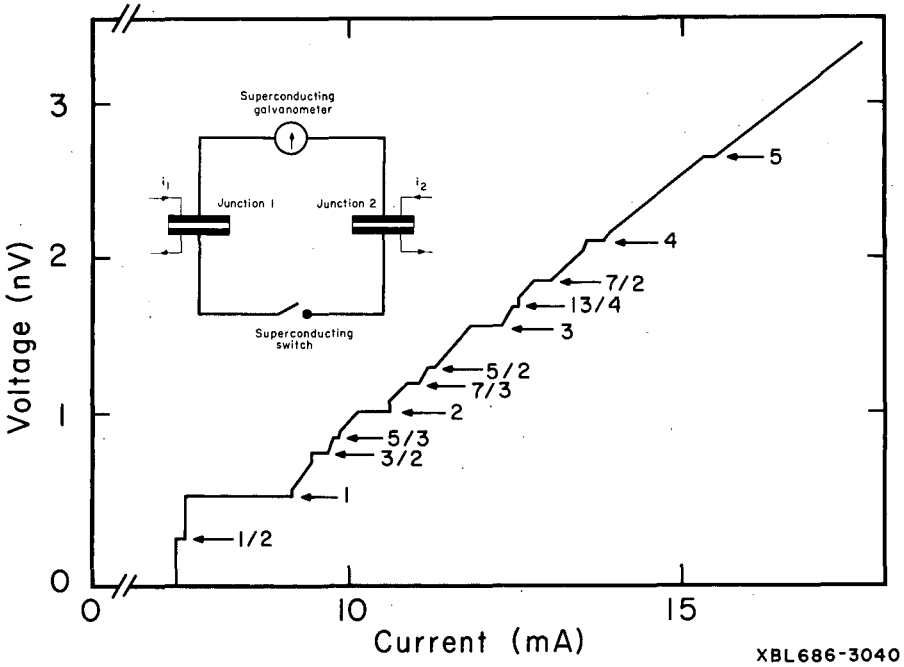

Fig. 2. The I-V characteristic of a lead-copper-lead junction at 4.2° K irradiated at a frequency of f_0 = 250 kHz. The numbers indicate the fractional harmonic equivalent using the Josephson frequency-voltage relation; e.g., 7/3 means $2_e v_0/h = (7/3)f_0$.

We expect to be able to continue our investigations into both the flux-jumping problem and the fluctuations in the thin-film microbridges.

Our all-dc method for taking I-V curve derivatives has been tested and proved effective. We intend to use this technique for doing a variety of studies on various configurations of tunnel junctions to study zero-bias anomalies, phonon spectra, etc. It is hoped that this technique will increase the resolution of second (d^2I/dv^2) derivatives sufficiently to enable us to study phonon spectra in weak-coupling superconductors in conjunction with the dilution refrigerator being constructed by Dr. T. Thorpe in this division.

A program to attempt to use the tunneling technique in investigating the properties of antiferromagnetic chromium is under way. Preliminary data have proved very encouraging, and a series of further investigations will be performed to analyze the observed structure and to identify its origin.

The studies of SNS sandwiches will be continued and amplified further to include systems where "N" is no longer a normal metal. It is believed that these junctions will prove to be a highly useful probe of the central material. A new theory of the harmonic and subharmonic structure of the steps induced by microwave fields is being developed.

In collaboration with Professor Y. R. Shen, an experiment is being performed to investigate the effect of an electric field on the coexistence curve and critical point of CO_2. Should these studies prove fruitful, we shall extend the work to the far more interesting cases of the liquid noble gases, such as Ar and He.

7. 1968 PUBLICATIONS

Gene I. Rochlin and Associates

Technical Journals

1. J. Clarke, The Magnetic Field Dependence of the Critical Current in a Self Field Limited Junction, in Proc. of the Conf. on Fluctuations in Superconductors, Asilomar, California (Stanford Research Inst., Menlo Park, California, 1968).
2. J. Clarke, The Proximity Effect Between Superconductors and Normal Metals, in Proc. of the Eleventh International Conference on

Low Temperature Physics, LT11 (to be published).
3. J. Clarke, An Experimental Comparison of the Josephson Frequency Voltage Relation in Different Superconductors, Phys. Rev. Letters 21, 1566 (1968).
4. C. Heiden and G. I. Rochlin, Flux Jump Size Distribution in Low-κ Type II Superconductors, Phys. Rev. Letters 21, 691 (1968).
5. G. I. Rochlin and C. Heiden, Size Distribution of Flux Bundles Entering or Leaving Type II Superconductors, Bull. Am. Phys. Soc. 13, 378 (1968).
6. G. I. Rochlin, Flux Jumping in Type II Superconductors, in Proc. of the Conf. on Fluctuations in Superconductors, Asilomar, California (Stanford Research Inst., Menlo Park, California, 1968).
7. G. I. Rochlin, "Noise" on Constant Current Steps in Aluminum Microbridges, in Proc. of the Conf. on Fluctuations in Superconductors, Asilomar, California (Stanford Research Inst., Menlo Park, California, 1968).
8. G. I. Rochlin, Noise Spectrum and Step Structure of Superconducting Microbridges at the Resistive Transition, in Proc. of the Eleventh International Conference on Low Temperature Physics, LT11 (to be published).

UCRL Reports

1. J. Clarke, Supercurrents in Lead-Copper-Lead Sandwiches, UCRL-18159, April 1968.

E. EXPERIMENTAL SOLID STATE PHYSICS AND QUANTUM ELECTRONICS

1. OPTICAL PROPERTIES OF SOLIDS

Ricardo Zucca and Y. Ron Shen

A spectrometer for the measurements of transmittive and reflective spectra by the wavelength modulation technique has been put into operation. The purpose is to obtain the derivative spectra rather than the ordinary spectra so as to get an improvement on the resolution of weak obscure structures. The advantage of this technique over other modulation techniques, e.g., electro-, piezo-, thermo-reflectance, etc., is that the sample is left untouched and consequently a simpler interpretation of the data is possible. The experimental difficulty lies in the fact that a background noise two orders of magnitude larger than the signal must be compensated through feedback.

During the past year the system has been assembled and tested. Several modifications have been made to the original design to improve the overall performance and reliability. The frequency range has also been extended to around 2000 Å. Finally, an optical dewar with temperature variable from 4°K to room temperature has been installed in the spectrometer.

Preliminary measurements have been made on a Ge sample as a test on the spectrometer. Figure 1 shows the ordinary reflectivity spectrum R(w) of Ge, and Fig. 2 shows the corresponding derivative reflectivity spectrum $\Delta R(w)/R(w)$ over the range 4000 to 2000 Å. The results prove to be fairly satisfactory. Note that some of the fine structures in the derivative spectrum cannot be resolved in the ordinary spectrum.

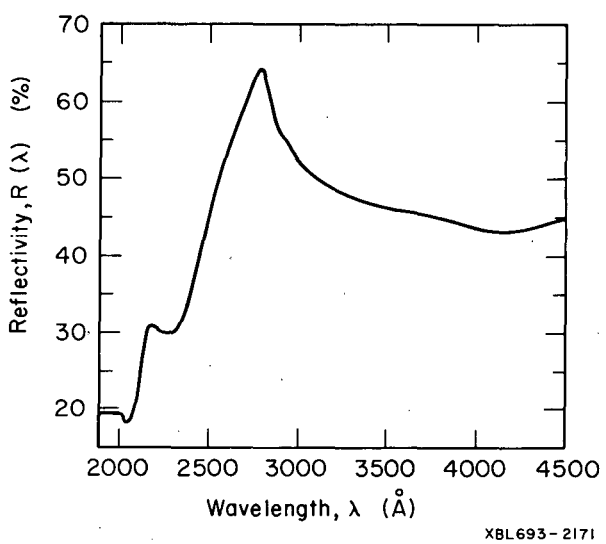

Fig. 1

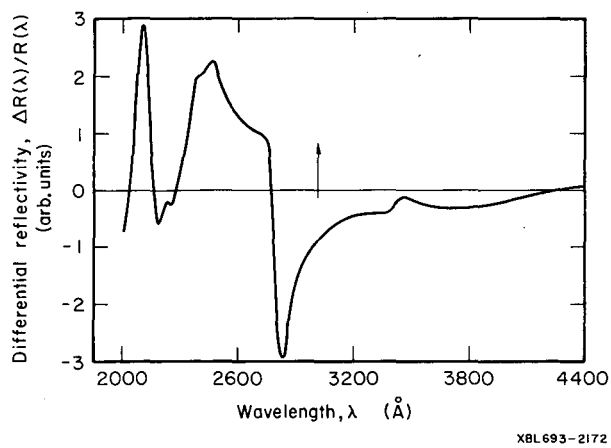

Fig. 2

2. SPONTANEOUS LIGHT SCATTERING

Hal Rosen, Folke Stenman, and Y. Ron Shen

The Raman spectrometer, consisting of a He-Ne laser, a double monochromater, and a photon counting detection unit has been set up, and has been used to investigate the Raman spectra of iodine complexes in solution. Frequency shift and intensity change of the Raman line corresponding to the I_2 stretching vibrational mode have been measured as a function of benzene concentration in the mixture of benzene and n-hexane. The frequency measurements are accurate to within 0.1 cm^{-1}. The results agree surprisingly well with the theoretical calculation (Fig. 1) based on a simple statistical model taking into account the charge transfer interaction between iodine and benzene. On the other hand, neither Benesi-Hildebrand's nor Ongel-Mulliken's model can explain our results satisfactorily. Using our statistical model we are able to deduce from the experimental results the value of the charge-transfer interaction potential between iodine and benzene, and also the average number of benzene molecules inter-

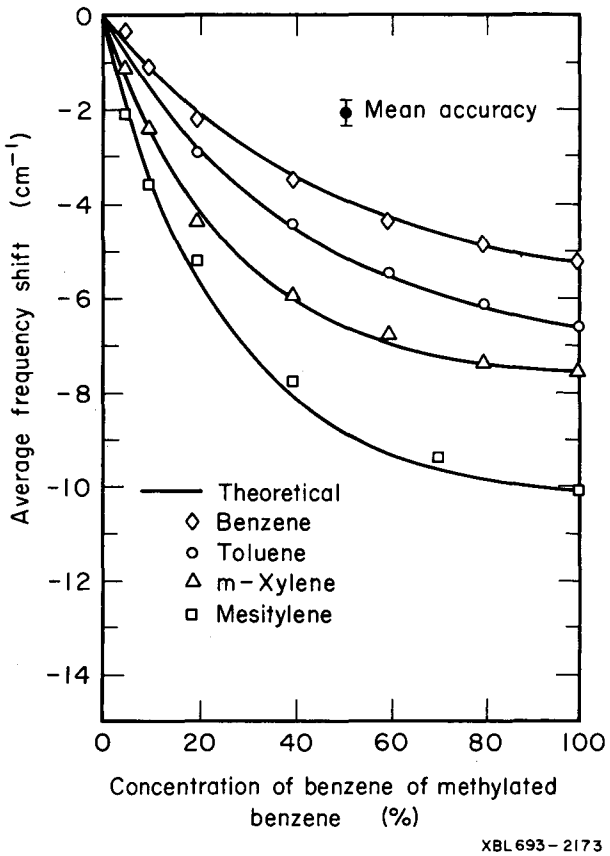

Fig. 1. Average frequency shift of the iodine stretching vibration as a function of the concentration of benzene (or methylated benzene) in the liquid mixture of benzene (or methylated benzene) and n-hexane.

acting simultaneously with each iodine molecule.

The success of our model led us to re-examine the existing optical absorption data for the I_2-benzene complexes. We found that our theory actually fits the data better than the Benesi-Hildebrand equation. The physical parameters derived from the optical data and from the Raman data agree to within 20%.

3. ULTRASHORT LIGHT PULSES

John Shelton and Y. Ron Shen

A mode-locked Nd-glass laser has been assembled and tested. The output consists of a series of equally spaced short pulses. From two-photon fluorescence measurements, the pulse duration is found to be $\sim 5 \times 10^{-12}$ sec as anticipated. The peak power of the pulses is about 1 GW.

The mode-locked laser has been used to study the third-harmonic generation from a dye solution, in particular the third-harmonic reflection from the dye near the critical angle of total reflection. A sharp increase in the signal at the critical angle has been observed in solution where the fundamental and the third harmonics are phase matched. However, the project will be terminated since we now realize that the research group in Naval Ordinance Laboratory is working on the same problem and is going to publish their results soon.

4. NONLINEAR OPTICS*

a. Theory

Y. Ron Shen

The permutation symmetry for generalized nonlinear susceptibilities of a medium is derived from the microscopic theory. It is shown that this permutation symmetry is essential for the existence of a time-averaged stored energy density or free energy for wave propagation in a nonlinear non-dissipative medium.

The steady state self-trapping of light in a medium is discussed from the thermodynamic point of view. The state of self-trapping corresponds to a minimum of the Gibb's energy of the system. Semi-quantitative features of self-trapping can be described readily with little calculation. Self-trapping for various nonlinear responses of the medium, with or without phase transition, is discussed. It is suggested that multiphoton transitions could be responsible for stable filaments. (This work was presented at the 1968 Gordon Conference on Nonlinear Optics.)

b. Experiments

Dillard Faries, Michael Loy, Roland Ribbota, and Y. Ron Shen

Far infrared radiation generated from the difference frequency between two temperature-tuned ruby lasers has been observed over the frequency range from 1.2 to 8.1 cm^{-1}. Lithium niobate and quartz were used as mixing crystals. The conversion efficiency was measured as a function of angle around the phase matched direction. The expected spectral content and frequency of the far infrared radiation has been verified, using a far infrared Fabry-Perot interferometer. (This project is accomplished in cooperation with K. Garing and P. L. Richards.)

We have performed the first accurate measurements on the duration of light pulses from the small-scale self-focusing region (generally believed to be a small-scale self-trapped filament). Consistent results were obtained from two independent ways of measuring. In toluene the pulse duration was found to be 0.05-0.2 nsec for an incoming laser power not much higher than the threshold for self-focusing. The diameter of the "filament" and the energy content in the pulse were obtained from simultaneous measurements to be 10 ± 2 μ and ~ 30 ergs respectively. Therefore, the peak intensity in the "filament" should be of the order of 30 GW/cm^2. This leads to suspicion of the existence of the self-trapped filaments, since a filament of such high intensity would not last over 1 mm before its power is depleted by various nonlinear processes.

The dynamics of self-focusing and the existence of self-trapped filaments were then carefully investigated. It was found that under our experimental conditions with a single mode laser, the self-trapped filaments do not exist. What was believed to be a filament is actually composed of a continuous series of self-focusing spots arising from the intensity variation with time of the incoming laser pulse. Correlation between self-focusing and stimulated Raman and Brillouin scattering has also been studied. In toluene, stimulated Brillouin scattering is seen before the beam is self-focused to the final 10 μ size, but stimulated Raman scattering appears almost concurrently as the self-focused beam reaches its final size. No spectral broadening on the spectrum of the self-focused beam has been observed.

*Research supported by the Office of Naval Research.

5. RESEARCH PLANS FOR CALENDAR YEAR 1969

Y. Ron Shen

The differential reflectometer will be used to study the derivative spectra of many semiconductors at various temperatures, in particular, the III-V and the II-VI compounds. Effort will be concentrated on the fine structures in the spectra. The results will be used for modification of the existing band structures for these compounds. Exciton states in the semiconductors can hopefully be identified.

Work on the Raman spectra of I_2-complexes will soon be finished. The Raman spectrometer will then be used to study liquid crystals and magnetic crystals. Information about molecular correlation in liquid crystals and about spin-phonon coupling in magnetic crystals can be provided by the Raman scattering results. An optical dewar with a superconducting magnet is being built for these measurements.

Lifetime measurements using ultra-short pulses will be continued with some modifications in techniques. Hopefully, the time resolution can be improved so that lifetimes less than 10^{-11} sec of either optical or vibrational excited states can be measured. Coherent transient effects may also be encountered.

Theoretical calculations on far infrared generation through optical beating in nonlinear crystals and on the general problem of self-focusing of light will be attempted. Experiments on far infrared generation will be continued, with the aim to extend the frequency of the far infrared output to 300 cm^{-1} or more. Self-focusing and self-trapping under various different conditions will be investigated. It is hopeful that the great mystery of the appearance of "self trapped filaments" can be solved before long. Other nonlinear optical experiments such as stimulated Raman and Brillouin scattering, spectral broadening, etc. will also be conducted.

6. 1968 PUBLICATIONS

Y. Ron Shen and Associates

Technical Journals

1. Y. R. Shen, Permutation Symmetry of Nonlinear Susceptibilities and Energy Relation, Phys. Rev. 167, 818 (1968).
2. Y. R. Shen, Optical Phenomena in Magnetic Materials, Magnetic Materials Digest, 1968, p. 244.
3. Y. R. Shen, H. Rosen, and F. Stenman, Frequency Shift of the Stretching Vibration of I_2 in Liquid Mixtures, Chem. Phys. Letters 1, 671 (1968).

UCRL Reports

1. D. W. Faries, K. A. Gehring, P. L. Richards, and Y. R. Shen, Tunable Far Infrared Radiation Generated from the Difference Frequency Between Two Ruby Lasers, UCRL-18525, October 1968.

F. NUCLEAR SPIN INTERACTIONS

1. NUCLEAR SPIN RELAXATION AND DOUBLE RESONANCE IN KH_2PO_4

Dietmar Stehlik and Per-Eric Nordahl

After improvement of the proton (or ^{31}P) signal detection system (shortening the recovery time to 5-10 μsec, new probe arrangement, stabilization, etc.) and after installation of a variable temperature unit, data were gathered concerning the proton relaxation following adiabatic demagnetization in the rotating frame (ADRF). The double resonance of rare nuclei is being carried out, including temperature and orientation dependence.

Relaxation Phenomena

Nuclear relaxation of KDP (short for KH_2PO_4) has become of great interest only recently. Usually nuclear spin diffusion to paramagnetic impurities is the dominating mechanisms for relaxation. In high purity crystals, high field proton relaxation has been reported due to the modulation of the dipole-dipole coupling by intraband jumping. This leads to an estimate of the correlation time in the ferroelectric phase. We find a similar effect for the proton relaxation after ADRF in less pure samples. However, we also find an enormous increase of this relaxation rate (more than an order of magnitude) in the vicinity of room temperature in a rather narrow temperature range. Moreover the signal decay in this temperature range is no longer exponential, but is made up of a superposition of two exponential decays. There exists no detectable orientation dependence for this effect. More data at room temperature and above are required to explain this anomalous relaxation effect.

Double Nuclear Resonance Detection in KH_2PO_4

We are able to sweep the search frequency from 250 kHz to 3 MHz in search of other nuclear moment isotopes in KDP. This range covers all nuclei of interest (^{39}K, ^{40}K, ^{41}K, ^{17}O, ^{2}D). The already known resonances of ^{39}K are used for crystal orientation, calibration of the search field, and check of the sensitivity. The double resonance sensitivity can be increased significantly by going from room temperature to about -30°. Here the effective time for nuclear spin irradiation, equal to the relaxation time T_1 after ADRF and proportional to the sensitivity, is increased by almost an order of magnitude. Together with a signal-to-noise ratio of about 50, quite favorable conditions are realized for nuclear double resonance. Preliminary data show a great number of double resonances. A detailed study of the orientation dependence by using the more informative audio saturation technique is underway to identify these resonances.

2. LEVEL-CROSSING DETECTION OF NQR TRANSITIONS

Jackson C. Koo

The nuclear electric quadrupole spectrum of ^{14}N in 4-chloro-3-nitrobenzenesulfonic acid potassium salt has been observed by means of the level-crossing detection method, formerly described in UCRL-18043. Values of $e^2qQ/\hbar = 1010 \pm 5$ kHz, the asymmetry parameter $\eta = 0.287 \pm 0.003$, and the spin lattice relaxation time $T_1 = 187$ sec were deduced from the experiment at 77°K. It is believed that this was the first time the NQR of ^{14}N of a NO_2 bond in an organic compound has been observed. It is also the first NQR reported of ^{14}N with the smallest $e^2qQ/\hbar$ value.

In order to detect the NQR spectrum of the naturally abundant deuterium, a multiple level-crossing detection method has been successfully developed by simply repeating the level crossing process many times before the proton signal is detected. The NQR spectrum of deuterium in a slightly enriched sample of tetra-chlorobenzene (about five times natural abundance) has been observed. Values of $e^2qQ/\hbar = 179.3 \pm 0.5$ kHz and the asymmetry parameter $\eta = 0.078 \pm 0.003$ were deduced from the experiment at 77°K.

A number of ways to further improve the above method, in order to detect the NQR of deuterium in a naturally abundant sample, have been considered. Marginal signals from naturally abundant deuterium have recently been detected.

3. EXCITON-PRODUCED NUCLEAR POLARIZATION

Dietmar Stehlik and Michael Schwab

It has been reported[1-3] that optically excited paramagnetic triplet excitons[3] in anthracene are capable of shortening the proton spin-lattice relaxation time (T_1) and

inducing a non-thermal proton polarization. In that the observed T_1 in anthracene and other pure molecular crystals are long (greater than an hour) there is considerable difficulty in gathering a significant amount of data in a reasonably short time. By taking advantage of a scheme of nuclear double resonance developed in our laboratory, [4] we are able to study these exciton effects in a sample of paradichlorobenzene. The intent of the study is to understand the nature of the polarization process and make use of the polarization effect in further experiments.

Paradichlorobenzene was chosen because of (1) the presence of an abundant proton spin system suitable for polarization by optically excited excitons, (2) the presence of an abundant ^{35}Cl spin system which can be used to monitor the proton spin polarization, (3) the availability of optical data on paradichlorobenzene concerning the first excited singlet and triplet exciton states, and (4) the availability of clean material out of which single crystals can be grown.

Excitons are excited by ultraviolet light available from a filtered mercury vapor arc. A change in the zero-field T_1 of protons has been observed in the ultraviolet-irradiated crystal at 77°K. The main factors causing a nuclear polarization are the selective electron polarization due to the optical excitation mechanisms of the triplet excitons and the electron-nuclear interactions. Experiments are under way to observe T_1 and the exciton-induced polarization as a function of external field, crystal orientation, exciton density, and impurity doping.

Impurity doping seems to be an important effect, as the induced proton polarization is strongly dependent on the number of exciton traps present. [3] In tetracene-doped anthracene crystals, polarization enhancement as large as -3700 (in the earth's magnetic field) have been reported. As the induced polarization should be proportional to the number of excitons present (for low exciton concentrations), an increase in polarization can be obtained by using a more efficient lamp or a laser to pump the exciton states. This should produce large polarizations, and conceivably the pumped sample can be used as a polarized target for high energy experiments, as a means to study the magnetic resonance properties of an essentially aligned nuclear system, and as a means to achieve a more sensitive nuclear double-resonance experiment.

1. G. Maier, M. Hasberlen, H. C. Wolf, and K. H. Hauser, Phys. Rev. Letters 25A, 384 (1967).
2. P. R. Moran and W. M. Yen, Phys. Rev. Letters 21, 70 (1968).
3. G. Maier and H. C. Wolf, Z. Naturforsch. 23a, 1068 (1968).
4. M. Schwab and E. L. Hahn (to be published).

4. ELECTRON PARAMAGNETIC RESONANCE STUDIES OF COHERENT OPTICAL TRANSITIONS IN RUBY

Lance Riley

This reports a summary of a thesis completed on the interaction of a passive ruby sample with intense coherent radiation from a Q-switched ruby laser.

Using epr monitoring techniques at X-band, optical pumping efficiencies at fixed laser temperature are investigated for sample temperatures in the range 60-120°K. Two ground state transitions, the $|+\overline{3}/2\rangle \leftrightarrow |-\overline{1}/2\rangle$ and the $|+\overline{3}/2 \leftrightarrow |+\overline{1}/2\rangle$ were studied. As the sample temperature is varied, the sample absorption frequency shifts relative to the laser emission frequency by many optical line widths. During the course of a complete temperature sweep the various allowed optical transitions between $^4A_2$ and $\overline{E}(^2E)$ sublevels compete with or reinforce each other as regards their effect on altering equilibrium values of $^4A_2$ Boltzmann population differences. A mathematical model of the optical pumping process based on rate equations, microwave circuit theory, and theoretical expressions for temperature-dependent frequency shifts and line width broadening is used to successfully interpret the results of these thermal tuning experiments. Predictions of rate equations concerning hole burning in inhomogeneously broadened lines are examined. Absolute measurements of changes in $^4A_2$ spin level populations are consistent with the hypothesis of hole burning. Finally, the model is critically examined and suggestions for a more accurate analysis put forth.

Optical pumping experiments are also carried out with the sample at 4.2°K. At this temperature the slow rate of incoherent dephasing, imposed by long optical lifetimes T_2, requires that the problem be analyzed in terms of the density matrix rather than by rate equations. The problem of an atom at a general position within an inhomogeneously broadened line which is subject to a resonant laser pulse of arbitrary time envelope is considered. A mathematical transformation leads to a second-order differential equation with time-varying coefficients. Perturbation solutions for atoms both very near and very far from resonance are derived, and are shown to converge to closed-form analytic expressions in the case

of a 2π hyperbolic secant pulse. An exponentially growing or decaying pulse yields an exact solution in terms of Bessel functions.

Results of experiments designed to verify the predictions of the foregoing analysis are presented. The data indicate that either the density matrix or rate equations provide an adequate description of the experiments. This ambiguity is shown to originate in the ronuniform transverse intensity distribution of the laser beam; the process of averaging over regions of different intensity washes out the characteristic features of coherent pumping. A Fortran computer program is presented that is capable of solving the density matrix equation for arbitrary pulses. Predictions regarding hole burning by pulses of various shapes are presented, and the possibility of using inhomogeneously broadened resonant systems as envelope detectors for very fast pulses is discussed.

---

1. L. Riley, Ph. D. Thesis, UCRL-18395, University of California, Berkeley, August 1968.

5. ELECTRON CYCLOTRON ECHOES IN PLASMAS

John Shaner

An apparatus for observing transient microwave response of precessing electron gyromagnetic and gyroelectric systems is completed, capable of generating one or several 10-nanosecond 10-watt x-band pulses. This apparatus is suitable for studying collision processes in gaseous plasmas by observing cyclotron echoes. During the initial tests 10^{-6} watt cyclotron echoes from a weakly ionized argon afterglow were measured. Efforts are now under way to enhance the receiver sensitivity to its bandwidth-limited value of 10^{-11} watt, and to reduce timing jitter to less than 10^{-9} sec.

When these technological advances have been accomplished, the apparatus will be used to search for cyclotron echoes in weakly ionized Cs vapor and to investigate the possibility of electron-cyclotron Cs-hyperfine double resonance effects. Theoretical calculations have indicated that fairly strong echoes should be observed in such a system.

6. NMR STUDIES OF THE SUPERCONDUCTING SURFACE STATE IN ALUMINUM

Robert Macklin

In contrast to work prior to 1968 which involved extensive mechanical design and construction to fabricate a ^{3}He apparatus suitable for NMR experiments at temperatures below 1°K, research during the past year has centered around improving and developing electronic apparatus to better observe NMR signals from an aluminum sample.

After a brief series of experiments observing NMR signals in doped water (constant polarizing field, pulsed polarizing field, spin echoes), a sample of 99.9% pure powdered aluminum (paint pigment) was obtained from IMRD. The first liquid ^{4}He was transferred and attempts to see free precession signals from the aluminum were begun. After the first signals were observed some brief and unsuccessful attempts were made to improve damping of the transmitter pulse and receiver recovery time. A slightly modified version of the Arenberg video-amplifier/detector was constructed to overcome the difficulty of envelope detecting an rf signal which has appreciable amplitude modulation during one cycle of the carrier, a problem which arises when doing low frequency (~ 1 MHz) NMR where the time constant associated with recovery of the receiver from saturation is approximately 5 μsec. The Arenberg circuit is partially effective in that it does act as a full wave detector; however, it also saturates at rather low input levels, introducing distortion. An old "boxcar" integrator was rehabilitated, checked for linearity, and used for sampling the nuclear signal and allowing it to be displayed on a chart recorder. Modifications were made in the receiver with the intent of reducing recovery time, but little improvement was noted.

At this point a zero-field audio absorption experiment was run on aluminum powder sample at ~2.5°K. Very recently the first signals from a layer of aluminum on Mylar film base has been observed. The dipolar absorption spectrum in the powder sample was consistent with the results of McLaughlin and Hahn for normal state aluminum, and it was noted that this sample is not as pure as theirs.

Experimental work in the immediate future will center around applying previously constructed equipment to physical problems, both to verify past experiments and extend the techniques to new systems.

Initial work will be directed toward verification of the results of McLaughlin and Hahn on three existing samples of powdered aluminum. The full low temperature capabilities of the cryogenic apparatus will be activated with the addition of ^{3}He to the system and assembly of existing temperature-measurement equipment. The system will then be used to conduct studies of cross relaxation between ^{27}Al nuclei in superconducting aluminum and other nuclei which are not superconducting. Depending on the sensitivity of the apparatus, a sample of aluminized Mylar film is to be used to investigate cross relaxation between ^{27}Al nuclei and the protons in the Mylar under the very desirable theoretical conditions of simple geometry, physical separation of the spin systems, but good interaction because of the intimate contact of the aluminum film with the Mylar surface. Irrespective of whether the sensitivity of the apparatus is sufficient for this sample, a sample of powdered aluminum containing dissolved Cu impurity atoms will be investigated.

7. 1968 PUBLICATIONS

Erwin Hahn and Associates

Technical Journal

1. R. Slusher and E. L. Hahn, Sensitive Detection of Nuclear Quadrupole Interactions in Solids, Phys. Rev. 166, 326 (1968).

UCRL Reports

1. L. Riley, Electron Paramagnetic Resonance Studies of Coherent Optical Transition (Ph. D. Thesis), UCRL-18395, University of California, Berkeley, September 1968.
2. M. Schwab, Nuclear Magnetic and Nuclear Quadrupole Double Resonance in Solids (Ph. D. Thesis), UCRL-18278, University of California, Berkeley, July 1968.

Appendices

IMRD STAFF FOR 1968

CHEMISTRY

Principal Investigator	Postdoctoral Fellows and Other Scientists	Graduate Students
Leo Brewer	D. Green C. Meyer L. Phillips G. Rosenblatt J. Smith	W. Callins C. Chang S. Chang P. Cunningham D. Green H. Johansen W. Keller B. King J. Roberts D. Solan J. Wang P. Wengert
George Jura		T. Chen J. Przybylinski C. Wu A. Yee
Ronald Herm		L. Gundel S. Lin L. Loh C. Mims D. Parrish
William Jolly	J. Campbell M. Savet P. Kuznesof R. Tsina	R. Dreyfuss P. Finn D. Hendrickson S. Lipp M. Mendelsohn R. Patton L. Prizant K. Strom F. Wang J. Webster
Charles Harris	E. Eletr	M. Buckley B. Holian R. Millikan R. Panos M. Silverman P. Voitoff
Robert Connick	G. Johansson K. Kustin J. Vriesenga C. Merideth	H. Charles W. Earl R. Lee J. Neely

Principal Investigator	Postdoctoral Fellows and Other Scientists	Graduate Students
Rollie J. Myers	A. Falick	W. Batchelder J. Chang J. Feiffer T. Hynes A. Jindo P. McKinney C. Pao J. Tevebaugh A. Wilkerson
Norman Phillips	J. Hoffer C. Waterfield	M. Conway J. Hoffer G. Schwartz B. Triplett S. Wang
Charles W. Tobias	D. Landolt	R. Acosta R. Alkire K. Beach J. Jorne K. Kinoshita K. Kojima U. Landau J. Selman
Bruce Mahan	E. Gislason R. Lambert	M. Cheng M. Chiang R. Horton M. Mosesman C. Tsao A. Werner
Rolf Muller	H. Gerischer R. Steiger	C. Churchman R. Gupta R. Turney
Harold Johnston	E. Marti	C. Crews P. Dow S. Gabelnick A. Harker M. Moran E. Morris T. Paukert S. Schwartz J. Van Den Bogaerde C. Wu
John Newman		L. Hsueh V. Marathe K. Nisancioglu W. Parrish P. Sih B. Starr K. Tan

Principal Investigator	Postdoctoral Fellows and Other Scientists	Graduate Students
Gabor Somorjai	J. Morabito A. Morgan	J. Davy H. Farrell T. French R. Goodman R. Hempton D. Howlett C. Lou F. Szalkowski W. Szeto L. West
Otto Redlich		I. Edelweiss V. Ngo
	NUCLEAR ENGINEERING	
Donald Olander	W. Siekhaus	J. Finucane R. Jones V. Kruger G. Moore R. Olstad R. Omberg J. Schofill
	PHYSICS	
Erwin Hahn	M. Schwab D. Stehlik	R. Fisher J. Koo R. Macklin S. McCall T. Pierce L. Riley M. Schwab J. Shaner
Marvin Cohen	C. Fong T. Thorp	P. Allen R. Cahn R. Ramirez Y. Tung J. Walter
Alan Portis	J. Aubrun	M. Bancroft B. Chornik R. Estrella W. Holzer E. Katz E. Shaw J. Siebert
Paul Richards	K. Gehring	G. Brackett J. Cosier B. Enders R. Joyce J. Paterson S. Sterling K. Yang
Y. Ron Shen	N. Amer R. Ribotta F. Stenman	I. Ku M. Loy H. Rosen J. Shelton R. Zucca

Principal Investigator	Postdoctoral Fellows and Other Scientists	Graduate Students
Gene Rochlin	J. Clarke	P. Hansma M. Jack G. Shen Y. Song J. Sweet
	METALLURGY	
John Dorn	M. Victoria	M. Abo-El-Fotoh K. Amin J. Bird C. Dharan L. Jacobson D. Klahn S. Lau C. Liu F. Mohamed R. Niccolls T. Stefansky C. Syn
Leo Brewer Earl Parker Victor Zackay	M. Pickus	R. Goolsby P. Guest L. Hartsough R. Jones J. Roberts M. Suenaga
Earl Parker		S. Ambekar C. Bruggemann R. Goolsby P. Guest R. Jones P. Key W. Ludemann R. McCoy F. Padilla D. Porter M. Raghavan
Gareth Thomas	W. Bell E. Bulter S. Ranganathan H. Warlimont	W. Bell I. Cheng S. Das L. DeJonghe G. Geiken D. Huang M. Kodera R. Livak P. Mangonon P. Okamoto P. Rao T. Tan

Principal Investigator	Postdoctoral Fellows and Other Scientists	Graduate Students
Jack Washburn	B. Escaig H. Tong	T. Astrup V. Kannan T. Kosel J. Lira-Olivares Y. Miura A. Nes K. Stolt J. Tartour T. Trebert G. Vellaikal M. Yokota
Ralph Hultgren	P. Desai M. Glesier K. Kelley G. Somayajulv	D. Hawkins H. Yoon
Victor Zackay	M. Merz W. Gerberich	D. Bhandarkar J. Challande G. Chanani Y. Chung M. Collver C. Dokko J. Dunning D. Fahr J. Hall P. Hemmings Y. Katz D. Klahn R. McCoy E. Page
Marshal Merriam Robert Hammond	E. Nembach	G. Geiken
Joseph Pask	R. Langston T. Sugita	I. Aksay M. Appel J. Brennan D. Cropper R. Davis R. Edwards C. Hoge A. Lacy R. Schweinberg
Alan Searcy	O. Herstad R. Mar D. Meschi	J. Austin R. Coyle J. Dudash D. Feather R. Leonard R. Mar H. Skinner C. Washburn

Principal Investigators	Postdoctoral Fellows and Other Scientists	Graduate Students
Richard Fulrath		R. Atkin C. Hoge D. Lee J. Masaryk M. Moyles Y. Nivas J. Playter G. Pryor B. Semans J. Shackelford M. Stett

DEGREES AWARDED

Ph. D. Degrees

1. R. Alkire, Reaction Distribution in a Dissolving Porous Anode (UCRL-18425, September 1968).
2. M. Appel, Interdiffusion in NiO, CaO and MgO Single Crystals (UCRL-18258, June 1968).
3. M. Bancroft, Nuclear Relaxation of Cu^{63} in Ni-Cu (UCRL-18461, September 1968).
4. W. L. Bell, Anomalous Absorption of Electrons (UCRL-18158, May 1968).
5. P. Cunningham, Measurement of Lifetimes by the Phase-Shift Method. I. Radiative Lifetimes of Some Excited Atomic States. II. Lifetimes of Some v' Regions of the $B^3\Pi_{0+u}$ State of I_2 (UCRL-18419, November 1968).
6. C. K. H. Dharan, The Dynamic Behavior of Aluminum at High Strain Rates (UCRL-18549, October 1968).
7. C. Y. Fong, Empirical Pseudopotential Method for Electronic Band Structure Calculations in Insulators (UCRL-18356, August 1968).
8. D. Green, Molecular Beam Studies of Scandium Monofluoride. I., UCRL-17961; Arc Spectrum of Magnesium Oxide, II., UCRL-17878 Rev. (January 1968).
9. J. K. Hoffer, The Thermodynamic Properties of He^4 Near the Melting Line (UCRL-18409, August 1968).
10. W. C. Holzer, Standing Spin Wave Resonance in Magnetic Thin Films (UCRL-18311, June 1968).
11. L. Hsueh, Diffusion and Migration in Electrochemical Systems (UCRL-18597, December 1968).
12. L. Jacobson, Solute Atom Locking of Dislocation (UCRL-18310, August 1968).
13. B. King, Optical Absorption Spectra of Matrix-Isolated Copper, Silver and Gold (UCRL-18618, November 1968).
14. P. L. Manganon, Strengthening the Phase Transformation in 304 Stainless Steel (UCRL-18230, August 1968).
15. R. W. Mar, Sublimation Kinetics of Zinc Single Crystals (UCRL-18257, June 1968).
16. R. Millikan, Part I. The Microwave Spectrum and Ring Puckering Potential of 1,1-Difluorocyclopentane. Part II. Computers as Interactive Devices in Chemical Experiments (UCRL-18621, November 1968).
17. M. Mosesman, Mass Spectrometric Study of Photoionized Gases (UCRL-18431, September 1968).
18. L. Riley, Electron Paramagnetic Resonance Studies of Coherent Optical Transition (UCRL-18395, September 1968).
19. M. Schwab, Nuclear Magnetic and Nuclear Quadrupole Double Resonance in Solids (UCRL-18278, July 1968).
20. S. E. Schwartz, Kinetics of Nitrogen Dioxide Fluorescence (UCRL-18431, September 1968).
21. J. F. Siebert, Electron Resonance Studies of Critical Fluctuation in Antiferromagnets (UCRL-18119, March 1968).
22. T. Stefansky, Strain Energy Interaction Between Solute Atoms and Dislocations (UCRL-18332, July 1968).
23. J. L. Strudel, Precipitation of Vacancies in Quenched Aluminum (UCRL-18407, September 1968).
24. G. Vellaikal, Dislocation Motion, Multiplication, and Interactions in the Preyield Region of Copper Polycrystals (UCRL-18435, November 1968).
25. M. Yokota, Hardening and Recovery of Quenched Gold (UCRL-17785, August 1968).

M. S. Degrees

1. K. N. Beach, A Laser Interferometer for Mass Transfer Studies (UCRL-18037, February 1968).
2. J. Challande, Corrosion Resistance of Metastable Austenitic Steels (UCRL-18475, September 1968).
3. Y. Chung, The Effect of Strain Aging on the Fracture Toughness of Steel (UCRL-18116, June 1968).
4. S. K. Das, Structure and Mechanical Properties of Fe-Ni-Co-C Steels (UCRL-18652, December 1968).
5. J. J. Dudash, The Melting Point, Vapor Pressure and Heat of Vaporization of Stannous Fluoride (UCRL-18164, May 1968).
6. I. Edelweiss, Clay Leachings with Acids (UCRL-18099, February 1968).
7. R. Goolsby, The Critical Temperature on Nb_3Sn in Various Microstructures (UCRL-18452, October 1968).

8. R. Gupta, Techniques for the Measurement of Small Amounts of Heat Released on Planar Surfaces (UCRL-18089, February 1968).
9. J. Hall, Structural Observations in a Metastable Austenitic Steel (UCRL-18282, June 1968).
10. P. Hemmings, The Influence of Strain-Induced Transformation on Fracture of Steels (UCRL-18458, June 1968).
11. R. Jones, The Superconducting Critical Current and Critical Fields of Nb_3Sn-NbC and Nb_3Sn-Nb Composites (UCRL-18437, September 1968).
12. C. A. Liu, Orientation Effect on the Plastic Deformation Behavior of Molybdenum Single Crystals (UCRL-18063, January 1968).
13. V. Marathe, Current Distribution on a Rotating Disk Electrode (UCRL-18264, June 1968).
14. J. S. Masaryk, Permeation in Fused Silica (UCRL-18393, August 1968).
15. Y. Nivas, Limitation of Griffith Flaws in Glass Matrix Composites (UCRL-18586, November 1968).
16. V. T. Ngo, Calculation Methods in Chemical Thermodynamics (UCRL-18510, December 1968).
17. E. W. Page, Structure and Properties of Dynamically Strain Aged Steels (UCRL-18244, June 1968).
18. G. A. Pryor, Impurity Effects in Sintering Lead Zirconate Titanate, (UCRL-18191, May 1968).
19. R. N. Schweinberg, Conductivity and Electrode Polarization in Molten Sodium Disilicate Glass (UCRL-18200, April 1968).
20. B. F. Semans, Densification and Electrical Properties of Lead Zirconium Titanate (UCRL-18126, March 1968).
21. R. Tremper, R-F. Plasma Microspheroidization of Ceramics (UCRL-17896, January 1968).
22. H. I. Yoon, Thermodynamic Properties of Indium-Lead Alloys (UCRL-18402, September 1968).

1968 RESEARCH SEMINARS

1. The Development of Directionally Solidified and Monocrystalloy Turbine Blades.
2. Science and Technology of Surfaces and Interfaces.
3. Crystal Excitations in Low Energy Electron Diffraction.
4. Magnetomechanical Damping Effects in Pure Nickel and Copper-Nickel Alloys.
5. Passivity of Iron.
6. Electrotransport in Current-Carrying Metal Films.
7. Experimental Confirmation of the Lifshitz-Wagner Theory of Particle Coarsening.
8. A Laser Interferometer for Mass Transfer Studies. (S)*
9. High Damping Capacity Manganese-Copper Alloys. (S)
10. The Characterization of 'TRIP' Steels in Terms of Microstructure. (S)
11. Development of the Lucalox Material and Subsequently the Lucalox Lamp.
12. Solution Kinetics Over Extended Temperatures and Negative Activation Energies.
13. Diffusion in Ferrous Sulfide.
14. The Entropy Surface and the Phase Diagrams of ^4He Below 2° K. (S)
15. The Dependence of the Superconducting Transition Temperature of Alloys on Various Physical and Metallurgical Parameters. (S)
16. Nonuniformaties in the Motion of a Dislocation Through a Random Distribution of Point Obstacles. (S)
17. Kinetic and Acrodynamic Aspects of the Attack of Refractory Materials by Dissociated Gases.
18. Far-Infrared Spectra of Ti and V Doped Al_2O_3. (S)
19. A Relation Between Crack Surface Displacements and the Strain Energy Release Rate. (S)
20. Diffusion-Limited High Temperature Metal Vaporization With Nucleation in the Boundary Layer. (S)
21. Techniques for the Measurement of Small Amounts of Heat Release on Planar Surfaces. (S)
22. How Does A Crack Grow? (S)
23. Electronic Spectra of Solid Low Temperature Solutions. (S)
24. Empirical Pseudopotential Method and the Ultraviolet Optical Properties of Insulators. (S)
25. Hinder Pseudo-Rotation in 1, 1-Diflurocyclopentane. (S)
26. A Study of the Optical Properties of Silver Single Crystals and of the Physical Adsorption of Gases on Silver by LEED and Ellipsometry. (S)
27. Reactions of Disulfur Dinitride with Antimony Pentachloride and Boron Trihalides. (S)
28. Damping of Dislocations at High Strain Rates. (S)
29. High Rate Anodic Metal Dissolution Studies. (S)
30. Some Aspects of Passivity and Transpassivity of Zirconium in Perchoric Acid Solution.
31. Least-Squares Digital Analysis of EPR Spectra. (S)
32. Sensitive Nuclear Quadrupole Resonance Detection of D and ^{14}N in Organic Compounds. (S)
33. Heat of Formation of Solid Indium-Lead Alloy. (S)
34. Determination of Surface Mean Displacements on Lead and Bismuth Single Crystal Surfaces by Low Energy Electron Diffraction. (S)
35. Sublimation of CrO_3. (S)
36. Crossed Beam Studies of Lithium Atom Reactions. (S)
37. The Bainite Reaction.
38. Intensity Analysis in Low Energy Electron Diffraction (LEED). (S)
39. Permeation in Fused Silica. (S)
40. Raman Spectrum of I_2 Complexes. (S)
41. Chemistry of Molten Fluoride Fuels for Nuclear Reactors.
42. LEED Studies of Gas Adsorption on Platinum Surfaces. (S)
43. Thermodynamic Stability of Intermetallic Transition Element Compounds. (S)

*(S) denotes student seminars.

Key-Word-Plus-Title Subject and Author Index

The following pages are an alphabetical permuted index of the material in this report. Author's names are included. The index was prepared by the IBM-1401 computer using the key-word-plus-title program KWPT. All significant words are indexed; insignificant words have been automatically rejected by the computer. In some cases the titles have been edited slightly to ensure proper word combination during automatic indexing and to provide maximum meaningful information.

Indexed terms are alphabetized and displayed in the left column of the index. The middle column shows the complete title and authors. The page number is given in the right column.

Your comments about the usefulness of this index and possible improvements are invited. Address such comments to Miss Gloria Smith (ext. 6308) who is responsible for the automated indexing, or to the editor, Mr. Charles Pezzotti (ext. 6003).